NOTICE

The quality of this microform is heavily dependent upon the quality of the original thesis submitted for microfilming. Every effort has been made to ensure the highest quality of reproduction possible.

If pages are missing, contact the university which granted the degree.

Some pages may have indistinct print especially if the original pages were typed with a poor typewriter ribbon or if the university sent us an inferior photocopy.

Reproduction in full or in part of this microform is governed by the Canadian Copyright Act, R.S.C. 1970, c. C-30, and subsequent amendments.

AVIS

La qualité de cette microforme dépend grandement de la qualité de la thèse soumise au microfilmage. Nous avons tout fait pour assurer une qualité supérieure de reproduction.

S'il manque des pages, veuillez communiquer avec l'université qui a conféré le grade.

La qualité d'impression de certaines pages peut laisser à désirer, surtout si les pages originales ont été dactylographiées à l'aide d'un ruban usé ou si l'université nous a fait parvenir une photocopie de qualité inférieure.

La reproduction, même partielle, de cette microforme est soumise à la Loi canadienne sur le droit d'auteur, SRC 1970, c. C-30, et ses amendements subséquents.

Geochemistry of Proterozoic Carbonates, Belt Supergroup, Montana and Idaho, U.S.A.

by

Susan Margaret Hall

A thesis submitted to the School of Graduate Studies in partial fulfillment of the requirements for the degree of PhD in Geology

UNIVERSITY OF OTTAWA

OTTAWA, CANADA, 1990

ISBN 0-315-60036-5

UNIVERSITÉ D'OTTAWA
UNIVERSITY OF OTTAWA

Acknowledgements

I thank Dr. Jan Veizer for his support throughout my thesis work and for his interest in the project. He provided me with good advice, strong direction and timely publications throughout my stay at the University of Ottawa. For sample collection and field logistics, Drs. Don Winston, Bob Horodyski, Jack Harrison and David Kidder were extremely helpful and generous with their time and enthusiasm. Thanks are due to the Superintendent of Glacier National Park for permission to collect in the park boundaries. Financial support was provided via N.S.E.R.C. grants to Dr. Veizer, a Sigma Xi grant to the author, teaching assistant salaries and a foreign student tuition waiver from the University of Ottawa.

John Loop was both helpful and supportive during my work in his laboratory, I thank him for both his aid and his friendship. Paul Middlestead and Gilles St. Jean assisted me greatly during my time in the stable isotope laboratory, and allowed me to fit my work into their busy schedules. Bill Carrigan helped me with KIBA extractions, and I thank him also for many helpful discussions throughout my work on this thesis. Wilma Schmiedel was of great assistance during factor analysis of the chemical results. Drs. Keith Bell and John Blenkinsop were helpful in strontium isotope analyses, and in particular in locating and analyzing several misplaced samples. I am especially grateful to have been able to discuss my results with Martine Savard and Ihsan Al-Aasm, who helped me to expand and refine my knowledge of diagenesis and low temperature geochemistry.

Special thanks are due to Edward, Miriam, Carolyn and Janis Hearn, without whose generosity and friendship this thesis never would have been completed. My mother was encouraging and supportive throughout this endeavour. Thanks to my stepmother, Pat, for harboring the 'houseguest who wouldn't leave'. And finally, thanks to Roger who has remained encouraging throughout the protracted thesis process.

Table of Contents

List of Tables

List of Figures

Abstract

Carbonates from the Proterozoic Belt Supergroup (≈ 850 - 1450 Ma old) were collected from well constrained stratigraphic sections throughout Montana and Idaho, U.S.A. The sampled sequences, in ascending stratigraphic order, include the Newland, Altyn, Spokane/Greyson transition, Empire, Wallace, Helena, Siyeh, Snowslip, Shepard and Libby Formations.

An increase in the degree of post-depositional alteration of Belt limestones is reflected in a diminution of Sr and Mg content, increase in Mn and by depletion in ^{13}C and ^{18}O. $\delta_i^{18}O$ of limestones ranges from +13.4 to +22.9 ‰ SMOW and $\delta^{13}C$ from -5.6 to +2.4 ‰ PDB. Two diagenetic trends can be resolved for the limestones. One, affecting the presumed originally aragonite-rich sediments, comprises the Newland, Libby and perhaps the Snowslip Formations. The other trend is confined to the Middle Belt Carbonate and may have been controlled by high-Mg calcitic sediments. A regional westward depletion in ^{18}O of 8 ‰ and ^{13}C of 2.5 ‰ reflects a higher temperature of alteration (< 300 °C) and an increased contribution from CO_2 derived from thermal cracking of hydrocarbons in the western Belt basin. The $\delta^{18}O$ and $\delta^{13}C$ compositions of the Belt limestones are within the ranges of the values reported for coeval Proterozoic basins. If compared to the modern ocean, the $\delta^{18}O$ of the Belt sea may have been lighter by perhaps 7 ‰. $\delta^{13}C$ averages close to 2 ‰, similar to modern values.

Dolostones in the Belt basin are dominantly micritic, with good preservation of depositional textures. $\delta^{18}O$ of dolomite ranges from 18.1 to 27.9 ‰ SMOW and $\delta^{13}C$ from -2.2 to 1.9 ‰ PDB. Post-depositional alteration of dolostone is indexed by a decrease in Sr and Na contents, increase in Mn and by depletion in ^{18}O and ^{13}C. Dolostones of the Mt.Shields and Altyn Formations have low Sr and heavy $\delta^{18}O$ and $\delta^{13}C$ (if compared to the bulk of Belt samples), show pervasive and destructive dolomitization and may have formed in a mixed water zone of the Dorag type. The remainder of the Belt dolostones resemble typical 'early' diagenetic micritic dolostones in their high Sr content and may have formed in an evaporative setting.

Carbonates of mixed dolomite and calcite composition show depletion in ^{18}O and ^{13}C and increase in Mn content with progressive diagenetic alteration. Secular variations in $\delta^{13}C$ are superimposed on diagenetic trends in this population, showing that carbonates of the Spokane/Greyson, Libby and Newland Formations are ≈ 2 ‰ heavier than those of the Middle Belt Carbonate.

$^{87}Sr/^{86}Sr$ of Belt carbonates ranges between 0.70484 and 0.74991. Progressive diagenesis, as indexed by decreasing elemental Sr and depletion in ^{18}O and ^{13}C, results in an increase in $^{87}Sr/^{86}Sr$ values. $^{87}Sr/^{86}Sr$ is better preserved in

dolomitized rocks and rocks with initially high Sr content (the Newland and Greyson/Spokane Formations). The 'best', that is the least radiogenic values, are similar to those for previously published coeval Proterozoic carbonates and they are more radiogenic than the contemporaneous mantle. A comparison of $^{87}Sr/^{86}Sr$ for the dissolved vs. the suspended load of the Belt basin indicates that the rivers supplying strontium to the basin did not exclusively drain young volcanic or plutonic terrain, but this terrain must have contained a significant source of Sr with marine isotopic composition. Alternatively, the source of nonradiogenic Sr might have been marine waters.

As in the Archean, the dominant redox controlling process in the Belt basin may still have been the coupling of C-O-Fe,Mn cycles and not of C-O-S typical of the Phanerozoic. The $\delta^{34}S$ of sulfates and sulfides suggest that the bacteriogenic sulfide reduction may have been limited in the Belt basin by a limited sulfate supply. Alternatively, the sulfides may represent late diagenetic phases derived from fluids at the end of the Rayleigh fractionation process. The $\delta^{34}S$ of sulfides and sulfates of the Belt basin is comparable to those of coeval Proterozoic sequences.

RESUME

Les formations à carbonates du Supergroupe de Belt (850 - 1450 Ma), Protérozoïque, ont été échantillonnés, au Montana et en Idaho, Etats-Unis, dans des sections dont le cadre stratigraphique est solidement établi. Par ordre stratigraphique, il s'agit des Formations de Newland, Altyn, Spokane/Greyson, Empire, Wallace, Helena, Siyeh, Snowslip, Shepard et Libby.

Le degré d'altération post-sédimentaire des calcaires de Belt est exprimé par une diminution du contenu en Sr et Mg, une augmentation en Mn et par une diminution en ^{13}C et ^{18}O. Les vaieurs de $\delta^{18}O$ varient de +13.4 à 22.9 o/oo (SMOW) et celles de $\delta^{13}C$ de -5.6 à 2.4 o/oo (PDB). Deux patrons diagénétiques sont reconnus dans les séquences calcaires. Le premier, dans les Formations de Newland, de Libby et possiblement de Snowslip, fut vraisemblablement produit par la calcitisation de sédiments riches en aragonite. Le deuxième est restreint aux carbonates du Groupe de Middle Belt et est possiblement relié à la stabilisation de calcites magnésiennes. A l'échelle régionale, d'est en ouest, une diminution de 8 o/oo de $\delta^{18}O$ réflète une augmentation des températures de recristallisation, alors qu'une diminution de 2.5 o/oo de $\delta^{13}C$ indique une contribution accrue en CO_2 organique vers l'ouest du Bassin de Belt. Les valeurs de $\delta^{18}O$ et $\delta^{13}C$ des calcaires se situent dans l'intervalle des valeurs documentées pour d'autres bassins du même âge. Lorsque comparée aux océans modernes, il semble que la mer de Belt devait être jusqu'à 7 o/oo plus légère en ^{18}O et qu'elle avait un signal similaire en ^{13}C, soit 2 o/oo en moyenne.

Les dolomies du Bassin de Belt sont à dominance micritique et montrent une bonne préservation des textures de dépôt. Leurs valeurs de $\delta^{18}O$ et $\delta^{13}C$ varient entre 18.1 et 27.9 o/oo (SMOW), et entre -2.2 et 1.9 o/oo (PDB), respectivement. Leur altération post-sédimentaire est réflétée par une baisse en Sr et Na, un enrichissement en Mn et un appauvrissement en ^{18}O et ^{13}C. Les dolomites des Formations de Mt. Shields et de Altyn sont plus pauvres en Sr, et plus riches en ^{18}O et ^{13}C que celles de l'ensemble du Bassin, elles résultent d'une dolomitization pénétrative et destructrice, probablement de type "Dorag". Ailleurs dans le bassin, les dolomites sont micritiques, d'aspect sédimentaire, et ont peut être été formées par évaporation.

Chez les carbonates mixtes, composés à la fois de dolomites et calcites, le degré d'altération progressif est affiché par un appauvrissement en ^{18}O et en ^{13}C, ainsi que par un enrichissement en Mn. Des variations séculaires de $\delta^{13}C$ se sont superposées aux patrons diagénétiques dans ces carbonates et ont entraîné un enrichissement de 2 o/oo dans les Formations de Spokane/Greyson, Libby et Newland, ceci par rapport aux carbonates du Groupe de Middle Belt.

Les rapports $^{87}Sr/^{86}Sr$ des carbonates du Supergroupe de Belt varient entre 0.70484 et 0.74991. L'altération diagénétique, indiquée par une baisse du contenu en Sr, ^{18}O et ^{13}C, a provoqué un enrichissement en isotopes radiogéniques. Les rapports $^{87}Sr/^{86}Sr$ sont mieux préservés dans les roches dolomitisées et dans les roches initialement enrichies en Sr (Formations de Newland et Greyson/Spokane). Les valeurs les mieux préservées, i.e. les moins radiogéniques, sont similaires à celles d'autres carbonates protérozoïques et sont plus radiogéniques que les valeurs du manteau contemporain. Une comparaison

entre les rapports $^{87}Sr/^{86}Sr$ obtenus pour les charges fluviatiles dissoute et flottante indique que les rivières qui ont amené le strontium au Bassin de Belt n'ont pas érodé qu'un jeune terrain volcanique et plutonique, mais un terrain devant aussi contenir une importante source de Sr marin. Alternativement, le Sr non-radiogénique auraient pu provenir d'eaux marines.

Dans le bassin de Belt, tel que pendant l'Archéen, le couplage cyclique C-O-Fe-Mn pouvait toujours être le principal contrôle du redox, au lieu du couplage C-O-S qui fut le principal contrôle au Phanérozoïque. Le $\delta^{34}S$ des sulfates et sulfures suggèrent que la réduction bactériogénique du souffre était possiblement limitée par une réserve restreinte en sulfates. Alternativement, les sulfures ne représentent peut être que des phases diagénétiques tardives, marquées par le fractionnement excessif d'un processus Rayleigh avancé. Finalement, les $\delta^{34}S$ des sulfures et sulfates du Bassin de Belt sont comparables à ceux de séquences contemporaines.

Introduction

This study of the geochemistry of Proterozoic Belt Supergroup carbonates aims at 1) reconstruction of trace element and isotope stratigraphy for the Belt basin, and 2) reconstruction of the geochemistry of the late Proterozoic oceans, a period particularly devoid of isotopic data.

Previous studies have linked progressive diagenesis of carbonate rocks to predictable changes in their chemistry (Brand and Veizer, 1980, 1981; Al-Aasm and Veizer, 1982, 1986; Brand and Morrison, 1987). The techniques developed during these studies (cf. Veizer, 1983a,b), and utilized previously for Archean rocks (Veizer, 1989a,b), are here applied to dominantly micritic carbonates (limestones and dolostones) from the Belt basin in order to establish their diagenetic rank and any preserved regional and temporal geochemical variations. These results, complemented by data from coeval sequences, will be utilized to track the evolution of Proterozoic seawater.

The stratigraphy of the Belt Supergroup has been reviewed and revised only recently (Hobbs, 1984). The first two chapters in this thesis are a review of the sedimentology, stratigraphy and tectonics of the Belt basin. The chemical composition of Belt sediments was first addressed by Harrison and Grimes (1970). They concluded that the dominant sediment source for Belt argillites was granitic (later corroborated by

$^{87}Sr/^{86}Sr$ studies of Belt argillites), that regional variation in trace element composition was related to metamorphism, and that the Belt sediments were chemically homogeneous. Frost and Winston (1987) confirmed this homogeneity and concluded that the sediments were multi-cyclic; while Schieber (1985, 1986) concluded that a granitoid gneiss and migmatite complex was the principal source rock during deposition of the Belt sediments. The last author attributed variations in REE chemistry in the eastern Belt sediments to periodic tectonic pulses and/or to variations in the degree of chemical weathering of the hinterland. Frost and Winston (1987), utilizing Sm-Nd systematics of fine-and coarse-grained siliciclastic sediments, showed that the age of the source of Belt sediments exceeded their depositional ages by ≈ 200 to 800 Ma.

In contrast to argillic sediments of the Belt Supergroup, carbonates in the basin have been largely ignored by geochemists. In an effort to determine the style of copper mineralization, some carbonates have been analyzed for oxygen and carbon isotopes (Rye et al., 1984; Lange et al., 1987). These authors also measured the $\delta^{34}S$ of sedimentary sulfides and sulfates and Ueda et al. (1987) reported $\delta^{34}S$ of trace sulfides and sulfates in one carbonate unit. Additional measurements of $\delta^{13}C$ and $\delta^{18}O$ values for carbonates have been reported by Winston et al. (1984). Schieber (1985) reported

elemental analyses of some carbonate-rich sediments from the eastern Belt basin. At the time the present study was initiated no comprehensive study of the geochemistry of Belt carbonates has been published.

The following study is timely because the stratigraphy and sedimentology of the Belt basin has recently been coordinated, the age of the sediments has been substantially constrained, and because the data complement the extensively studied siliciclastic sediments. This regional investigation of the geochemistry of carbonate sediments in the Belt basin thus should provide a framework for localized and more detailed analyses of sedimentology and diagenesis.

Chapter 1

Stratigraphy, Tectonics and Paleogeography of the Belt Basin

The Belt Supergroup is a succession of rocks of Proterozoic age, specifically = 850 - 1450 Ma (Harrison, 1972; Obradovich et al., 1984), deposited in a basin which extends from southwestern Canada (southern Alberta and British Columbia) into the northwest United States (northern Idaho, western Montana and eastern Washington; Figure 1-1). The Belt Supergroup is dominantly a sequence of fine grained clastic sediments with subordinate carbonates and igneous rocks.

1.1 Geometry of the Belt Basin

The Belt basin is bounded on the east by the Montana Disturbed Belt, an orogenic belt which extends along the eastern margin of the Rocky Mountains (Figure 1-2; Harrison, 1972). Facies changes along this belt, which probably represents the easternmost depositional edge of the Belt basin, are the most pronounced of the entire supergroup (Price, 1964; Mudge, 1970). Discovery of the previously unrecognized lower Belt strata east of the Montana Disturbed Belt indicates that the lower Proterozoic Belt basin may have extended slightly east of this boundary (Reynolds and Lindsey, 1979). South of Helena, Montana, the Willow Creek

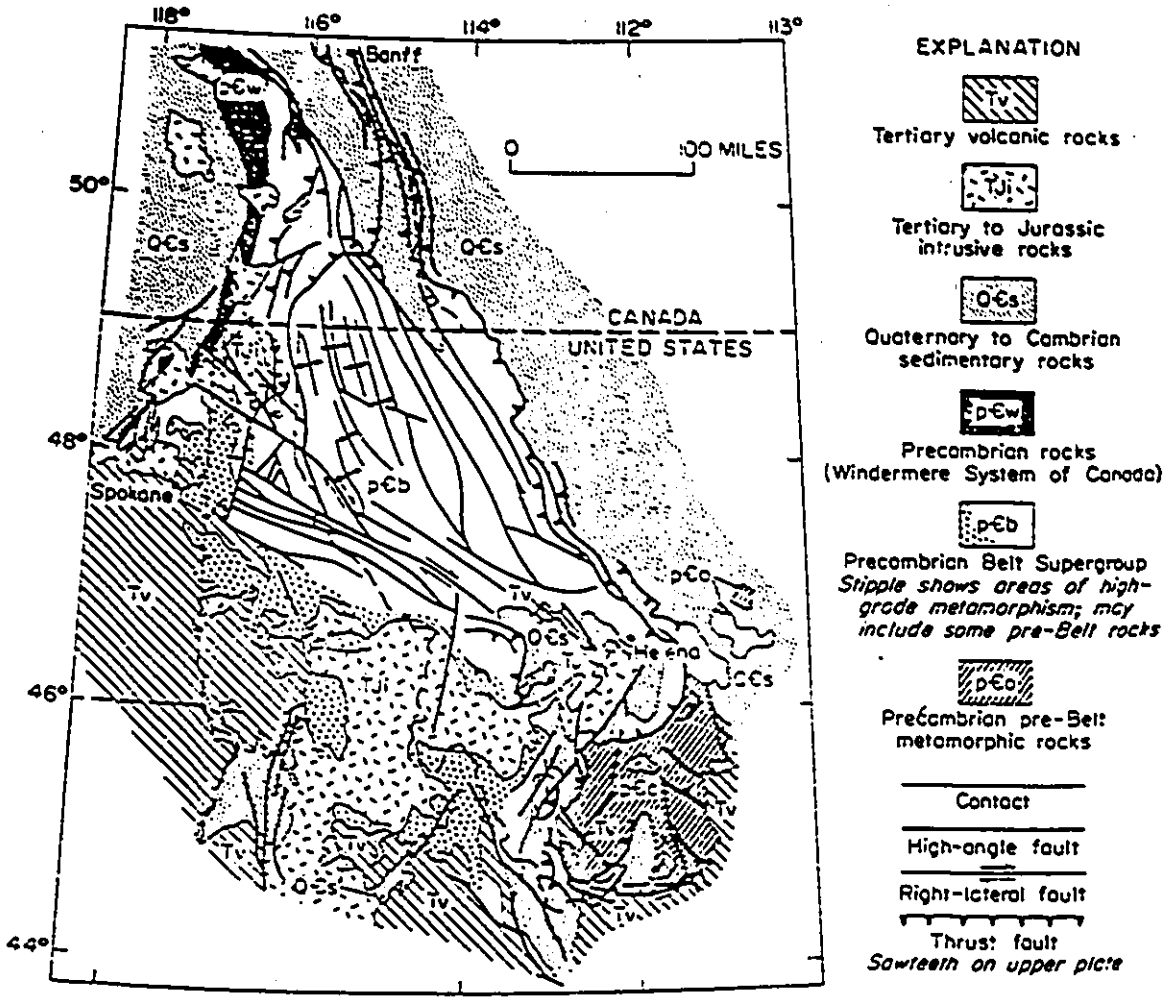

Figure 1-1.
Regional geology of the Belt basin (Harrison, 1972).

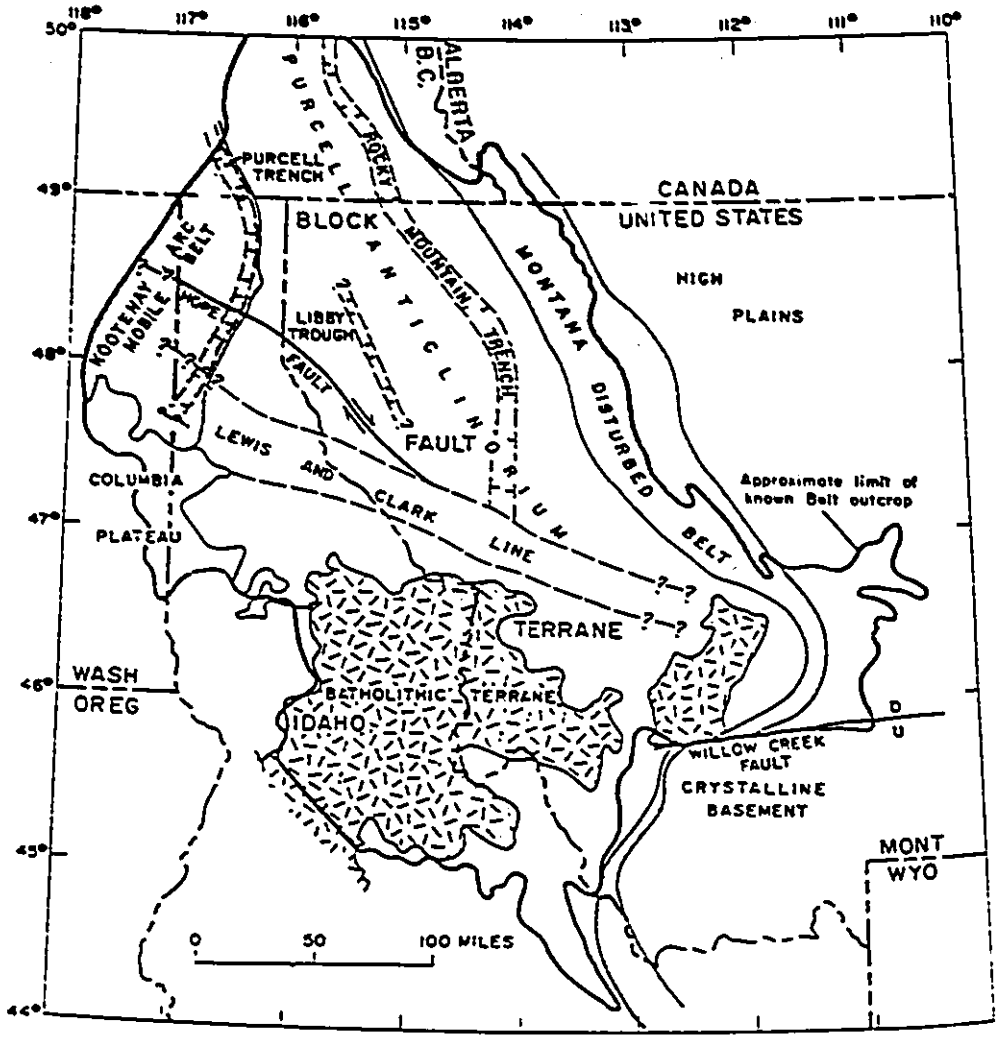

Figure 1-2.
Geologic and tectonic provinces in northern Idaho, eastern Washington, western Montana and southern British Columbia. U-upthrown side of fault, D-downthrown side of fault (Harrison, 1972).

fault separates Belt sediments from the southern crystalline basement rocks (Figure 1-2; McMannis, 1963). In the northwest, the Belt Supergroup is overlapped by the younger Windermere system (Figure 1-1; Harrison, 1972). Belt sediments show no apparent thinning as they pass underneath a cover of Tertiary Columbia River basalt on the western edge of the basin. The depositional edge of the Belt basin in the west is therefore unknown (Figure 1-1; Harrison, 1972, Harrison et al., 1974). The southern and southwestern Belt sediments are injected with Jurassic to Tertiary intrusive rocks (the Idaho Batholith; Figure 1-1) and as such are highly metamorphosed and deformed, making correlations with the less deformed Belt sediments difficult.

1.2 Thickness and General Stratigraphy of the Belt Basin

The measured thickness of Belt sediments varies from 52,000 feet (≈ 16 km) in the basin centre (Wells, 1972) to 3,700 feet (≈ 1128 m) in the western part of the basin (Rice, 1941) and the sequence pinches out along the eastern basin edge (Harrison, 1972). These thicknesses are exaggerated in places by Phanerozoic thrusting (Harrison et al., 1980).

The Belt Supergroup is divided into four major stratigraphic units which are, in ascending order, the Lower

Belt Prichard Formation with its eastern equivalent Chamberlain Shale and Newland Dolomite, the Ravalli Group, the Middle Belt Carbonate and the Missoula Group (Figure 1-3).

Provenance studies based on facies changes and paleocurrent indicators indicate a southern source for most sediments in the Belt basin (Figures 1-4 and 1-5). In lower Belt and Ravalli group sediments, a southern and western source is strongly indicated for the western Belt basin (Figure 1-4; Myers, 1952; Hrebar, 1971; Bowden, 1977; Mauk, 1983; Cressman, 1984b; Finch and Baldwin, 1984; Hoy, 1984). In the southeastern Belt basin (the Helena embayment), a carbonate ramp which dips north to south has a northern provenance for lower Belt sediments (Godlewski and Zieg, 1984). Middle and upper Belt sediments also indicate a dominantly southern sediment source (Figure 1-5; Harrison, 1984; Wallace et al., 1984). During upper and middle Belt time, there was an increased sediment influx from the eastern basin edge (Figure 1-5; Harrison, 1984; Wallace et al., 1984). Some Missoula Group sediments are derived from a northern basin margin (Figure 1-5; Wallace et al., 1984). A comprehensive study of paleocurrent indicators is now being undertaken by the U.S. Geological Survey and will doubtless yield a more complete understanding of sediment source directions throughout the Belt basin.

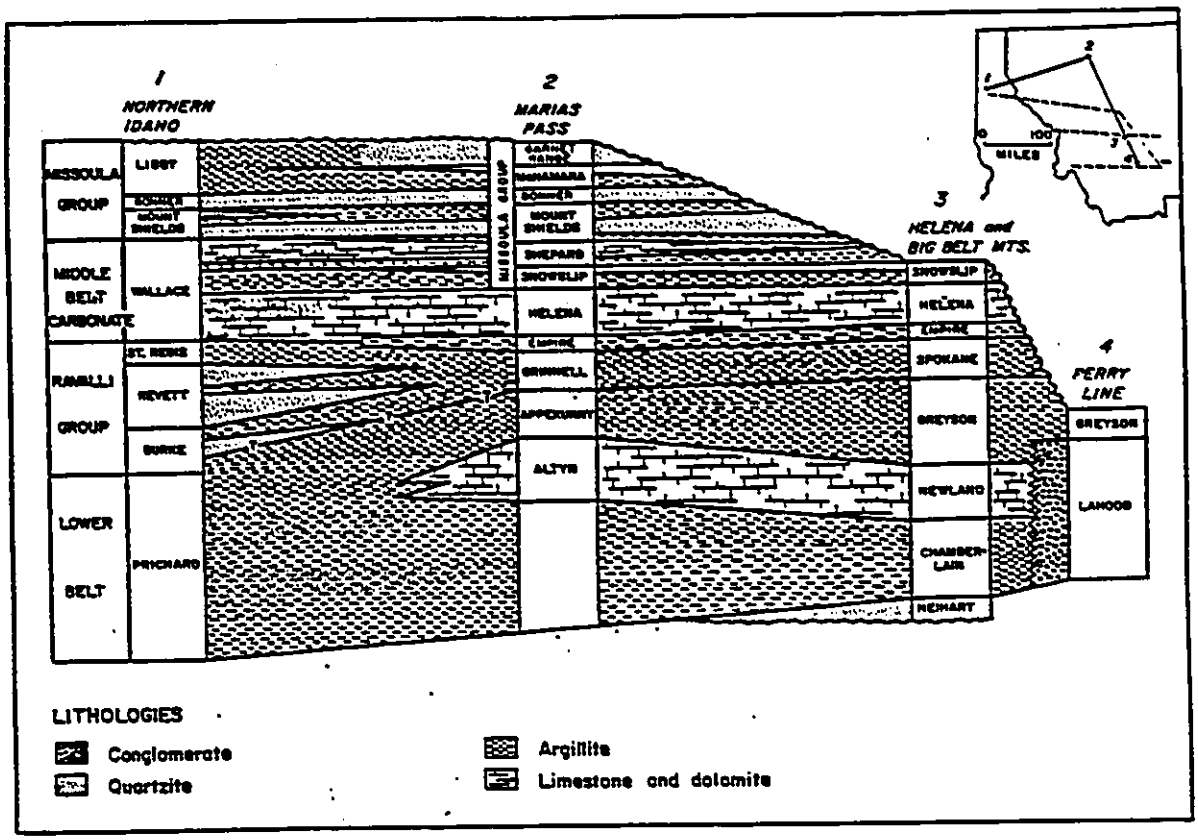

Figure 1-3.
Stratigraphy of the Belt Supergroup, not to scale (Winston, 1986).

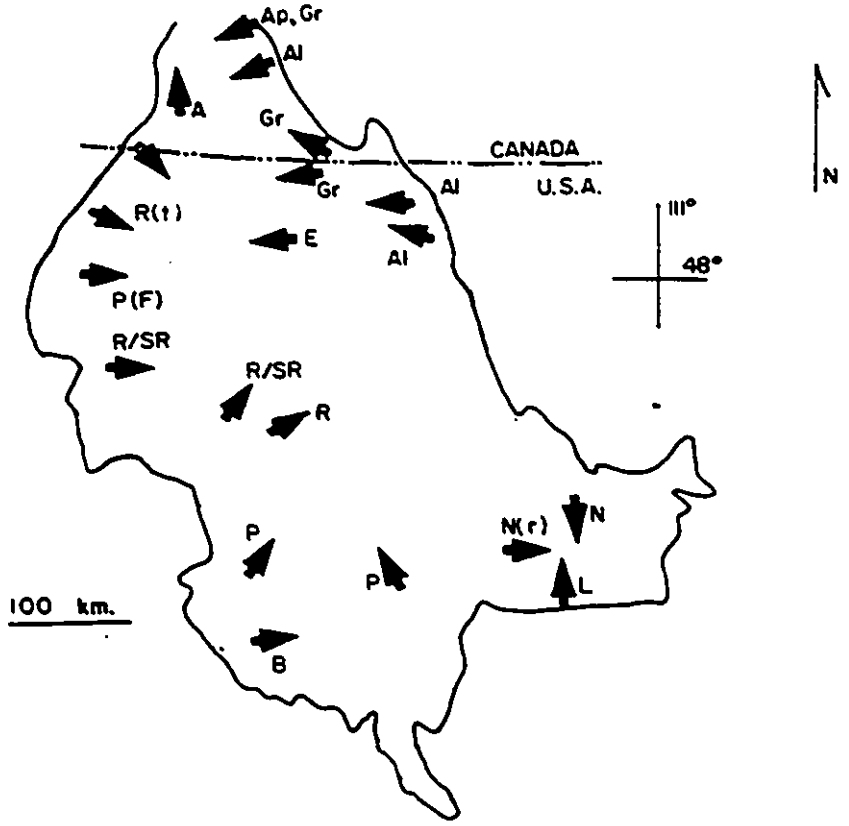

Figure 1-4
Lower Belt and Ravalli Group paleocurrent/sediment source directions. A - Aldridge Fm. (Prichard equivalent), sole marks indicating direction of sediment transport (Hamilton et al., 1983). Al - Altyn Fm., current directions at the site of deposition and facies changes (Hoy, 1982; Horodyski, pers. com., 1987). Ap, Gr - Appekunny and Grinnell Fms., Facies changes in quartz arenite units and cross-bedded sands (Horodyski, pers. com., 1987). B - Belt age rocks with westward coarsening grain size and a westward increase in the feldspar content of feldspathic quartzites indicating a western granitic source (Myers, 1952). E - Empire Fm., more feldspathic units to the east and westward tapering of sedimentary units (Harrison, pers. com., 1987). L - LaHood Fm., facies changes indicate location of basin margin (Hamilton et al., 1983). N - Newland Fm., facies changes indicate location of basin margin and centre (Godlewski and Zieg, 1984). N(r) - ripples in the Newland Fm. (Zieg, 1981). P - Prichard Fm. Turbidites (based on slumping and distribution of turbidity flows and sole marks (Cressman, 1984a; Finch and Baldwin, 1984). P(F) - Prichard Fm. facies progradation towards eastern Belt basin (Cressman, pers. com., 1987). R, R/SR - Revett and St. Regis Fms., ripple marks and facies changes (Bowden, 1977; Hrebar, 1971; Mauk, 1983). R(t) - continuation of Revett thickness into British Columbia (McMechan, 1981) and into eastern Washington (Miller and Clark, 1975).

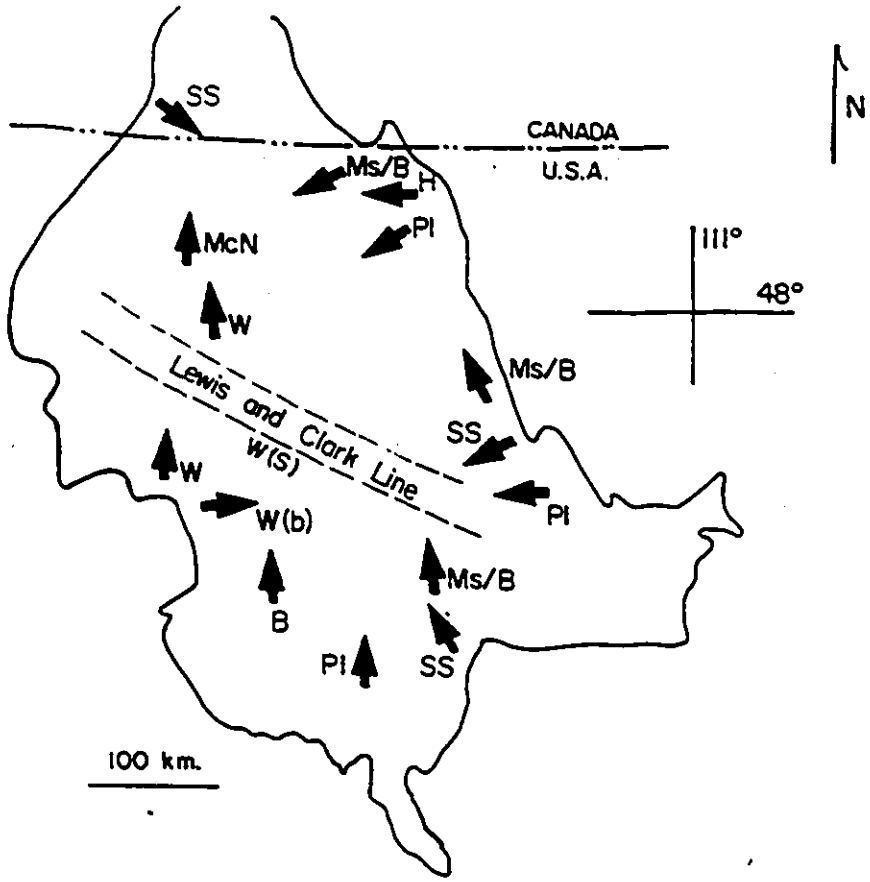

Figure 1-5
Middle Belt Carbonate and Missoula Group paleocurrent/sediment source indicators. B - Bonner Fm., southward thickening of sand wedge (Winston, 1973). H - Helena Fm., eastern source for quartz arenite sands at cycle boundaries (Harrison, pers. com., 1987). Ms/B - Mt. Shields and Bonner Fms., based on facies changes and paleocurrent directions (Wallace et al., 1984) and the existence of granitic pebbles in the south/southwestern part of the basin (Wallace pers. com., 1987). McN - McNamara Fm., based on a greater volume of sand in the south/southwest (Winston, 1986). Pl - Pilcher Fm., cross-beds and facies distribution (Wallace et al., 1984). SS - Snowslip and Shepard Fms., based on thickening direction of sediment wedges (Wallace et al., 1984) and by crossbed and facies distributions (more quartz arenite rich units on the western edge of the basin) and on the existence of granitic pebbles in the south/southwestern part of the basin (Wallace pers. com., 1987). W - Wallace Fm., based on facies changes (Harrison, 1984). W(b) - Wallace Fm., sand facies restricted along the western side of the basin (Winston, pers. com., 1987). W(S) - Wallace Fm., slumps caused by movement on the Lewis and Clark line during sedimentation (Godlewski, 1977).

1.3 Age of Belt Sediments

Controls on the age of Belt sediments are summarized in Figure 1-6. The oldest dated rock in the Belt Supergroup is the Cressport C (Moyie) sill intruded into the base of the middle Prichard Formation from which a U-Pb age of 1,433 ± 10 Ma was determined (Zartman et al., 1982). This sill was probably intruded into the Prichard before lithification of the formation as evidenced by deformation of the sediments within 1 foot of the sill. The age of the sill is therefore close to the age of deposition of the Prichard Formation. K-Ar dates of metamorphic biotite in the Prichard give a slightly younger age of > 1,335 Ma for its metamorphism (Obradovich and Peterman, 1968). Rb-Sr whole rock isochrons determined from argillites in the Neihart Quartzite through Greyson shale from the Little Belt Mountains (east-central Belt basin) yield an age of 1,300 Ma, which may record the age of low-grade metamorphism of these sediments. The younger age of these lower Belt units may pose some problems for correlation of the Prichard and Newland Formations (Obradovich et al., 1984), although if we accept 1,300 Ma as the age of metamorphism this may instead record a metamorphic overprint on Prichard equivalent rocks deposited in the eastern Belt basin. Obradovich and Peterman (1968) indicated a U/Pb age of 1360 to 1270 Ma for bentonites in the Neihart Quartzite. K-Ar and

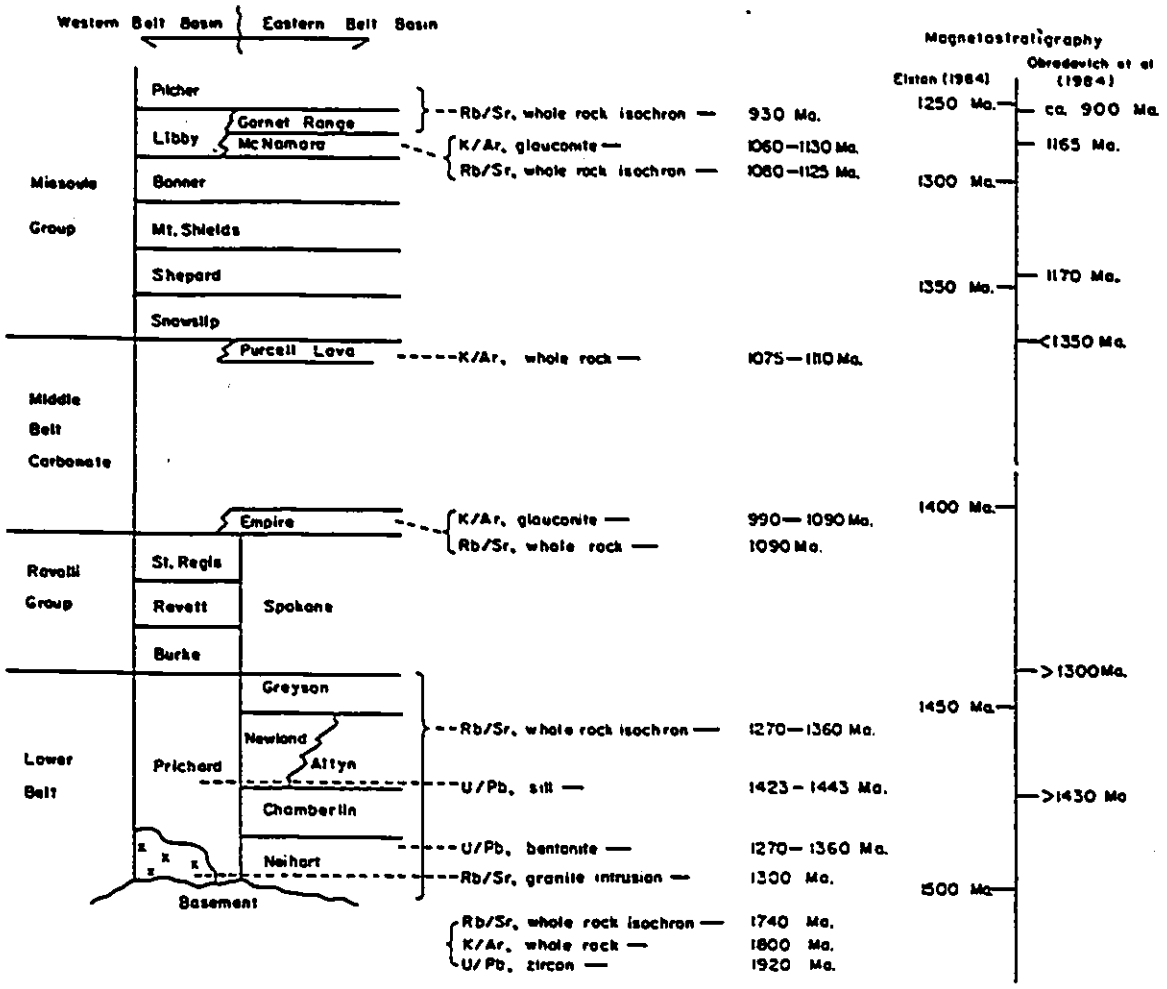

Figure 1-6
Age controls on Belt Supergroup Sediments.

Rb-Sr isochrons determined from glauconite and Rb-Sr isochrons from whole rock samples yielded an age of 1,100 Ma for the upper Ravalli group, the Middle Belt Carbonate and most of the Missoula Group (Figure 1-6; Obradovich et al., 1984). The Garnet Range Formation and Pilcher Quartzite have been dated at 900 Ma by Rb-Sr whole rock isochrons (Obradovich et al., 1984). Burwash (1984) reported Rb-Sr mineral isochrons for a sill in the Siyeh Formation (northern equivalent of the Middle Belt Carbonate) of 1665 to 1317 Ma and for the Purcell Lava (extruded into the Mt. Shields/Shepard Fms.) of 818 to 1237 Ma. Nd model ages of clastic sediments in the Belt basin indicate a 1600 to 2100 Ma old provenance, the average crustal residence age of the fine grained sediments being 2000 Ma (Frost and Winston, 1987).

Magnetostratigraphy of the Belt Supergroup suggests that the Belt may be older than 1,300 Ma (Elston, 1984). Elston (1984) dated the Missoula Group sediments as 1,250 Ma, extrapolating this date to infer an age of 1,450 to 1,500 Ma for the lower Belt Prichard Formation. Although polarity reversals seem well controlled stratigraphically, some controversy surrounds the use of magnetostratigraphy as a dating tool for this interval of the Proterozoic. Insufficiently dated pole positions prevent accurate dating of Belt sediments by magnetostratigraphy (Obradovich et al., 1984). To further undermine Elston's (1984)

magnetostratigraphic time frame, Obradovich et al. (1984) have pointed out that several poles determined for Belt formations fall well outside the polar limits set by those few rocks which have good geochronologic data. This indicates that post-depositional structural rotation is a significant problem in some of the Belt sediments. The poor time resolution inherent in analyzing structurally rotated Proterozoic rocks precludes the use of magnetostratigraphy as anything but a rough estimate of the age of Belt sediments.

The oldest rocks in the Belt Supergroup are probably older than 1400 Ma and a tectonic event at 1300 Ma resulted in low grade metamorphism of lower Belt sediments, causing anomalously young dates throughout the lower Belt, and intrusion of granite into the Prichard Fm. The age of Ravalli Group, Middle Belt Carbonate and Missoula Group sediments is poorly constrained, but the bulk of the evidence indicates that these sediments were deposited between 1300 and 1100 Ma ago. Subsequently, low grade metamorphism may have affected these rocks resulting in a significant scatter of age dates and implying a younger age (≈ 900 Ma) for the upper limit of deposition of Belt sediments.

1.4 Proterozoic Tectonics of the Belt Basin

It is unclear if Belt sediments were deposited in a basin isolated from or connected with the open ocean (Winston et al., 1984). Figure 1-7 summarises the major ideas on tectonic settings of the Belt basin. These ideas range from an early miogeoclinal concept (Walcott, 1914; Price, 1964; Figure 7A) to a marine epicratonic reentrant of the sea along the edge of western North America (Harrison et al., 1974; Figure 7C). The Belt basin may have been one of a number of roughly coeval reentrants along the west coast of present North America. Imprecise dating of sediments in these basins allows only their superficial correlation (Harrison et al., 1974).

Paleocurrent analysis, facies analysis and geochemical studies (Frost and Winston, 1987) indicate a western provenance for many of the Belt sediments, and thus neither the marine epicratonic reentrant (7C) or miogeoclinal (7A) concepts are wholly accurate. Harrison et al. (1974) introduced the concept of an island or large cratonic 'prong' which lay to the west of the Belt basin and provided a western source terrane for the Belt basin sediments. The most recent thoughts on the tectonic setting of the Belt basin call for a western continental block which partly enclosed the basin (Cressman, 1984b; Figure 7D). Winston et al. (1984) and

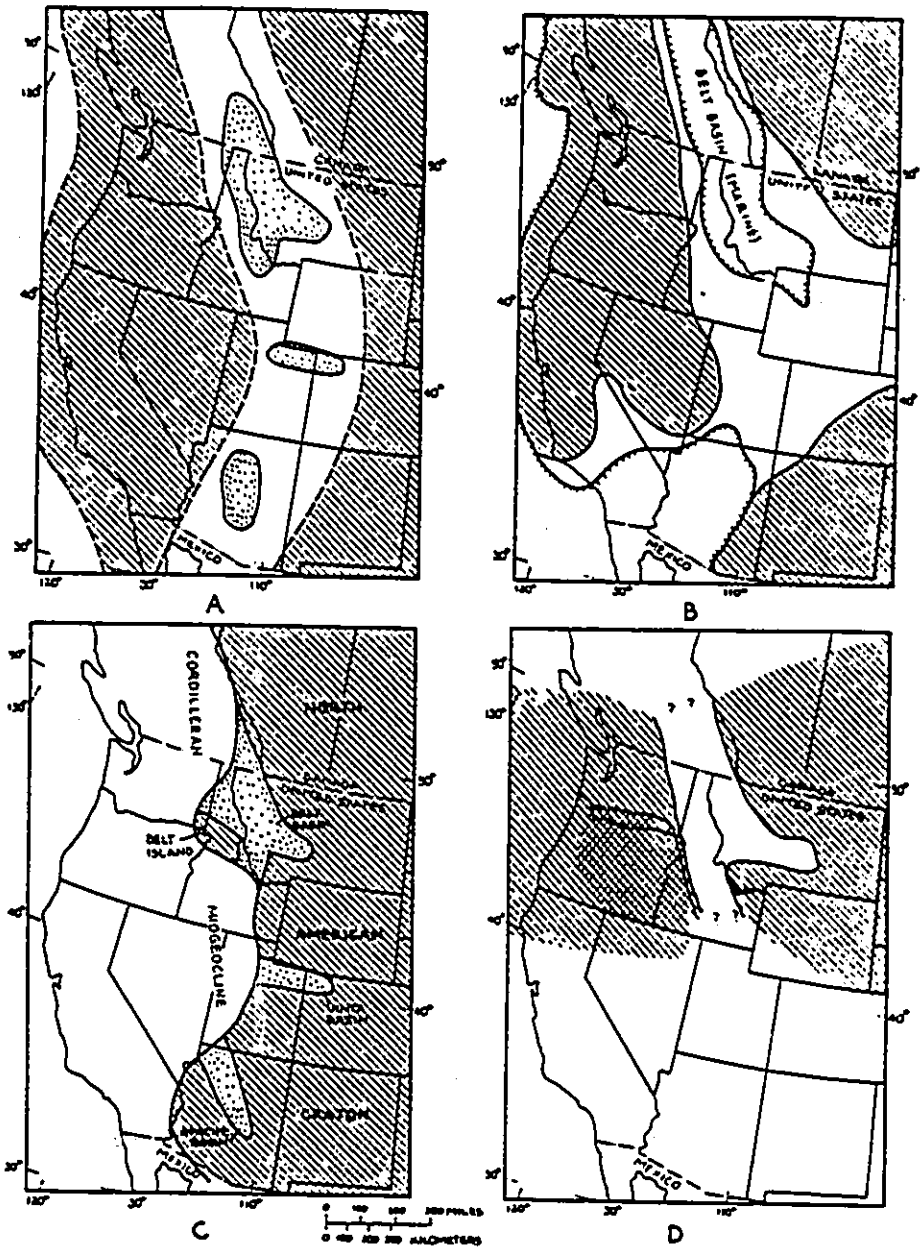

Figure 1-7.
Middle Proterozoic paleogeography of western North America sketched from ideas of various authors (from Winston et al., 1984). A) Isolated basins within a continental geocline (Walcott, 1914). B) Marine epicontinental sea surrounded by continental deposits (Fenton and Fenton, 1937). C) Marine miogeocline with embayments into western North America, including the Belt basin embayment which is further isolated by the Belt island to the west of the basin (Harrison et al., 1974). D) Partly enclosed Belt basin bordered on the west by a continent (Cressman, 1984a).

Frost and Winston (1987) proposed that the Belt basin was wholly enclosed and is in fact an intracratonic basin.

Interpreting paleomagnetic poles determined from Proterozoic sediments worldwide, Piper (1982) concluded that there was a Proterozoic supercontinent from 2600 to 570 Ma. The correlation of poles is poor after 800 Ma which may indicate that the supercontinent was beginning to fragment at 800 Ma. This breakup correlates well with geochronological age estimates for the end of Belt sedimentation (Figure 1-6) and corroborates Stewart's (1972, 1976) and Eisbacher's (1981) assumption of a continental break-up of North America at ≈ 850 Ma. The rifted western equivalent of the Belt Supergroup may be found in the Siberian Platform (Sears and Price, 1978). The correlation is difficult to specify since Proterozoic rocks of Belt age are only poorly exposed in the Siberian Platform. The similarity of structural style (tectonic grain), good fit of the North American platform and the Siberian platform, and synchronous ages for stabilization and onset of sedimentation in a series of aulacogens along both platforms (1570 - 1450 Ma) are arguments for stabilization of both continents at around 1700 Ma, and their rifting at 1500 Ma.

Between 1700 and 850 Ma, active spreading along the western edge of the North American craton as well as within the craton seems to have occurred (Stewart, 1972). About 850

Ma ago, tectonism on the continent changed, initiating the onset of continental separation. In the Belt basin this change is evidenced by the uplift and erosion of the upper Belt strata (850 - 900 Ma) and in initiation of Windermere sedimentation unconformably over the Belt strata. Armin and Mayer (1983) and Bond and Kominz (1984) examined sedimentation and subsidence in the Cordilleran miogeocline and date the initial continental separation at 600 Ma.

The Proterozoic structural regime of the Belt basin is complicated by Phanerozoic structures. Some pre-existing faults have been reactivated, as indicated by clear correlation of the present-day Lewis and Clark line with the well-established existence of Proterozoic movements along this lineament (Reynolds and Kleinkopf, 1977; Hobbs et al., 1965; Godlewski, 1977). Where no data exist for delineation of Proterozoic faults, Winston (1986) has utilized Phanerozoic faults as an approximation for the Proterozoic structural pattern.

The basement of the Belt basin was apparently dissected by a series of east-west and northwest trending faults (Winston, 1981, 1982, 1983; Kleinkopf and Reynolds, 1982), inferred from abrupt increases in sediment thickness across the proposed faults (Winston, 1986). The faults break the basement into blocks (Figure 1-8) and the relative uplift

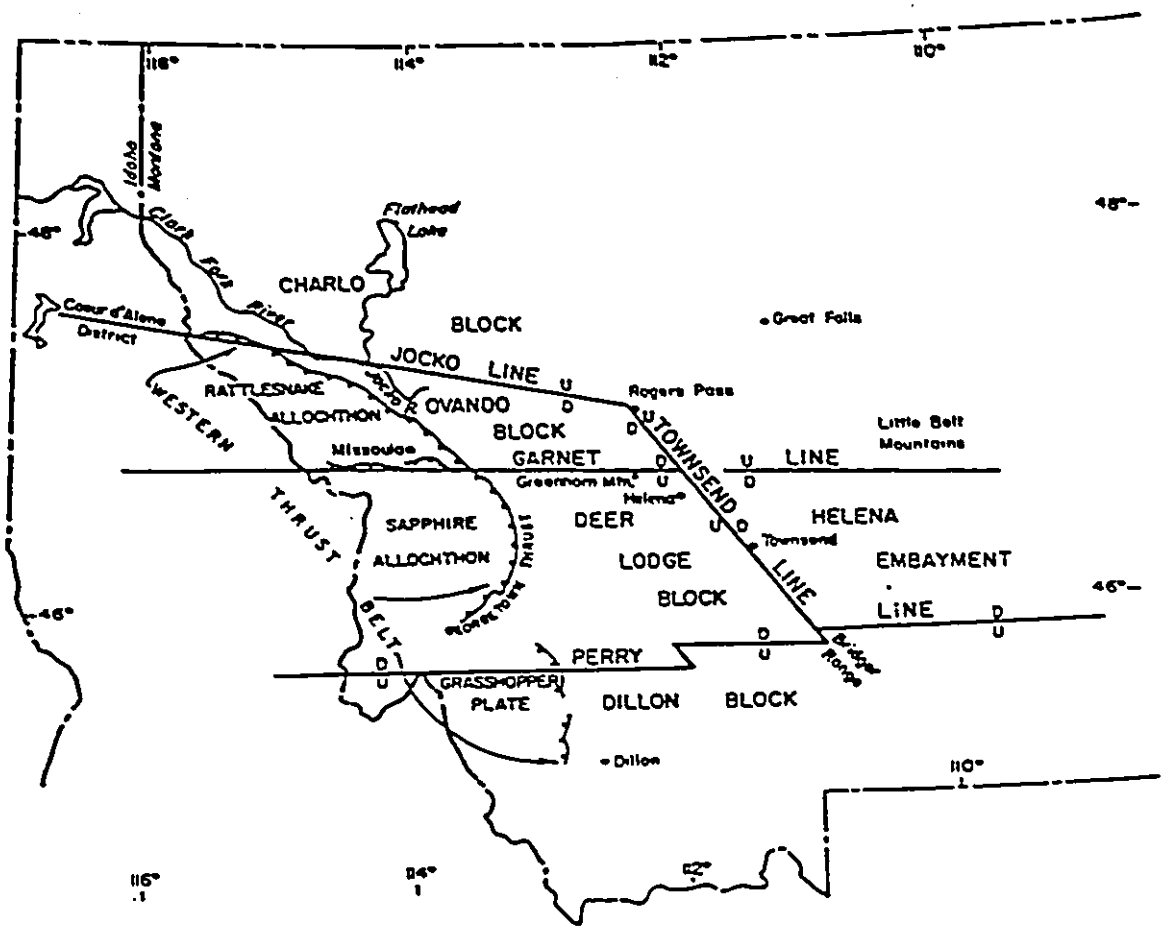

Figure 1-8
Proterozoic crustal blocks of the Belt basin, D-downthrown block, U-upthrown block (Winston, 1986)

and subsidence along these faults apparently initiated and controlled sedimentation in the Belt basin (Winston, 1986).

The Perry Line (Figure 1-8) was the southern limit of the Belt basin and is now delineated by the Willow Creek, Soap Creek and Pass faults. Proterozoic movement along the Perry line was down to the north, as is dramatically defined by the Lahood Formation, a coarse-grained arkose and arkosic conglomerate, the components of which were shed from the uplifted Dillon block into the Helena embayment.

North of the Perry line, the Belt basin is dissected by the Lewis and Clark line (Figure 1-2), now recognised as the Osburn fault in its western part. The Osburn strike slip fault is thought to have been active with vertical movement predominating during the Precambrian (Hobbs et al., 1965; Godlewski, 1977, Reynolds, 1977) and is defined by Winston (1986) as consisting of two east-west fault zones, the Garnet and Jocko lines (Figure 1-8). The eastern end of the Lewis and Clark line shows strike slip, oblique slip and normal dip slip movement (Reynolds, 1977). Using stratigraphic evidence, Reynolds (1977) deduced that the movement on the eastern Lewis and Clark line from the Precambrian to Mesozoic was vertical. During the late Mesozoic and early Tertiary, the movement became left lateral strike slip in response to intrusion of the Boulder batholith. During the late Cenozoic, movement became

right lateral strike slip with displacements of 13 to 26 km (Harrison et al., 1974). Winston (1986) controversially defined the Lewis and Clark line as consisting of two east-west fault zones during Belt time, the southern Garnet and northern Jocko lines (Figure 1-8). The Townsend line supposedly separated the Helena embayment (graben) from the western Belt basin (Winston, 1986). Movement along the Townsend line was down to the east in the south and down to the west in the northern part of the basin.

1.5 Tectono-Stratigraphic History of the Belt Basin

Initial subsidence of the basement blocks of the Belt basin resulted in a basin deeper in the western part of Montana and structurally elevated in eastern Idaho and along the eastern edge (as defined by the Townsend line; Winston, 1986). The Helena embayment may have been partly restricted even during this time, as is indicated by thinning of Belt strata across the Townsend line. The northern Jocko line was active during this period, as is illustrated by thickening of the Lower Belt Prichard Formation south of the Jocko line (Webster,1981). The lowermost Precambrian igneous rocks in the Belt basin are the dioritic Moyie sills (and accompanying dikes) which were intruded into the Prichard Formation. The Moyie sills are believed to have intruded the Lower Belt strata shortly after deposition of the sediments

(Leech, 1962) and are dated at 1430 Ma (Zartman et al., 1982). The Moyie sills indicate that the Belt basin was undergoing a period of tensional tectonism. A hiatus in igneous activity, which followed the intrusion of the Moyie sills, lasted until the upper Middle Belt Carbonate time.

The lower Ravalli Group marks upward shallowing of the basin, and uplift of a source area to the south. The Revett Formation (of the lower Ravalli Group) represents an alluvial fan which aggraded northeastward across the Belt basin (Hrebar, 1971; Bowden, 1977; Mauk, 1983). As sediment from the upland source to the south became depleted (as a result of the end of tectonic activity in the south), siltite-argillite couplets were the predominant deposits. The uppermost Revett contains sand wedges which may indicate renewed tectonic uplift and coincident transgression of the Belt sea (Winston, 1986). Movement along the Jocko line continued during deposition of the Revett, as is evidenced by thickening of the Revett south of the Osburn fault (White and Winston, 1982; Alleman, 1983; Mauk, 1983). The predominant sediment source was to the south and west during deposition of the Ravalli Group (Figure 1-4). Mudstones predominate in the strata of the Ravalli Group on the eastern margin of the basin, with some coarse grained sandstones (presumably derived from the adjacent Hudsonian basement) interfingering with these mudstones (Winston, 1986).

The Belt sea transgressed over the Revett depositing the St. Regis and Spokane Formations, with a small regression occuring during deposition of the lower St. Regis (Winston, 1986). In the south, movement continued along the Jocko line, as indicated by southern thickening of sediments (Wallace and Hosterman, 1956) and by slumping in the St. Regis (Chevillon, 1977) and Wallace Formations (Winston, 1986).

Transgression of the Belt sea continued into the Middle Belt Carbonate interval. During deposition of the Middle Belt Carbonate, the Ovando block also subsided (Winston, 1986). The uppermost Middle Belt Carbonate interval records a basinwide regression which restricted the Belt sea to the north-central part of the basin (Winston, 1986). Volcanic glass shards are reported in the uppermost Siyeh Formation (Middle Belt Carbonate) but they may record a volcanic event extrinsic to the Belt basin (Horodyski, 1983).

The Missoula Group represents a change in sediment source direction from west and south to the south and east (Figure 1-5). Sand wedges in the Bonner and Mt. Shields Formations built out from the south into the northwest Belt basin while down-to-the-north movement continued along the Garnet line, as reflected in the Snowslip and Shepard Formations (Winston, 1986). Down-to-the-south movement along

the Jocko line is also discerned by southern thickening of the Snowslip and Shepard Formations. Extrusion of the Purcell Lavas, the only volcanic rocks in the Belt basin, coincides with the shift in sediment source direction in the Missoula Group. The composition of the Purcell Lavas grades from tholeiitic basalts in the west to alkaline basalts in the east (Hunt, 1964). Schieber (1985) postulated that this compositional change indicates that continental crust thinned westward below the Belt basin. Synchronous with extrusion of the Purcell Lavas onto Missoula Group sediments, diabasic sills and concomitant dikes intruded the Siyeh Formation (Horodyski, 1983). These sills are dated at 1,100 Ma (K-Ar; Hunt, 1964), comparable to dates from the Purcell Lavas of 1,100 Ma (Harrison et al., 1974) and 818-1237 Ma (Burwash, 1984). Emplacement of the Purcell Lavas and associated sills marks a major tectonic event in the Belt basin which resulted in uplift of the southern margin of the basin and changed the sediment source direction for Missoula Group rocks as described earlier. The tectonic pulse at around 1,100 Ma appears to have been coincident throughout the North American craton, as reflected in the Cardenas Lavas of the Grand Canyon Series (1,100 Ma; Lucchitta and Hendricks, 1983); the Keweenawan basalts (1,100 Ma), and the abundance of mafic dikes and igneous complexes (Muskox, Duluth; Windley, 1977).

A transgressive marine influx in the Belt basin may have culminated in deposition of the Garnet Range and Libby Formations (D. Kidder, pers. comm., 1986). The subsequent regression marked the deposition of the Pilcher Quartzite. There is some doubt as to the age of the Pilcher Formation, which may be Cambrian and thus correlative with the Flathead Quartzite (the lowermost Cambrian unit in the northwest U.S.: Nelson and Dobell, 1961; Hall, 1968; Illich and Winston, 1968; Winston, 1973, 1977; Elston, 1984).

Small granitic plutons of Precambrian age intrude Belt sediments at the northwestern edge of the basin (Leech, 1962; Gabrielse and Reesor, 1964; Gabrielse, 1972). These plutons are thought to have been formed during orogeny in the East Kootenay Arc (Figure 1-2), and mark the end of Belt deposition and the onset of Windermere sedimentation (Gabrielse, 1972). Ages of the intrusions have been determined by K-Ar as 675 to 790 Ma and thus are younger than the Belt Supergroup (Leech, 1962).

1.6 Metamorphism of Belt Sediments

Most Belt sediments are unmetamorphosed or have undergone lower greenschist facies metamorphism. Metamorphism in the Belt increases from east to west and with depth in the stratigraphic section. This metamorphic

trend is demonstrated by the transformation of illite to its 2M polymorph (Maxwell and Hower, 1967), oxygen isotope geothermometry on co-existing quartz and illite (Eslinger and Savin, 1973) and by an increase in biotite in the western part of the basin (Harrison, 1972; Hobbs et al., 1965). In the lower Prichard Formation, the garnet isograd is reached in northeastern Idaho. In southern Idaho, upper greenschist and amphibolite facies rocks have been reported (Norwick, 1977; Lang and Rice, 1981; Lang, 1983). These higher metamorphic grades are restricted to the southern edge of the Belt basin which is intruded by plutonic rocks. Plutonism and tectonic activity along this southern margin undoubtedly metamorphosed sediments locally to anomalously high grades.

The carbonate samples collected for this study were either unmetamorphosed or were found to contain muscovite and rarely chlorite (Appendices A and B).

Chapter 2

Stratigraphy, Sedimentology and Depositional Environments of the Belt Basin

The sedimentology, depositional environments, petrography and diagenesis of formations in the Belt Supergroup are discussed below in ascending stratigraphic order. The characteristics of formations sampled in this thesis are summarized in Table 2-1 and the sample locations are summarized in Figure 2-1 and detailed in Appendix A. Formations not sampled for the present project are not described here.

2.1 Prichard Formation

Above and interfingering with Neihart Quartzites (Figure 1-3), deep-water Prichard Formation sediments derived from the south or southeast (Figure 1-4) predominated during initial fill of the Belt basin (Figure 1-3). The Prichard Formation is an overall regressive sequence composed mostly of sands and muds deposited by turbidites plus some shelf carbonates in the northern basin (McMechan, 1981; Cressman, 1982, 1984a; Finch and Baldwin, 1984).

Some sub-wave base calcareous and dolomitic mudstones were sampled from the Prichard Formation for this thesis, but their carbonate content was

Table 2-1 Characteristics of Belt Carbonate Formations Sampled in this Thesis

Formation	Age	Facies	Depositional Environment
Libby	930-1125 Ma	Upper: Hummocky cross-stratified siltite and quartzite with argillite partings Lower: Parallel laminites, oolitic siltites, stromatolites, channel sands	Deep Water, Open Marine; northern basin partly euxinic, southern, mud-flats
Mt. Shields	1050-1110 Ma	4- black to green argillite 3- carbonate and red argillite 2- red to grey quartzite 1- red argillite	4,3-carbonate = shallow water,occasionally emergent mud- flats 2- northern braided stream and southern deltaic complex 1- mud-flats and pro-delta sands
Shepard	1050-1110 Ma	Upper: black argillite, tan dolomite Lower: greenish-black argillite with red and green quartzites	Upper: shallow sub-tidal with occasional subaerial exposure Lower: mud flats and distributary channel sands
Snowslip	1050-1110 Ma	Red and green argillites, scattered cross-bedded quartzites and fine-grained laminated quartzites, carbonates and stromatolites increase up section	shallow water,inter-tidal with sheet and channel sands

Table 2-1 cont.

Formation	Age	Facies	Depositional Environment
Middle-Belt Carbonate	1040-1110 Ma	E- Helena and Siyeh Fms.; cycles of argillite, calcite dolomite and fine-grained sand W- Wallace Fm.; graded siltstone couplets grading up section into carbonate cycles then to sand	Lower: E- mudflats W- deep water turbidites Middle: E- shallow subtidal to intertidal W- subtidal Upper: intertidal to supratidal
Empire	1040-1090 Ma	Carbonate-rich siltites and argillites	Subtidal
Spokane	1075-1270 Ma	Red argillites and calcareous sandstones, local evaporites and oolite-rich horizons	Shallow water seasonally exposed; ephemeral streams
Greyson	1270-1360 Ma	Grey siltite to argillite, increase in fine sand and stromatolites up section	Debris-flow deep water deposits shallowing upward to shallow water deposits
Altyn	1270-1360 Ma	Cycles of doloarenite, dolomicrite, chert and quartzite, abundant stromatolites	Shallow sublittoral to intertidal
Newland	1270-1360 Ma	Cycles of laminated grey to brown siltstone and calcareous and dolomitic mudstone	Sub-wave base

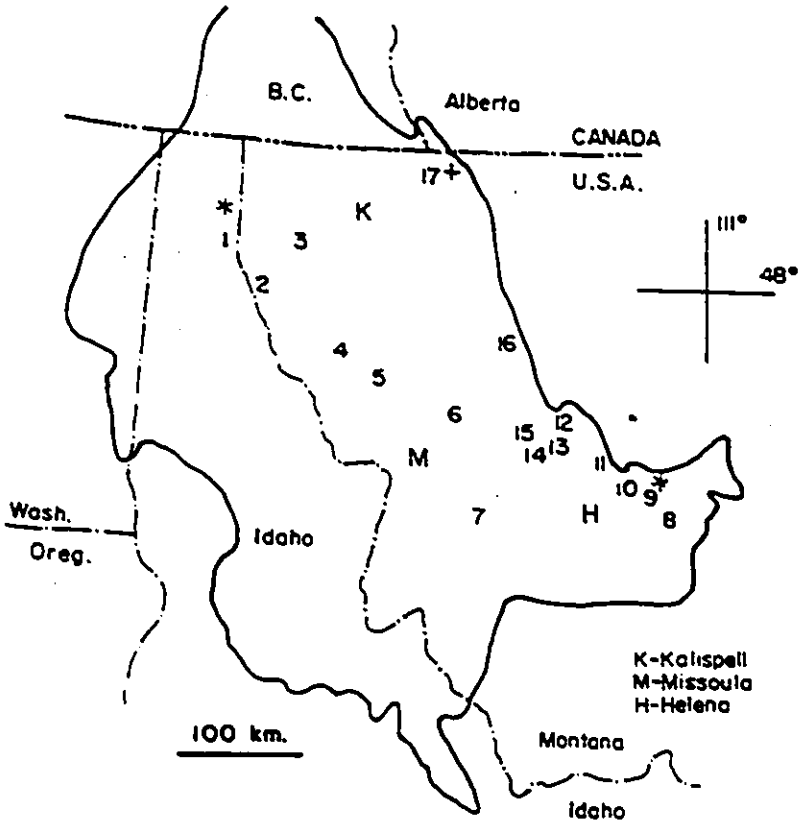

Figure 2-1
Approximate location of samples collected in the Belt basin. See Appendix A for complete descriptions.

1 CF - Clark Fork, Wallace Fm.
2 DF, RR - Delye Fork, Ruen Road, Mt. Shields Fm.
3 7/23/86, 7/25/86, 7/28/85, 7/29/85, FC, FB, FM, MP - Libby area, Shepard, Libby, Mt.Shields, Empire and Prichard Fms.
4 GC - Graves Creek, Wallace Fm.
5 BHP - Big Hole Peak, Wallace Fm.
6 HL - Holland Lake, Helena Fm.
7 PH - Phillipsburg, Helena Fm.
8 NC - Newlan Creek, Newland Fm.
9 DG - Decker Gulch, Newland Fm.
10 SC - Smith Creek, Newland Fm.
11 TC,WC - Trout Creek, Wolf Creek, Spokane/Greyson Fms.
12 DRC - Dearborn River Canyon, Helena Fm.
13 FCR - Falls Creek Ridge, Helena Fm.
14 RP - Rogers Pass, Helena Fm.
15 RM - Red Mountain, Helena Fm.
16 WL - Wood Lake, Helena Fm.
17 SN/LC, GTS/SY, PP/SY, AF/AL, RM/SH - Snowslip, Sieyh, Altyn and Shepard Fms.
* Sampled by Maxwell and Hower (1967)
\+ Sampled by Eslinger and Savin (1973)

too low for geochemical study (Appendices A and C).

2.2 Newland Limestone

A transgression of the Belt sea in the Helena embayment resulted in deposition of the Newland Limestone. It is dominated by 10- to 100-metre thick units of thin bedded to laminated grey to brown siltstones alternating with 10 metre thick carbonate units (Schieber, 1985). Zieg (1981) divided the upper Newland into distinct lithologic units. These are composed of cycles with dolomitic or calcitic microspar at the base, silty calcitic microspar with cross-laminated silt in the middle, and silty shale with cross-laminated silt and microspar nodules at the top. These units may represent intrinsically controlled sedimentary cycles or repetitions generated by episodic faulting during deposition of the sequence. A similar cyclic pattern has been observed in the stratigraphically equivalent Altyn Formation in the north, but not in deep-water sediments of the western Belt basin.

Ripple marks which have been observed in the section mostly indicate an east to west or southeast to northwest current direction. However, Zieg (1981) reported west-trending ripples suggesting a western source for sediments. If so, the Helena embayment may have been isolated

at times from the Belt basin by an eroding upland, the latter a result of down-to-the east movement along the Townsend line (Figure 1-8; Zieg, 1981). According to Zieg (1981) the Newland sequence contains sparce distal debris flows, but lacks shallow-water features. This observation contrasts with the description of flat pebble conglomerates, cross-bedded sands and erosion surfaces at the top of some cycles by Schieber (1985) which he interpreted as shallow-water to emergent features. Field observations do not corroborate the shallow water interpretation for these particular conglomerates.

The Newland Limestone was deposited on a south-dipping ramp of the northern shoreline, now defined by the Volcano Valley Fault (eastern Garnet Line extension; Figure 1-8), as inferred from debris-flow paleocurrent directions and soft-sediment slumping (Godlewski and Zieg, 1984; Schieber, 1985).

The samples of Newland Formation collected for this thesis were mostly calcareous mudstones deposited below effective wavebase (Appendix A, Table 2-2). Alternating clastic and carbonate-rich layers define laminations. Fine-grained dolomite crystals are disseminated in the calcite matrix. Both carbonates show neomorphic crystal textures. The samples contain traces of chlorite and muscovite.

2.3 Altyn Limestone

The Altyn Limestone is considered to be the northern

Table 2-2 Summary of Petrographic Analyses of Belt Carbonates

		Classification							Diagenetic Textures											
Formation	#	M	IM	OM	S	IS	OS	BL	P	MT	CC	AN	V	D	DR	DD	SI	ST	M	C
Libby	1						1							1			1	1	1	
Mt.Shields	4				2	1		1	3			2		4	2				3	
Shepard	7	3	3			1			1	1		1	1	5	1				4	
Snowslip	4	1	2					1	3		2			3	3	1			2	1
MBC	36	25	10	1					2	5	1	5	11	30	11	1		6	17	1
Empire	2	2										1		2					1	
Greyson/ Spokane	3	1	2						2	2			1	1	1	1		2	2	1
Altyn	2			1		1			1					2	2		1		1	
Newland	3	1	1			1							2	1				1	1	2

- Number of Thin Sections

M - micrite; IM - intramicrite; OM - oomicrite; S - sparite; IS - intrasparite
OS - oosparite; Bl - biolithite (Folk, 1962); micrite = < 0.005 mm; microspar = 0.005-0.02 mm; sparite = > 0.02 mm

P - contains primary cement; MT - molar tooth; CC - calcite replacing siliciclastics; AN - aggrading neomorphism; V - calcite veinlets; D - dolomitization; DR - dolomite rhombs; DD - dedolomitization; SI - silicification; ST - stylolites; M - muscovite; C - chlorite.

platform equivalent of the Prichard Formation (Figure 1-3; Winston, 1986). This formation represents the oldest unit in the northeast section of the Belt basin (White, 1977) and records an overall regression in the basin, grading upward and westward in o the Appekunny Argillite (Horodyski, 1983; Connor et al., 1984; Fermor and Price, 1984).

The Altyn Limestone is a 140- to 300-metre-thick unit of peritidal doloarenites, dololutites, cherts, quartzites and litharenites (White, 1977). It is commonly cyclic, with an undulatory to erosional base several centimetres thick which is overlain by low-angle to planar cross-stratified sandy doloarenite containing rare dolostone intraclasts. The uppermost unit in the Altyn cycles is a thinly bedded, wavy, rippled sandy doloarenite interbedded with silty dololutite (Horodyski, 1983). These cycles are several metres thick and fine and thin upward. Stromatolites are common, particularly in the lower cyclic units (Horodyski, 1983).

The Altyn is believed to have been deposited in a nearshore environment. This is based on primary sedimentary structures such as mud cracks, algal mats and columnar stromatolites, bimodal current indicators, intraformational breccias and tidal channels (White, 1977). Horodyski (1983) interpreted the cycles in the Altyn to have been created by tidal channels migrating over a tidal flat. Alternatively, these cycles could represent progradational shallow subtidal

to intertidal deposits. Dolomite in the formation is interpreted to have been formed in a hypersaline environment as evidenced by collapse breccias and evaporite pseudomorphs, including length-slow chalcedony which is presumably diagnostic of evaporites (Folk and Pittman, 1971; White, 1977).

Samples of oosparites, sparites and stromatolites of the dolomitic intertidal facies of the Altyn Formation were collected (Appendices A and B, Table 2-2). Dolomite is predominantly spar-sized, with stromatolitic laminae defined by alternating dolosparite and dolomicrite layers. Sparry dolomite cross-cuts silica clasts in the more clastic portions of the rock. Some ooids show radial textures (Figure 2-2), others have been recrystallized with only concentric laminae remaining, and some are silicified (Figure 2-3). Igneous and metamorphic rock fragments (Figure 2-2), monocrystalline quartz and chert constitute 1% of these samples. White (1977) interpreted these clasts as evidence for the proximity of a Hudsonian basement. Primary cement textures (isopachous rims, blocky cement dominated by enfacial junctions, etc.) are visible in one sample. Minor muscovite is present in one sample; in another, an igneous rock fragment has been chloritized.

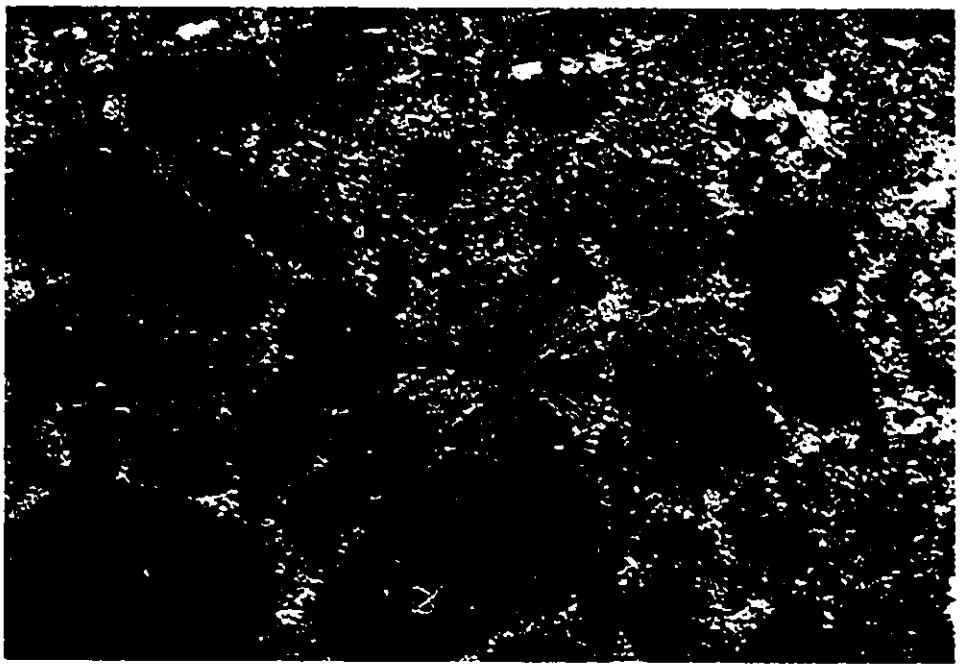

Figure 2-2
Thin section view of recrystallized dolomitic ooids from Altyn Formation sample AF/AL-3, an oodolosparite, or grainstone (Appendix B). Crossed polars, scale bar is 1 mm.

Figure 2-3
Thin section view of silicified ooids in a dolosparite matrix. Altyn Formation, sample number AF/AL-3, an oodolosparite, or grainstone (Appendix B). Dolomite postdates silicification and is found in the interior of some ooids. Crossed polars, scale bar is 1 mm.

2.4 Ravalli Group

According to established stratigraphic nomenclature the western Ravalli Group includes the Burke, Revett and St. Regis Formations; the north eastern Appekunny, Grinnell and Empire Formations; and the eastern Greyson, Spokane and Empire Formations. Only the St. Regis, Grinnell and Spokane Formations are correlative across the Belt basin. Discontinuous exposures in the lower Ravalli Group obscure other stratigraphic relationships. The two members of the Ravalli Group which were sampled for this thesis are the Greyson and Empire Formations, described below.

2.4.1 Greyson Formation

Deep-water argillites and siltstones were dominantly deposited by debris flows from basin margins during early Greyson time (Connor et al., 1984). Siltstones of the upper Greyson record shallow water sedimentation and regression of the Belt sea in the Helena embayment (Nelson, 1963). This regression culminated in the deposition of a basin-wide redbed marker, comprising the St. Regis, Grinnell and Spokane Formations.

The Greyson Formation was sampled at the Spokane/Greyson transition in the eastern Belt basin (Figure 2-1; Appendix A). The carbonates in this transition zone are intertidal calcitic micrites and intramicrites with up to 10% disseminated

monocrystalline quartz and feldspar clasts (Table 2-2, Appendix B). Albite crystals, reportedly pseudomorphs after halite and gypsum (Lange et al., 1987), and blocky calcite fill birdseye vugs (Figure 2-4). Calcite crystals show neomorphic textures. Disseminated dolomite, where present, is mostly micritic, generally shows the same neomorphic textures as calcite, and occasionally has a rhombic outline (Figure 2-5). Chlorite is locally abundant, and trace muscovite is pervasive. Molar-tooth structures, described later, are filled with clastics and calcite.

2.4.2 Empire Formation

Laminated calcareous and dolomitic siltites and argillites of the Empire Formation were deposited in subtidal environments in the Helena embayment during a period of subsidence and basinwide transgression which continued during deposition of the overlying Middle Belt Carbonate (Connor et al., 1984; Winston, 1986).

Two samples were collected from the Empire Formation in the western Belt basin (Figure 2-1). These samples were collected from below wave-base facies and are parallel laminated dolomicrites (Table 2-2; Appendices A and B). The dolomite has uniformly sized crystals, is fine-grained and has indistinct crystal boundaries. Some patchy aggrading neomorphism has produced coarser grained sparry dolomite.

Figure 2-4
Thin section view of albite pseudomorphs after gypsum which, with blocky calcite, fills birdseye vugs in a micrite matrix: Spokane/Greyson transition sample WC-3, an intramicrite or wackestone (Appendix B). Crossed polars, scale bar is 0.5 mm.

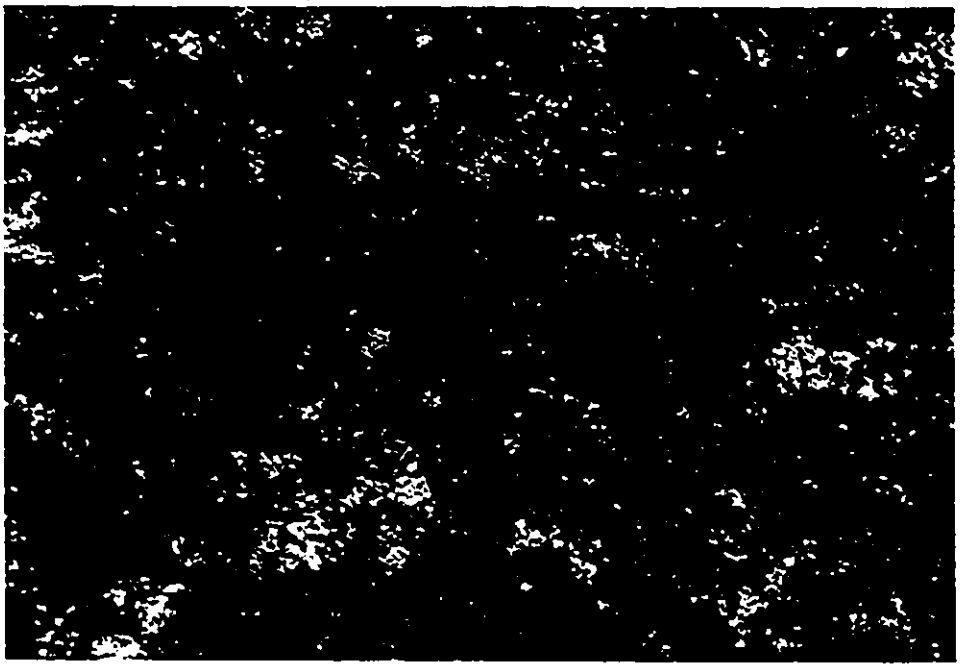

Figure 2-5
Thin section view of Spokane/Greyson sample TC-1, a dolomitic and calcitic intrasparite/wackestone . Alizarin Red-S has stained the calcite red while dolomite and siliciclastics are unaffected. Note dolomite rhombs, indicated by arrows, which are undergoing dedolomitization. Scale bar is 0.25 mm.

2.5 Middle Belt Carbonate

The Middle Belt Carbonate is divided into a western and an eastern facies. The western Wallace Formation, divided by Grotzinger (1981) into three members, correlates in the east with the Helena (and its northern equivalent the Siyeh Limestone), Snowslip and Shepard Formations. The last two are traditionally included in the overlying Missoula Group, and such assignment will be followed in this thesis. Deposition of the Middle Belt Carbonate was initiated by a transgressive cycle which began during upper Ravalli time, followed by a regression during uppermost Middle Belt Carbonate time (Winston, 1986).

The lowermost unit of the Wallace is a 1,200-metre-thick succession of parallel and wavy laminated laterally continuous (0.3 to 3 cm. thick) graded couplets of dolomitic argillite (Harrison, 1984; Winston, 1986) with calcite ribbons and pods, stromatolites and quartzites (Harrison, 1984). Additional features include ripple marked fine sand and silt, mud-cracked muddy layers, ooid packstones and intraclast breccias (Harrison, 1984).

The middle Wallace is defined as thin (0.3 to 3 cm) graded couplets of fine sand to clay (Harrison, 1984). The terrigenous middle Wallace grades eastward into the thinner - bedded and more calcareous Helena Formation. Large slump folds and breccias are found in the middle Wallace Formation south

of the Lewis and Clark Lineament (Wallace et al., 1976; Godlewski, 1977). These breccias probably represent slope deposits formed adjacent to the contemporaneously active Lewis and Clark Line.

Beds of the upper Wallace Formation increase in thickness up section, but maintain the general depositional character of graded couplets described earlier. The sequence is marked by microlaminated (less than 1 cm) silt and clay grading eastward into the lower Snowslip Formation (Figure 1-3). Stromatolitic dolomite underlies the laminated siltstone (Harrison, 1984). Near the Canadian border, the upper Wallace is missing and the red and green siltites of the Snowslip Formation rest directly on the middle member of the Wallace Formation.

The Helena is divided into a western and an eastern facies, with the paleoshoreline at the eastern edge of the Helena embayment. The thickness of stratigraphic sections increases from 180 metres in the east to 1480 metres in the west. In the west, the formation was deposited in cycles supposedly recording basinwide transgressive/regressive events (Eby, 1977). The cycles are more calcareous proximal to the eastern shelf, and more terrigenous westward towards the centre of the basin.

The Siyeh is composed of (a) muddy and sandy dolostone, dolomitic limestone and limestone, (b) dolomitic and calcitic argillite, calcitic argillite, and sandy argillite, and (c)

calcitic sandstone (Horodyski, 1983). The presence of mud-cracks in the lower part of the Siyeh Fm. suggests an intertidal to supratidal environment. Throughout most of the formation, a shallow sub-tidal environment probably prevailed. The upper Siyeh Fm. (the top 175 m) was deposited in an environment with strong tidal influences, as is evidenced by herringbone cross-stratification, reactivation surfaces, and flaser, wavy, and lenticular bedding (Horodyski, 1983).

Cyclic sediments (dark grey mudstone and dolomitic mudstone overlain by impure dolostone) have been interpreted as transgressive mudstones overlain by regressive dolostones (Horodyski, 1983). Stromatolites are abundant throughout the Siyeh Fm., and Baicalia/Conophyton cycles have been reported near the top of the succession by Horodyski (1983). An equivalent Conophyton zone can be seen in the Dearborn River Canyon section of the Helena Fm. (Figure 2-1, Appendix A) and represents a prominent marker unit in the eastern Belt basin.

Overall, the lower Middle Belt Carbonate formations represent a series of periodically exposed mud-flats which were gradually submerged during a basinwide transgression. Deep-water and shelf-facies carbonate sediments were deposited in the east (Helena Fm.) and terrigenous sediments from a westward source filled the western Belt basin (Wallace Fm.). The terrigenous sediments of the Wallace Formation were likely deposited by turbidity flows which were generated along

the south and west basin margin (Winston, 1986). A basinwide transgression continued during deposition of the Middle Belt Carbonate and is reflected both in deep water and shelf facies carbonate deposits of the upper Middle Belt Carbonate. The upper Middle Belt Carbonate is typified by shoaling-upward carbonate cycles, reflecting evaporitic peritidal environments on the eastern edge of the Helena embayment and a deeper water carbonate shelf within the embayment (O'Connor, 1972; Eby, 1977; Grotzinger, 1986). Alternatively, the cycles represent events along the basin margins (Horodyski, 1983). If the Belt basin were an epicratonic reentrant, the cycles may reflect 3rd or 4th order changes in the eustatic sea level. If the Belt basin were to represent an intracratonic basin, these cycles may record periodic climatic changes. An intriguing possibility is that these cycles might be related to a lithospheric flexure, with concomitant loading and subsidence of the lithosphere underlying the Belt basin (cf. Cisne, 1985). However, the time resolution is so poor that such a link is difficult, if not impossible, to prove.

Evaporite pseudomorphs (halite, gypsum and shortite) are reported throughout the Middle Belt Carbonate (Eby, 1977; Grotzinger, 1981; Horodyski, 1983; Harrison, 1984). Other indicators of hypersalinity, as reported by Eby (1977), are synsedimentary breakage and deformation of ooids, molar-tooth carbonates, reduced stromatolite diversity and local collapse

breccias. Further evidence for high salinity in the Middle Belt Carbonate is the recognition of chlorine-rich scapolite in metamorphosed portions of the Wallace Formation in Idaho (Hietanen, 1963).

Carbonates of the Middle Belt Carbonate were collected in the centre (Figure 2-1; RP, WL, DRC, RM, BHP, HL, and PH), along the western (Figure 2-1; 7/28/85 series, CF) and eastern edges (Figure 2-1; FCR, GTS/SY, PP/SY) of the Belt basin. The samples from the centre and western edge were dominantly deposited below wave base and are micritic. Samples from the eastern margin were deposited in higher energy environments reflecting their proximity to the paleoshoreline. These samples are also dominantly micritic, but more are intramicrites, oomicrites and biolithites (stromatolites; Appendix B). Carbonate cycles were sampled in the western (7/28/85-4 to 6) and the central Belt basin (BHP-9 to 18). Sampling was systematic throughout the Middle Belt Carbonate. To ensure that geochemical signatures of the Belt sea water were untainted by samples containing clasts derived from outside the Belt basin, and to exclude possible vital effects of organisms (algae, bacteria), mudstones were dominantly sampled. Along its eastern and western margin the Middle Belt Carbonate is more dolomitic than in the basin centre. Limestones and dolostones are dominantly fine-grained and can be concentrated in layers or disseminated throughout the

samples. Siliciclastics in thinly laminated samples are concentrated along laminae, whereas in thick bedded samples the clasts are dispersed evenly throughout the carbonate matrix. Dolomite rhombs are usually restricted to the coarser grained and more clastic rich portions of the rocks and constitute a minor percentage of the dolostone. Carbonates uniformly show diagenetic textures, such as wavy indistinct crystal boundaries, diffuse crystal contacts, uniform grain size, and few enfacial junctions (Bathurst, 1975). Aggrading neomorphic textures are common as are crosscutting calcite and dolomite veinlets. Some clastic-rich samples have muscovite, and one has chlorite, cross-cutting previous diagenetic textures. Only the sections WL, DRC and RP have no muscovite, whereas the Clark Fork section (CF) at the western basin edge has the strongest metamorphic overprint.

Molar tooth textures are present in many Belt carbonates and ubiquitous in the Middle Belt ones, particularly at the tops of cyclic depositional units. Molar tooth structures have been discussed at length by other authors, especially Eby (1977), and will not be addressed in detail here. These textures are uniformly sized, fine-grained, convolute layers and lenses of carbonate which occur in carbonate units of similar grain size (Figure 2-6). Typical molar tooth structures are calcite, whereas the wall rock is dolomite (Figure 2-7). Molar tooth structures commonly contain siliciclastic clasts (Figure 2-

Figure 2-6
Molar tooth carbonate "veins" at the top of a depositional cycle from Rogers Pass (RP) (Figure 2-1). Molar tooth structures weather grey in contrast to the brown weathering of the bulk of the carbonate. The scale is approximately 15 cm long.

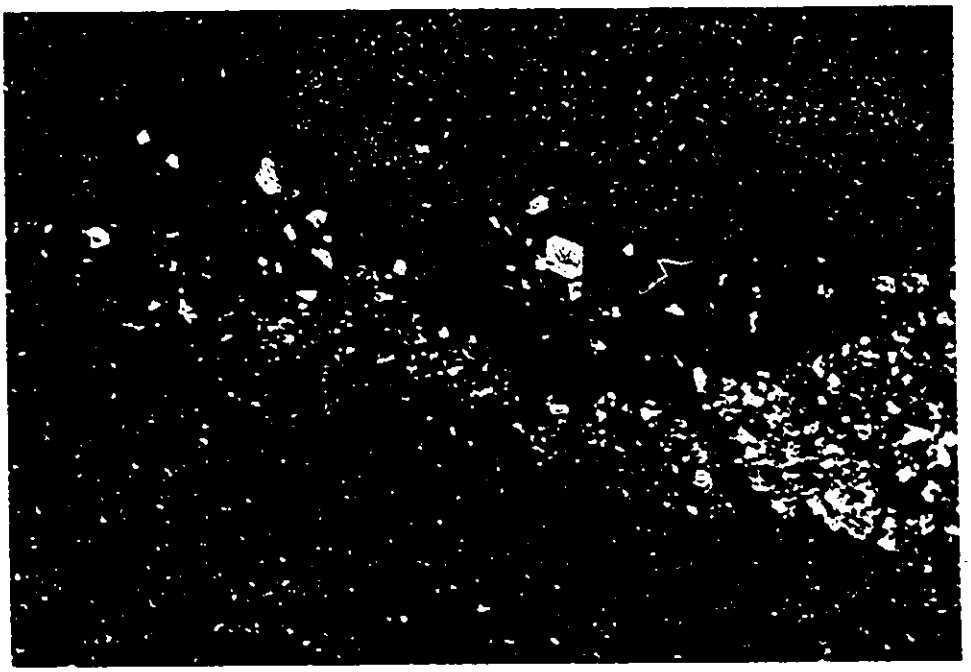

Figure 2-7
Thin section of the contact of a molar tooth carbonate "vein" (filled with micrite) with dolomicrite. Alizarin Red-S has stained the calcite red while not affecting dolomite. Sample number BHP-9, micrite or mudstone (Appendix B). Crossed polars, scale bar is 1 mm.

7) and are postulated to be fluidization textures which formed early in the diagenetic history of the rock (Eby, 1977; Horodyski, pers. comm., 1985).

2.6 Missoula Group

Missoula Group sediments crop out for the most pare in the western Belt basin, and are divisible into three units (Wallace et al., 1984). The lower Missoula Group includes the Snowslip and Shepard Formations, the middle the Mt. Shields Formation, Bonner Quartzite and laterally equivalent Striped Peak Formation, and the upper Missoula Group includes the McNamara and Garnet Range Formations plus the laterally equivalent Libby Formation (Figure 1-3). During deposition of the Missoula Group, the principal sediment source in the western basin changed from west to south, and sediments were deposited in fans which transgressed over lower Belt sediments in a northwesterly direction, interfingering with shallow water terrigeneous and carbonate muds (Figure 1-5; Winston, 1986). From the Missoula Group the Snowslip, Shepard, Mt.Shields and Libby Formations were sampled for this study.

2.6.1 Snowslip and Shepard Formations

The Snowslip and Shepard Formations are predominantly redbed sequences, with more abundant redbeds in the east and south and green-beds in the north and west (Wallace et al.,

1984). The Snowslip red-beds (argillites) are thought to have been deposited in mudflats, and scattered quartzites of the Snowslip were deposited as sheet sands and distributary channel sands (Wallace et al., 1984). Green argillites of the Snowslip Formation and black argillites, red and green quartzites and dolostones of the Shepard Formation represent deposition in shallow water, with rare subaerial exposure (Horodyski, 1983; Wallace et al., 1984).

The Snowslip Formation was sampled in the northern Belt basin (Figure 2-1) where it is dominated by micritic limestone deposited in supratidal, subtidal, intertidal and sublittoral environments (Appendix A). Of the samples studied petrographically, two are stromatolitic, one is oolitic and the remainder, depending on the percentage of siliciclastic clasts, are wackestones or mudstones (Appendix B; Table 2-2). Visible siliciclastics are composed of mono- and polycrystalline quartz and chert and make up 10 to 40 % of the rock. Some monocrystalline quartz fragments have overgrowths, indicating that they are polycyclic grains. Calcite crystals in the Snowslip range from < 0.005 to 0.05 mm, are equant with indistinct crystal boundaries, and are arranged in thin laminae (< 0.3 cm) alternating with quartz and feldspar clasts (Appendix B). Coarse-grained calcite (0.4 mm) replaces quartz and feldspar in the more siliciclastic rich sections of one sample, but is volumetrically minor. Dolomite is rhombic, with

crystals ranging from 0.005 to 0.5 mm. Dolomite rhombs cross-cut both calcite and siliciclastics in some samples. Dolomite also shows textures indicating recrystallization to neomorphic spar or 1:1 replacement of calcite which was undergoing aggrading neomorphism. Trace muscovite occure in some samples, and chlorite makes up 4% of one sample.

The Shepard Formation sampled in the northern Belt basin is dolostone and in the western basin it is dolostone and dolomitic limestone mirroring the distribution of dolostone on the basin edges noted earlier in the Middle Belt Carbonate. Shepard Formation samples are roughly 50 % soluble (Appendix C); the insoluble residue is quartz and feldspar which is mostly monocrystalline and sometimes strained (Appendix B). Dolomite crystals in the Shepard are usually less than 0.0025 mm, with wavy and indistinct boundaries. Graded bedding occasionally occurs within dolomite laminations. Dolomite occurs in the coarser grained sections of the rock and embay quartz. Micritic dolomite is recrystallized to neomorphic sparite in patches in some samples. Glauconite intraclasts are recorded from one thin section (DRC-SI-345; Figure 2-8). Although glauconite as a rule indicates marine conditions, it is also reported from non marine environments (McRae, 1972). Trace opaques are disseminated throughout Shepard samples as is muscovite (Appendix B; Table 2-2).

Figure 2-8
Thin section view of Shepard Fm. sample DRC-SI-345 through crossed polars. Glauconite, quartz and feldspar intraclasts in micrite form a matrix in this intrasparite/packstone (Appendix B). Alizarin Red-S has stained calcite red, scale bar is 0.5 mm.

2.6.2 Mt. Shields Formation

The Mt.Shields Formation is composed of red and green occasionally calcareous argillites, fine- to medium-grained feldspathic quartzite, and some stromatolitic carbonates in the northern basin (Wallace et al., 1984).

The Mt.Shields Formation represents deposition as mud-flats with some prodeltaic sheet sands. Quartzites and siltites represent braided stream channel, delta channel, delta plain and delta front deposits which were deposited in the southern Belt basin. These deltas grade northward into pro-delta sheet sands and mud flats of the upper Striped Peak Formation (Figure 1-3; Wallace et al., 1984). The Mt. Shields stromatolite-bearing units and green argillites were deposited in shallow water with occasional subaerial exposure.

The Mt. Shields carbonate units, which were sampled in the western Belt basin (Figure 2-1), are dominantly thinly bedded to thickly laminated (0.3-10.0 cm). The samples are parallel laminated, dolomitic and occasionally stromatolitic (Appendix A). Because sampled carbonates show few primary sedimentary structures, a deep-water depositional environment has been assumed (Appendix A). Regional geologic considerations place these rocks in shallow but quiet water below effective wave base, with the exception of sample 7/29/85-5, which has rippled crossbeds implying deposition above wavebase. Mono and polycrystalline quartz fragments, chert and metamorphic rock

fragments compose < 5% of the total volume of the samples studied petrographically (Table 2-2). Solubility of the Mt. Shields Formation is high, mostly 70 to 80 % (Appendix C). Dolomite in the Mt. Shields is fine grained, dominantly < 0.0025 to 0.025 mm and shows patchy recrystallization (aggrading neomorphism) to sparry dolomite (up to 0.05 mm). Some dolomite rhombs are present in the coarser grained sections of the rock, but most of the dolomite has wavy and indistinct crystal boundaries. Up to 1% muscovite occurs in most of Mt. Shields Formation samples.

2.6.3 Libby Formation

The Libby Formation was deposited in a partly euxinic shallow basin with a southeast sediment source (Wallace et al., 1984; Kidder, 1985). Its lower part is composed of parallel laminated dark grey and greenish grey argillites and siltites which are overlain by stromatolitic and oolitic siltites. Southward the lower Libby Fm. consists of channel sands interbedded with mud-cracked argillites and siltites (Kidder, 1985). The upper Libby is composed of metre-thick beds of hummocky cross-stratified coarse grained siltite, which is interpreted to have been deposited by storms in a marine environment, and fine-grained quartzite with thin argillaceous partings (Kidder, 1985). It is overlain by structureless, crudely laminated, greenish-grey silty

argillite. The transition from the lower to the upper Libby Fm. may have been caused by a major change in the character of the Belt basin, specifically the transition to more open marine conditions compared to partly to wholly restricted marine or fresh water conditions which may have existed throughout much of the Belt 'time' (Kidder, pers. com., 1986).

Samples collected from the Libby Formation in the western Belt (Figure 2-1) are dominantly micritic, with shallow water features such as oolites and some cross-bedding (Appendix A). Stromatolites are common in these sections. The depositional environment of the Libby samples was intertidal to subtidal, with stromatolites indicating that many carbonates were formed in relatively shallow water, at least in the photic zone. Intraclasts of chert and monocrystalline quartz are common in these samples. Some ooids are relatively unaltered, retaining their original radial textures (Figure 2-9), but most have been recrystallized and replaced by silica and sparry calcite (Figure 2-10).

2.7 Diagenetic Sequence of Belt Carbonates

Table 2-2 summarises the diagenetic features observed in those carbonates studied petrographically, and Table 2-3 outlines their diagenetic sequence. The latter is derived from direct observations, but not all features are present in any

Table 2-3 Generalized Diagenetic Sequence for Carbonates of the Belt Supergroup

Deposition	Progressive Diagenesis
micritic calcite	
micritic dolomite	
	molar tooth
	aggraging neomorphism
	sulfide
	gypsum & halite
	silicification
	albitization
	blocky calcite
	rhombic dolomite
	dissolution of dolomite
	calcite replacement
	compaction
	calcite veins

Figure 2-9
Thin section view of Libby Fm. sample 7/29/35-4 through crossed polars. Relatively unaltered oolid in a sparite matrix shows original radial textures. Both oolid and matrix are calcite. Scale bar is 0.5 mm.

Figure 2-10
Thin section view of Libby Fm. sample 7/29/85-4 under crossed polars. Recrystallized and silicified ooid in a sparry calcite matrix. The sparry calcite matrix is replacing the silicified ooid as evidenced by the embayment of the calcite into the ooid. Some dolomite rhombs cross-cut the silicified portion of the ooid. Scale bar is 5 mm.

one thin section. The timing of the events is therefore relative. Micritic calcite, dolomite and intraclasts of both siliciclastics and carbonates represent depositional phenomena and are commonly interlaminated. Aggrading neomorphism recrystallized this micrite to microspar and sparite, often in a patchy or porphyroid fashion. Molar tooth (fluidization) structures transect the rock after lithification, but before compaction. These molar tooth structures are filled with blocky calcite cement, indicating another phase of calcite cementation or a replacement of a metastable mineral phase which originally filled the molar tooth structure. Diagenetic opaque minerals, chalcopyrite, pyrrhotite and pyrite, as well as halite and gypsum formed locally. The halite and gypsum is occasionally replaced by albite and silica. Locally, ooids were silicified at about the same time. Blocky calcite cement fills the vugs which previously were partially filled with now-replaced evaporites, and may correspond to the same phase of blocky calcite cement that fills molar tooth structures. Dolomite rhombs crystallized during the next phase of diagenesis. These rhombs were subsequently etched and occasionally replaced by calcite. Calcite partially replaced silicates at a similar time in the sequence. When iron rich carbonate is present, its Fe content increases in the later stage calcites and dolomites (Figures 2-11, 2-12). Occasionally crystals show zonation with iron-poor centres

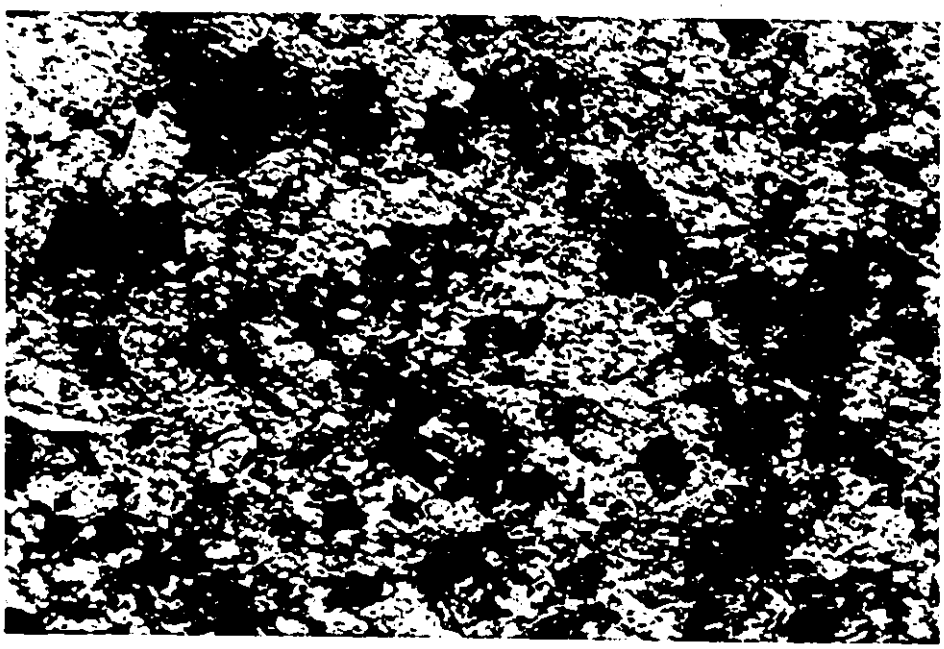

Figure 2-11
Dolomite rhombs showing increasing iron content (marked by blue stain) in crystal rims. The rhombic dolomite is more iron rich than earlier phase dolomite which it is cross-cutting. Thin section of sample Sh/Lc-8, uncrossed polars, and stained with Alizarin Red-S and Potassium Ferricyanide. The scale bar is 25 μm.

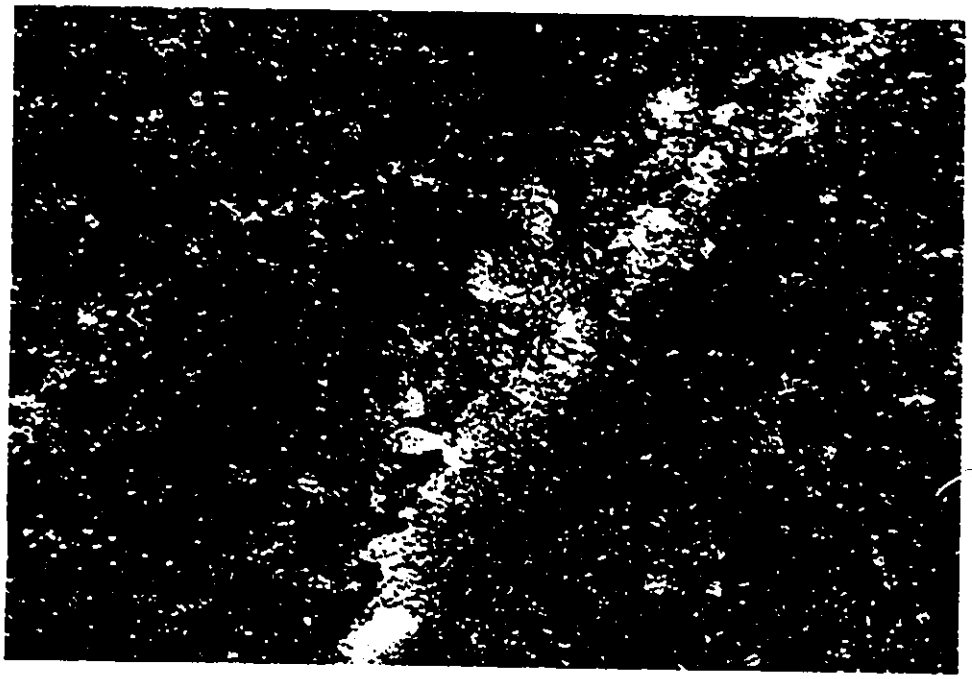

Figure 2-12
Late stage calcite veins show iron enrichment as indicated by purple staining. The scale bar is 1 mm. Thin section of sample RP-5, viewed under uncrossed polars, and stained with Alizarin Red-S and Potassium Ferricyanide.

grading outward into iron-rich rims (Figure 2-11). Compaction of the rocks produced stylolites, as defined by Fe-oxides, siliciclastics, carbonaceous matter, and by sutured siliciclastic grains. After stylolite formation, brittle fracture has produced iron-poor calcite veins which are typically oriented parallel and perpendicular to bedding. Minor muscovite transects rock fabrics, and traces of chlorite has replaced mafic minerals in rock fragments.

2.8 Dolomitization of the Belt Supergroup

Most carbonate units in the Belt Supergroup are dolomitized to some extent; the Altyn, Empire and Mt. Shields Formations, where collected, show pervasive dolomitization. Dolomite in the Belt carbonates is dominantly micritic (<.0025 to .01 mm; Figure 2-13) and commonly shows primary depositional structures, including interlamination with calcite (Figure 2-14), and neomorphic textures (Figure 2-13). Rhombs of dolomite are found in the more siliciclastic-rich, coarser grained sections of these formations (Figure 2-15). The Altyn Formation is a dolosparite, with dolomitization destroying some primary rock textures (Figure 2-3).

The predominance of micritic dolostones with a high Sr content (>100 ppm) throughout the Belt Supergroup may indicate that the most important mode of dolomitization involved the

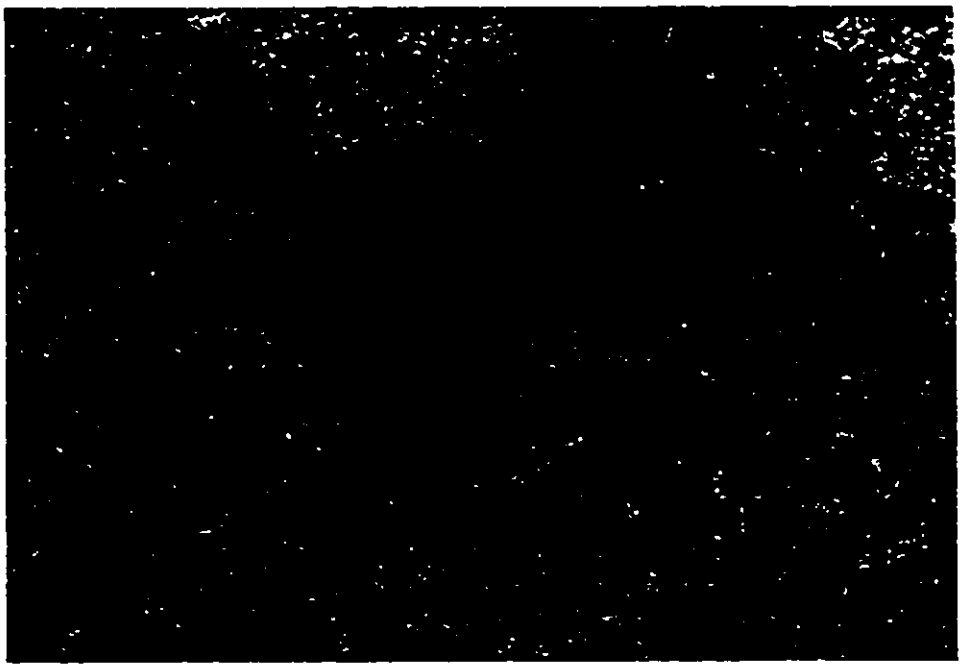

Figure 2-13
Thin section view of Empire Formation sample 7/28/85-13 under uncrossed polars. The carbonate in this thin section is 100% dolomite, as determined by staining with Alizarin Red-S. Dominantly micritic, patches of sparite are formed by aggrading neomorphism of the dolomicrite. Scale bar is 1 mm.

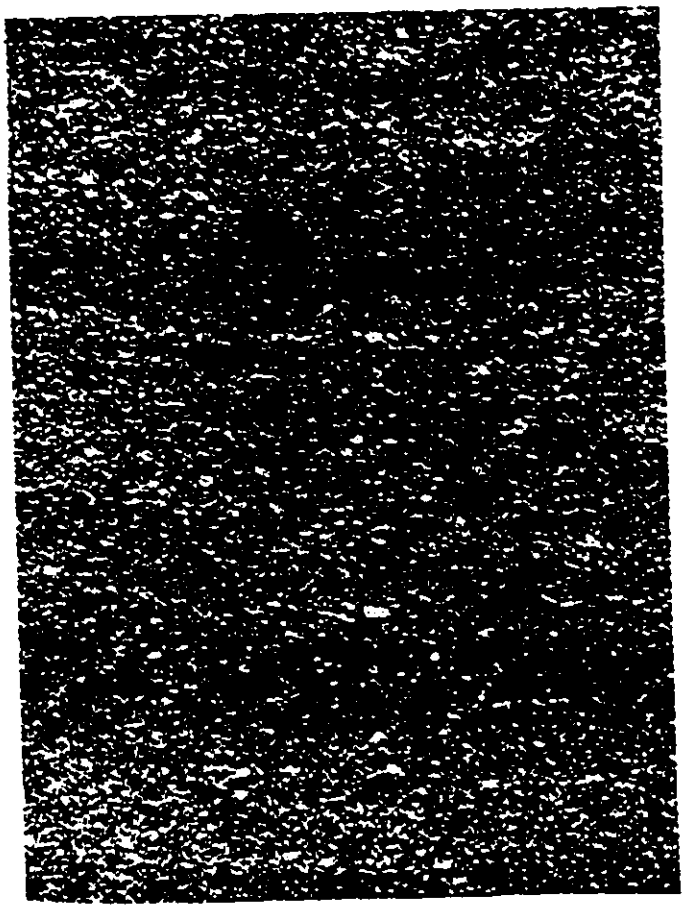

Figure 2-14
Thin section view of Siyeh Formation sample GTS/SY-14. Alizarin Red-S has stained calcite pink. Dolomite and calcite is commonly interlaminated with sharp contacts between laminations. Scale bar is 1 mm.

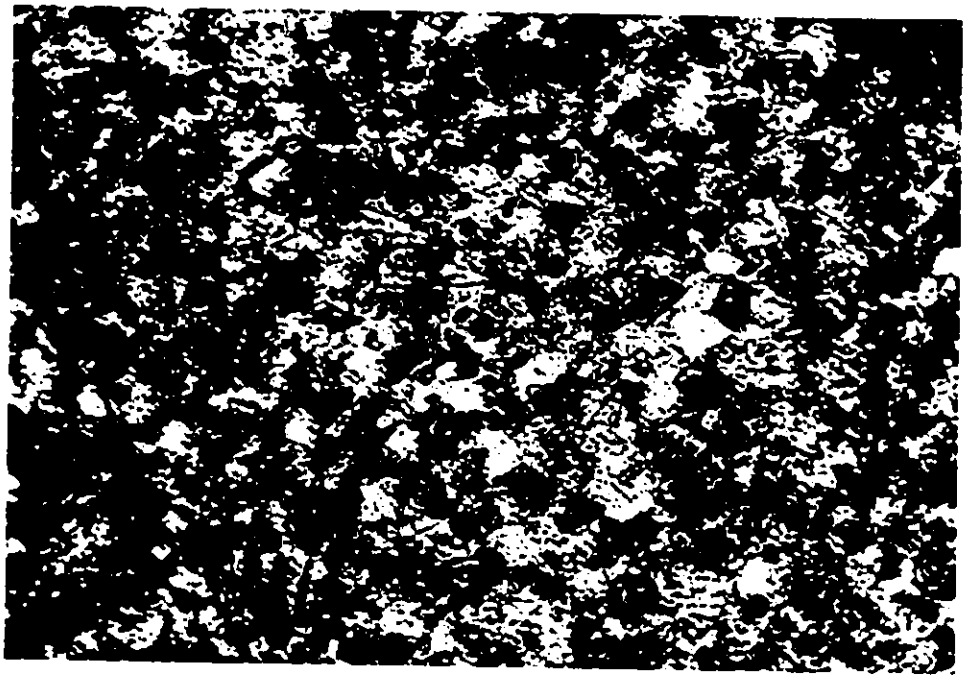

Figure 2-15
Thin section view of Newland Formation sample NC-2. Larger dolomite crystals are commonly found in coarser grained, more siliciclastic-rich sections. Calcite is stained pink by Alizarin Red-S. Both rhombic (low temperature) and xenotopic (high temperature) dolomite (Bathurst, 1986) is present, forming between cross-cutting silicate grains. Scale bar is 0.5 mm.

percolation of hypersaline brines through carbonate sediments (King, 1947; Adams and Rhodes, 1960; Illing et al., 1965; Veizer and Demovic, 1974; Veizer et al., 1978; Land, 1986). Evaporites, commonly associated with this mode of dolomitization, are mostly lacking in Belt sediments, except occasionally as pseudomorphs, but may have been seasonally dissolved (cf. Muir et al., 1980). In contrast, the Mt. Shields and Altyn Formation dolostones contain low Sr (≈40 ppm), are dominantly sparry with poor textural preservation, and may have been formed in a mixed-water zone following the Dorag model of dolomitization (Hanshaw et al., 1971; Badiozamani, 1973; Veizer and Demovic, 1974; Veizer et al., 1978).

Chapter 3

Trace Elements, Carbon and Oxygen Isotopes in Carbonate Sediments

Carbonates are chemical sediments and when they precipitate from ambient water they incorporate Sr, C, O and other elements into the carbonate lattice and between lattice sites. Aragonite, high Mg-calcite ($CaCO_3$ with 12 - 17 mole % $MgCO_3$) and low Mg-calcite ($CaCO_3$ with < 4 mole % $MgCO_3$) are in equilibrium with ocean waters (Bathurst, 1975), with calcite containing 4 - 12 mole % $MgCO_3$ rarely found in nature. Only high Mg-calcite and aragonite have been observed to be precipitating from shallow tropical ocean water (James and Choquette, 1984).

Carbonates precipitated from surface waters usually undergo subsequent mineralogical and chemical diagenetic stabilization and may even eventually be converted to dolomite. The conversion of aragonite to calcite (dLMC) at normal diagenetic temperatures of less than 150^0 C can proceed at a geologically reasonable rate only through a water medium which effectively reduces the activation energy that must be overcome for the reaction to proceed (Bathurst, 1975). Calcites with a high Mg content will dissolve more readily than those with low Mg because their crystal lattice becomes distorted as more Mg is absorbed into the lattice (James and

Choquette, 1984).

Neomorphism of carbonates is internally driven by the different saturation limits of aragonite, high Mg-calcite and low Mg-calcite as well as the force of crystallization of the stable mineral phases (Malvia and Siever, 1988). Deep sea carbonates do not seem to undergo neomorphism after 30 Ma or 300 m depth of burial (Baker et al., 1982), although some deep sea carbonates show continually decreasing Sr content, indicative of ongoing neomorphism, for 100 ± 20 Ma (cf. Manghnani et al., 1980).

Because kinetic factors inhibit primary precipitation of dolomite from ocean water of normal salinity and temperature, most dolomite is presumed to be diagenetic in origin (Lippman, 1973; Baker and Kastner, 1981; Machel and Mountjoy, 1986). Table 3-1 illustrates several alternative chemical pathways whereby calcite or aragonite can be converted to dolomite. Increases in time, temperature, Mg/Ca ratio, CO_3^{-2} activity, or reduction in SO_4^{-2} activity of seawater will favour the precipitation of dolomite (King, 1947; Adams and Rhodes, 1960; Illing et al., 1965; Lippman, 1973; Folk and Land, 1975; Muir et al., 1980; Morrow, 1982; Carballo and Land, 1984; Saller, 1984; Baker and Burns, 1985; Mullins et al., 1986).

3.1 Trace element distribution in carbonates

Trace elements are incorporated into carbonates as : 1) minor elements absorbed onto crystal surfaces during the

Table 3-1 Some Stoichiometric Formulas for the Transformation of Calcite or Aragonite to Dolomite and the Characteristics of These Reactions

Formula	Volume Change	ΔG^0_r *	Comments
$2\ CaCO_3 + Mg^{+2} = CaMg(CO_3) + Ca^{+2}$ [2]	loss of 6-13%	A-D: -1.83 C-D: -1.38	External source for Mg Transport of Ca^{+2} away from reaction site Local $CaSO_4$ precipitation
$CaCO_3 + Mg^{+2} + CO_3^{-2} = CaMg(CO_3)_2$ [1]	gain of 75-88%	A-D: -13.24 C-D: -13.01	External source for CO_3^{-2} & Mg^{+2} No Ca^{+2} removal necessary
$(2-x)CaCO_3 + Mg^{+2} + xCO_3^{-2} = CaMg(CO_3)_2 + (1-x)Ca^{+2}$ [3]	no change	A-D: -3.08 C-D -4.29	x = .11 for aragonite x = .25 for calcite Local $CaSO_4$ precipitation
$(2-x)CaCO_3 + Mg^{+2} + xHCO_3^- = CaMg(CO_3)_2 + (1-x)Ca^{+2} + xH^+$ [4]	no change	not reported	x = .1 CO_3^- is present as HCO_3^- due to alkaline conditions (pH = 6.3-10.4) which exist in a sabkha

* Free energy of reaction, KCal/Mole; calculations by Morrow (1982) from data of Helgeson et al., 1978.
A = aragonite, C = calcite, D = dolomite

[1] from Weyl (1960)
[2] from Lippman (1973)
[3] from Morrow (1982)
[4] from Patterson (1972)

growth of crystals by excess electrical charges on these surfaces, 2) occlusions onto the surfaces of rapidly forming minerals and through incorporation between crystal surfaces as liquid inclusions or silicates, 3) occupants of free lattice positions created by defects in the structures of the minerals, or 4) substitutions for Ca^{+2} or Mg^{+2} in carbonate lattices (McIntire, 1963).

Trace elements are randomly included in minerals by processes 1 to 3, and their behaviour is not easily predictable but is volumetrically subordinate to that of process 4 (Veizer, 1983b). Sodium concentration is an exception and most of it may be linked to noncarbonate fluid inclusions (Fritz and Katz, 1972; Land and Hoops, 1973; White, 1977; Ishikawa and Ichikuni, 1984; Busenberg and Plummer, 1985).

If the trace element is incorporated into a mineral by substitution for Ca^{+2} or Mg^{+2} (4 above), experimental distribution coefficients (K) can predict the partitioning of trace elements between the mineral and the fluid (McIntire, 1963):

$$\left(\frac{Tr}{L}\right)_{solid} = K \left(\frac{Tr}{L}\right)_{fluid}$$

where:

Tr = molar concentration of trace element
L = molar concentration of element for which the trace element is substituting
K = distribution coefficient

This equation is valid for homogeneous distribution of the trace element in the fluid phase resulting from the fact that the fluid reservoir is 'unlimited', that is large, in comparison to the precipitating solid.

Distribution coefficients for various carbonate minerals are partly known from experimental growth studies carried out at fixed physicochemical parameters (see Mucci and Morse, 1983; Veizer, 1983a, Ishikawa and Ichikuni, 1984; and Ohde and Yasuki, 1984 for a compilation of K's for sedimentary carbonates). Distribution coefficients are sensitive to changes in temperature and kinetic factors of precipitation, especially the rate of precipitation (Kinsman, 1969; Ishikawa and Ichikuni, 1984). Most studies of trace element sorption on calcite describe an initial rapid adsorption of trace elements onto the crystal surface followed by slow solid-solution precipitation (McBride, 1979; Mucci and Morse, 1983; Farley et al., 1985; Mucci et al., 1985; Davis et al., 1987). As the rate of precipitation increases, distribution coefficients approach unity (Lorens, 1981). These factors of uncertainty allow only order of magnitude assumptions for calculated distribution coefficients.

When the volume of the fluid is small, as in the case of many diagenetic systems, the situation becomes more complex. As mineral phases are precipitated, the water composition evolves. The distribution of a trace element is then

controlled by the Doerner-Hoskins heterogeneous distribution law (Gordon et al., 1959):

$$\log\left(\frac{Tr^i}{Tr^f}\right)_{solid} = K \log\left(\frac{L^i}{L^f}\right)_{solution}$$

where:

Tr = molar concentration of trace element
L = molar concentration of lattice element
i = initial concentration of element
f = final concentration of element
K = distribution coefficient

As a first order approximation (and keeping in mind all the uncertainties involved), the original marine carbonate sediments should have chemical compositions similar to those in Table 3-2. Such sediments subsequently are involved in diagenetic transformation of the original metastable assemblage of carbonate minerals into the stable low-Mg calcite (dLMC). In a simple case of open system diagenesis (water dominated system), the dLMC will acquire chemical attributes of the diagenetic fluid through repartitioning similar to the 'homogeneous' case. For example, if the diagenetic fluid were meteoric water, the composition of dLMC could approximate the end member listed in Table 3-2. Even this simple consideration indicates that diagenetic/epigenetic recrystallization should lead to a loss of Sr and Na as well as the gain of Mn and Fe with increasing 'degree of alteration'. In nature, the matter is more complex, because the diagenetic systems are only partially open, that is have

Table 3-2
Trace Element Concentration of Ocean Water, Meteoric Water and Ground Water with Corresponding Trace Element Concentrations of Carbonates Deposited in Equilibrium with these Waters

Trace Element	Concentration in ocean water		Concentration in meteoric water[1]
Sr	7.7	ppm	60 ppb
Na	10,760	ppm	5 ppm
Mn	.2	ppb	8 ppb
Fe	2	ppb	40 ppb
Mg	1,290	ppm	3.8 ppm

Carbonates Precipitated From Ocean Water[3]

	Aragonite	Calcite	Dolomite
Sr	7,000-9,400 ppm	1000 ppm	470-550 ppm
Na	1,500 ppm	200-300 ppm	<110-160 ppm
Mn	0.1-0.6 ppm	1 ppm	1 ppm
Fe	-	2-39 ppm	3-50 ppm
Mg	750-6300 ppm	16,300-75,400 ppm	130,400 ppm

Diagenetic Calcite Deposited by Meteoric Water[3]

Sr	24 ppm
Na	7-10 ppm
Mn	13,000 ppm
Fe	24,000-478,000 ppm
Mg	1,950-8980 ppm

1 - Drever, 1982
2 - Faure, 1986
3 - Veizer, 1983a

low water/rock ratios. As a consequence, the water composition evolves and the situation approximates the above 'heterogeneous' case. However, the water evolves not only due to continuous precipitation of dLMC, but also because of concomitant dissolution of the metastable carbonate precursor. In the extreme case of a completely closed system the fluid may attain a composition where the dissolving and precipitating phase have identical chemistry (Baker et al., 1982). In nature the intermediate situation is the most frequent. Apart from this temporal evolution of the fluid, localized concentration gradients may exist in the fluid adjacent to specific mineral surfaces. This results in partial transposition of chemical attributes of the precursor into its diagenetic successor of dLMC. In detail, the matter is complex and discussed more completely in Veizer (1983a,b), Brand and Morrison (1987) and Brand (1989).

For our consideration it is important to point out that most diagenetic to low grade metamorphic processes result in a general loss of Sr, Na and gain of Mn and Fe. The overall trends are presented in Figure 3.1. The actual slopes and the magnitudes of these trends are variable and difficult to calculate, but their general signs have been confirmed in many studies of Phanerozoic and Precambrian carbonates (Brand and Veizer, 1980, Al-Aasm and Veizer, 1982, 1986, Veizer et al., 1982, 1989a,b; Brand and Morrison, 1987; Brand, 1989). As a

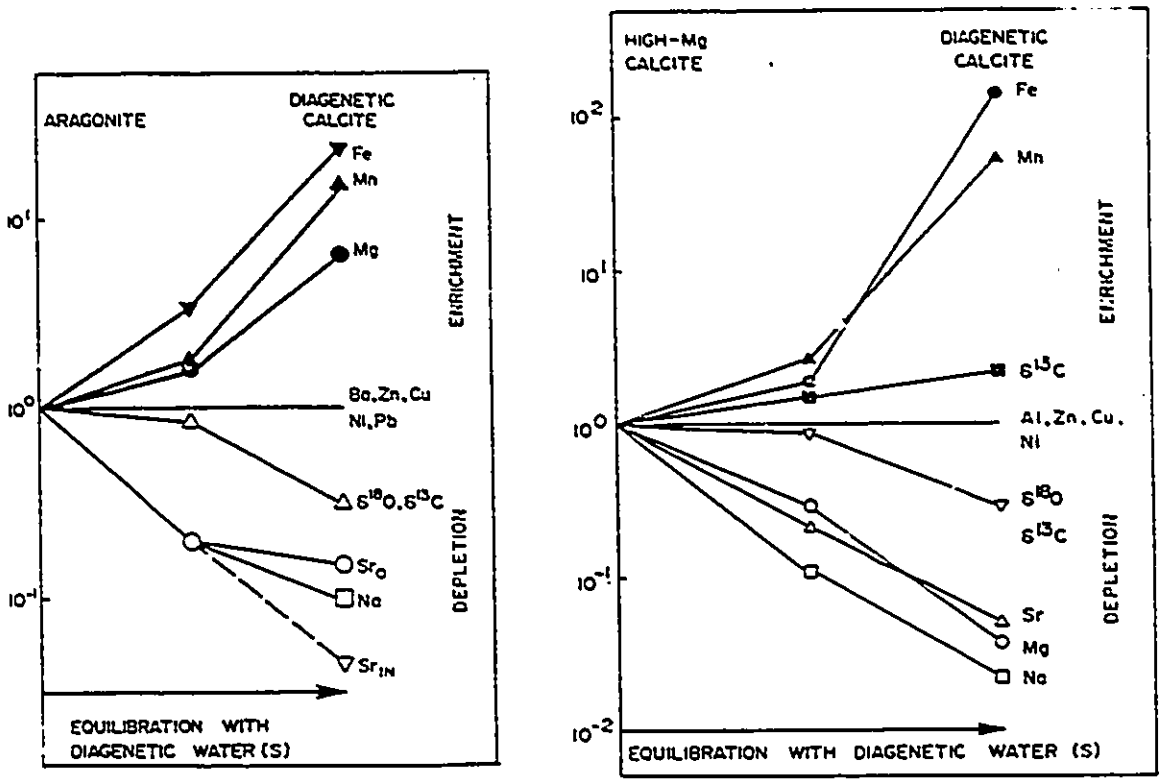

A B

Figure 3-1
General trends for trace elements and stable isotopes caused by diagenetic repartitioning during transformation of (A) aragonite and (B) high-Mg calcite into diagenetic low-Mg calcite. These trends were determined from well preserved and altered fossils by Brand and Morrison (1987).

result, the covariance of trace elements, particularly the negative correlation between Mn and Sr, may be utilized for determination of the relative 'degree of alteration' from a suite of coeval samples.

The situation for dolostones is more complicated than for limestones. Nevertheless, the general rules of partitioning theory apply and the covariant trends of trace elements, if documented, may be utilized as an index of the relative 'degree of alteration' in a manner similar to that of limestones (Figure 3.2). This will be the approach taken in the study of the Belt carbonates. Dolomite crystals typically show zonations of trace element concentrations, with Sr and Na enriched centres (Fritz and Katz, 1972; Choquette and Steinen, 1980) and Fe and Mn enriched rims (Morrow, 1982). This zonation may represent a nonstoichiometric, trace element rich core (Reeder and Sheppard, 1984; Land, 1986; Randzaao and Cook, 1987) and a more ordered dolomite rim which better reflects the composition of the diagenetic fluid.

3.2 Oxygen and carbon isotopes

Fractionation of oxygen isotopes into carbonates is inversely proportional to temperature (^{0}K) and is expressed as:

$$10^3 \ln \alpha \text{ (aragonite-water)} = 2.69\ (10^6 T^{-2}) - 3.24$$

$$10^3 \ln \alpha \text{ (calcite-water)} = 2.78\ (10^6 T^{-2}) - 2.89$$

(O'Neil et al., 1969)

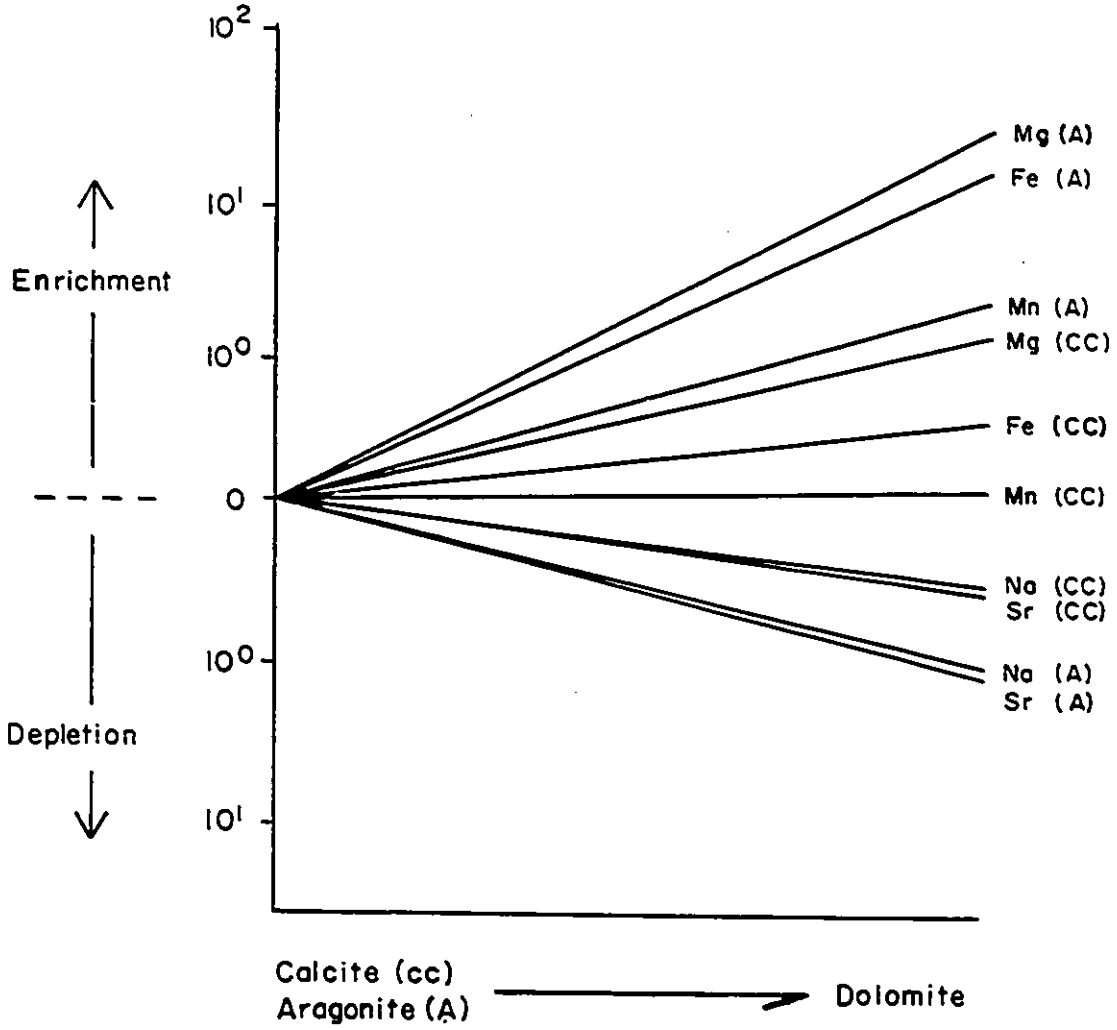

Figure 3-2
Theoretical enrichment and depletion factors for dolomites as compared with a calcite or aragonite precursor, presuming the diagenetic fluid was dominated by marine water. (A) - enrichment of element relative to aragonite, (CC) - enrichment of element relative to calcite. These trends are not based on actual observed trends, but solely on trends predicted by distribution coefficients and the trace element content of diagenetic fluids (Table 3-2).

$10^3 \ln \alpha$ (dolomite-water) = $3.06 (10^6 T^{-2}) - 3.24$

(Matthews and Katz, 1977)

The oxygen isotope composition of modern ocean water of normal salinity and standard temperature and pressure is $\delta^{18}O$ = 0 $^0/_{00}$ (SMOW; Standard Mean Ocean Water) by definition, and deviates by less than 1 $^0/_{00}$ worldwide (Hoefs, 1980). $\delta^{18}O$ of recent marine limestones ranges from 28 to 30 $^0/_{00}$ SMOW (Faure, 1986). $\delta^{18}O$ of dolomite should theoretically be some 5 - 7 $^0/_{00}$ heavier than that of coexisting calcite at surface temperatures (Clayton et al., 1968; Land, 1980). However, the observed $\Delta^{18}O$ (dolomite-calcite) for some Holocene and ancient dolomites is considerably less (Degens and Epstein, 1964; Land, 1980; Aharon et al., 1987; Andrews et al., 1987). This may reflect the fact that dolomitization was a later phenomenon proceeding at higher temperatures and/or it may mirror problems with fractionation factors which were determined at temperatures much above those typical of natural dolomite forming environments (Northrop and Clayton, 1966; Fritz and Smith, 1970; Sheppard and Schwartz, 1970).

The $^{18}O/^{16}O$ ratio of meteoric water is controlled by evaporation and Rayleigh distillation. Meteoric water is depleted in ^{18}O, with regional variations controlled by latitude and altitude, and ranges between 0 and -60 $^0/_{00}$ SMOW (Faure, 1986).

The isotopic content of pore water, originally that of sea or meteoric waters, evolves as it passes through reactive carbonate rocks. During diagenesis of sediments, pore waters show a trend of increasing $\delta^{18}O$ with increasing temperature and salinity (Sheppard, 1986). The resulting range of $\delta^{18}O$ for pore waters is -20 to 10 $^{0}/_{00}$. The isotopic composition of metamorphic and pore waters overlaps, as do the geologic processes, and $\delta^{18}O$ of metamorphic fluids ranges from 3 to 20 $^{0}/_{00}$ (Shieh and Taylor, 1969; Muehlenbachs and Clayton, 1971; Taylor, 1974; O'Neil and Ghent, 1975; Magaritz and Taylor, 1976; Sheppard, 1981).

The carbon isotopic composition of carbonates is dependent on 1) the $\delta^{13}C$ value of CO_2 gas in equilibrium with carbonate and HCO_3^- ions in solution, 2) the fractionation of carbon isotopes between CO_2 gas, carbonate and bicarbonate in solution and the solid carbonate:

calcium carbonate - bicarbonate	1.00185 ± 0.00023
bicarbonate - carbon dioxide gas	1.00838 ± 0.00012
calcium carbonate - carbon dioxide gas	1.01017 ± 0.00018

(as determined experimentally at 20^0 C by Emrich et al., 1970), 3) the temperature at which the minerals were equilibrated, 4) the hydrogen ion activity (pH) and other chemical parameters of the system which would change the concentrations of carbonate and bicarbonate in the solution (Faure, 1986). Fractionation factors vary with temperature, but in the case of carbon isotopes, this should not be significant at surface

and diagenetic temperatures (Emrich et al., 1970; Faure, 1977). Carbon isotopic values are reported relative to the PDB (Peedee Belemnite) standard.

There are two main reservoirs of carbon, reduced (organic) carbon and oxidized (carbonate sediments and total dissolved) carbon. These reservoirs are separated by two processes: 1) kinetic effects during photosynthesis (Park and Epstein, 1960; Smith and Epstein, 1971; Whelan et al., 1973; Monson and Hayes, 1982) which lead to a depletion of ^{12}C in CO_2 and its enrichment in the synthesised organic matter, and 2) a chemical exchange between atmospheric CO_2 and HCO_3^- which enriches HCO_3^- in ^{13}C (Deuser and Degens, 1967; Wendt, 1968; Emrich et al., 1970; Vogel et al., 1970).

In the modern ocean the dissolved organic matter has $\delta^{13}C$ of -21.8 $^0/_{00}$ (Hoefs, 1980), whereas the total dissolved (oxidized) carbon has $\delta^{13}C$ of 0.5 to 1 $^0/_{00}$ (Kroopnik, 1980). The range of carbon isotopic composition of meteoric waters is wide, with average river water TDC $\delta^{13}C$ between -6 and -9 $^0/_{00}$, while $\delta^{13}C$ of groundwater varies from -30 to +3 $^0/_{00}$ (Anderson and Arthur, 1983).

Organic matter in recent sediments has $\delta^{13}C$ values mostly between -20 and -27 $^0/_{00}$ (Eckelman et al., 1962; Sackett and Thompson, 1963; Welte et al., 1975; Schultz and Calder, 1976; Gearing et al., 1984). The average $\delta^{13}C$ value for organic matter in pre-Tertiary sedimentary rocks is -28 (Hoefs, 1980).

In contrast, the average $\delta^{13}C$ value for marine carbonate rocks is 0.56 ± 1.55 $^{0}/_{00}$ (Keith and Weber, 1964).

As with trace elements, diagenetic stabilization of carbonate sediments results in repartitioning of oxygen and, to a lesser degree, carbon isotopes. Numerous studies, summarized for example in Bathurst (1975), Hudson (1977), and Allan and Matthews (1982), show that this usually results in ^{18}O depletion, while the $\delta^{13}C$ is mostly buffered by the isotopic composition of the carbonate precursors. Previous work, synthesized by Lohman (1983), documents three basic types of 'alteration' trends for oxygen and carbon isotopes in limestones (Figure 3-3). The trend A indicates diagenetic alteration at a high water/rock ratio, where the $\delta^{13}C$ is buffered by the $CaCO_3$ precursor and the ^{18}O depletion is inherited from the meteoric component in diagenetic fluid. This trend may extend to highly depleted ^{18}O values as a consequence of recrystallization (at whatever diagenetic/epigenetic stage) at higher temperatures. Invariant $\delta^{18}O$ and decreasing $\delta^{13}C$ (trend B) implies alteration in near surface, low latitude environments where temperature, and $\delta^{18}O$ of diagenetic waters, did not deviate much from that of seawater, but ^{12}C was contributed by organic carbon (Al-Aasm and Veizer, 1986). Covarying $\delta^{13}C$ and $\delta^{18}O$ (trend C) suggests burial diagenesis, with ^{18}O depletion caused by increasing temperatures of equilibration and ^{12}C supplied to carbonates by

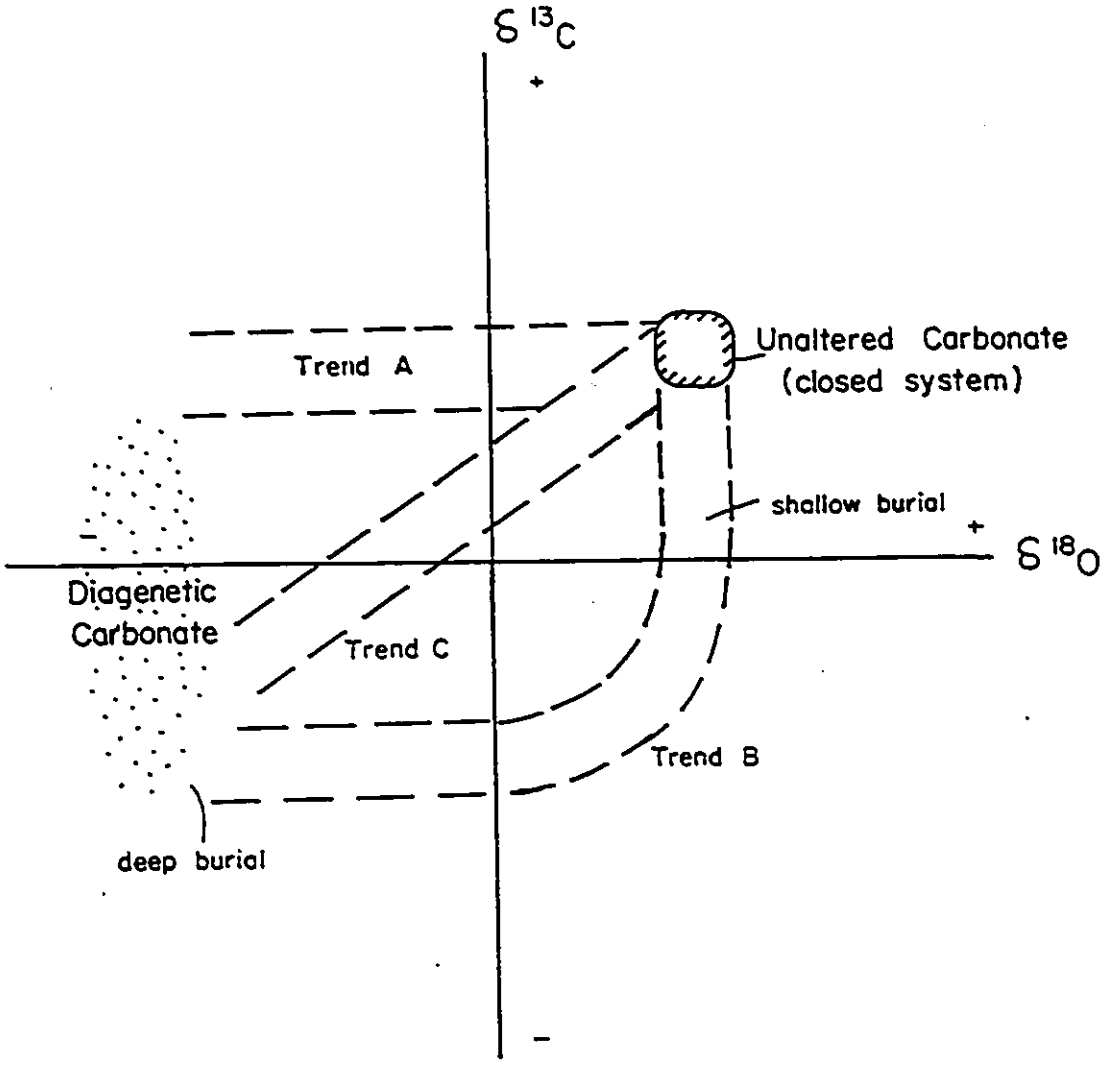

Figure 3-3
$\delta^{18}O$ and $\delta^{13}C$ trends for the diagenesis of carbonate rock. The trends are described in the text. Figure abstracted from Lohmann (1983).

CO_2 or CH_4 generated by thermal cracking of hydrocarbons within the sequence (McKirdy and Powell, 1974; Eichman and Schidlowski, 1975; Hoefs and Frey, 1976; Hudson, 1977). Dolomites should show complementary diagenetic trends, with the least altered dolostones enriched in ^{18}O when compared to coexisting limestones.

3.3 Secular Variations

Carbonates of different ages that have undergone comparable degrees of diagenetic alteration have time dependent trace element concentrations which implies secular variations in depositional fluids. Only trace elements with ocean residence times longer than 10^3 years (the mixing time of the oceans; Broecker, 1963) can be considered in this respect, since their long residence times enable their thorough mixing and thus homogeneous distribution in the ocean. The elements of interest to us are Ca, Mg, Sr, Mn and Na (Holland, 1978).

The controls on sea water chemistry of the modern ocean are 'continental' river flux (F^C), 'mantle' flux (F^M) at hydrothermal cells on mid-ocean ridges, sedimentation (F^S), diagenetic flux (F^D) and possibly subduction (F^T) (Garrels and Mackenzie, 1971; Holland, 1978; Veizer et al., 1982). F^M and F^C are the dominant fluxes, and will change as the rates of water recycling through rivers as opposed to recycling through oceanic crust changes. Fluctuations in F^M are interpreted to

cause variations in Sr, Mg and Ca observed in pelagic carbonates, chiefly through the contribution of Ca to and removal of Mg from the oceans due to enhanced F^M caused by higher spreading rates (Renard, 1986). Although Fe and Mn increases in pelagic carbonates have been predicted for an increase in F^M, their temporal distribution is more complicated because these elements are also affected by the redox conditions of the ocean, paleo-depth, distance from mid-ocean ridges, and by Fe and Mn contribution through F^C (Renard, 1986).

Archean carbonates have orders of magnitude higher Mn and Fe concentrations than their Phanerozoic counterparts (Veizer et al., 1982, 1989a,b). Iron and Mn may have been present in higher concentrations in oxygen-poor Precambrian oceans (Veizer, 1985) or, more likely, have been supplied at a higher rate into the coeval exogenic system from the ubiquitous volcanic and fumarolic sources characteristic of the early stages of planetary evolution (cf. Veizer, 1989a).

The oxygen isotope composition of marine cherts, carbonates, phosphorites and glauconites decreases with increasing age (Baertschi, 1957; Clayton and Degens, 1959; Degens and Epstein, 1962; Keith and Weber, 1964; Weber, 1965; Perry, 1967; Longinelli and Nuti, 1968; Bausch and Hoefs, 1972; Dontsova et al., 1972; Perry and Tan, 1972; Schidlowski et al., 1975, 1983; Knauth and Epstein, 1976; Veizer and

Hoefs, 1976; Knauth and Lowe, 1978; Perry et. al., 1978; Shemesh et al., 1983; Friedrichsen, 1984; Luz et al., 1984; Keppens and O'Neil, 1985; Popp et al., 1986; Veizer et al., 1986). There exist three disparate explanations for this trend: 1) an increasing probability of post-depositional recrystallization in meteoric water and/or at higher temperatures with increasing age of sediments; 2) a decrease in the temperature of the oceans from the Archean high of about 70° C to < 30° C at present (Knauth and Epstein, 1976; Kolodny and Epstein, 1976; Knauth and Lowe, 1978; Shemesh et al., 1983; Luz et al., 1984); 3) an increase $\delta^{18}O$ of seawater since the Archean (Weber, 1965; Perry, 1967; Dontsova, 1970; Fritz, 1971; Dontsova et al., 1972; Perry and Tan, 1972; Perry et al., 1978).

Post-depositional alteration undoubtedly accounts for a portion of the ^{18}O depletion in ancient sediments. Nevertheless, it is difficult to justify the entire secular trend by this factor alone, as is discussed in detail in Veizer et al. (1986, 1989a,b). An elevated temperature for Proterozoic oceans, the case 2 above, is also an unlikely explanation since glacial events have been recorded for both the early and the late Proterozoic (Visser, 1971; Young, 1973; Frakes, 1979; Trendall, 1979; Hambrey and Harland, 1985). The third alternative could yield ^{18}O depleted ocean water, providing the low temperature (<350°C) sea water-silicate rock

exchange has been enhanced in the geologic past (Muehlenbachs and Clayton, 1971, 1972; Chase and Perry, 1972; Perry et al., 1978; Gieskes and Lawrence, 1981; Gregory and Taylor, 1981; Lawrence and Gieskes, 1981, Lohman and Walker, 1989). This would, however, require that the counteracting process of ^{16}O removal from sea water into silicates (e.g. basalts of oceanic crust) at temperatures exceeding 350°C did not compensate for the low-temperature flux (Walker and Lohman, 1989).

Secular oscillations in carbon isotopic composition of sea water of about 5 $^{0}/_{00}$ have been documented throughout the Phanerozoic (Veizer et al., 1980; Schidlowski et al., 1983) and higher order variations, reflecting perhaps CO_2 balance of the atmosphere-ocean system (Renard, 1986), changes in ocean circulation patterns or phosphate supply to continental shelves (Broecker, 1982) have been documented for the Cenozoic (Shackleton and Kennett, 1975). The original $\delta^{13}C$ composition of the oceans must have been controlled by ^{12}C enriched volcanic carbon ($\delta^{13}C = -6 \pm 1$ $^{0}/_{00}$; Deines, 1980). Lighter carbon isotopes were fractionated into organic matter as life evolved prior to 3.5 - 3.8 Ga ago, leaving the residual carbon in the ocean enriched in ^{13}C to values of about 0 $^{0}/_{00}$ (Schidlowski et al., 1983). Variations in the relative sizes of organic and inorganic terrestrial reservoirs of carbon through geologic time have been the cause of secular oscillations of $\delta^{13}C$ with a wavelength of about 10^7 years

(Veizer et al., 1980). Because of problems with stratigraphic resolution, these second order oscillations have not yet been resolved for the Precambrian.

Chapter 4

Diagenesis of Carbonates in the Belt Basin

This thesis is a reconnaissance study of carbonates in the Belt Supergroup and as such will yield patterns of diagenesis on a regional scale. Because of the broad nature of this study, the number of samples for any particular formation is limited, and furthermore they are of variable lithology (limestones, dolostones, dolomitic limestones). Earlier geochemical studies of carbonates demonstrated that lithology is the first order controlling factor of chemical attributes. For all these reasons, it is more appropriate to define statistical populations through lithology rather than formations. Within a given lithology it is then possible to compare the relative chemical signatures of specific formations. In the present study, carbonates containing less than 10% dolomite (Mg < 1.7%) are classified as limestones, carbonates with less than 10% calcite as dolostones (Mg > 11.7%), and the intermediate population is designated as dolomitic limestone (Figure 4-1). Samples containing less than 25% soluble fraction (Figure 4-1) are disregarded in the subsequent evaluation because of the intrinsic error in calculation of carbonate-bound trace element concentrations. Further subdivision of lithologic populations is not possible because of the small number of samples in each subpopulation.

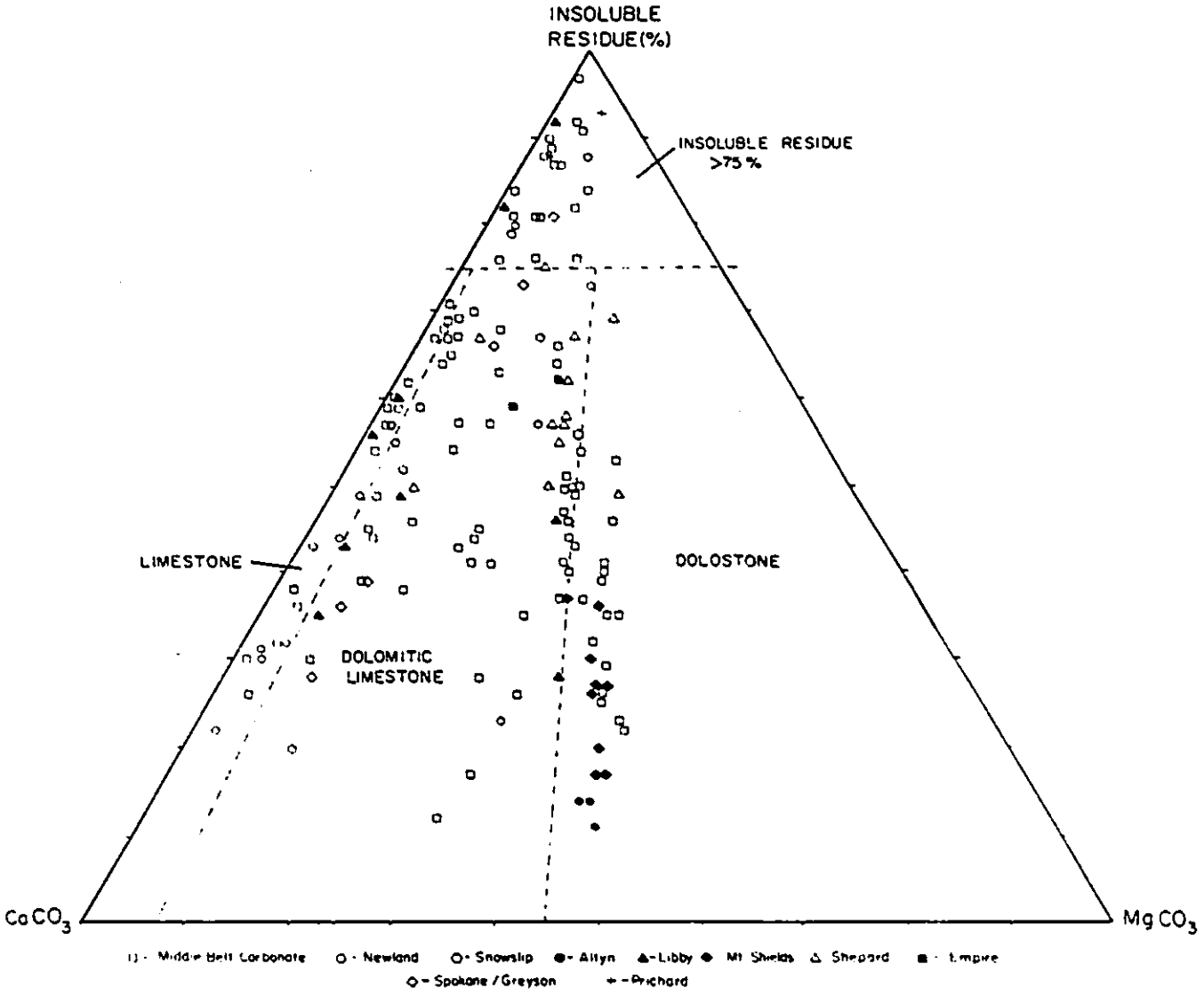

Figure 4-1
Compositional fields used in statistical analysis of Belt carbonates. Molar Ca and Mg fractions were calculated presuming that the total of Ca and Mg of carbonates accounted for 100% of the soluble fraction.

Formation specific studies of Belt carbonates await future efforts.

4.1 Diagenesis of Belt limestones

In order to determine if Belt carbonates show diagenetic trends similar to those of their Phanerozoic and Archean counterparts (Brand and Veizer, 1980, 1981; Veizer, 1983a,b; Al-Aasm and Veizer, 1982, 1986; Veizer et al., 1989a,b), the amassed geochemical data (Appendix C) have been analyzed through R-mode factor analysis. This evaluation yields groups of correlative factors that can be interpreted as a function of geology, diagenesis or laboratory techniques. Dolostones, limestones and carbonates of intermediate composition are discussed as separate populations.

Table 4-1 shows the results of a rotated factor analysis of all Belt limestones. The underlined values represent the controlling loadings. These results were obtained using the statistical program SPSSx (S.P.S.S.x., 1986), with the particular parameters of the factor analysis program shown in Appendix D.

The first factor, which accounts for 36.5% of the total variance, antithetically links percent solubility with Al, Fe and Na. This factor probably represents leaching from aluminosilicate impurities during laboratory digestion of carbonate rocks. With decreasing solubility, and therefore

Table 4-1
Varimax Rotated Factor Analysis for Belt Limestones

Variable	Factor 1	Factor 2	Factor 3	Communality
% Sol.	-0.68	0.21	0.49	0.74
log Ca	-0.25	-0.35	-0.09	0.19
log Mg	0.03	0.92	-0.08	0.86
log Mn	0.18	-0.88	-0.21	0.86
log Sr	0.00	0.03	0.93	0.87
log Al	0.88	0.04	-0.34	0.90
log Na	0.91	-0.01	0.22	0.88
log Fe	0.88	0.10	0.09	0.80
$\delta^{18}O$ cc	0.00	0.84	0.41	0.89
$\delta^{13}C$ cc	0.00	0.41	0.88	0.95
Eigenvalue	3.65	2.89	1.46	
% Variance Explained	36.5	29.0	14.6	

N = 24 for trace elements and % soluble
N = 22 for isotopes
Underlined loadings are those that are statistically dominant.

Interpretation:

Factor 1	Laboratory leaching
Factor 2	Formation of sparry calcite and burial diagenesis
Factor 3	Early (shallow) diagenetic mineral transformations

increasing insoluble residue, more Fe, Na and Al are leached from the aluminosilicate fraction of the rocks.

The second factor, accounting for 29.0% of the total variance, links an increase in Mn content with depletion in Mg, ^{18}O and to a lesser degree ^{13}C. A scatter plot of Mn vs. $\delta^{18}O$ shows clearly this negative correlation (Figure 4-2). Trace elements in rocks have usually a log normal distribution (Graf, 1960; Veizer and Demovic, 1974) and are plotted on a log scale throughout this thesis. The different Belt formations plot as two populations, the Libby Formation and one limestone sample from the Snowslip Formation consistently have the most depleted $\delta^{18}O$. The Newland Formation and the Middle Belt Carbonate samples overlap, although the former has on average less Mn and heavier $\delta^{18}O$ (Figure 4-2). Plots of Mn/Mg and Mg/$\delta^{18}O$ yield analogous trends and groupings. Comparison with Figure 3-1 shows that the observed covariance is as predicted from 'alteration trends'. The gain of Mn and depletion in ^{18}O may result either from early (shallow burial) stabilization of the carbonate precursors in an environment dominated by meteoric waters or from recrystallization of the rocks (and precipitation of Mn/Fe rich spar cement) during deeper burial at elevated temperatures. Any combination of the above is of course a possibility. The overall shift in $\delta^{18}O$ of about 8 $^{o}/_{oo}$ would be exceptional for early diagenetic environments in low latitude climates favouring carbonate

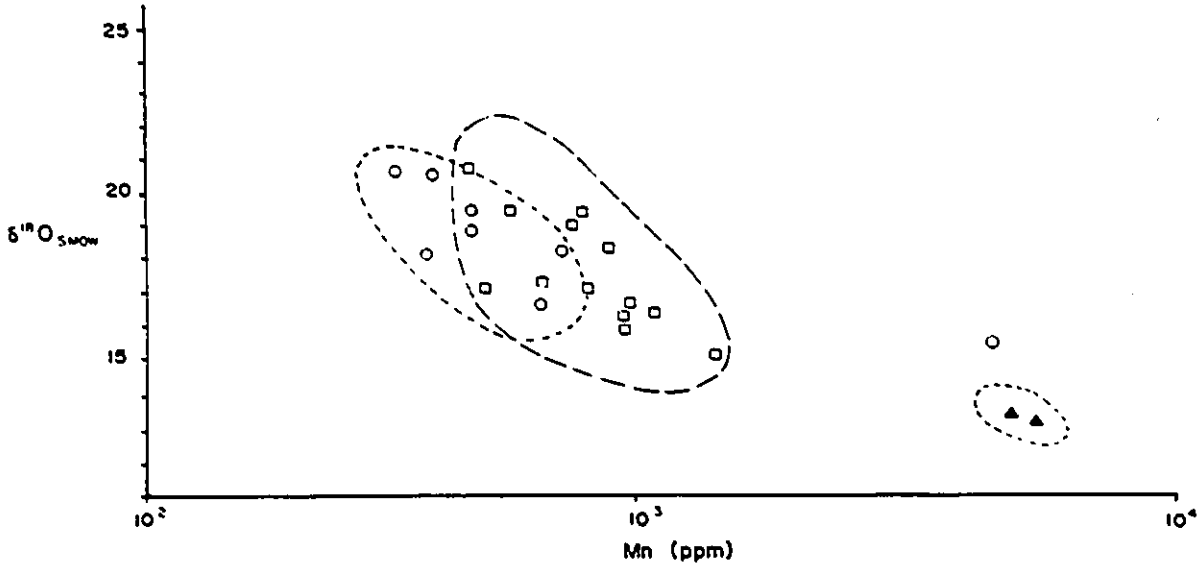

Figure 4-2
Scatter diagram of Mn content vs. $\delta^{18}O$ for the Belt limestones. ○-Newland Fm., □-Middle Belt Carbonate, ⬡-Snowslip Fm., ▲-Libby Fm.

deposition and this argues for a role of burial at elevated temperatures in the development of the observed trend. This proposition will be substantiated in the subsequent text. It appears therefore, that the Belt limestones define a trend of increasing alteration in the order of Newland < Middle Belt Carbonate << (Snowslip) < Libby.

The third factor, which accounts for 14.6% of the total variance, relates antithetically Sr content with $\delta^{13}C$ (Table 4-1, Figure 4-3). The Newland Formation contains the most Sr and the heaviest δ^{13}, while the Middle Belt Carbonate, Libby and Snowslip Formations are depleted in Sr and ^{13}C. Again, this is a covariance predicted by alteration trends (Figure 3-1), although the 'alteration' sequence for formations other than the Newland is not identical. This suggests that the alteration sequence is somewhat more complex, with three distinct populations well separated in the standard Sr/Mn plot (Figure 4-4). The Newland Formation is therefore the least altered, best preserved, limestone analyzed in the Belt basin, followed by the Middle Belt Carbonate and finally the most altered Snowslip and particularly Libby Formations.

Petrographic evidence substantiates the above conclusions. The least chemically altered limestones are micritic calcites (NC-1, Figure 4-5; RP-15, PP/SY-2, Appendix B) which lack textures indicative of advanced diagenesis (Table 2-3). Progressive alteration is usually accompanied by

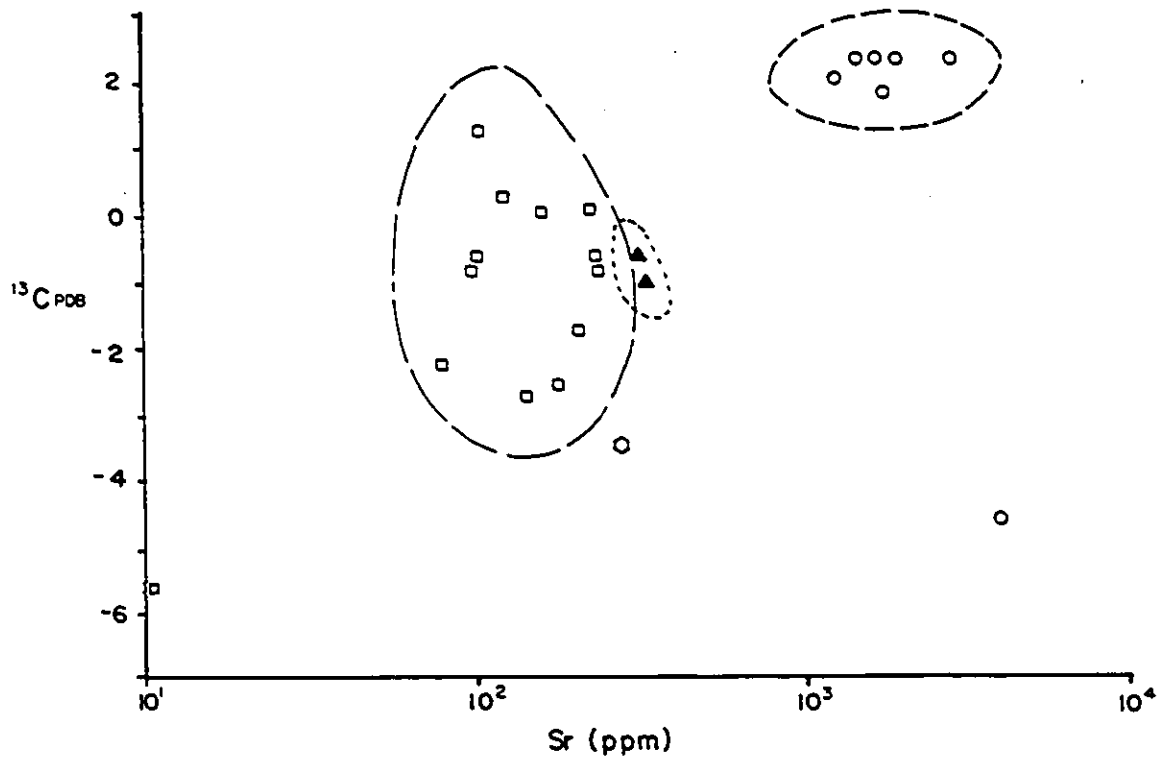

Figure 4-3
Scatter diagram of Sr vs. $\delta^{13}C$ for the Belt limestones.
○-Newland Fm., □-Middle Belt Carbonate, ○-Snowslip Fm., ▲-Libby Fm.

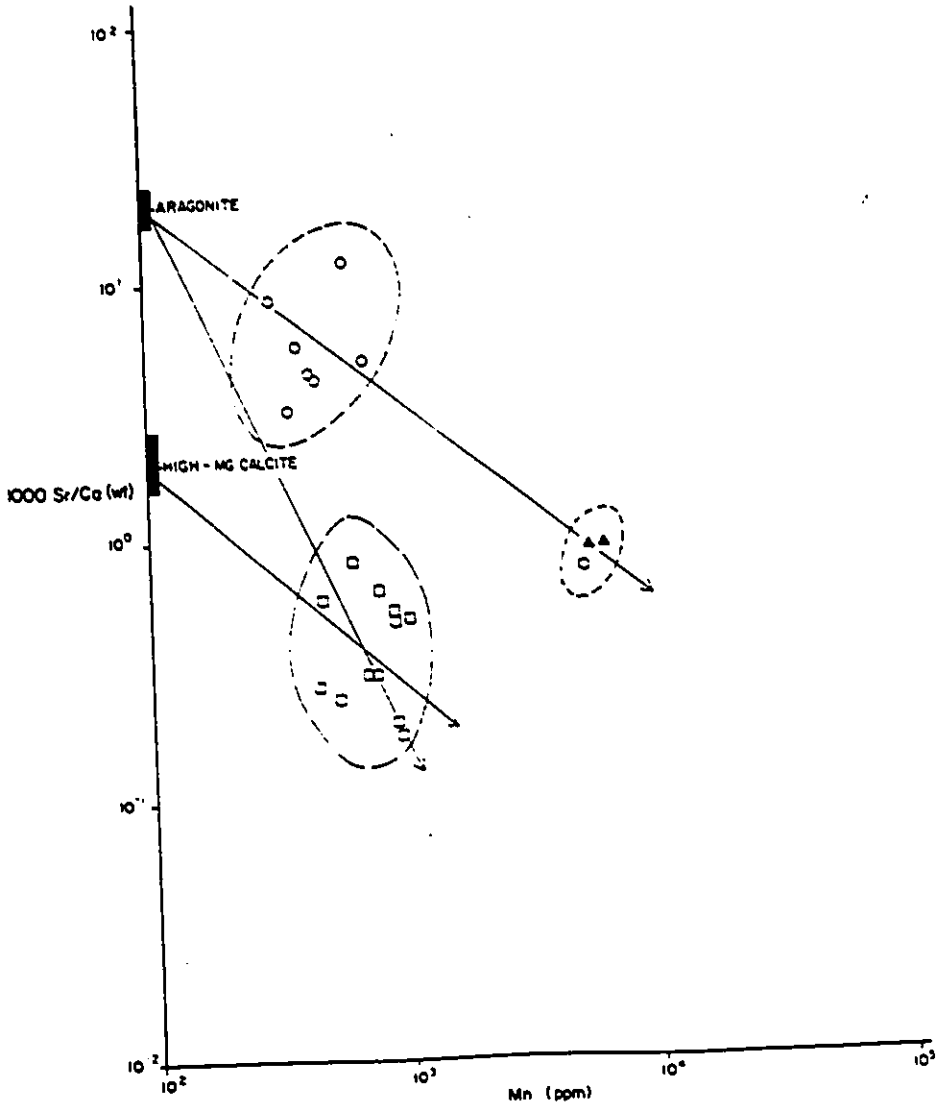

Figure 4-4
Scatter diagram of Sr/Ca vs. Mn for limestones of the Belt Supergroup. ○-Newland Fm., □-Middle Belt Carbonate, ⊙-Snowslip Fm., ▲-Libby Fm. The aragonite and high-Mg calcite fields are those of modern carbonates. The arrows indicate possible alteration pathways.

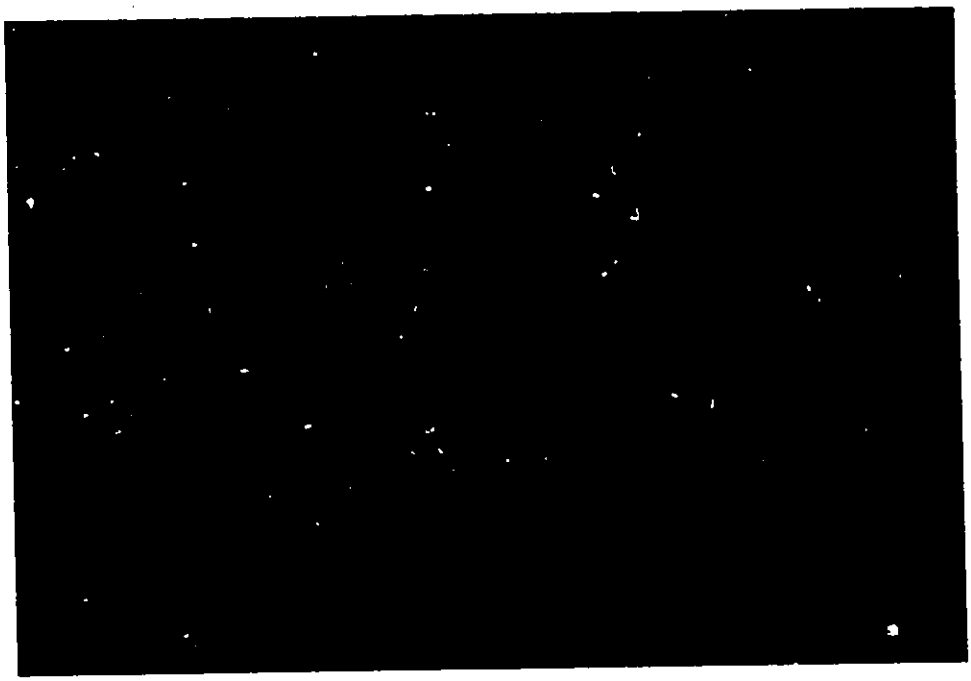

Figure 4-5
Thin section view of micritic calcite. Newland Formation sample NC-1 viewed under uncrossed polars. Alizarine Red S has stained calcite pink, scale bar is 1 mm.

the development of calcite veins (BHP-9, NC-2, Appendix B), and by increasing grain size (SN/LC-7,Figure 4-6; NC-2, Figure 4-7). Those calcites which are most altered (in this case within the Newland Formation population) show advanced diagenetic textures when compared with other carbonates of this population such as the recrystallization of ooids (NC-2, Appendix B), the replacement of siliciclastics by blocky calcite (NC-2. Figure 4-8) and the development of stylolites (NC-2, Figure 4-9).

Many studies of carbonate diagenesis show that an increase in diagenetic alteration of limestones is accompanied by Sr loss and Mn gain (cf. Veizer, 1983a,b). Although Sr and Mn loaded on separate factors when all Belt limestones were considered (Table 4-1), and thus were related to different textural components of limestones, their negative correlation is clearly distinguishable when details of the relationship are considered (Figure 4-4). The high Sr content of the Newland Formation limestones, with a geometric mean of 2137 ppm, necessitates an aragonite precursor (Davies, 1977; Wardlaw et al., 1978; Singh, 1987). Sr in calcite deposited in equilibrium with ocean water is theoretically 1,000 ppm, whereas for aragonite it is 7,000 to 9,400 ppm (Table 3-1). Considering the $\delta^{18}O$ depletion of Libby and Snowslip Formation limestones (≈ 8 $^{0}/_{00}$ compared with the Newland and ≈ 5 $^{0}/_{00}$ with Middle Belt Carbonate limestones) and their high Mn content,

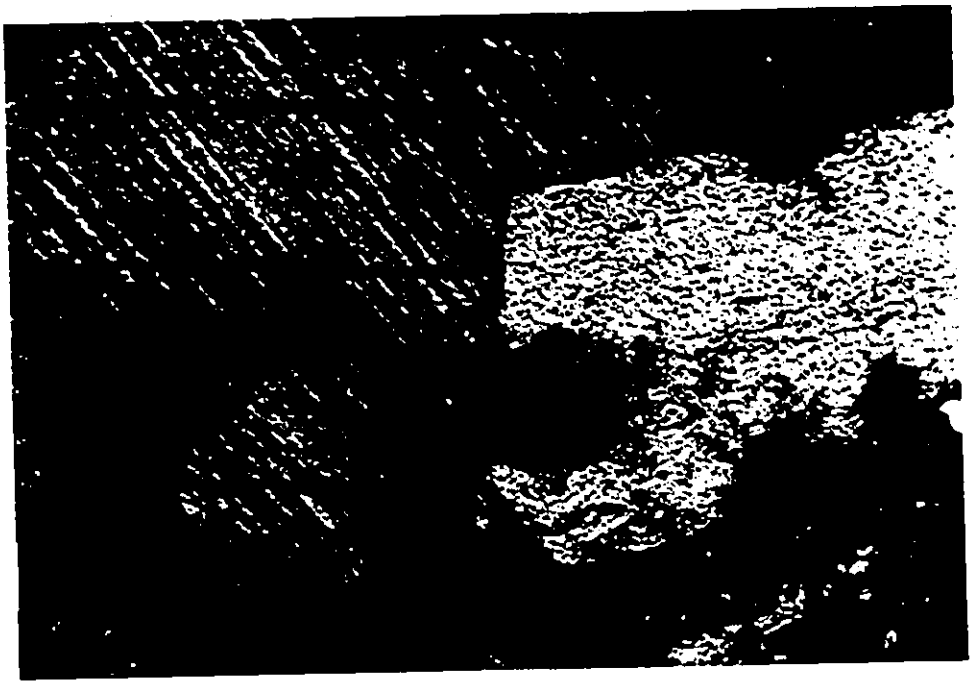

Figure 4-6
Thin section view of large (5 mm) calcite crystals of Snowslip Formation sample Sn/Lc-7 viewed under uncrossed polars. These calcite crystals are growing at the expense of quartz (surrounded by calcite crystals near the centre of the photograph). Alizarine Red S has stained the calcite crystals pink, scale bar is 0.25 mm.

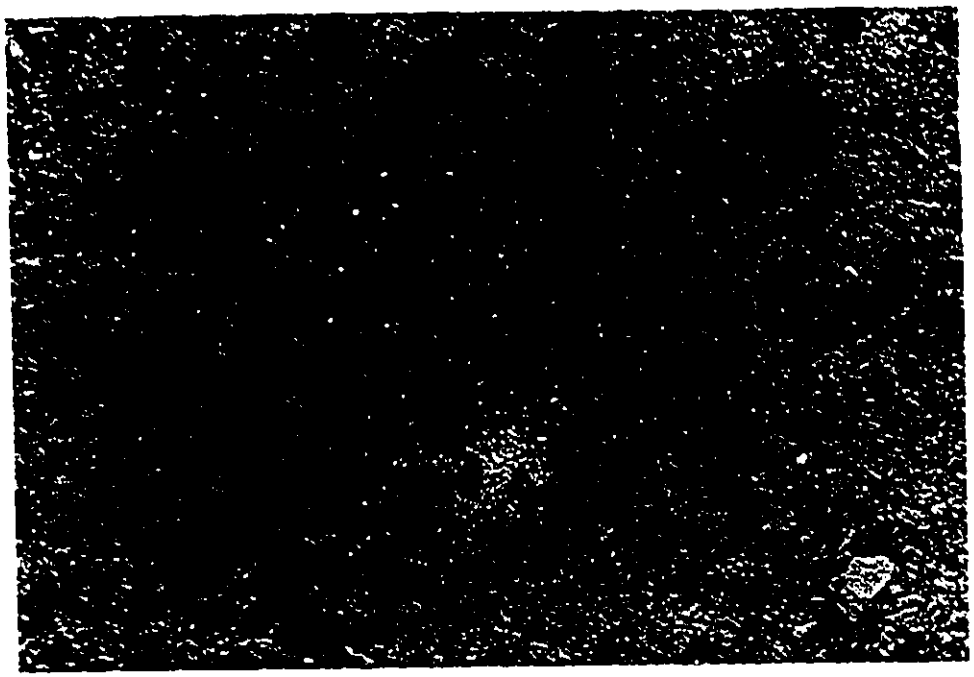

Figure 4-7
Thin section view of sparite crystals, Newland Formation sample NC-2, scale bar is 0.05 mm. Alizarine Red S has stained calcite pink, although this colour is not clear under crossed polars. Scale bar is 0.5 mm.

Figure 4-8
Thin section view of diagenetic calcite replacing quartz and chert clasts. Newland formation sample number NC-2 viewed through crossed polars. Alizarine Red S has stained calcite pink, although this colour is not clear under crossed polars. Scale bar is 0.05 mm.

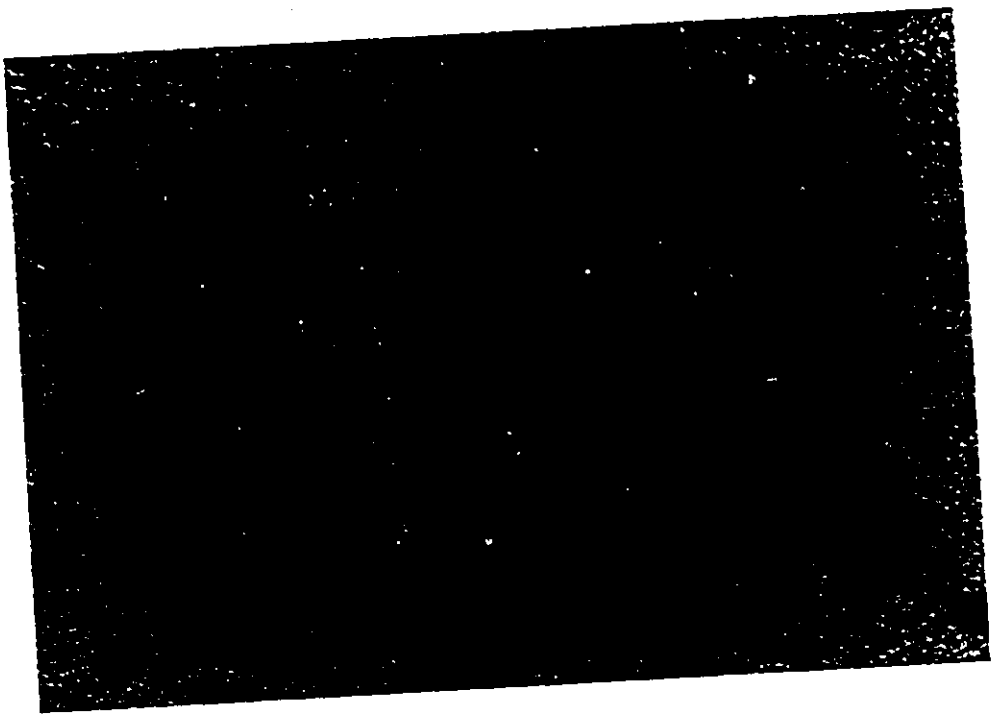

Figure 4-9
Thin section view of a stylolite in Newland Formation sample NC-2, as defined by concentrations of iron oxides, viewed under uncrossed polars. Scale bar is 0.05 mm.

this population represents limestones which have been strongly recrystallized during post-depositional alteration, perhaps at high temperatures. Considering the degree of alteration the rocks have been subjected to, their Sr content is relatively high. I propose therefore that the Libby and Snowslip Formation sediments may have been originally aragonitic. Petrographic evidence supports the existence of an aragonite component in the Libby Formation limestones. Some ooids in the Libby Formation are completely recrystallized and replaced by silica and blocky calcite (Figure 2-10), but others still retain their original radial textures (Figure 2-9). A possible interpretation is that the former represent a complete void dissolution of aragonitic precursors, whereas the latter originated by early neomorphic replacement of the highly reactive high-Mg calcite (Kidder and Hall, in prep.).

The existing data for the Middle Belt Carbonate limestones do not preclude conclusively an aragonitic precursor, but this population is easier to reconcile with a precursor which contained less Sr, such as a high-Mg calcite (Figure 4-4).

Both ^{18}O and ^{13}C of Belt limestones become progressively depleted with continuing post-depositional alteration (Figure 4-10) mimicking the burial trend C in Figure 3-3. The entire Newland to Libby range, if attributed to temperature variations, implies a 20° C gradient, that may have been

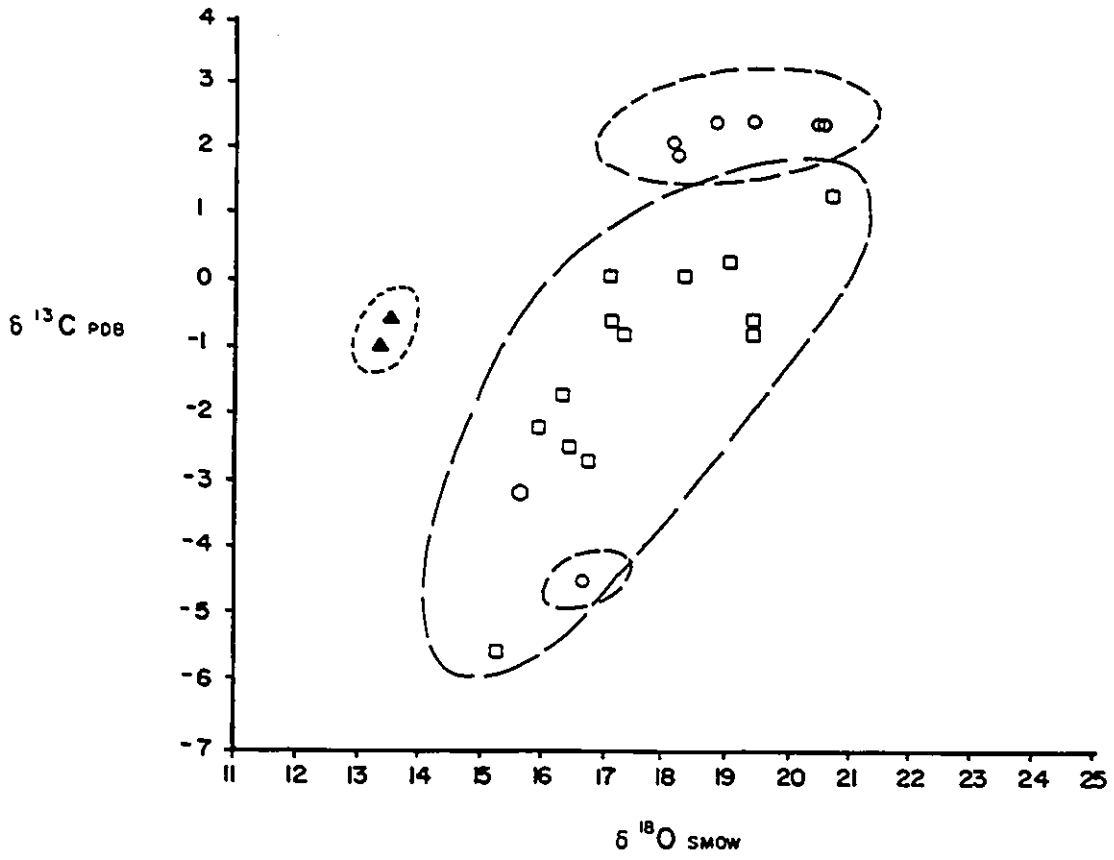

Figure 4-10
Scatter diagram of $\delta^{18}O$ vs. $\delta^{13}C$ for Belt limestones. ○-Newland Fm., □-Middle Belt Carbonate, ○-Snowslip Fm., ▲-Libby Fm.

regional, a proposition discussed in the subsequent text. The Middle Belt Carbonate defines a parallel, but separate trend, projecting to a $\delta^{13}C$ value of ≈ + 1 ‰, in contrast to + 2.5 ‰ for the Newland. This may indicate intraformational $\delta^{13}C$ variations which have not yet been erased by post-depositional evolution. The light carbon encountered in more altered samples likely originated from thermal cracking of organic matter in deeply buried Belt sediments, whereas the ^{18}O depletion reflects recrystallization at elevated temperatures during burial diagenesis.

The least altered Newland Formation attains the highest degree of closed system alteration, therefore most closely representing the original $\delta^{18}O$ and $\delta^{13}C$ of the Belt rocks. The $\delta^{13}C$ signature of Newland limestones is 2.4 ‰ PDB (Figures 4-3, 4-10), similar to values for Phanerozoic carbonates (Keith and Weber, 1964; Veizer et al., 1980). The $\delta^{18}O$ of the least altered Newland limestone is 22.9 ‰ SMOW (DG-3, Figures 4-2, 4-10), depleted by ≈ 5-7 ‰ if compared to their Phanerozoic and modern counterparts.

4.1.1 Facies control of trace element and isotope distribution

Although it has been established above that the alteration trends observed in the Belt limestones variously affect different formations in the sequence, the possibility

exists that some of these variations may have been caused by initial facies differences in trace element compositions or isotopic ratios of carbonates. However, scatter diagrams of Sr vs. Mn and $\delta^{13}C$ vs. $\delta^{18}O$ show that there is no correlation between depositional environment (as reported in Appendix A) and geochemical variations. I therefore conclude that the controls on Sr, Mn, $\delta^{18}O$ (and $\delta^{13}C$) distributions do not include any facies component, or if a facies component did once exist, it has been eradicated by diagenetic overprint. The only vestige still preserved is that of a possible difference in original mineralogy.

Some samples were collected through several sedimentary 'cycles' (as described in Chapter 2) in the Wallace Formation (Figure A-1 and some samples in the 7/28 and 7/29 series) in the hope that an analysis of the geochemistry of the carbonates in these cycles might give some clue as to their origin. In particular, I was interested in whether or not restricted water conditions could be recognised in the cycles. Even in this case, the diagenetic overprint clearly was the dominant control. Molar tooth dolomite was depleted in Sr, if compared to carbonates in close proximity, and had the highest Mg/Ca ratio of the sequence suggesting that this facies is more pervasively dolomitized than the bulk of the carbonate. The heaviest isotopic ratios in limestones are associated with intraclast breccias and thus may reflect the isotopic

composition of the clasts rather than a change in water chemistry of the basin. Both $\delta^{18}O$ and $\delta^{13}C$ of the 'poddy' brown weathering limestones in the cycles was depleted, which I interpret to imply a diagenetic, possibly meteoric, origin for these pods or concretions. Unfortunately the high insoluble residue in these pods precludes analysis of trace element variations. $\delta^{18}O$ and $\delta^{13}C$ of dolostones was remarkably uniform throughout the cycles, indicating that dolomites were formed from diagenetic fluid of the same isotopic composition. Further and more detailed study of isotopic ratios and variations of trace element concentrations within depositional cycles might yield important information on chemical changes in the Belt basin during deposition of one of these cycles if the diagenetic overprint can be eliminated.

4.1.2 Regional Isotopic Variations in the Belt limestones

Previous studies have shown that metamorphism of the Belt Supergroup increases towards the west and with depth in stratigraphic sections. Using the transformation of illite from its 1M to its 2M polymorph, Maxwell and Hower (1967) showed that the eastern Belt (Figure 4-11) had not been metamorphosed sufficiently to cause illite recrystallization. The western Belt section that they sampled (Figure 4-11) contained from 24 to 100% illite in its 2M polymorph, with the percentage of this higher temperature polymorph increasing

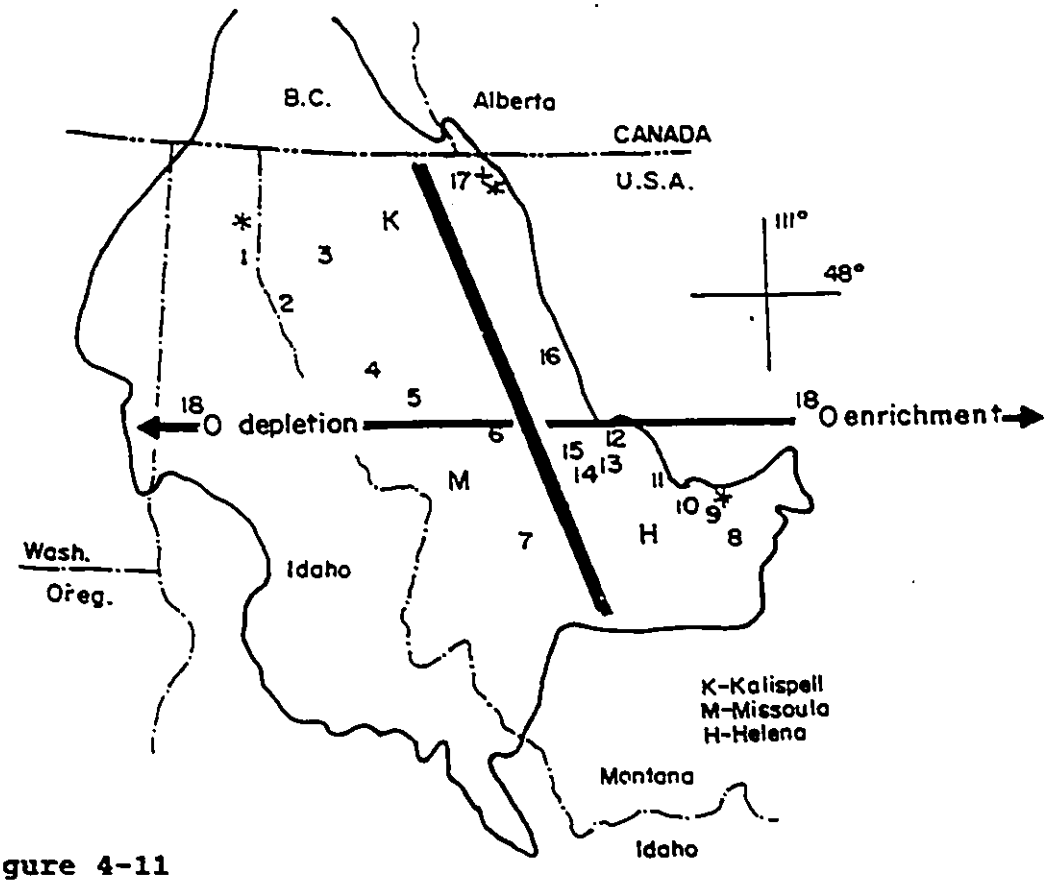

Figure 4-11
^{18}O enrichment and depletion in the Belt basin. See Appendix A for exact sample location descriptions. H - Helena, K - Kalispel, M - Missoula. See the text for further descriptions of this figure.

1 CF - Clark Fork, Wallace Fm.
2 DF, RR - Delye Fork, Ruen Road, Mt. Shields Fm.
3 7/23/86, 7/25/86, 7/28/85, 7/29/85, FB, FM, FC, MP, - Libby Area, Shepard, Libby, Mt.Shields, Empire and Prichard Fms.
4 GC - Graves Creek, Wallace Fm.
5 BHP - Big Hole Peak, Wallace Fm.
6 HL - Holland Lake, Helena Fm.
7 PH - Phillipsburg, Helena Fm.
8 NC - Newlan Creek, Newland Fm.
9 DG - Decker Gulch, Newland Fm.
10 SC - Smith Creek, Newland Fm.
11 TC, WC - Trout Creek, Wolf Creek, Spokane/Greyson Fm.
12 DRC - Dearborn River Canyon, Helena Fm.
13 FCR - Falls Creek Ridge, Helena Fm.
14 RP - Rogers Pass, Helena Fm.
15 RM - Red Mountain, Helena Fm.
16 WL - Wood Lake, Helena Fm.
17 SN/LC, GTS/SY, PP/SY, AF/AL, RM/SH - Glacier National Park Section, Snowslip, Siyeh, Altyn and Shepard Fms.
* Sampled by Maxwell and Hower (1967)
+ Sampled by Eslinger and Savin (1973)

with depth from 24-33% in the Libby Formation, 54 to 79% in the Wallace, 71-87% in the St.Regis and Burke Formations, and 83-100% in the Prichard. The northern section (Figure 4-11) contains 41 to 62% 2M illite increasing with depth; 41-62% in the Missoula Group, 45-50% in the Grinnell and 50-62% in the Appekunny Formation. Illite crystallinity is controlled by increasing temperature (Kubler, 1967; Frey, 1969). Maxwell and Hower (1967) reported that the 2M polymorph becomes stable once a temperature of 200 to 350^0 C is reached. Eslinger and Savin (1973) calculated the maximum temperature attained in the Glacier National Park section (Figure 4-11) of the Belt Supergroup sediments from oxygen isotope fractionation between coexisting quartz and illite. Temperatures ranged from 225 to 310^0 C for quartz-illite pairs, with quartz-feldspar pairs yielding 40 to 865^0 C, and two quartz-calcite pairs indicating 170 and 340^0 C. Temperatures attained for quartz-illite pairs closely fit the illite 2M polymorph data of Maxwell and Hower (1967) indicating a geothermal gradient of 36^0 C per km depth. Missoula Group sediments attained 225^0 C and temperatures increased down section to a maximum of 310^0 C for a sample from the Altyn limestone (Figure 4-11).

Because there is a well-defined regional and depth related increase in temperatures in the Belt basin, it may be possible that this very-low grade metamorphic fingerprint is visible in trace element contents or stable isotopic ratios of

the carbonates. For trace elements, there is no clear pattern of increasing 'alteration' northward or westward in the studied Belt formations, although the least altered carbonate, the Newland Limestone, is from the eastern Belt and the most altered Libby Formation, is on the western edge of the basin (Figure 4-11). Neither is there any clear relationship with depth in any single area or with stratigraphic horizon across the basin. It appears, therefore, that the original mineralogy of the facies ('aragonite' vs. 'calcite') exerted the dominant control on trace element chemistry of the rocks, a feature not yet completely overprinted by post-depositional phenomena. This suggests that, when considering the trace element contents of carbonates, the post-depositional alteration has occurred in environments where the rock was buffering the fluids (low water/rock ratio). This was probably partially the case also for carbon isotopes. For oxygen isotopes, however, this is an unlikely proposition, since oxygen in water far exceeds the amount of oxygen originating from dissolution of carbonates (cf. Veizer, 1983a). If so, oxygen isotopes will be the most likely tracer to show an open system (high water/rock ratio) behaviour and thus reflect any post-depositional gradients in temperature.

Oxygen and carbon isotopes appear to become lighter towards the western Belt basin (Figure 4-10). The Middle Belt Carbonate units of similar 'alteration' degrees (Mn and Sr

concentration; Figures 4-2, 4-3) have lighter $\delta^{18}O$ and $\delta^{13}C$ in the western section (Wallace Formation) than in the east (Siyeh and Helena Formation, Figure 4-12). The regional variation in $\delta^{18}O$ allows a division of the Belt basin at $\delta^{18}O$ = 19 $^{0}/_{00}$ SMOW, with projection of this division onto a map of the Belt basin delineating regions of relatively depleted and enriched oxygen isotopic composition for limestones (Figure 4-11). Dolostones, as will be shown later, fit this pattern as well. The overall 6-8 $^{0}/_{00}$ shift in $\delta^{18}O$ between east and west would indicate a temperature difference of some 24-32^{0} C, perhaps related to the < 1 km greater overburden in the western part. This estimate is, however, dependent on the $\delta^{18}O$ of fluids involved in the deep burial alteration and the temperature differences could have been therefore more or less than the above value. Other formations have not been sampled at sufficient density to allow similar contouring of isotope values.

I did not observe any ^{18}O depletion with increasing depth, as would be expected if oxygen isotope signatures of limestones had been reset at the elevated temperature calculated by Maxwell and Hower (1967) and Eslinger and Savin (1973). Even for a single area, with no regional overprint, this was not the case. For example, in the Glacier National Park section (Figure 4-11) the stratigraphically deeper Siyeh Formation has actually a heavier oxygen isotopic signature

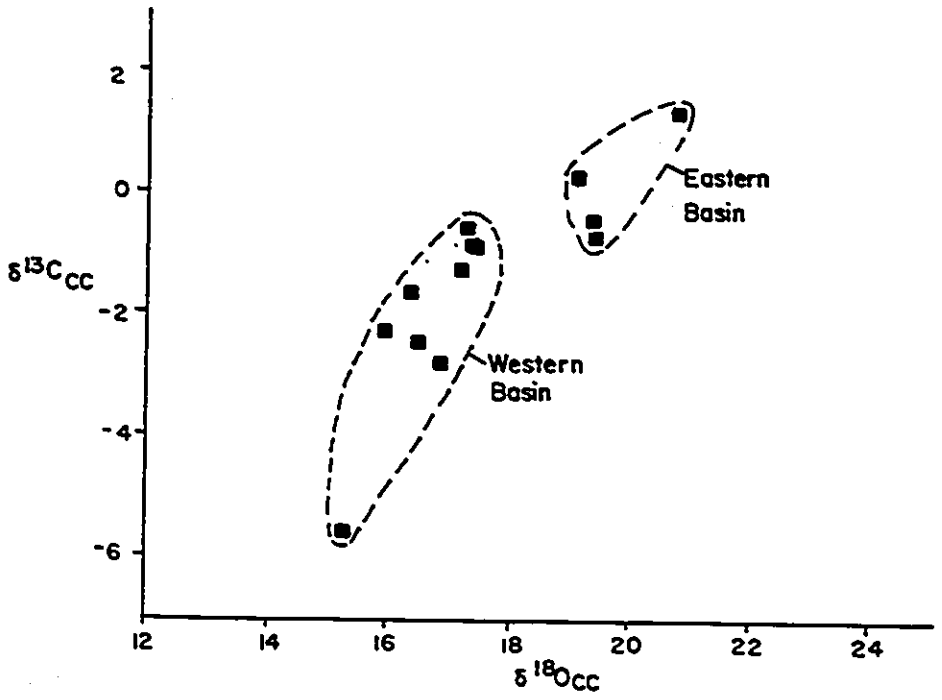

Figure 4-12
$\delta^{18}O$ (SMOW) vs. $\delta^{13}C$ (PDB) of Middle Belt Carbonate samples from the eastern (Red Mountain and Glacier Park) and western (Big Hole Peak) portions of the Belt basin. See Figure 4-11 for the location of these sections.

than the overlying, partly dolomitized, Shepard Formation. This is in accord with the trace element contents of the carbonates, with the latter sequence having higher Mn concentrations and thus a higher degree of diagenetic alteration. Consequently, diagenesis along with secular variations and not later burial metamorphism are the primary controls of isotopic ratios in these carbonates.

$\delta^{13}C$ variations show a trend of ^{13}C depletion westward in the Belt basin, as did ^{18}O. There is a regional decrease from the east to the west of 1.1 $^{0}/_{00}$ when considering mean $\delta^{13}C$ values of the eastern and western facies of the Middle Belt Carbonate (Figure 4-12). For single samples of this sequence the greatest E-W depletion is > 3 $^{0}/_{00}$. It is improbable that temperature differences alone created this depletion if the dominant carbon species in solution was HCO_3^-, unless the ambient temperature was less than 15^0 C in the eastern and greater than 400^0 C in the western basin (cf. Emrich et al., 1970, for temperature dependence of carbon isotope fractionation). The $\delta^{13}C$ of pure carbonate is commonly changed little from its initial value during diagenesis (Veizer et al., 1980) and even during metamorphism (Shieh and Taylor, 1969; Sheppard and Schwartz, 1970). The necessity for a ^{12}C source in the western Basin, coupled with the evidence of higher temperatures, suggests a greater contribution of CO_2 from thermal decomposition of organic carbon during deep

burial (McKirdy and Powell, 1974; Eichman and Schidlowski, 1975; Hoefs and Frey, 1976).

4.2 Diagenesis of Belt Dolostones

Factor analysis of Belt dolostones yields 4 factors (Table 4-2). In the first factor, which explains 30.6% of the variance, increase in insoluble residue correlates positively with increasing Al and Fe content and ^{13}C enrichment. The second factor shows a positive correlation of Ca, Mg and Sr and explains 19.6 % of the variance. Factors 1 and 2 are complementary; factor 1 represents the insoluble fraction of the samples (with concomitant leaching of Al and Fe from this fraction) while factor 2 represents the soluble rock fraction, which in this case is dolomite. The link of Sr with factor 2 is probably due to Sr substitution for Ca in the dolomite lattice.

Factor 3, the negative correlation of Mn with Sr, Na and $\delta^{13}C$, accounts for 15.3% of the variance. This relationship is typical of carbonate diagenesis (Figure 3-2). A standard scatter plot of Sr/Ca vs. Mn shows that dolostones were significantly altered during post-depositional recrystallization (Figure 4-13). Dolostones of all formations plot near or below the field for Middle Belt limestones. The oldest and easternmost Altyn Formation has the least Mn content and is thus the 'least altered'. The stratigraphically

Table 4-2

Varimax Rotated Factor Analysis for Belt Dolostones

Variable	Factor 1	Factor 2	Factor 3	Factor 4	Communality
% Soluble	-0.79	0.02	-0.04	0.14	0.66
log Ca	0.11	0.89	-0.10	0.12	0.84
log Mg	-0.25	0.86	0.05	0.02	0.81
log Mn	0.48	-0.25	-0.61	-0.03	0.76
log Sr	0.13	0.49	0.48	-0.54	0.79
log Al	0.90	0.12	0.12	0.01	0.84
log Na	0.25	-0.17	0.78	-0.18	0.75
log Fe	0.70	-0.18	-0.15	0.06	0.56
$\delta^{18}O$ do	0.00	0.14	0.05	0.91	0.86
$\delta^{13}C$ do	-0.56	0.04	0.65	0.32	0.85
Eigenvalue	3.06	1.95	1.53	1.20	
% Variance Explained	30.6	19.6	15.3	12.0	

N = 28
Underlined loadings are those that are dominant

Interpretation:
Factor 1 Laboratory leaching of siliciclastics
Factor 2 Presence of dolomite (carbonate content)
Factor 3 Post-depositional recrystallization
Factor 4 Intraformational overprint of variations within the Middle Belt Carbonate

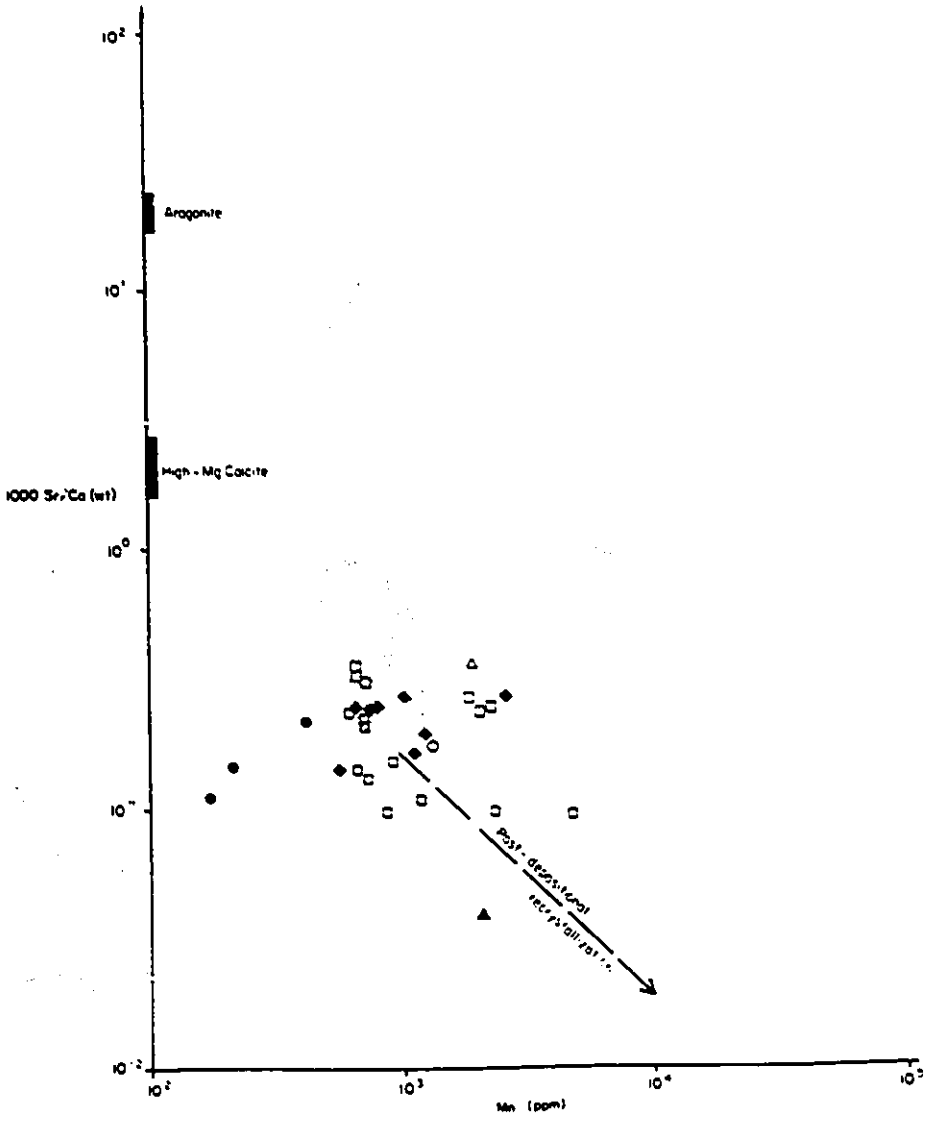

Figure 4-13
Scatter diagram of Sr/Ca vs. Mn in the Belt Dolostones. The shaded patterns represent the Libby, Newland and Middle Belt Carbonate limestone fields (Figure 4-4). ●- Altyn Fm., -□ Middle Belt Carbonate, ◆- Mt. Shields Fm., ▲- Libby Fm., △- Shepard Fm., ○ - Snowslip Fm.

higher Middle Belt and Mt. Shields dolostones are intermediate. Finally, one sample from the uppermost Libby Formation falls at the most altered terminus of this trend (Figure 4-13). Thus, as for limestones, the alteration rank increases upwards stratigraphically, or in reality from east to west. $\delta^{13}C$ is controlled by progressive post-depositional alteration as measured by increasing Mn concentrations (Figure 4-14). The least altered population, the Altyn Formation, gives a 'best' $\delta^{13}C$ value for Belt dolostones of + 1.9 $^{0}/_{00}$ PDB, close to that of the least altered limestone population and to modern carbonate sediments.

The fourth factor links Sr with $\delta^{18}O$ and accounts for 12 % of the variance (Table 4-2). ^{18}O depletion is accompanied by increasing Sr content (Figure 4-15). The negative correlation of Sr and $\delta^{18}O$ is probably due to the overwhelming influence of the Middle Belt Carbonate population, which contains the bulk of the samples, but the reason for this correlation is unknown. Accepting that Altyn dolostones represent the least altered group of samples (see discussion of factor 3), the best sample has $\delta^{18}O$ = 27.9 $^{0}/_{00}$ SMOW (AF/AL-1). This is 5 $^{0}/_{00}$ heavier than the least altered Belt limestone, but the difference is within the limits of uncertainty for theoretically predicted dolomite/calcite fractionation.

The pattern of covariant $\delta^{18}O$ and $\delta^{13}C$ noted in the Belt limestones is repeated in dolostones (Figure 4-16). Again, the

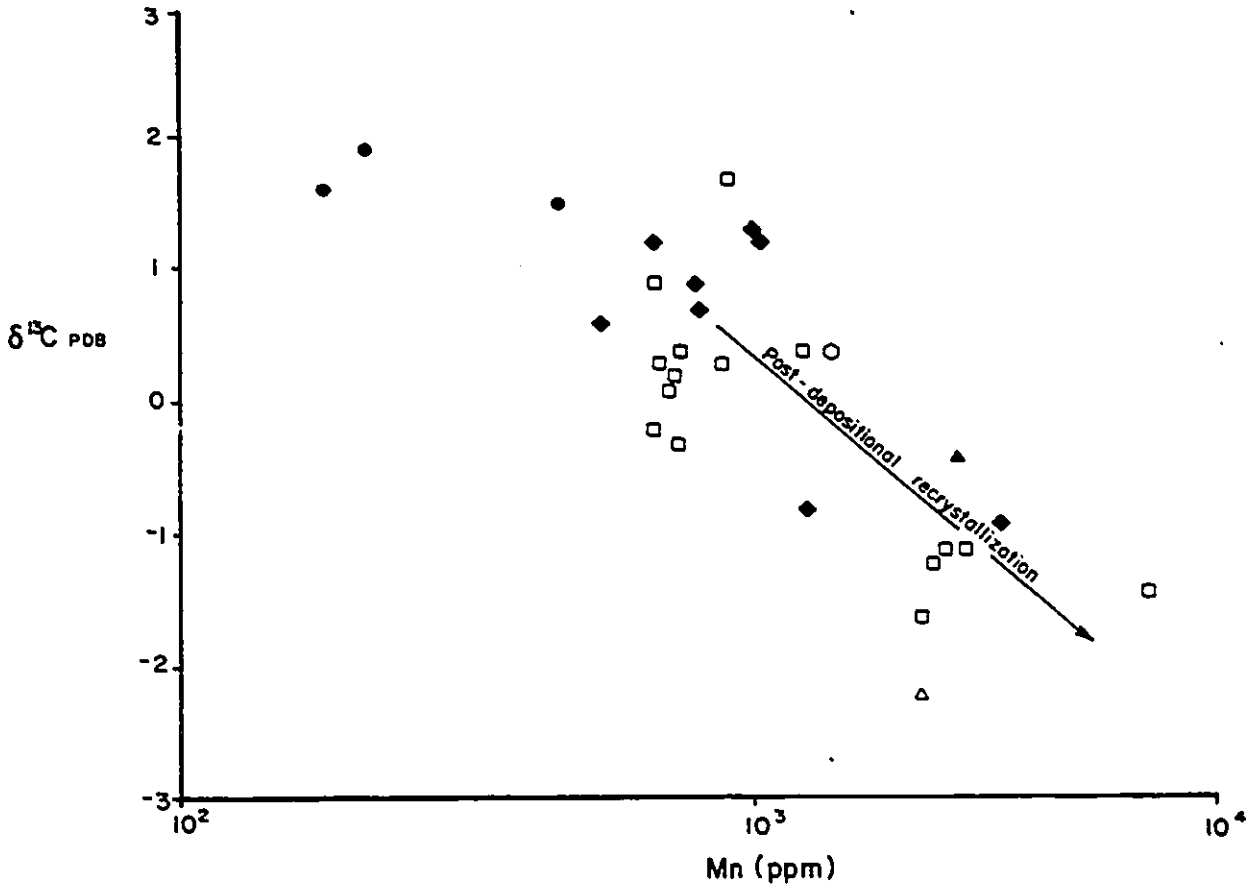

Figure 4-14
Scatter diagram of $\delta^{13}C$ vs. Mn (ppm) for the Belt dolostones. ● - Altyn Fm., □ - Middle Belt Carbonate, ◆ - Mt. Shields Fm., ▲ - Libby Fm., △ - Shepard Fm., ○ - Snowslip Fm.

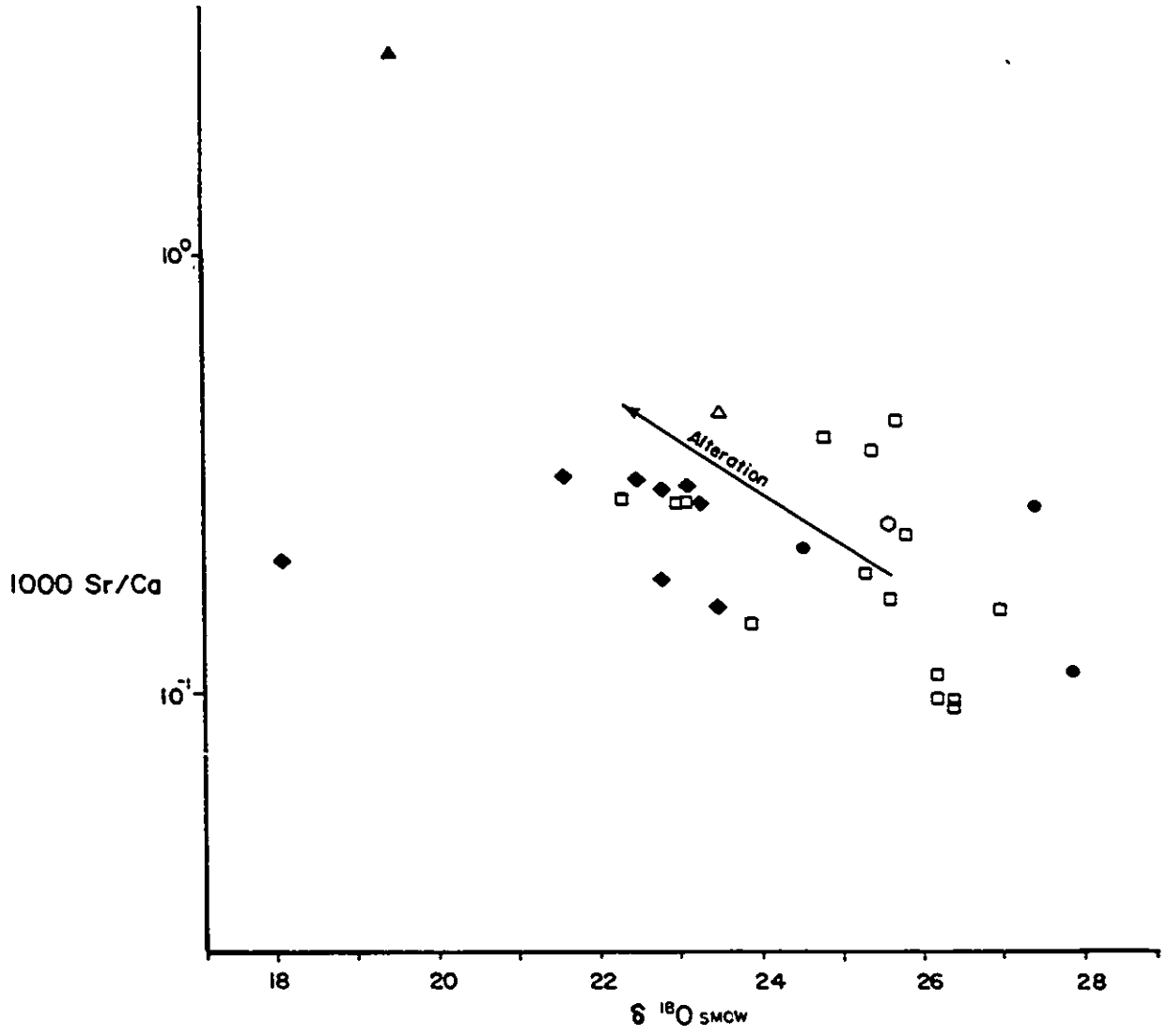

Figure 4-15
Scatter diagram of Sr/Ca (wt.) vs. $\delta^{18}O$ for the Belt dolostones. ● - Altyn Fm., □ - Middle Belt Carbonate, ◆ - Mt. Shields Fm., ▲ - Libby Fm., △ - Shepard Fm., ○ - Snowslip Fm.

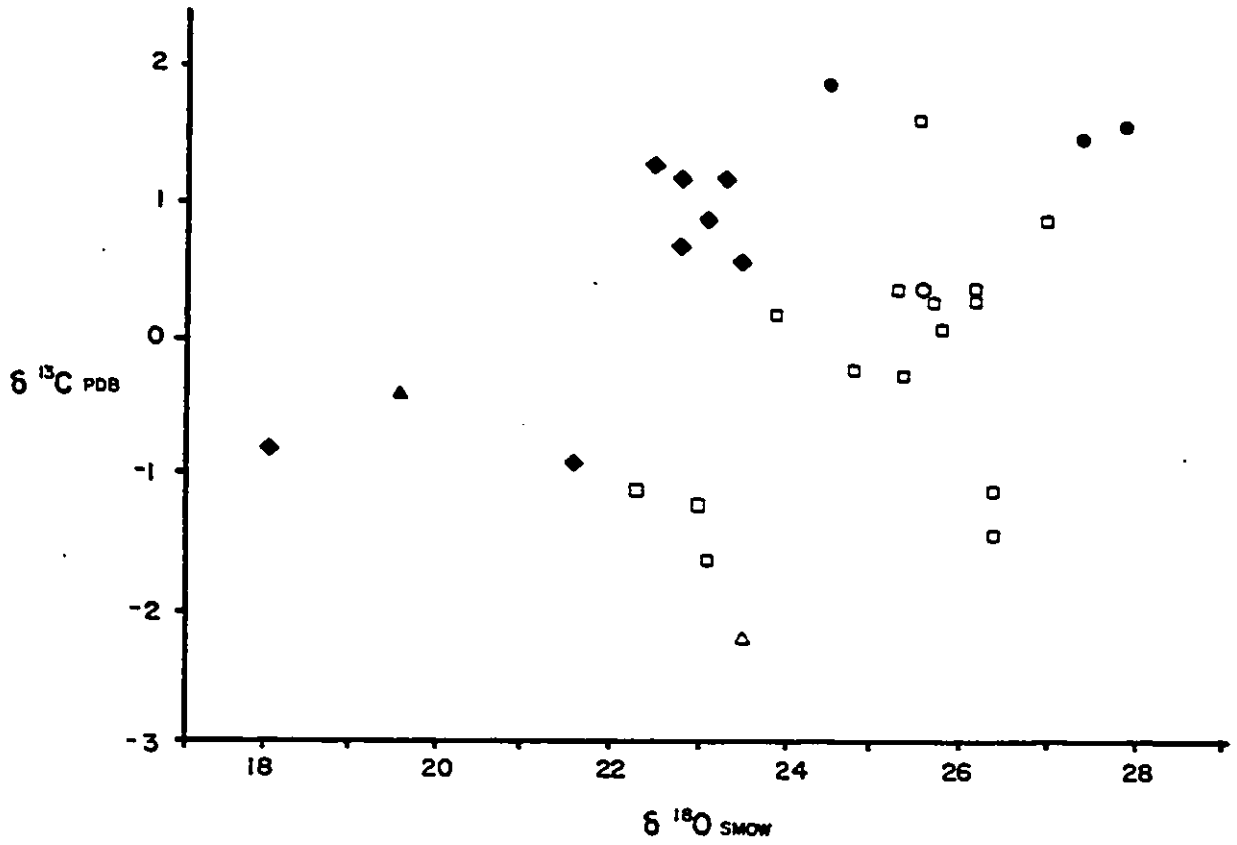

Figure 4-16
Scatter diagram of $\delta^{18}O$ vs. $\delta^{13}C$ for the Belt dolostones.
●- Altyn Fm., □- Middle Belt Carbonate, ◆- Mt. Shields Fm.,
▲- Libby Fm., △- Shepard Fm., ○ - Snowslip Fm.

Altyn Formation, representing the stratigraphically oldest and easternmost population of Belt dolostones, is least altered with heaviest ^{18}O and ^{13}C. Post-depositional recrystallization resulted in depletion of ^{18}O and ^{13}C, with regional variations superimposed on this pattern. Dolostones of the Libby and Mt. Shields Formations, the youngest populations, were collected in the western Belt basin and show the greatest ^{18}O depletion (Figure 4-16), while dolostones of the Middle Belt Carbonate are intermediate. As with limestones, this is evidence for recrystallization of carbonates under higher temperature conditions in the western Belt basin.

4.3 Diagenesis of Dolomitic Limestones

Trace element and isotope variations of Belt carbonate samples of mixed dolomite and calcite composition are used only to verify the conclusions drawn from 'pure' dolomite and calcite populations. Factor analysis of carbonates of mixed composition yields 3 factors (Table 4-3). Factor 1, accounting for 30.7 % of the total variance, is interpreted to represent the dolomite/calcite ratio of the samples (Mg/Ca, Sr/Ca) which, in turn, controls also $\delta^{18}O$. Factor 2, accounting for 24.2% of the total variance, reflects the effect of insoluble residue on trace element composition via laboratory leaching of Al, Na and Fe from insoluble silicates.

Table 4-3

Varimax Rotated Factor Analysis Dolomitic Limestones

Variable	Factor 1	Factor 2	Factor 3	Communality
% Soluble	0.21	-0.86	0.17	0.82
log Ca	-0.82	-0.21	0.04	0.73
log Mg	0.88	-0.06	-0.03	0.79
log Mn	0.09	0.01	-0.71	0.52
log Sr	-0.07	0.12	-0.01	0.51
log Al	-0.01	0.89	0.00	0.79
log Na	0.02	0.82	-0.14	0.69
log Fe	0.39	0.56	-0.23	0.52
$\delta^{18}O$ cc	0.68	0.02	0.60	0.84
$\delta^{13}C$ cc	0.03	-0.10	0.73	0.54
$\delta^{18}O$ do	0.45	-0.14	0.63	0.63
$\delta^{18}O$ do	-0.11	-0.31	0.87	0.88
Eigenvalue	3.68	2.89	1.73	
% Variance Explained	30.7	24.2	14.5	

N = 87 for trace elements and % soluble
N = 82 for $\delta^{18}O$ cc and $\delta^{13}C$ cc
N = 65 for $\delta^{18}O$ do and $\delta^{18}O$ do

Underlined loadings are statistically dominant.

Interpretation:
Factor 1 Dolomite/Calcite ratio
Factor 2 Laboratory leaching
Factor 3 Burial diagenesis

Factor 3 links increasing Mn content with depletion of ^{18}O and ^{13}C (Figures 4-17, 4-18). The general pattern of alteration once again shows progressively more profound post-depositional alteration in upper than in the lower Belt Formations (Figures 4-17, 4-18, 4-19, 4-20). The least altered samples from the mixed population yield $\delta^{18}O_{CALCITE}$ = 25 $^{0}/_{00}$ SMOW, about 2 $^{0}/_{00}$ heavier than that of the least altered limestone. $\delta^{18}O_{CALCITE}$ in this mixed population is probably influenced by ^{18}O derived from partial dissolution of dolomite during the reaction with phosphoric acid (Appendix C). This is illustrated by a plot of Mg/Ca vs. $\delta^{18}O$ (Figure 4-21) which shows that $\delta^{18}O_{CALCITE}$ increases with the increasing proportion of dolomite in the sample, while $\delta^{18}O_{DOLOMITE}$ is unaffected by the Mg/Ca ratio. $\delta^{18}O$ selected from the least altered sample in the limestone population is therefore determined to be a better approximation of the original value of Belt limestones. The best estimate of initial $\delta^{13}C$ derived from this mixed population is, as with the limestone and dolostone populations, close to 2 $^{0}/_{00}$ PDB (Figures 4-18, 4-19). There appear to be secular variations of $\delta^{13}C$ superimposed on alteration trends. The Spokane-Greyson and perhaps the Libby and Newland Formations may have originally contained $\delta^{13}C$ = 2 $^{0}/_{00}$ heavier than that of the Middle Belt Carbonate, as determined by comparison of samples of similar alteration rank (Figures 4-18, 4-19). In contrast to all Belt samples, the

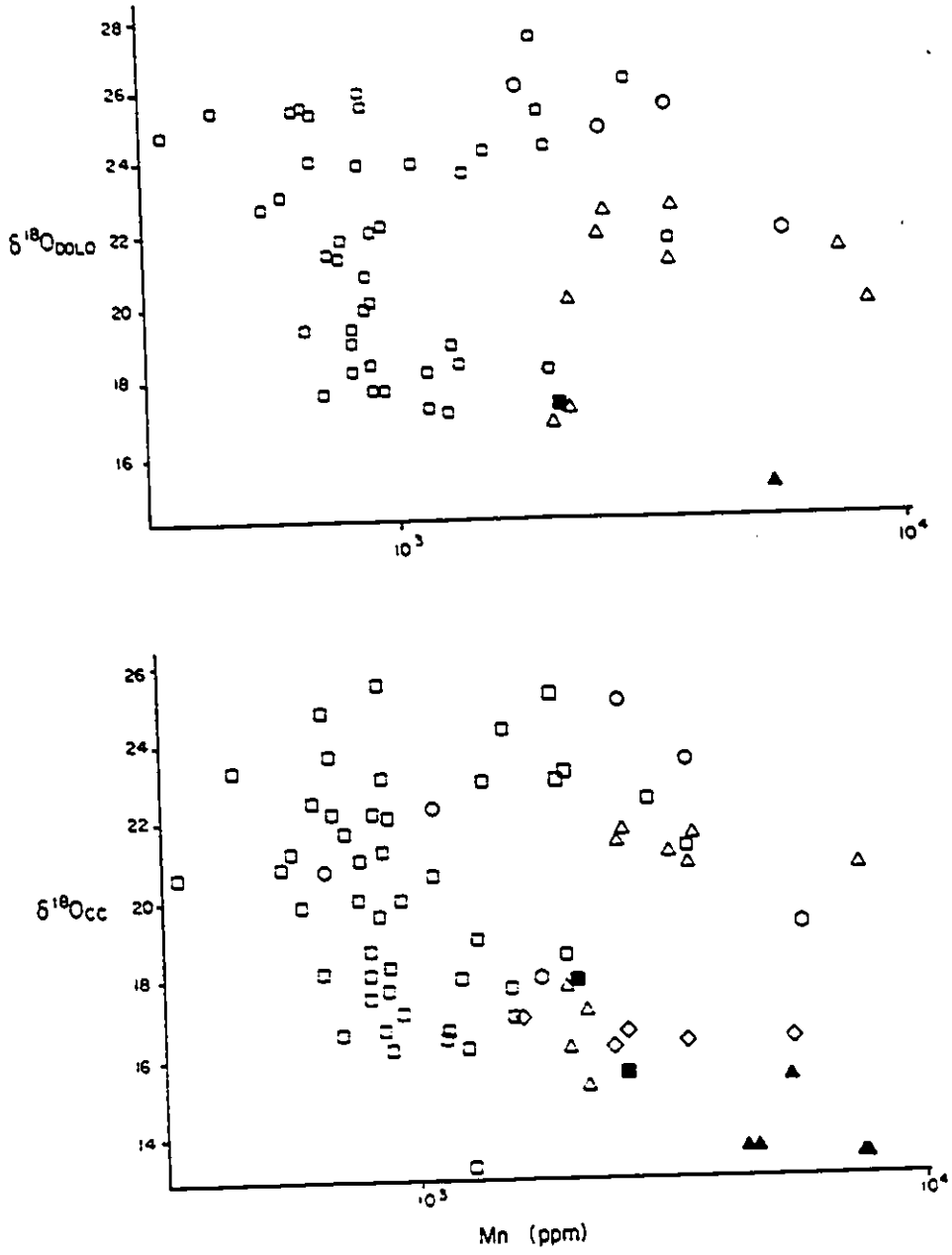

Figure 4-17
Scatter diagram of Mn vs. $\delta^{18}O$ SMOW (cc-calcite, and dolo-dolomite) for the mixed dolomite/calcite population. △-Shepard Fm., ▲-Libby Fm., ○-Snowslip Fm., ■-Empire Fm., ○-Newland Fm., ◇-Spokane/Greyson transition, □-Middle Belt Carbonate

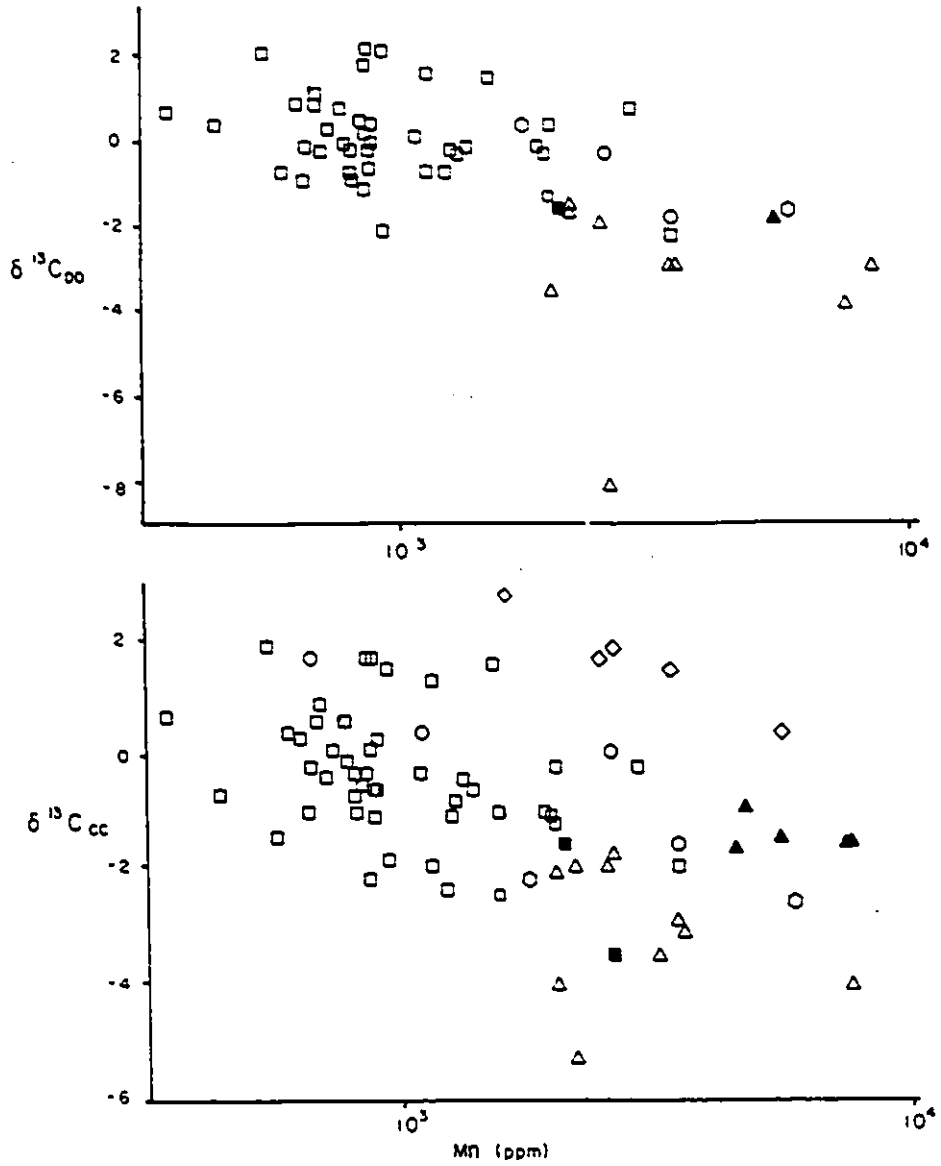

Figure 4-18
Scatter diagram of Mn and $\delta^{13}C$ PDB (cc-calcite, and do-dolomite) for the mixed dolomite/calcite population. △-Shepard Fm., ▲-Libby Fm., ○-Snowslip Fm., ■-Empire Fm., ○-Newland Fm., ◇-Spokane/Greyson transition, □-Middle Belt Carbonate

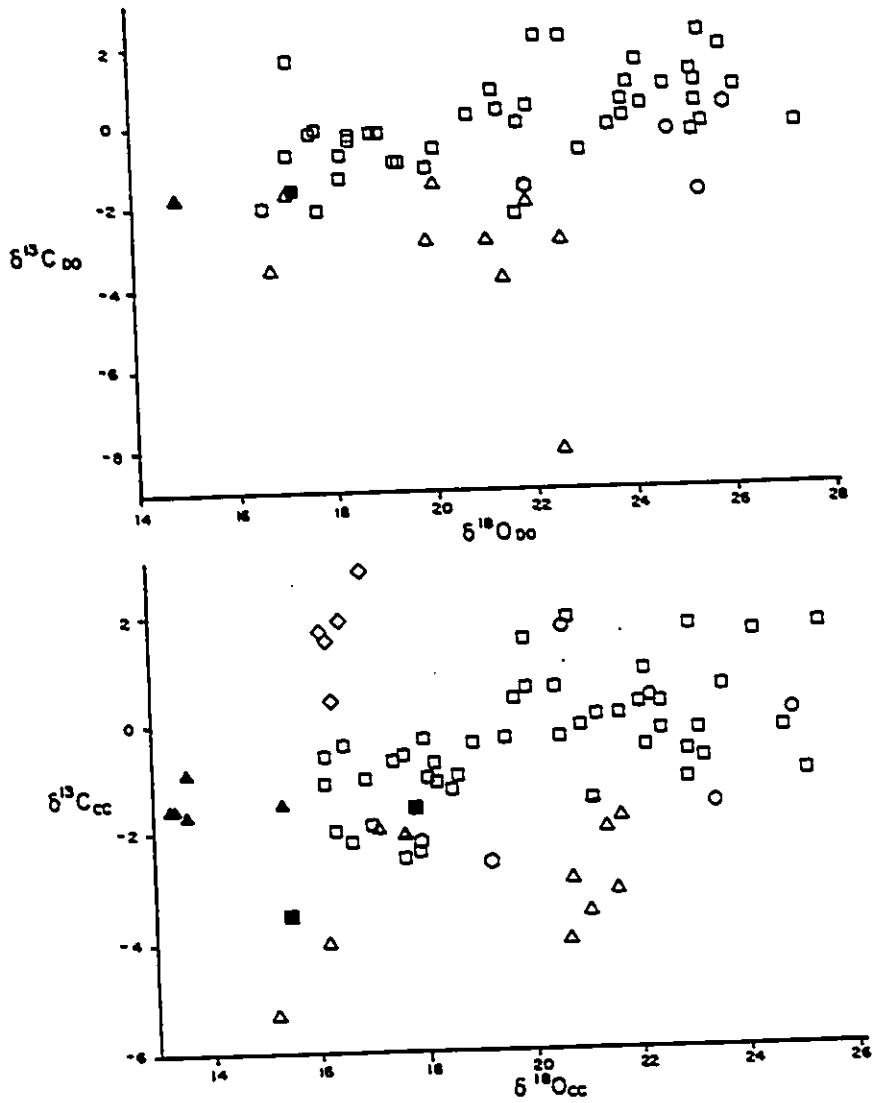

Figure 4-19
Scatter diagram of $\delta^{18}O$ (SMOW) vs. $\delta^{13}C$ (PDB) for calcite (cc) and dolomite (do) fractions of samples of mixed dolomite and calcite composition. △-Shepard Fm., ▲-Libby Fm., ⬡-Snowslip Fm., ■-Empire Fm., ○-Newland Fm., ◇-Spokane/Greyson transition, □-Middle Belt Carbonate

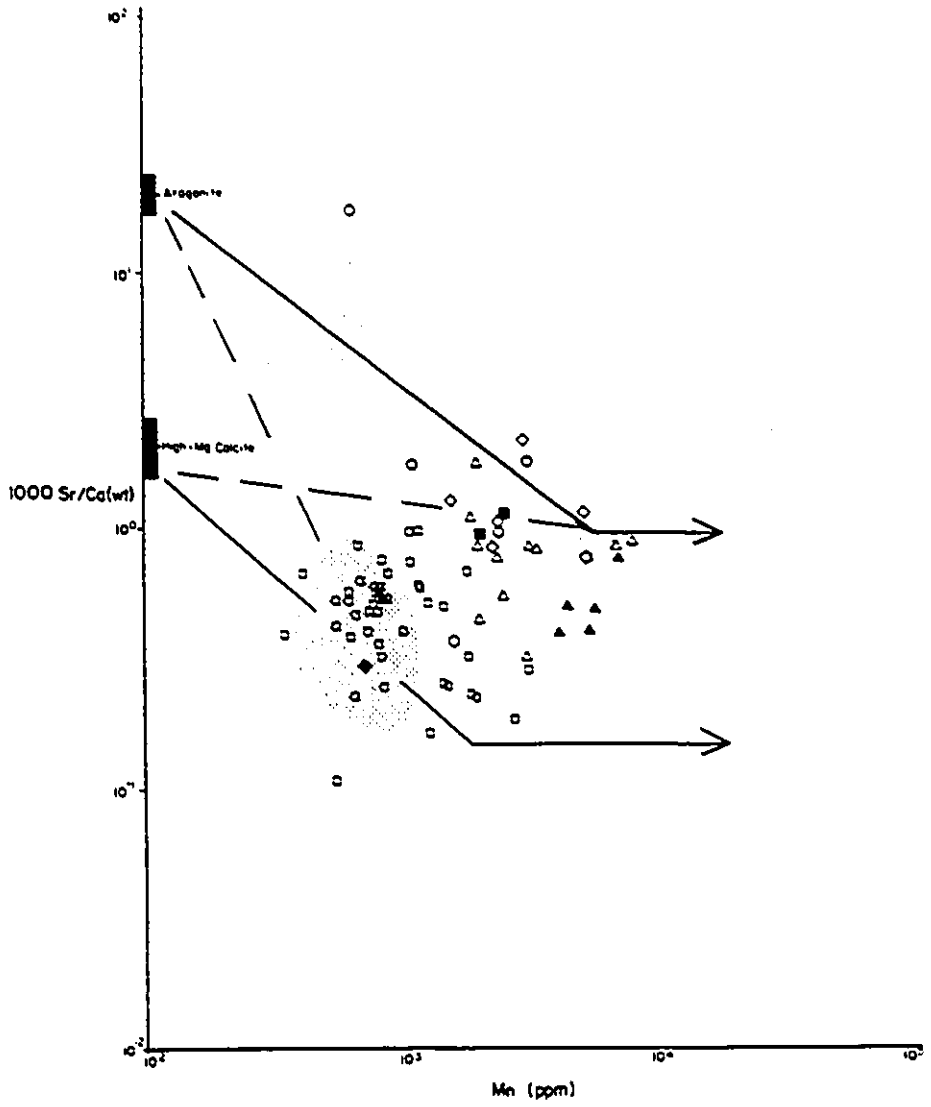

Figure 4-20
Scatter diagram of Sr/Ca vs. Mn for the mixed dolomite - calcite samples of the Belt Supergroup. The Libby, Newland and Middle Belt Carbonate Fields are those of Belt limestones (Figure 4-4). △-Shepard Fm., ▲-Libby Fm., ○-Snowslip Fm., ■-Empire Fm., ○-Newland Fm., ◇-Spokane/Greyson transition, □-Middle Belt Carbonate

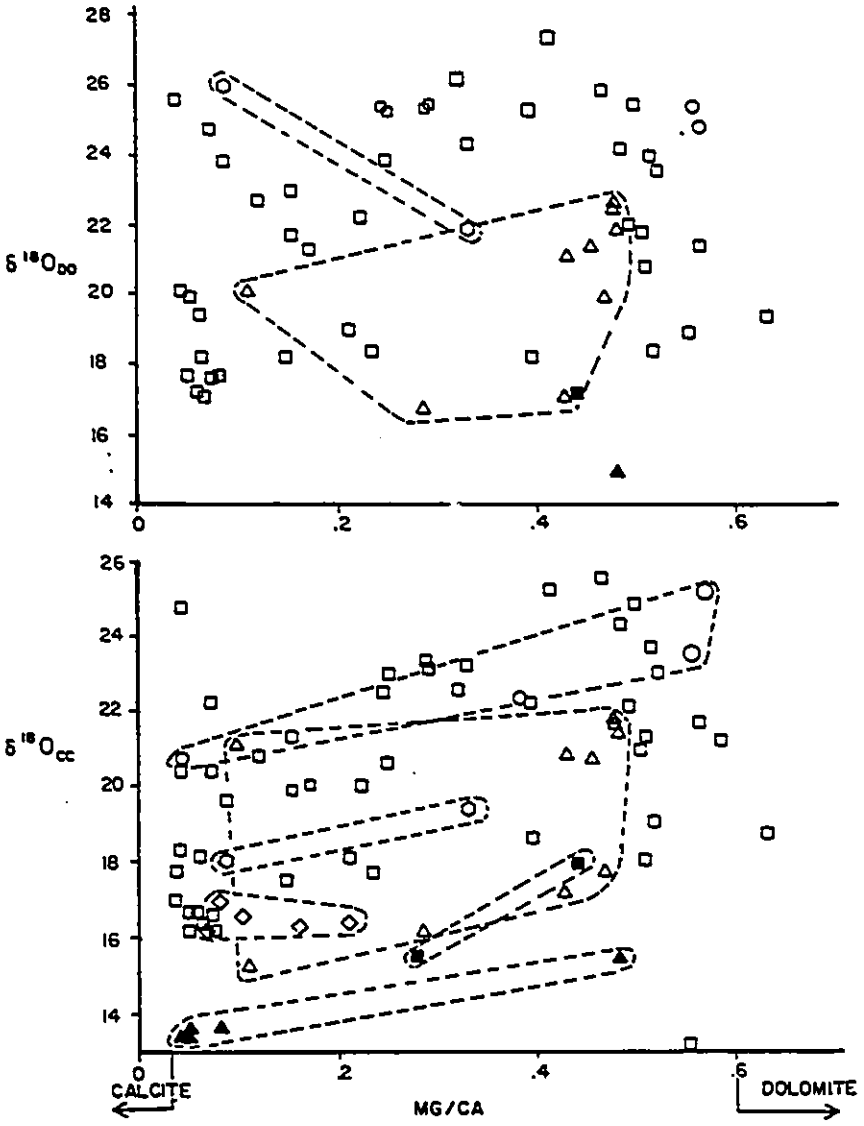

Figure 4-21
Percent dolomite, as measured by Mg/Ca (wt.) ratio, vs. $\delta^{18}O$ (SMOW) variations of the dolomite and calcite fractions of mixed dolomite/calcite Belt samples. △-Shepard Fm., ▲-Libby Fm., ○-Snowslip Fm., ■ -Empire Fm., ○-Newland Fm., ◇-Spokane/Greyson transition, □-Middle Belt Carbonate

Shepard Formation seems to record a ^{13}C depletion of ≈ 2 $^{0}/_{00}$ (Figures 4-18, 4-19). Intraformational variations of $\delta^{13}C$, independent of alteration rank, noted in both limestone and mixed dolomite-limestone populations, appear to record secular variations in $\delta^{13}C$ of up to 4 $^{0}/_{00}$. $\delta^{13}C$ variations of this magnitude observed throughout the rock record are thought to represent variations in the relative sizes of the organic vs. inorganic carbon reservoirs at different times during geologic history (Veizer et al., 1980; Schidlowski et al., 1983). This may also be the case for the Belt carbonates.

4.4 Oxygen and carbon isotope composition of depositional fluids

The possible range for oxygen isotope compositions of the depositional fluids can be calculated from consideration of the most and the least altered carbonates combined with reasonable formational temperature estimates (Maxwell and Hower, 1967; Eslinger and Savin, 1973). Assuming the temperature range of 10 to 350^{0} C, $\delta^{18}O$ of 22.9 $^{0}/_{00}$ SMOW for the least altered sample from the limestone population (Newland sample DG-3), 13.4 $^{0}/_{00}$ for the most altered limestone of the 'aragonite trend' (Libby sample FC-431) and 15.3 $^{0}/_{00}$ for the most altered limestone of the 'calcite trend' (Middle Belt Carbonate sample BHP-7), the possible range for oxygen isotopic values for depositional fluids of the Belt basin

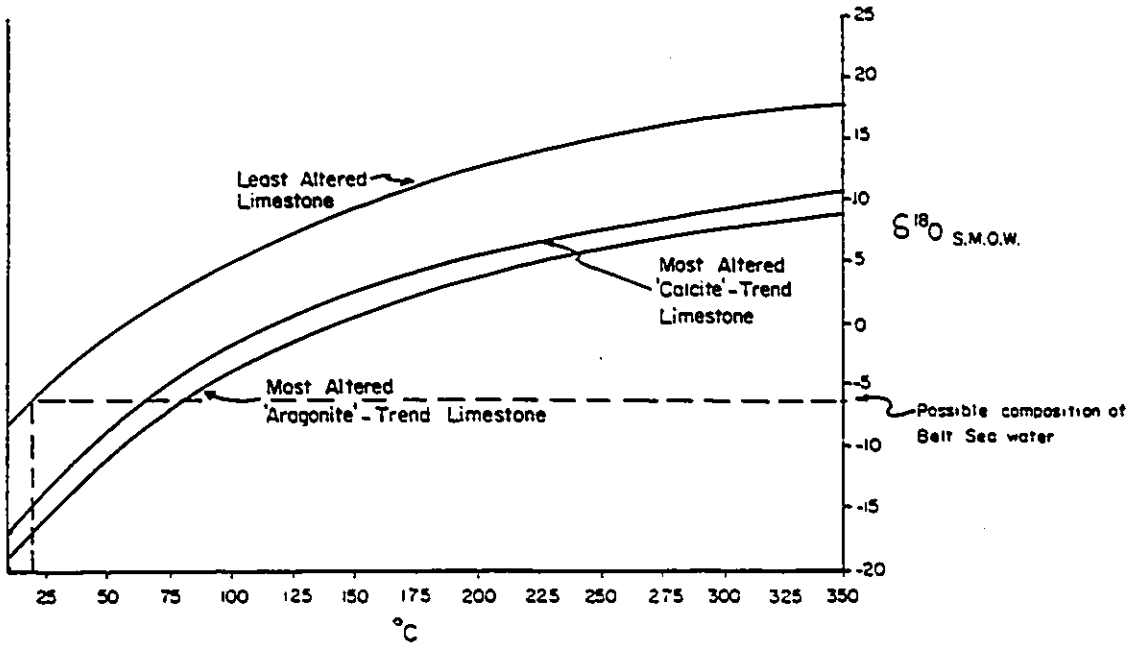

Figure 4-22
Ranges of possible oxygen isotopic compositions for depositional fluids of the Belt Supergroup limestones. The least altered limestone trend most closely approximates the $\delta^{18}O$ of the Proterozoic Belt Sea. The most altered limestone samples for carbonates of originally aragonite or calcite composition are the maximal $\delta^{18}O$ compositions of diagenetic fluids.

facies is approximated in Figure 4-22. Because the oxygen isotope fractionation for dolomites is not well understood at low temperatures (< 300° C), samples containing > 10% dolomite are not considered. Assuming a depositional temperature of about 20° C, the least altered carbonate indicates a depositional fluid (seawater) with oxygen isotope composition of -7 °/₀₀ SMOW (Figure 4-22), considerably lower than that of modern seawater. For comparison, diagenetic fluids might have ranged from -20 to 11 °/₀₀ SMOW, depending on the temperature of diagenetic equilibration (Figure 4-22). $\delta^{13}C$ value of depositional fluids was close to 2 °/₀₀, close to that of the modern ocean.

Chapter 5

Strontium Isotope Geochemistry of Belt Carbonates

5.1 Strontium isotope systematics

Strontium is incorporated into carbonate minerals with negligable isotopic fractionation (Peterman, et al., 1970). Thus the isotopic composition of unaltered calcite is a direct measure of the isotopic composition of the water from which it was precipitated. ^{87}Sr is generated by the beta decay of ^{87}Rb, therefore if there is significant Rb within the originally deposited carbonate, the decay of ^{87}Rb will increase the $^{87}Sr/^{86}Sr$ ratio of the carbonate with time. Fortunately, Rb is rarely found in pure carbonate minerals (Veizer, 1983a) and the effect of Rb decay on Sr isotope composition in unaltered carbonates can usually be discounted.

The $^{87}Sr/^{86}Sr$ ratio of the modern ocean is uniform, 0.70912 ± 0.00003 when standardized for an Eimer and Amend standard of 0.70802 (Burke et al., 1982). In the subsequent discussion, an E & A standard of 0.70802 and NBS 987 standard value of 0.71023 will be adopted. The uniform $^{87}Sr/^{86}Sr$ ratio of the modern ocean is due to the long residence time of Sr in the oceans (4-5 x 10^6 years; Holland, 1978) as compared to the mixing time of the oceans of 10^3 years (Broecker, 1963; Goldberg, 1963). The major Sr fluxes affecting the $^{87}Sr/^{86}Sr$ ratio of modern as well as ancient oceans are 1) input from river water (F^c), 2) removal

of Sr by formation of sediments (F^s) and diagenetic reflux of their Sr to the oceans (F^D), 3) cycling of ocean water through hot and cold (< 300°C) MOR basalt (F^R). Figure 5-1 illustrates these fluxes, their relative magnitudes as well as their Sr isotopic ratios. The controlling fluxes of the isotopic composition of strontium in the ocean appear to have been the input from river water and the cycling of ocean water through MOR basalts. The average dissolved Sr concentration of river water is 0.068 ppm, and in the oceans it is 7.7 ppm (Faure, 1986). The input of Sr into the ocean has been estimated to be 2.24×10^{12} g yr^{-1} (Wadleigh et al., 1985) and the total amount of Sr in the ocean is 1.06×10^{19} g (calculated using information from Goldstein and Jacobsen, 1987). Consequently, the Sr composition of seawater is not affected by river water flux over short time intervals.

The Sr isotopic composition of river water is controlled by the Sr isotopic composition of the rocks comprising the drainage area of the river system. The average strontium isotope ratio of continental flux, as measured by dissolved Sr in modern river waters is 0.7111 (Wadleigh, 1982) to 0.7101 ± 0.0005 (Goldstein and Jacobsen, 1987). The $^{87}Sr/^{86}Sr$ of the major rivers of the world ranges from 0.7060 for the Nile to 0.7156 for the Nelson River (Goldstein and Jacobsen, 1987). Smaller rivers with more limited catchments range from 0.704 to 0.738 (Wadleigh et al., 1985; Goldstein and Jacobsen,

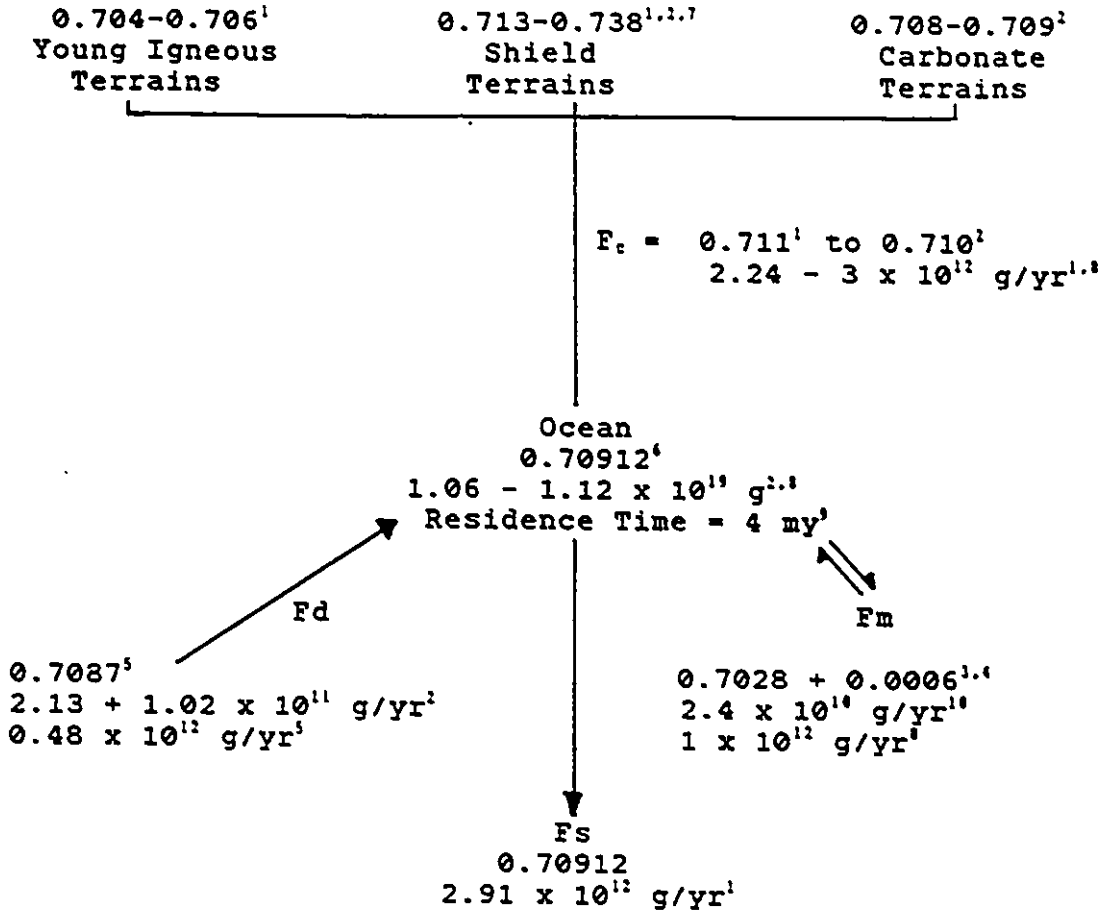

Figure 5-1
Major fluxes of the strontium cycle, Fc - continental (dissolved river) flux , Fm - flux through hot MOR basalt, Fd - diagenetic flux from sediments, Fs - sedimentary flux via sedimentation. [1] - Wadleigh *et al.*, (1985); [2] - Goldstein and Jacobsen, (1987); [3] - Hoffman and Hart, (1978); [4] - Albarede *et al.*, (1981); [5] - Elderfield and Gieskes, (1982); [6] -Burke *et al.*, (1982); [7] - Brass, (1976); [8] - DePaolo, (1987); [9] - Holland, (1978); [10] - Modified from Morton and Sleep, (1985) as suggested by Goldstein and Jacobsen, (1987). Standards are E. and A. = 0.70802 and NBS 987 = 0.71023.

1987). The uniformity of values for the major rivers of the world (0.7110 for the Amazon, 0.7101 for the Mississippi, 0.7111 for major Canadian rivers, 0.7112 for the Indus; Brass, 1976, Wadleigh et al., 1985, Goldstein and Jacobsen, 1987) is probably not coincidental but represents an average isctopic composition of Sr weathered from the dominant rock types in the world today. A river drainage dominated by young igneous rocks has a $^{87}Sr/^{86}Sr$ ratio of 0.704-0.706, for carbonate dominated drainages this ratio is 0.708-0.709 and shield terrains produce river waters with $^{87}Sr/^{86}Sr$ ratios from 0.713 to 0.738 (Brass, 1976; Wadleigh et al., 1985; Goldstein and Jacobsen, 1987). The $^{87}Sr/^{86}Sr$ ratio of rivers varies as tributaries with different isotopic compositions merge. Fisher and Stueber (1976) showed that the $^{87}Sr/^{86}Sr$ of the Susquehanna River changed from 0.7090 to 0.7128 as tributaries draining igneous, sedimentary and metamorphic rocks joined the main river. The concentration of Sr in the tributaries that drain carbonate provenances is higher than in those draining sandstone, schist and granite rocks. If a drainage is only 10% carbonate rock, the carbonate will nonetheless dominate the $^{87}Sr/^{86}Sr$ concentration of the stream that drains it (Faure, 1986). The amount of carbonate available for weathering on a world-wide basis can therefore effectively buffer the $^{87}Sr/^{86}Sr$ ratio of continental flux and, because the Sr ratio of carbonates is similar to that of ocean waters, buffers the

rapid fluctuation of $^{87}Sr/^{86}Sr$ in seawater.

The average $^{87}Sr/^{86}Sr$ of suspended material in rivers today is 0.7133 (Goldstein and Jacobsen, 1987). This strontium is considerably more radiogenic than the $^{87}Sr/^{86}Sr$ of dissolved Sr, the latter probably due to the influence of non-radiogenic $^{87}Sr/^{86}Sr$ derived from carbonates and evaporites.

The $^{87}Sr/^{86}Sr$ ratio of lake waters ranges from 0.7045 to 0.7950 (Goldstein and Jacobsen, 1988) and is highly dependent on the river systems supplying the lakes. Lakes which undergo extreme evaporation may concentrate Sr by precipitation of minerals which exclude it, but the $^{87}Sr/^{86}Sr$ value of the lake will not be changed by this process (Faure, 1986).

The Sr isotopic composition of groundwater and sub-surface brines is controlled by the composition of the original interstitial water, the strontium isotopic composition of the host rocks and by ion exchange reactions with clays in the host rocks. Sr released by diagenetic reactions will further modify the isotopic composition of Sr in ground and formation waters. Pore waters generally become more radiogenic through interaction with host sediments as these rocks are multi-cycle, 'shield'-type sediments with more radiogenic strontium values (Land, 1986; Collerson et al., 1988). Strontium isotope ratios measured from dolomitic rocks are those of the dolomitizing solution, perhaps modified by

dissolving calcite phases (Saller, 1984). Therefore using $^{87}Sr/^{86}Sr$ ratios of dolomitic rocks to determine the strontium isotope ratio of ocean water is suspect (Vahrenkamp et al., 1988).

The isotopic composition of seawater is influenced by Sr isotope exchange with MOR basalts. The concentration of Sr may change little during the cycling of seawater through basalt, although this parameter is poorly constrained, but the isotopic composition of seawater changes dramatically. The measurements of Sr concentration of undiluted and uncontaminated MOR hydrothermal waters ranges from 7.57 ± 1 to 15.3 ppm (Michard et al., 1984; Piepgras and Wasserburg, 1985). The flux of sea water through hot MOR basalts is estimated at 3.2×10^{15} g yr^{-1} as measured by ^{3}He flux (Jenkins et al., 1978; Craig and Lupton, 1981). This estimate may be high as suggested by Bowers and Taylor (1985) and Morton and Sleep (1985). The flux of Sr through hot MOR basalts is then $2.4 - 4.9 \times 10^{10}$ g yr^{-1}. The flux of Sr through cold MOR basalts (submarine weathering) is estimated to be 6.1×10^{11} g yr^{-1} (Holland, 1984). Reevaluation of the Sr isotope average for global river water to a less radiogenic value than previously estimated indicates that the flux of ocean water through submarine basalt may be a factor of 3 lower than estimates based on ^{3}He flux and is calculated to be closer to $2.9 \pm 2.5 \times 10^{14}$ g yr^{-1} (Goldstein and Jacobsen, 1987). The $^{87}Sr/^{86}Sr$

composition of seawater that has reacted with hot MOR basalt is close to that of the unaltered basalt (0.702-0.703; Albarede et al., 1981). Sr isotopic exchange of cold basalts with seawater is poorly understood, but seawater with a less radiogenic isotopic composition (0.705; Holland, 1984) should result from this interaction.

The strontium isotopic composition of calcite changes with diagenetic alteration. Diagenetic carbonate minerals reflect the isotopic composition of the diagenetic fluids. The strontium isotopic composition of this fluid depends on the interaction with both the carbonate and the non-carbonate fractions of the enclosing rock. If the silicate fraction of the rock is dominated by young volcanic clasts, the strontium isotopic ratio of the resulting diagenetic carbonate minerals may be less radiogenic than the original carbonate constituents. In contrast, if the silicates are dominantly from old shield areas, the diagenetic fluids and carbonate minerals formed from these fluids should have a more radiogenic strontium isotopic composition than the original carbonate. The geochemistry of diagenesis in this case predicts, in a very general sense, sediment provenance and vice versa.

5.2 Secular variation of strontium isotopic ratios

The strontium isotopic composition of carbonates, and thus presumably of seawater, has fluctuated throughout the Phanerozoic (Peterman et al., 1970; Veizer and Compston, 1974; Brass, 1976; Burke et al., 1982). These variations likely represent fluctuations in the influence of the two principal fluxes of strontium into the ocean: continental runoff and cycling of seawater through MOR basalts. $^{87}Sr/^{86}Sr$ ratios in a more 'continentally dominated' ocean will be more radiogenic than those in an ocean dominated by cycling of seawater through MOR basalts or continental weathering of young volcanic material. The influence of continental weathering on the strontium isotope composition of the ocean is a function of both the amount and the type of material available for weathering. The contribution of strontium isotopes from MOR cycling is a reflection of the rate of MOR spreading and the volume of MOR exposed. The variations in the Sr isotope curve should therefore be related to global tectonic events (cf. Veizer, 1985).

The strontium isotopic variation of carbonates during the Precambrian is less well known (Veizer and Compston, 1974). The strontium isotopic composition of Precambrian carbonates become more radiogenic with decreasing age (Veizer and Compston, 1976; Veizer et al., 1989b; Figure 5-2). Veizer et al. (1982) relate this pattern to the evolution of the earth's crust. The buildup of

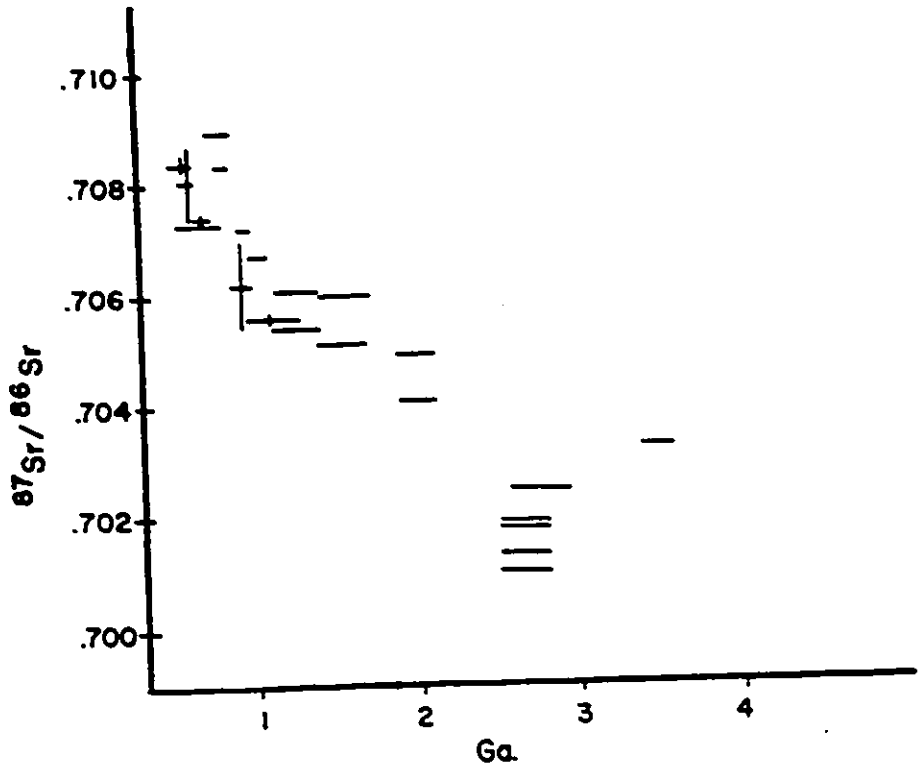

Figure 5-2
Variations of $^{87}Sr/^{86}Sr$ of Precambrian marine carbonates. Constructed from data of Veizer and Compston (1976), Veizer et al. (1983) Demaiffe and Fieremans (1981) and Veizer, 1989b, modified from Faure (1986). Normalized to E. and A. standard = 0.70800, NBS SRM 987 = 0.71014. Although the standards used in this figure are not the same as those used in treatment of raw data elsewhere, this variation is inconsequential when considering the scale of the diagram.

continents, and thus of rivers, in the Proterozoic is reflected in 'continental' $^{87}Sr/^{86}Sr$ of carbonates. The return of strontium ratios to more magmatic values in the Phanerozoic reflects the importance of plate tectonics, specifically the rapid cycling of seawater through MOR basalts and increased F^C from tectonically active (young) continental margins. Alternately this may be an artifact of better time resolution in Phanerozoic age rocks.

Strontium isotope evaluations of Proterozoic carbonates is still scarce with time resolution still only about 75 ± 25 Ma. (Veizer et al., 1983). As more Proterozoic basins are studied and the data base of chemically evaluated rocks increases, patterns of $^{87}Sr/^{86}Sr$ variation similar in magnitude and frequency to those determined for the Phanerozoic may emerge. Because of problems with time resolution in Proterozoic rocks, these patterns may never be as clear as they are in Phanerozoic rocks.

5.3 Strontium isotope systematics of Belt carbonates

The $^{87}Sr/^{86}Sr$ values of Belt carbonates range between 0.70484 and 0.74991 with a mean value of 0.72309 as normalized to an E. and A. standard of 0.70802 and NBS-987 of 0.71023 (Table 5-1). The observed $^{87}Sr/^{86}Sr$ ratios are least radiogenic at the base of the stratigraphic section (Newland and Altyn Formations) and the highest values are in the uppermost Belt

Table 5-1
Strontium Isotope Ratios of Belt Carbonates

Sample	$^{87}Sr/^{86}Sr$	Characteristics[1]	Dep. Environment
Libby:			
FM-303	0.74991	DOCC	Sub-Tidal
Mt. Shields:			
DF-4	0.71063	DO,TKL,TB,PLL	Sub-Littoral
Shepard:			
7/29/85-3	0.71521	DOCC,THB,PLL	Sub-Littoral
Snowslip:			
Sn/Lc-7	0.72715	CC,THL,STR	In Photic Zone
MBC:			
Sn/Lc-1	0.73897	CC,THB,STR,CR,RXB MC,PLL,WL,MT	Sub-Tidal
Gts/Sy-1	0.71841	DO,MB,AR	Sub-Tidal
Gts/Sy-8	0.72549	DOCC,THB,IC-cong.	Sub-Tidal
Rp-8	0.71441	DOCC,TKL,PB,AR	Inter-Tidal
Rp-13	0.72136	DOCC,THB,WB,MT	Sub-Tidal
Bhp-10	0.73143	DOCC,MB,PB,WB	Sub-Tidal
Bhp-15	0.73212	DOCC,MT	Inter-Tidal
Bhp-16	0.73206	CC,IC-congl.	Inter-Tidal
GC-1	0.73646	DOCC,TB,TNL,PLL,WB	Sub-Tidal
GC-4	0.74324	DOCC,MB,MT	Inter-Tidal
Drc-4	0.70951	DO,MB	Sub-Littoral
Drc-5	0.71627	DOCC,THL,THB,PLL	Sub-Littoral
7/28/85-4	0.72392	DOCC	Inter-Tidal
7/28/85-5	0.74087	DOCC,MT	Sub-Littoral
7/28/85-6	0.72492	DOCC,TB	Sub-Tidal
Empire:			
7/28/85-8	0.72608	DOCC,TKL,MB	Sub-Littoral
Spokane/Greyson:			
Tc-1	0.70908	DOCC,TNL	Inter-Tidal
Altyn:			
Af/Al-2	0.70923	DO,THB,RXB	Inter-Tidal
Newland:			
Nc-2	0.70514	CC,TNL,THB,PB	Sub-Littoral
Nc-4	0.70484	CC,THL,THB,PB	Sub-Littoral
SR-1	0.71050	DOCC,THL,MB,PB	Sub-Littoral

[1] Abbreviations and Descriptions of Depositional Environments are explained in Appendix A. DO - dolomite, CC - calcite, DOCC - dolomitic calcite.

(Libby Formation). The Middle Belt Carbonates show the largest variation in $^{87}Sr/^{86}Sr$, perhaps because this part of the section contains the bulk of the measured samples. Considerable variation in observed $^{87}Sr/^{86}Sr$ ratios could result from: 1) acid leaching of ^{87}Sr from the noncarbonate portion of samples during laboratory digestion of samples and/or post-depositional exchange of carbonate Sr with radiogenic Sr from the noncarbonate fraction, 2) Sr equilibration with pore waters which were enriched in radiogenic strontium during diagenetic and post-depositional history of the carbonates, and 3) some of the carbonates may perhaps be non-marine, thus reflecting the ^{87}Sr enriched nature of continental drainage systems. Unfortunately, factor analysis, which proved so useful in studies of trace element and stable isotopes, were not applicable for strontium isotopes. This is a function of the small sample size (n=25) and the heterogeneous nature of the samples. There is no correlation of strontium isotope ratio with facies as specified in Table 5-1.

If laboratory leaching were the cause of significant enrichment or depletion of ^{87}Sr in the Belt carbonates, a plot of aluminum vs. $^{87}Sr/^{86}Sr$ for the Belt carbonates should yield a correlation between these two variables. Figure 5-3 shows that this is not the case.

The influence of diagenesis on strontium isotopic ratios is implied by the correlation of this ratio with depletions in

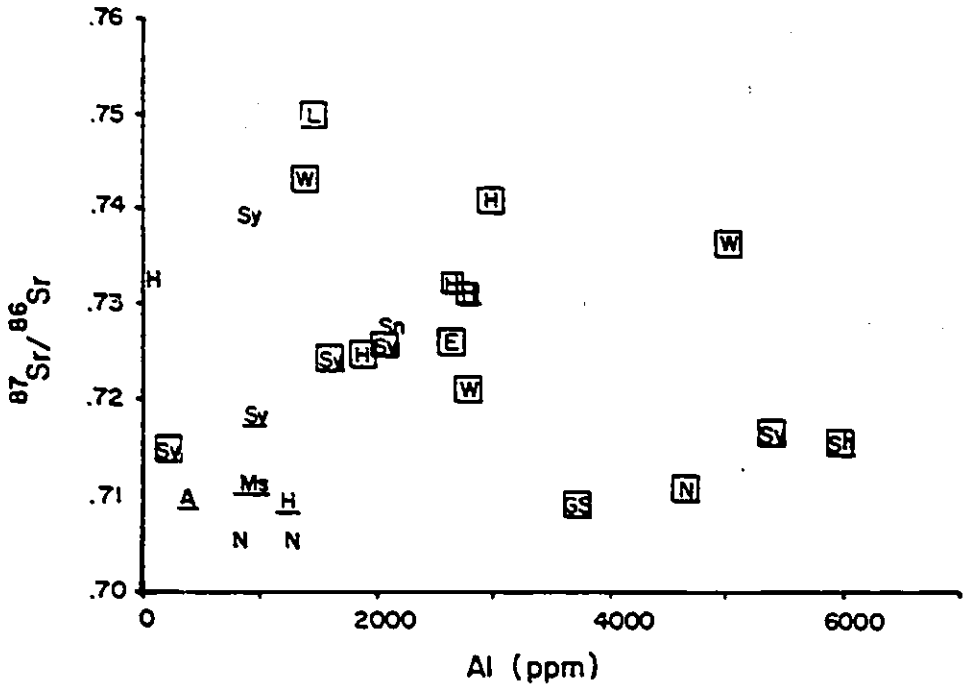

Figure 5-3
$^{87}Sr/^{86}Sr$ vs. Al for carbonates of the Belt Supergroup. Underlined samples denote dolomite, not underlined are calcite, and those in squares are of mixed dolomite and calcite composition. Higher Al concentration does not correlate with more radiogenic Sr as would be expected if acid digestion of carbonates leached significant radiogenic Sr from aluminosilicates. L - Libby Fm., Ms - Mt.Shields Fm., Sh - Shepard Fm., Sn - Snowslip Fm., W - Wallace Fm., H - Helena Fm., Sy - Siyeh Fm., E - Empire Fm., GS - Greyson/Spokane Fm., A - Altyn Fm., N - Newland Fm.. See Table 5-1 and Appendix C for geochemical data and sample descriptions.

^{18}O (Table 5-2). As $\delta^{18}O$, and marginally Sr, concentrations decrease, the $^{87}Sr/^{86}Sr$ ratio becomes more radiogenic (Figures 5-4 and 5-5), because the remaining quantity can be more easily contaminated by addition of extraneous ^{87}Sr during progressive diagenesis. Consequently, the formations with the least radiogenic strontium isotope ratios, the Altyn, Newland, and Spokane/Greyson, are those that are least diagenetically altered (cf. Chapter 4). The Libby Formation, at the top of the Belt stratigraphic succession, is the most diagenetically altered and also has the most radiogenic $^{87}Sr/^{86}Sr$ ratio. The discovery that $^{87}Sr/^{86}Sr$ is so clearly affected by post-depositional alteration frustrates the construction of a detailed $^{87}Sr/^{86}Sr$ stratigraphy of the Belt basin. Nevertheless, the lower stratigraphic sections may yield valid $^{87}Sr/^{86}Sr$ ratios reflecting those of the Belt sea waters.

On average, Belt limestones are more radiogenic $^{87}Sr/^{86}Sr$ (mean=0.72163) than Belt dolostones (mean=0.71194; Table 5-1). The least radiogenic strontium is uniformly found in dolostones with the exception of samples from the originally aragonitic Newland and Spokane/Greyson formations (Table 5-1). Models of dolomitization and studies of recently formed dolomites show that carbonates with initially high strontium concentrations (aragonite) retain their strontium isotope signature throughout the process of dolomitization whereas those with low strontium (calcite) attain $^{87}Sr/^{86}Sr$ values

Table 5-2

Correlation Matrix of $^{87}Sr/^{86}Sr$ with Trace and Major Elements and Oxygen and Carbon Isotopes

	$^{87}Sr/^{86}Sr$
% Soluble	-.21
Calcium	.34
Magnesium	-.39
Strontium	-.38
Manganese	.35
Aluminum	.07
Sodium	.33
Iron	.27
$\delta^{18}O$ calcite	-.70
$\delta^{18}O$ dolomite	-.65
$\delta^{13}C$ calcite	-.45
$\delta^{13}C$ dolomite	-.44

At the 99% level of confidence, $\delta^{18}O$ calcite and dolomite correlate significantly with $^{87}Sr/^{86}Sr$, at a 98 % level of confidence, $\delta^{13}C$ calcite correlates significantly with $^{87}Sr/^{86}Sr$, and at a 95 % level of confidence, $\delta^{13}C$ dolomite, Sr and Mg correlate significantly with $^{87}Sr/^{86}Sr$. Data are reported in Appendix C, n = 25.

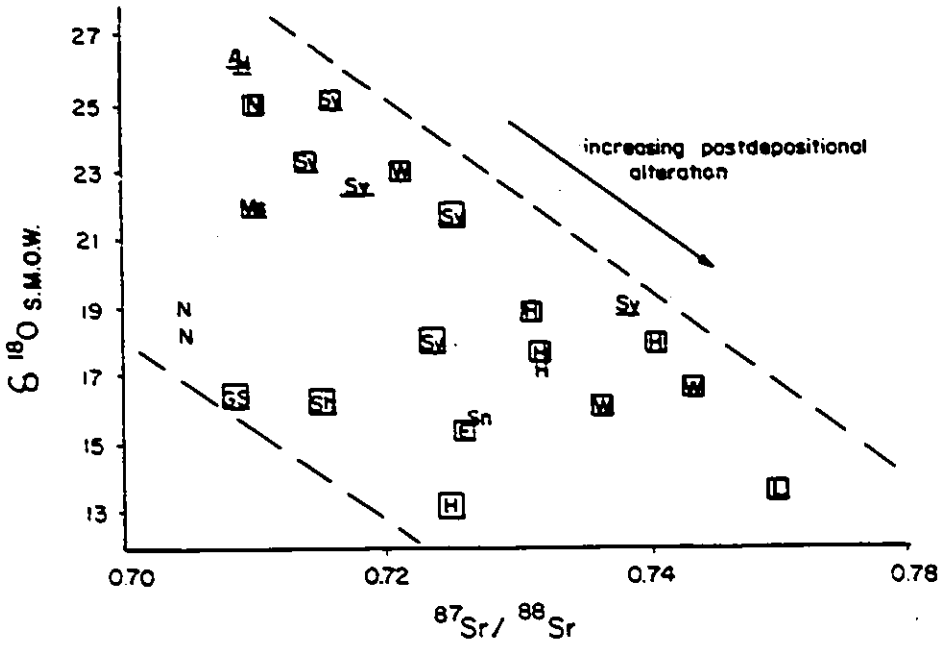

Figure 5-4
$\delta^{18}O$ vs. $^{87}Sr/^{86}Sr$ for Belt Supergroup Carbonates. Underlined samples denote dolostone, those not underlined are limestone, those in squares are of mixed dolomite and calcite composition. L - Libby Fm., Ms - Mt.Shields Fm., Sh - Shepard Fm., Sn - Snowslip Fm., W - Wallace Fm., H - Helena Fm., Sy - Siyeh Fm., E - Empire Fm., GS - Greyson/Spokane Fm., A - Altyn Fm., N - Newland Fm.. See Table 5-1 and Appendix C for geochemical data and sample descriptions. $\delta^{18}O$ of mixed samples is that of calcite.

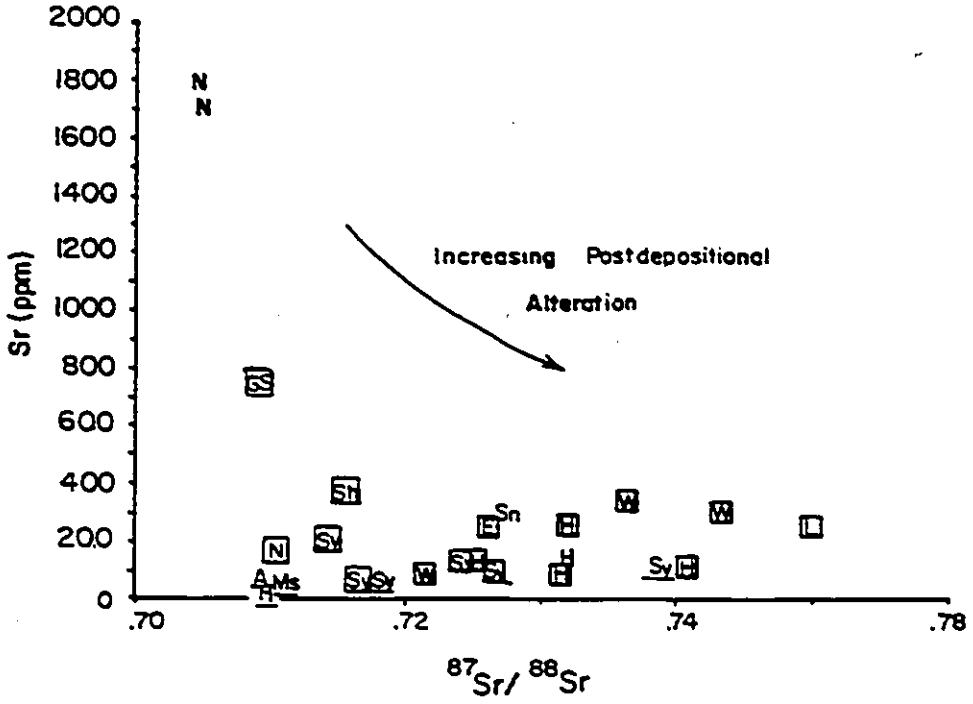

Figure 5-5
Strontium concentration vs. $^{87}Sr/^{86}Sr$ for Belt Supergroup carbonates. Underlined samples denote dolostone, not underlined are limestone, and those in squares are of mixed dolomite and calcite composition. L - Libby Fm., Ms - Mt.Shields Fm., Sh - Shepard Fm., Sn - Snowslip Fm., W - Wallace Fm., H - Helena Fm., Sy - Siyeh Fm., E - Empire Fm., GS - Greyson/Spokane Fm., A - Altyn Fm., N - Newland Fm.. See Table 5-1 and Appendix C for geochemical data and sample descriptions.

coincident with dolomitizing seawater (Vahrenkamp _et al._, 1988). If the dolomitizing fluid were a mixture of sea and fresh water, $^{87}Sr/^{86}Sr$ would still mirror that of seawater due to the high relative concentration of strontium in sea vs. fresh water. Belt carbonates show that those formations which were initially aragonitic and samples which are dolomitic retain non-radiogenic $^{87}Sr/^{86}Sr$. The process of dolomitization has aided in retention of less radiogenic ^{87}Sr in Belt carbonates, as has the presence of initially high Sr concentrations as described above.

The $^{87}Sr/^{86}Sr$ value of the early Belt waters may have fluctuated between 0.7048 and 0.7095 (Table 5-1, Figures 5-4, 5-5). Nevertheless, I cannot exclude that a portion of this fluctuation reflects in part, or perhaps even entirely, only post-depositional variations and will therefore accept only the least radiogenic value 0.70484 ± 0.00003 (see Veizer and Compston, 1974, for a detailed discussion of the approach) as a best estimate for Beltian seawater. This is a maximum $^{87}Sr/^{86}Sr$ ratio for Beltian seawater as every sample could contain radiogenic strontium. This $^{87}Sr/^{86}Sr$ value is similar to the roughly coeval Bangemal Group of the Hamersley Basin, Australia (0.70496 if normalized to E. and A. = 0.70802), but still well above the values for contemporaneous mantle (Figure 5-6).

Figure 5-6
$^{87}Sr/^{86}Sr$ for Proterozoic carbonates. All $^{87}Sr/^{86}Sr$ ratios are normalized to E. and A. standard = 0.70802, NBS SRM 987 = 0.71023. X - limestone, O - dolostone, △- mixed dolomite/calcite. Inset represents the entire ranges for all measurements, whereas the extended version is confined to $^{87}Sr/^{86}Sr$ <.710

a) Cango and Malmesbury Formations
b) Nama System
c) Adelaide Geosyncline: Wonoka, Nuccaleena, Willochra, Trezona and Etina Fms. and Amadeus basin: Pertatataka Fm.,
d) Yangtzee Gorges,
e) Adelaide Geosyncline: Brighton Lmst., Tapley Hill Fm., Tindelpina Shale, Apilla Tillite,
f) Adelaide Geosyncline: Skillogalee Dolomite,
g) Adelaide Geosyncline: River Wakefield Group,
h Mauritania, Adrar Fm.
i) Amadeus basin: Bitter Springs Fm., Elery Cr., Belt basin: Libby Dolomite,
j) Belt basin: Mt. Shields Fm.,
k) Hammersley basin: Bangemal Group,
l) Belt basin: Snowslip and Shepard Fms.,
m) Belt basin: Middle Belt Carbonate,
n) Belt basin: Empire Fm.,
o) Belt basin: Spokane/Greyson Fms.,
p) Belt basin: Altyn and Newland Fms.,
q) McArthur basin: Reward Dolomite, Cooley Mbr., Mitchell Yard Mbr., Mara Do., Leila Sst. ,
r) McArthur basin: Wollogorana Fm.

See Appendices C and E for lists and sources of the data.

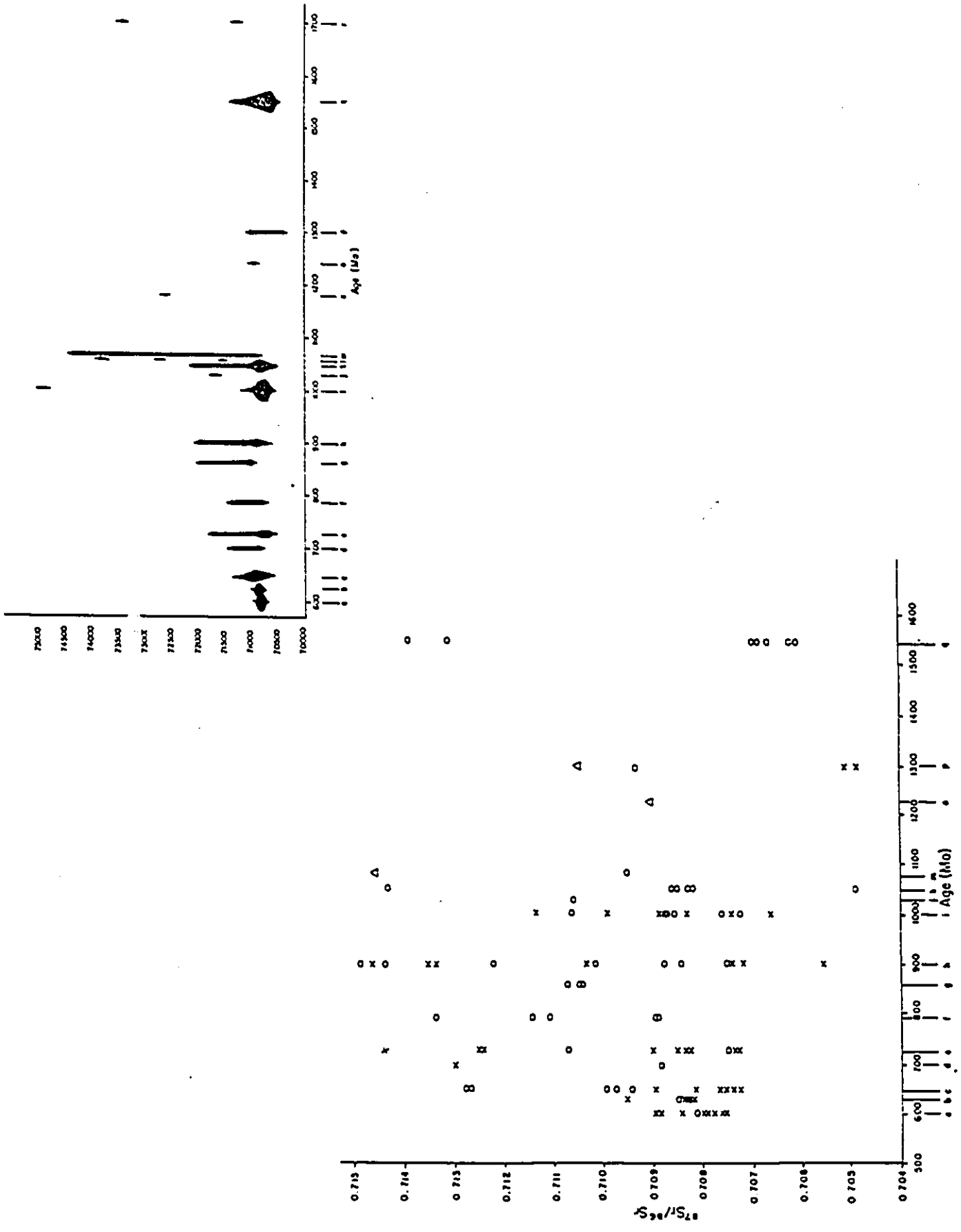

5.3.1 $^{87}Sr/^{86}Sr$ of Belt argillites and their provenance

The provenance for the siliciclastic rocks in the Belt basin appears to have been a 1.6-2.1 Ga old terrain which was close to granite in composition (Harrison and Grimes, 1970; Schieber, 1985, 1986; Frost and Winston, 1987). Frost and Winston (1987) determined an average Sm-Nd crustal residence age of 2.0 Ga for the fine-grained sediments. Coarse-grained samples showed more variation in Sm/Nd ratio and reflected the influence of local sources. The uniformity of Sm/Nd ratios for the Belt Supergroup was attributed by Frost and Winston (1987) to a mixing of the sediments en route to deposition in the Belt basin. The remarkable homogeneity of fine-grained siliciclastics in the Belt Supergroup was also noted by Harrison and Grimes (1970) in their study of the mineralogy and geochemistry of Belt rocks. They concluded that the source rock was granitic in composition from mineral ratios and from major and trace element chemistry of mostly siliciclastic rocks. Schieber (1986) noted the homogeneity of REE patterns within formations in the Helena embayment. He inferred a granitoid gneiss and migmatite source. The well mixed nature of these siliciclastics indicates that they are of multi-cycle origin.

If the sediment source of Belt sediments were dominantly granitic, its $^{87}Sr/^{86}Sr$ ratio would depend on the age of the source at the time of erosion. The crustal residence ages of

the fine-grained Belt sediments exceed their depositional ages by at least 200 to 1070 Ma. Obradovich and Peterman (1968) estimated that the $(^{87}Sr/^{86}Sr)_0$ for a whole rock Rb-Sr isochron of the argillaceous Belt sediments (Empire through McNamara formations in the east-central Belt basin) was 0.7325, for the sediments of the Neihart through Greyson formations in the eastern Belt basin it was 0.7070, and for the Pilcher Quartzite and Garnet Range Formations in the western Belt basin it may have been 0.7300. These values are within the range of $^{87}Sr/^{86}Sr$ values for granites exposed today (Taylor and McLennan, 1985) and may represent the original strontium isotope ratio of the granitic source rocks. The eastern Belt, however, may have derived its sediments from a less radiogenic (younger?) source.

$^{87}Sr/^{86}Sr$ in the Belt carbonates reflect partially the isotopic composition of the Belt sea water, but in most instances the ratios have been modified during post-depositional evolution of the sediments. It is difficult to pinpoint the timing of this alteration process and in all likelihood this was a protracted phenomenon. The radiogenic component undoubtedly originated from the siliciclastic portion and was imparted to carbonates via pore waters which leached radiogenic strontium from the siliciclastics. This may have commenced already during diagenetic stabilization of the rocks, but it continued undoubtedly through the times of

progressive burial, as indicated by the clear negative correlation with $\delta^{18}O$ (Figure 5-4).

5.3.2 $^{87}Sr/^{86}Sr$ of the suspended and dissolved river load in the Belt basin

The $(^{87}Sr/^{86}Sr)_0$ of Belt argillites may have been between 0.7300 and 0.7325 throughout most of the Belt basin, but may have been considerably lower, 0.7070, in the eastern basin (Obradovich and Peterman, 1968). As stated earlier, the $^{87}Sr/^{86}Sr$ of Belt waters probably ranged between 0.7048 and 0.7095. Argillites record the strontium isotope ratio of material deposited as suspended load in river systems which fed the basin, whereas limestones record the value of the dissolved load supplied by these same rivers. Taking the Belt basin as a unit, the $\Delta\ ^{87}Sr/^{86}Sr$ (suspended minus dissolved load) may have ranged between 0.00416 and 0.02516. This is considerably greater than for modern rivers (Figure 5-7). It may indicate that 1) the rivers supplying the Belt basin did not drain an exclusively young volcanic or plutonic terrain (Goldstein and Jacobsen, 1987), 2) there was an alternate source of nonradiogenic Sr to waters of the Belt basin, 3) chemical weathering of silicates preferentially enriched waters in nonradiogenic Sr, or 4) the $^{87}Sr/^{86}Sr$ of suspended sediments in the Belt basin is an overestimate. Although the chemical weathering of silicates does result in preferential

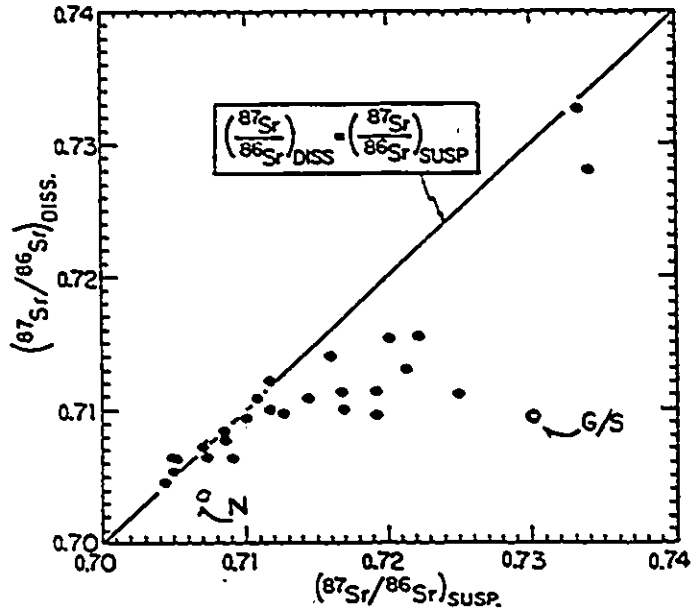

Figure 5-7
Relationship between $^{87}Sr/^{86}Sr$ in the dissolved and suspended load of rivers with $^{87}Sr/^{86}Sr < 0.740$. $^{87}Sr/^{86}Sr$ in the dissolved and suspended load of rivers draining young volcanic terrains are equal. If the $^{87}Sr/^{86}Sr$ in the dissolved load is less radiogenic than that in the suspended load, a terrain including marine precipitates is implied. The two Belt Supergroup values plotted on this figure are for the Newland (N) and Greyson/Spokane transition (GS). Modified from Goldstein and Jacobsen (1987).

dissolution of phases enriched in nonradiogenic $^{87}Sr/^{86}Sr$ (Dasch, 1969; Brass, 1975), Goldstein and Jacobsen (1987) note that in modern rivers differential chemical weathering accounted for a depletion < 0.001. If chemical weathering were more severe in the Proterozoic, this effect could have been enhanced but it seems unlikely that this was the primary cause of the difference in ^{87}Sr in suspended vs. dissolved load in the Belt basin. A provenance of marine precipitates is a possibility for the nonradiogenic Sr found in the Belt basin. As was discussed earlier, this provenance need only be 10% carbonate and/or evaporite for this component to dominate the $^{87}Sr/^{86}Sr$ in the dissolved load of the rivers which fed the basin. Alternately, the source of nonradiogenic Sr might have been marine waters. $^{87}Sr/^{86}Sr$ from carbonates of similar age are remarkably similar to the least radiogenic, and least post-depositionally altered, limestones in the Belt basin (Figure 5-6; Appendix E). The similarity between these values may indicate that the Belt sea was linked with the world ocean with carbonates precipitating in the Belt basin reflecting a world average $^{87}Sr/^{86}Sr$.

Chapter 6

Secular Variations in Proterozoic Carbonates

Second order secular oscillations of sulfur, carbon and strontium isotopic ratios and some trace element concentrations have been noted in Phanerozoic rocks (Nielsen, 1965; Holser and Kaplan, 1966; Peterman et al., 1970; Veizer and Compston, 1974; Monster et al., 1979; Claypool et al., 1980; Veizer et al., 1980, Boyle, 1981, Graham et al., 1981; Burke et al., 1982; Goodfellow and Jonasson, 1984; Holser, 1984; Veizer, 1985, Veizer, et al., 1986) but these variations have not yet been resolved in the Proterozoic because of poor temporal resolution and the incompletely preserved rock record. Sulfur, carbon and oxygen isotope and iron and manganese concentrations of Belt and other Proterozoic carbonates are presented below.

6.1 The redox cycle in Precambrian oceans

Prior to the development of the two biologically mediated sulfur reservoirs, free oxygen may have existed at lower levels in the atmosphere-hydrosphere system than is the case today. Consequently, Fe or Mn may have been present at higher concentrations in the early Precambrian ocean. The source of this Fe and Mn may have been an enhanced flux from lavas and immature volcanics either via direct seawater/oceanic crust

interaction or by weathering from continents (Veizer, 1985). If there were a higher concentration of Fe and Mn in the Precambrian oceans, these elements should be more concentrated in Precambrian rather than Phanerozoic carbonates. Archean carbonates do show increased concentrations of Fe and Mn if compared to their Phanerozoic counterparts (Figures 6-1 and 6-2). The contention by Veizer (1985) is that in the Archean and early Proterozoic, the C-O-S cycle was not yet established, but instead a C-O-Fe,Mn cycle dominated the redox balance of the exogenic system. Iron and Mn are present at higher concentrations in Belt carbonates than in Phanerozoic samples and are, in the case of Fe, comparable to Archean carbonates (Figures 6-1 and 6-2). This indicates that the redox cycle may still have been controlled partially by C-O-Fe,Mn as opposed to the C-O-S buffer of the Phanerozoic. The high Fe content of Belt samples may be a consequence of the fact that ankeritic phases were not excluded in this study in contrast to the Archean data of Veizer (1985).

6.2 The Sulfur Cycle

The sulfur cycle has two principal reservoirs: oxidized sulfate ($\delta^{34}S$ = 20 ± 10 $^{0}/_{00}$ CDM, Canon Diablo Meteorite; 2.4 x 10^{20} moles of sulfur) and reduced sulfide ($\delta^{34}S$ -20 ± 20 $^{0}/_{00}$ CDM; 2.9 x 10^{20} moles of sulfur; Claypool et al., 1980; Garrels and Perry, 1974).

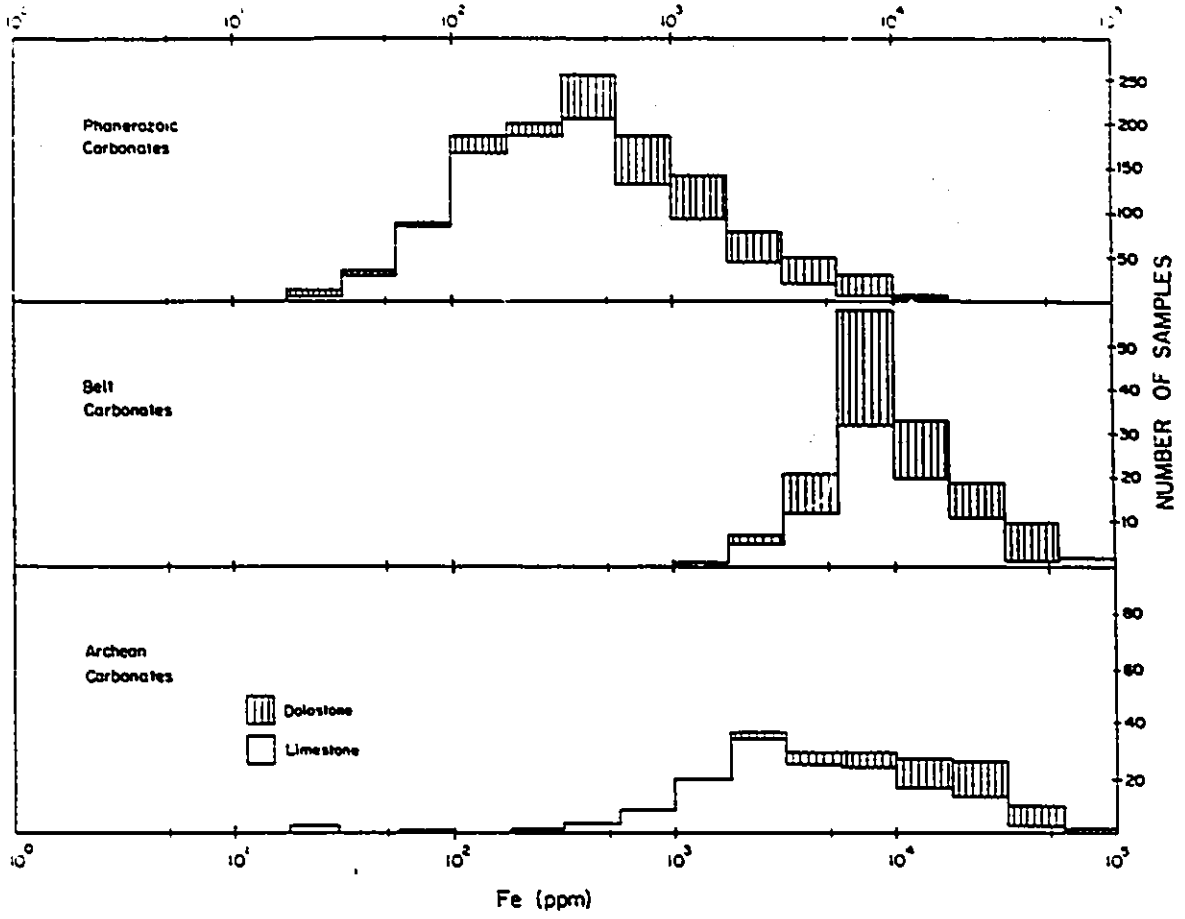

Figure 6-1
Histograms of Fe concentrations for Belt carbonates as compared to Fe distribution in Phanerozoic and Archean counterparts. Trace element data of Belt carbonates is repcrted in Appendix C of this thesis, Archean and Phanerozoic data are summarized from histograms in Veizer (1985). See also Veizer et al., (1989b).

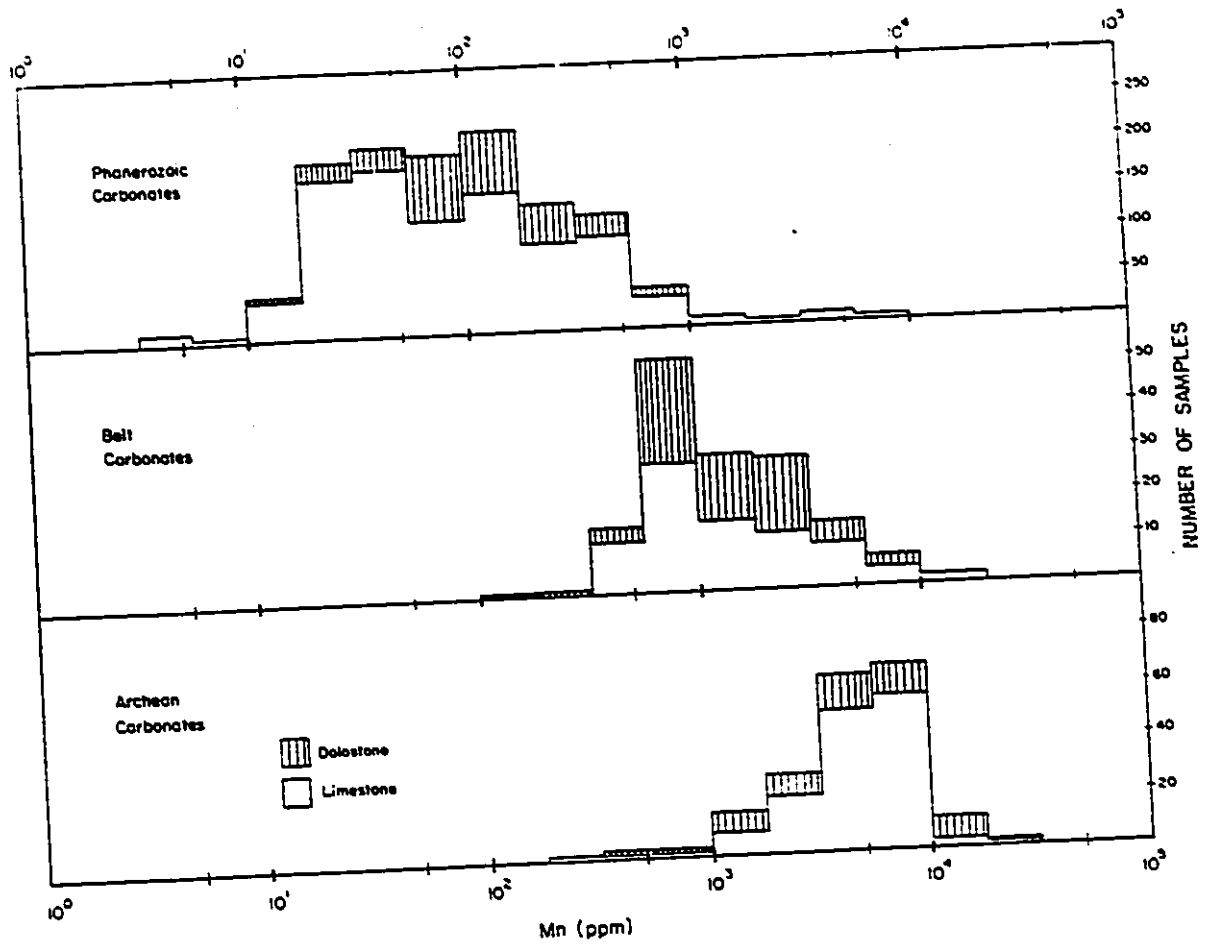

Figure 6-2
Histograms of Mn concentrations for Belt carbonates as compared to Mn distributions in Phanerozoic and Archean counterparts. Trace element data of Belt carbonates is reported in Appendix C of this thesis, Archean and Phanerozoic data are summarized from histograms in Veizer (1985). See also Veizer et al., (1989b).

The isotopic signature of the two reservoirs became distinct at 2.3 ± 0.4 Ga ago and is linked to the development of an oxidized reservoir and the concomitant evolution of bacteria that could reduce sulphate, performing dissimilatory sulfate reduction (Goodwin et al., 1976; Cameron, 1982b; Veizer et al., 1982, Hattori et al., 1983, Schidlowski et al., 1983; Cameron and Hattori, 1987). Prior to the establishment of the two sulfur reservoirs, $\delta^{34}S$ of both sulfide and sulfate clustered close to 5 ± 5 $^{0}/_{00}$ CDM (Lambert et al., 1978; Monster et al., 1979; Cameron, 1982b; Schidlowski et al., 1983), reflecting mantle sulfate of 0 $^{0}/_{00}$ CDM. The $\delta^{34}S$ of sulfate minerals is close to seawater SO_4^{-2} (Ohmoto and Felder, 1987). The fractionation of sulfur between the aqueous sulfate ion and sulfate minerals is negligible, usually yielding an enrichment of 1-2 $^{0}/_{00}$ in sulfate minerals (Schidlowski et al., 1983). The reduction of sulfate to sulfide is subject to kinetic fractionation by dissimilatory sulfate reducing bacteria that preferentially fractionate ^{32}S into H_2S. This H_2S is subsequently precipitated as a sulfide in sediments. The average fractionation attributed to the process of dissimilatory sulfate reduction is 35 to 40 $^{0}/_{00}$, as determined from coexisting sulfate and sulfide species (Schidlowski et al., 1983). The factors which control the degree of bacteriogenic sulfate fractionation and subsequent formation of sulfide minerals in sediments are: 1) sufficient

organic material in the sediment for the bacteria to consume, 2) a reducing environment in which the bacteria may survive, 3) sufficient sulfate for the bacteria to reduce, 4) trace metals to combine with the H_2S liberated by the bacteria and precipitate sulfide minerals. Rayleigh fractionation within a closed pore water environment can cause large variations in $\delta^{34}S$ of the resulting sulfide minerals.

The $\delta^{34}S$ of sedimentary seawater sulfate has varied systematically during the Phanerozoic (Figure 6-3; Thode and Monster, 1965; Nielsen, 1965; Holser and Kaplan, 1966; Claypool et al., 1980). Similar systematic variations of $\delta^{34}S$ in Precambrian oceans have not yet been demonstrated. Figure 6-4 is a compilation of the ranges of $\delta^{34}S$ values reported from the literature for sedimentary sulfates and sulfides from about .9 to 2.5 Ga ago. The paucity of sulfates from which to construct a curve similar to that reported for the Phanerozoic is obvious, and to further discourage such an endeavour, some of the sulfates reported here may have been deposited in a restricted marine or lacustrine environment (McArthur Basin and Belt Supergroup). The $\delta^{34}S$ of Proterozoic sulfides clearly illustrates that dissimilatory sulfate reduction was active in the exogenic sulfur cycle throughout this Eon.

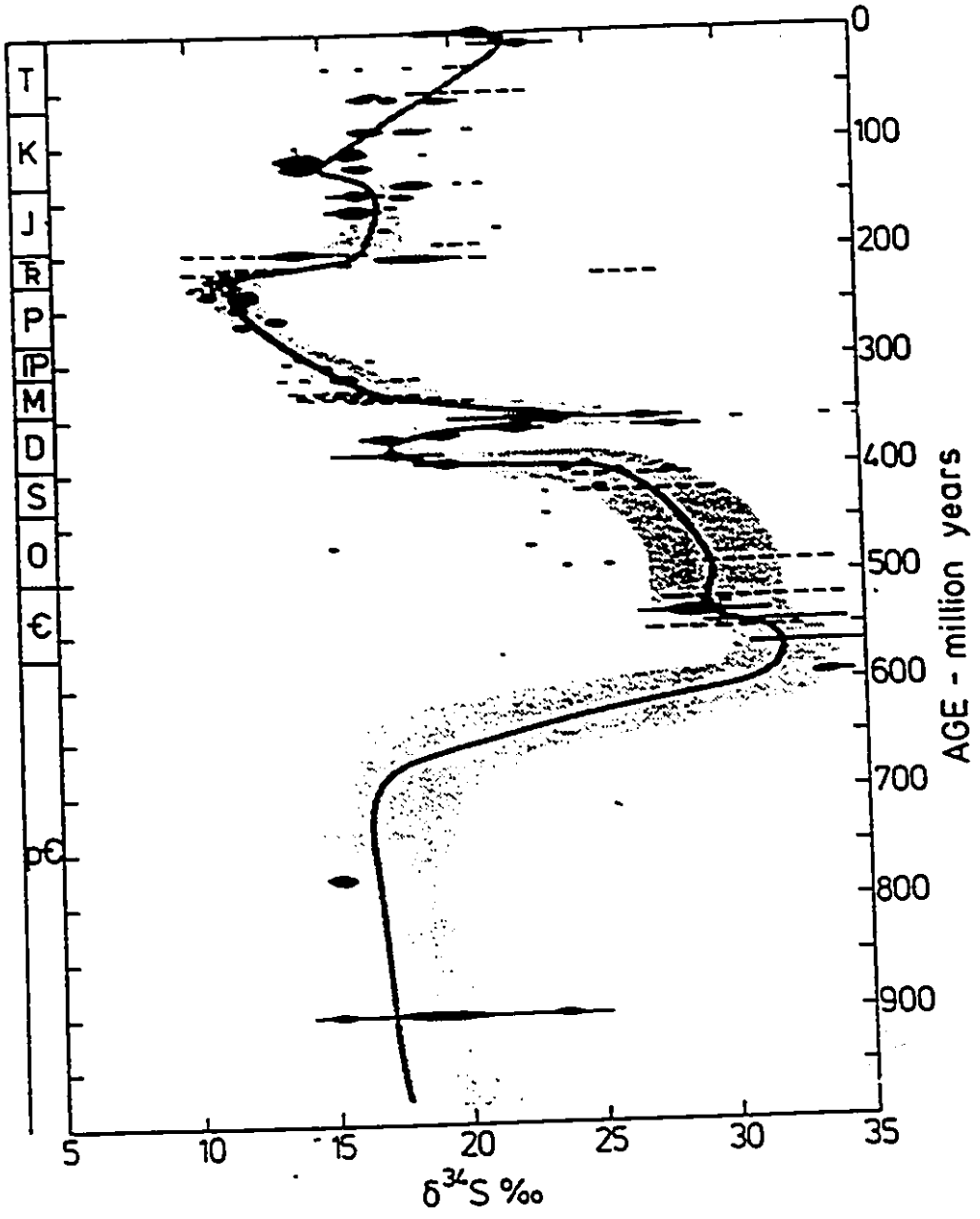

Figure 6-3
Variations in $\delta^{34}S$ of sulfates through time (Claypool et al., 1980).

Figure 6-4
Compilation of $\delta^{34}S$ of sulfides and sulfates reported from sediments of about .9 to 2.5 Ga age. Solid lines indicate sulfide, dashed lines denote sulfate.
1- Nonesuch Shale, White Pine, Michigan, Burnie et al. (1972)
2- Noonday Dolomite, Death Valley, Calif., Hall (1984)
3- Belt Supergroup, U.S.A., Campbell et al. (1978), Lange et al. (1987), Ueda et al.(1987), and this thesis
4- Northern China, Qin et al. (1985)
5- Grenville Province, U.S.A. and Canada, Buddington et al. (1969) and Whelan et al. (1984)
6- Roan Group, Zambia, Claypool et al. (1980)
7- McArthur Basin, Australia, Smith and Croxford (1975), Both and Smith (1975), Carr and Smith (1977), Smith et al. (1978)
8- Asen, Skellefte district, Sweden, Rickard et al. (1979)
9- Poorman, Homestake and Ellison Fms., U.S.A., Rye and Rye (1974)
10-Outokumpu, Finland, Makela (1974)
11-Belcher Group, Canada, Ueda et al., in press
12-Udokan U.S.S.R., Bogdanov and Golubchina (1971), Chukrov (1971)
13-Gunflint Fm., U.S.A.-Canada, Shegelski (1982), Cameron (1982a)
14-Kona Dolomite, U.S.A., Hemzacek et al. (1984)
15-Pine Creek Geosyncline, Australia, Donnelly and Ferguson (1980)
16-2.4 Ga. sediments, Canada, Cameron and Garrels (1980), Hattori et al. (1983), Thode et al. (1962)
17-Transvaal Supergroup, S.Africa, Cameron (1982b)
18-Cahill Fm., Pine Creek Geosyncline, Donnelly and Ferguson (1980)
19-Gordon Lake Fm., Canada, Cameron (1983)
20-Frood Series, Canada, Thode et al. (1962)
21-Hammersley and Turee Creek Groups, Hammersley Basin, Australia, Cameron (1982a)

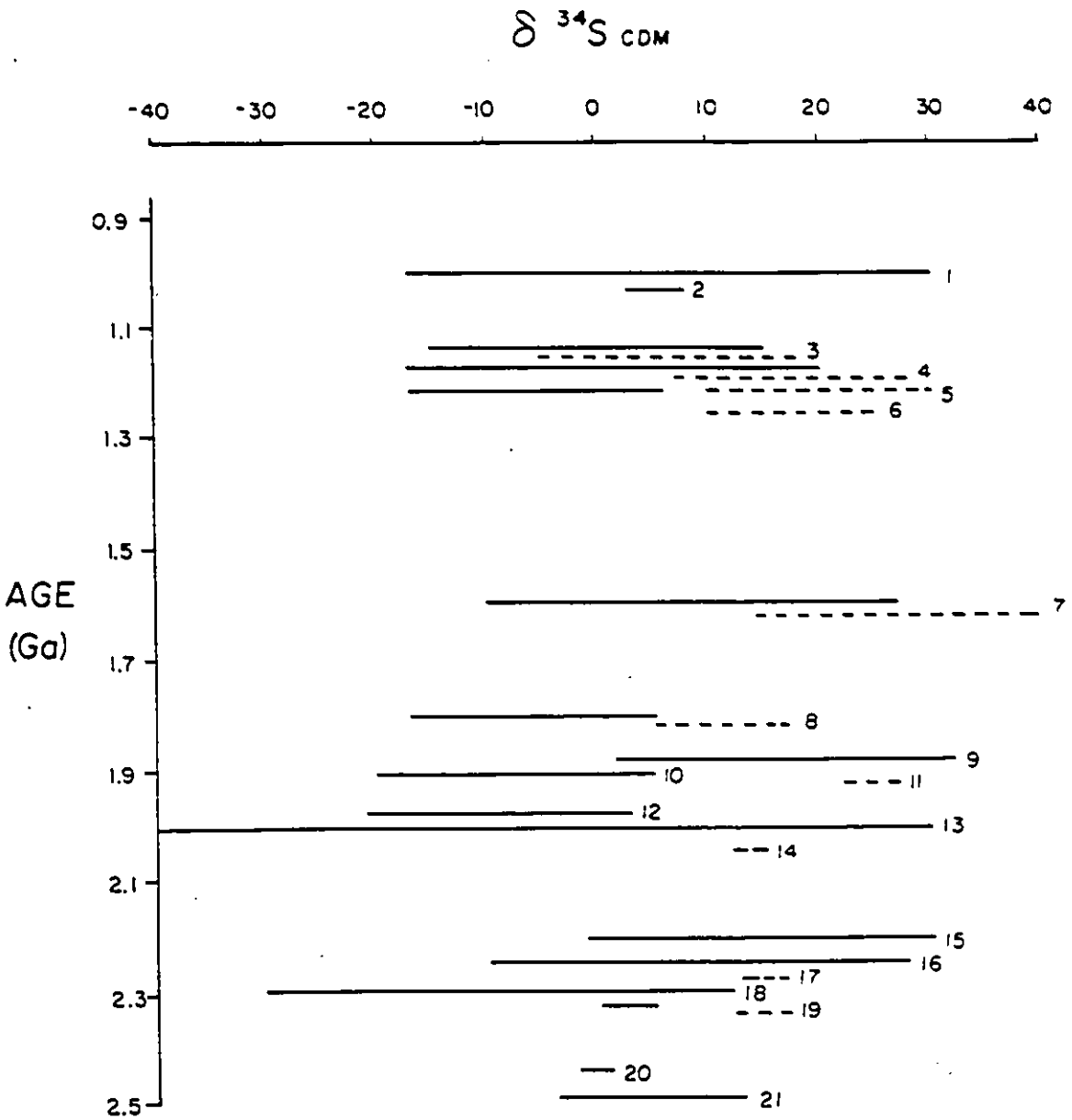
δ 34S CDM
-40
-30
-20
-10
0
10
20
30
40
AGE
(Ga)
0.9
1.1
1.3
1.5
1.7
1.9
2.1
2.3
2.5
1
2
3
4
5
6
7
8
9
10
11
12
13
14
15
16
17
18
19
20
21

6.2.1 Sulfur isotopes in the Belt basin

$\delta^{34}S$ of trace pyrite in carbonate was determined for some Belt samples (Appendix C; Table 6-1, Figure 6-5). $\delta^{34}S$ of pyrite in Belt carbonates, as determined in this thesis, ranges from +0.2 to +9.6 and averages 5.5 $^{0}/_{00}$ CDM. The sulfur concentrations range from 0.334 to <0.005 (Table 6-1 and Appendix C). $\delta^{34}S$ of trace sulfide and sulfate from limestones in the Siyeh Fm. range from 0.8 to 14.3 $^{0}/_{00}$ for sulfate and -7.4 to 14.2 $^{0}/_{00}$ for sulfide (Figure 6-5, Ueda et al., 1987). $\delta^{34}S$ of diagenetic sulfides (chalcocite, bornite, covelite, chalcopyrite and pyrite) in the Spokane Formation range from -17.0 to 2.1 (Figure 6-5, Lange et al., 1987). $\delta^{34}S$ of diagenetic copper sulfides and barite from the upper Spokane Fm, range from -4.9 to 18.0 $^{0}/_{00}$ for barite and -2.2 to 2 $^{0}/_{00}$ for sulfides.

The fractionation between sulfate and sulfide coexisting in carbonate samples from the Siyeh Formation was nearly constant at 5 ± 2 $^{0}/_{00}$ (Ueda et al., 1987). Rye et al. (1984) report that bacteriogenic sulfate reduction occurs in some lithologies in the Belt basin (the Revett Fm.) but not others (the Spokane Fm.). The small fractionation between sulfate and sulfide sulfur and the presence of heavy sulfides in some Belt strata argue against the importance of dissimilatory sulfate reducing bacteria in Belt carbonates during formation of sulfates and sulfides in the Siyeh and Spokane Formations. If

Table 6-1

Sulfur Isotope Composition of Trace Sulfide in Belt Carbonates

Sample Number	$\delta^{34}S$ CDM[1]	% Sulfur[2]
Libby:		
FC-72	2.7	0.010
7/25/85-5	0.2	0.334
Mt. Shields:		
7/29/85-5	7.9	
Shepard:		
7/29/85-3	5.7	
RM/SH-1	6.6	
Middle Belt Carbonate:		
HL-6	2.8	
GTS/SY-11	7.8	0.054
WC-3	9.6	0.290
	8.8	
Newland:		
NC-5	7.3	

[1] Acid (HCl) insoluble sulfides
[2] Determination by ion liquid chromatography (Appendix C)

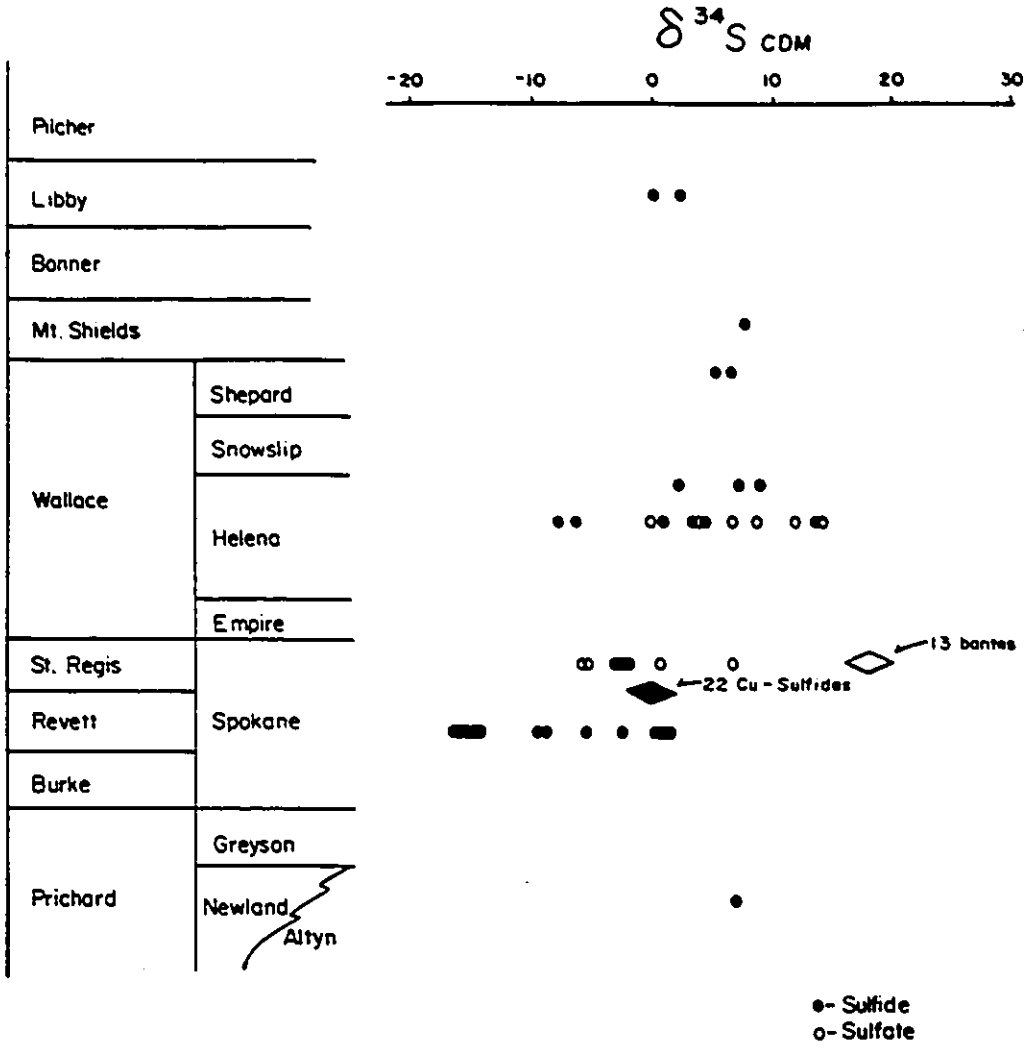

Figure 6-5
Variation in $\delta^{34}S$ of sulfides (●) and sulfates (O) in Belt sediments. $\delta^{34}S$ of pyrite from the Libby, Mt.Shields, Shepard, uppermost Helena and Newland Formations were determined in this thesis (Table 6-1). Trace sulfide and sulfate was analyzed from carbonates in the Siyeh (Helena) Formation by Ueda et al., 1987. Copper sulfides and barite were analyzed from mineralized sediments in the uppermost Spokane Formation (Rye et al., 1984) and lower in the Spokane Formation (Lange et al.,1987).

deposition of sulfate and sulfide from normal marine waters is presumed, photosynthetic bacteria could have formed sulfate from H_2S within the basin (cf. Schidlowski et al., 1983) in a scenario similar to that concluded for the 3.4 Ga. Pilbara Block of W. Australia (Lambert et al., 1978) and the 3 Ga old Swaziland system of the Barberton Mountain Land, S.Africa (Perry et al., 1971). Ohmoto and Felder (1987) argue that smaller Δ SO_4-H_2S is a result of the dominance of species of sulfate-reducing bacteria living in warmer ancient oceans, which reduce sulfate with less kinetic segregation of ^{32}S. Alternatively, there might have been insufficient organic matter and/or an oxygenated sedimentary environment in the Belt basin which would have limited the activity of sulfate-reducing bacteria. As Δ SO_4-H_2S is inversely proportional to the log of the rate of sulfate reduction (Kaplan and Rittenberg, 1964; Chambers et al., 1975), the low Δ SO_4-H_2S in Belt sediments might imply that the sulfate supply to the Belt basin was periodically limited. The Belt Supergroup contains no bedded and few disseminated evaporites and may have had a limited sulfate concentration which would lead to low sulfate fractionation. The enrichment of ^{34}S in sulfide and sulfate with decreasing trace sulfate within the Siyeh Formation, as reported by Ueda et al., (1987), argues for a limited sulfate supply for the Belt basin during lower Belt 'time'. However, this relationship was not observed in the sulfur analyses

performed for this thesis, although the sample size is too small for any far reaching conclusions. Total sulfur of the Belt carbonates ranges between < 5 and 4980 ppm (Appendix C, Table 6-1, and Ueda, et al., 1987), which suggests that the sulfur supply was occasionally limited in the Belt basin. Sulfate-reducing bacteria seem to have been periodically active in the basin as seen in strongly fractionated sulfates and sulfides in some facies of the Revett Fm. (Figure 6-5), although this fractionation might have been caused by Rayleigh fractionation within the pore waters of the Revett. It is possible that the activity of dissimilatory sulfate reducing bacteria was facies controlled, the limiting factors being reducing conditions and/or the presence of organic matter within different facies in the Belt basin. Coincident with the restricted existence of the necessary bacteria, sulfate reduction may be limited by a fluctuating sulfur supply to the basin.

The $\delta^{34}S$ of sulfates from the Belt Supergroup is on average lighter than $\delta^{34}S$ of sulfates from basically contemporaneous sequences in northern China, the Roan Group of Zambia and the Grenville Province of the U.S.A. and Canada (Figure 6-4). However, if isotopically light barites reported from mineralized areas are excluded, the $\delta^{34}S$ of sulfates in the Belt basin fall within the limits of these coeval sequences, where $\delta^{34}S$(sulfate) is approximately 10 to 30 $^{0}/_{00}$ CDM

(Figure 6-4). The $\delta^{34}S$ of Belt sulfides (-17 to 14 $^{0}/_{00}$) is comparable to sulfide $\delta^{34}S$ reported from sequences of similar age (Figure 6-4).

The majority of sulfide $\delta^{34}S$ values summarized in Figure 6-4 are from areas of mineralization and may therefore be representative of a population skewed towards heavier $\delta^{34}S$ (Schidlowski et al., 1983). If we take $\delta^{34}S$ of pyrite in this thesis as reflecting the $\delta^{34}S$ of the oceanic sulfate, such sulfate should have had a $\delta^{34}S$ of 40-45 $^{0}/_{00}$, heavier than any yet analyzed from either Phanerozoic or Proterozoic sequences. Because the $\delta^{34}S$ of sulfate analyzed from the Belt basin is between -4 and +17 $^{0}/_{00}$ CDM (Rye et al., 1984, Ueda et al., 1987), one of three alternate explanations is favoured: 1) bacteriogenic sulfate reduction was restricted in the Belt basin, 2) the sulfides are late diagenetic and the sulfur source for sulfides and sulfates in the Belt basin might have been basinal brines not representative of the Belt waters, or 3) sulfides and sulfates were deposited from non-marine waters. $^{87}Sr/^{86}Sr$, $^{18}O/^{16}O$ and $^{13}C/^{12}C$ ratios imply that the Belt Supergroup is a marine sequence, therefore eliminating 3) above. The second alternative, that the bulk of $\delta^{34}S$ measured thus far from Belt sediments is from diagenetic minerals, is the preferred hypothesis.

6.3 Carbon and oxygen isotopic composition of Proterozoic carbonates and seawater

Oxygen isotope values for the Belt group limestones range between 22.9 and 13.4 $^{0}/_{00}$ and dolostones from 27.9 to 18.1 $^{0}/_{00}$ SMOW (Appendix C). Published isotopic values for carbonates of similar age are scarce (Figures 6-5, 6-7, 6-8, 6-9). Carbonate sequences which temporally overlap those of the Belt (= 850 to 1450 Ma.) are the Indian Kaladgi and Badami Groups (1000-2000 Ma.; Sathyanartayan et al., 1987) and Kurnool system (800-1100 Ma.; Schidlowski et al., 1975), the Zambian Katanga System (600-1300 Ma.; Schidlowski et al., 1975), the Australian Bangemall (1000-1100 Ma.; Veizer and Hoefs, 1976; Veizer and Compston, 1976) and McArthur Groups (1400-1688 Ma.; Veizer and Hoefs, 1976; Schidlowski et al., 1983), the Greenland Eleonore Bay Group, Spitsbergen Akademikerbreen and Veteranen Groups and Nordaustlandet Roaldtoppen, Celisusberget and Franklinsundet Groups (900 Ma. Knoll et al., 1986), and the Noonday (900-1300 Ma.) and Beck Spring (1200-1400 Ma.) Dolomites from the U.S.A. (Tucker, 1982; Hall, 1984). The ranges of oxygen isotope values for the Belt Supergroup fall within the spread of values for other Proterozoic carbonates (Figures 6-6, 6-7).

The range of carbon isotopes for Belt dolomites is -2.2 to 1.9 $^{0}/_{00}$ PDB and for calcites it is -5.6 to 2.4 $^{0}/_{00}$ (Appendix C). The carbon isotope values of Belt carbonates are close to

Figure 6-6
$\delta^{18}O$ distribution in Proterozoic limestones as summarized from data listed in Appendices C and E. The ranges of values for Belt limestones from this thesis are indicated as bars.
A-India, Krol-Tal Succession;
B-S.Africa, Cango and Malmesbury Fms.;
C-S.W. Africa (Namibia): Nama System; Greenland; Spitsbergen: Nordauslandet succession;
D-S.W. Africa: Damara System;
E-Australia: Balcanoona & Tapley Hill Fm., Adelaidean Geosyncline; Greenland; Spitsbergen: Nordauslandet succession;
F-Greenland; Spitsbergen: Nordsauslandet succession, Australia: Bitter Springs Fm.;
G-India: Chattisgarh System, Nandini Series;
H-Mauritania: Taoudenni Syncline;
I-Greenland; Spitsbergen: Nordauslandet, succession; India: Kurnool System;
J-Zambian Cu-belt: Katanga System;
K-India: Kurnool System; U.S.: Belt Mt.Shields, Spokane, Missoula Group (from literature);
L-U.S.: Belt Middle Belt Carbonate (from literature);
M-U.S.: Belt Ravalli Group (from literature);
N-India: Kaladgi Group;
O-Canada: Coronation Geosyncline;
P-Fennoscandian Shield: Karelian/Svecofennian Fms.;
Q-S.Africa: Transvaal Supergroup;
R-Zimbabwe: Lomagundi Grp; Canada: Espanola Limestone.

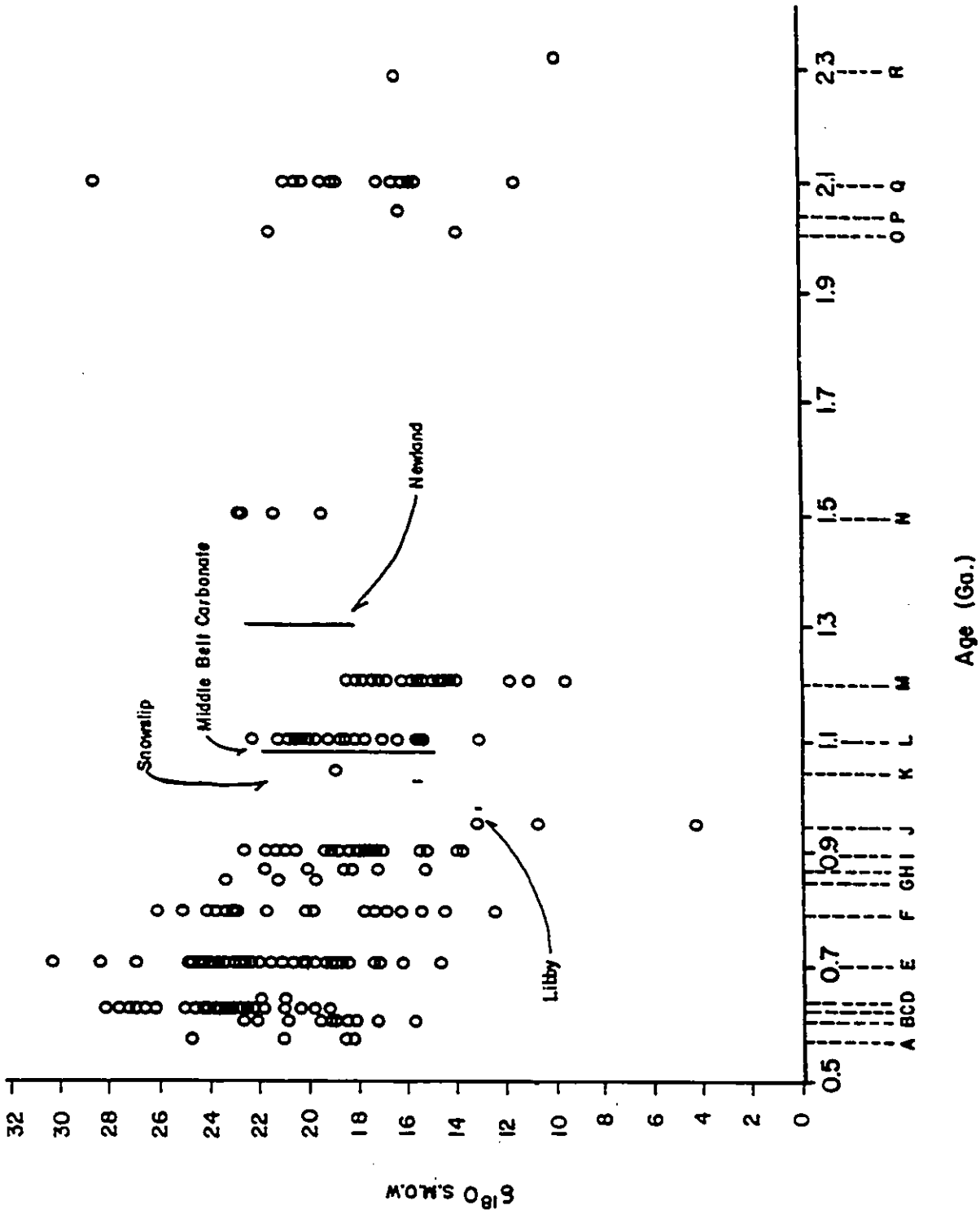
Newland
Middle Belt Carbonate
Snowslip
Libby
Age (Ga.)
$\delta^{18}O$ S.M.O.W
32
30
28
26
24
22
20
18
16
14
12
10
8
6
4
2
0
0.5
0.7
0.9
1.1
1.3
1.5
1.7
1.9
2.1
2.3
A BCD E F GH I J K L M N O P Q R

Figure 6-7
$\delta^{18}O$ distribution in Proterozoic dolomites as summarized from data listed in Appendices C and E. The ranges of values for Belt dolostones from this thesis are indicated as bars.
A-India: Krol-Tal succession;
B-S. Africa: Cango and Malmesbury Fms.;
C-Greenland: Nordauslandet: Spitsbergen succession;
D-Namibia: Damara System;
E-Greenland; Nordauslandet: Spitsbergen succession;
Australia: Adelaide Geosyncline, Brighton Lmst., Amadeus Basin; Pertataka Fm.;
F-Amadeus Basin, Bitter Springs Fm.; Greenland: Nordauslandet: Spitsbergen Fm.;
G-India: Belha Series, Bhatapara Do.; Mauritania: Taoudenni Syncline;
H-Greenland; Nordauslandet succession;
I-Zambian Cu-belt: Katanga System;
J-U.S.: Noonday Do.;
K-U.S.: Belt, Mt.Shields; Australia: Bangemall Group;
L-India: Badami Group;
M-Canada: Oakway Fm.;
N- U.S.: Belt Ravalli Group (from literature), Beck Spring Dolomite;
O-India: Cuddapah System; Canada: Sibley Fm.;
P-India: Kaladgi Group;
Q-Australia: Bungle Bungle Do., McAuthur Group;
R-Australia: Earaheedy Group;
S-Canada: Coronation Geosyncline;
T-Fennoscandia Shield: Karelian/Svecofennian Fms.;
U-Canada: Maintounuk Group;
V-Australia: Hammersley Basin, Mt.Bruce Supergroup; S-Africa: Transvaal Supergroup;
W-Canadian Shield: Epworth Group;
X-Zimbabwe: Lomagundi Group;
Y-Australia: Hammersley Group.

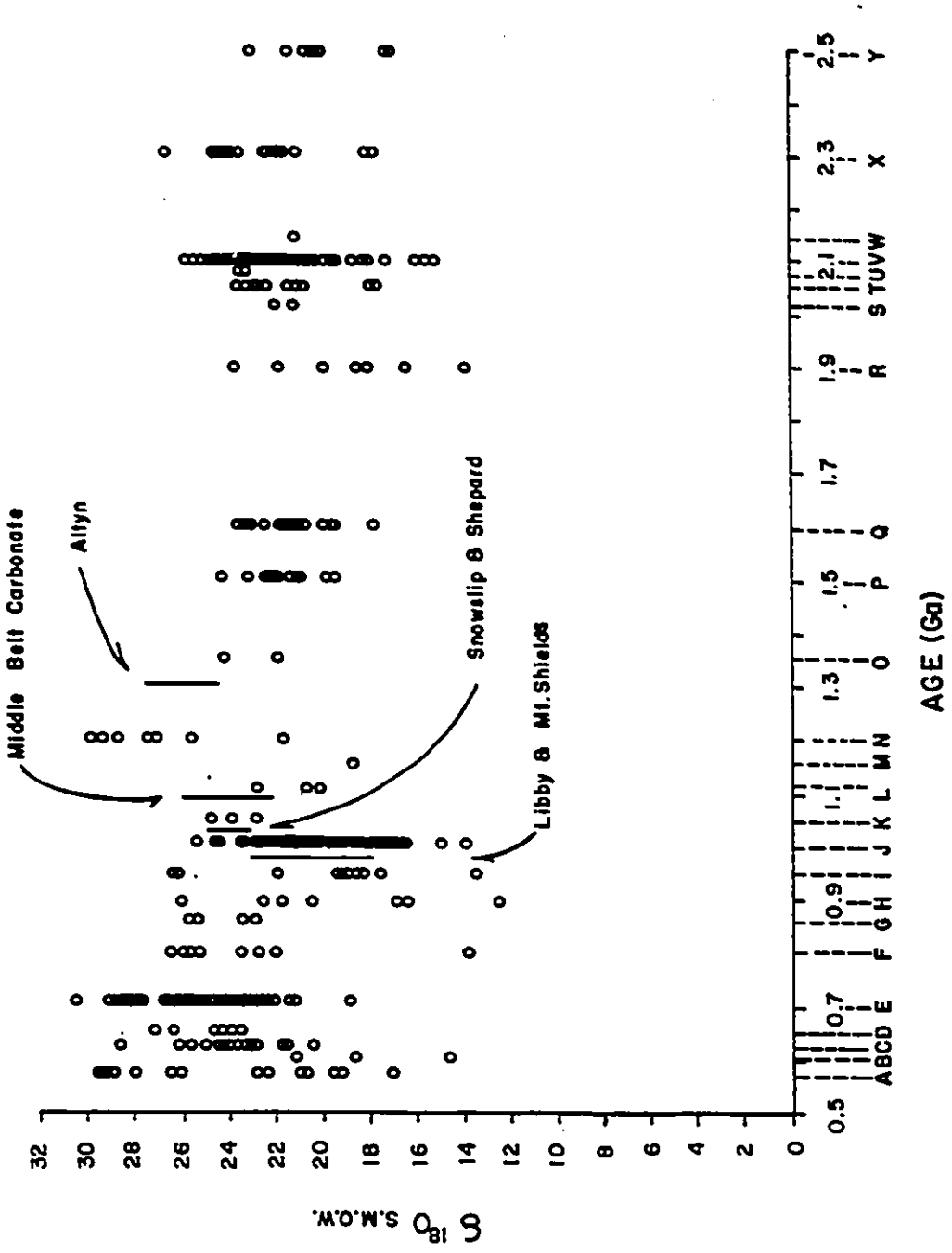
Middle Belt Carbonate
Altyn
Snowslip & Shepard
Libby & Mt. Shields
δ 18O S.M.O.W.
32
30
28
26
24
22
20
18
16
14
12
10
8
6
4
2
0
AGE (Ga)
0.5
0.7
0.9
1.1
1.3
1.5
1.7
1.9
2.1
2.3
2.5
ABCD E F G H I J K L M N O P Q R S TUVW X Y

Figure 6-8
$\delta^{13}C$ distribution in Proterozoic limestones as summarized from data listed in Appendices C and E. The ranges of values for Belt limestones from this thesis are indicated as bars.
A-India: Krol-Tal Succession;
B-S.Africa: Cango and Malmesbury Fms.;
C-S.W. Africa (Namibia): Nama System; Greenland; Spitsbergen; Nordauslandet succession;
D-S.W. Africa: Damara System;
E-Australia: Balcanoona & Tapley Hill Fm., Adelaide Geosyncline; Greenland; Spitsbergen; Nordauslandet succession;
F-Greenland; Spitsbergen; Nordsauslandet succession; Australia: Bitter Springs Fm.;
G-India: Chattisgarh System, Nandini Series;
H-Mauritania: Taoudenni Syncline;
I-Greenland; Nordauslandet; Spitsbergen succession; India:, Kurnool System;
J-Zambian Cu-belt: Katanga System;
K-India: Kurnool System; U.S.: Belt, Mt.Shields, Spokane, Missoula Group (from literature);
L-U.S.: Belt, Middle Belt Carbonate (from literature);
M-U.S.: Belt, Ravalli Group (from literature);
N-India: Kaladgi Group;
O-Canada: Coronation Geosyncline;
P-Fennoscandian Shield: Karelian/Svecofennian Fms.;
Q-S.Africa: Transvaal Supergroup;
R-Zimbabwe: Lomagundi Grp; Canada: Espanola Limestone.

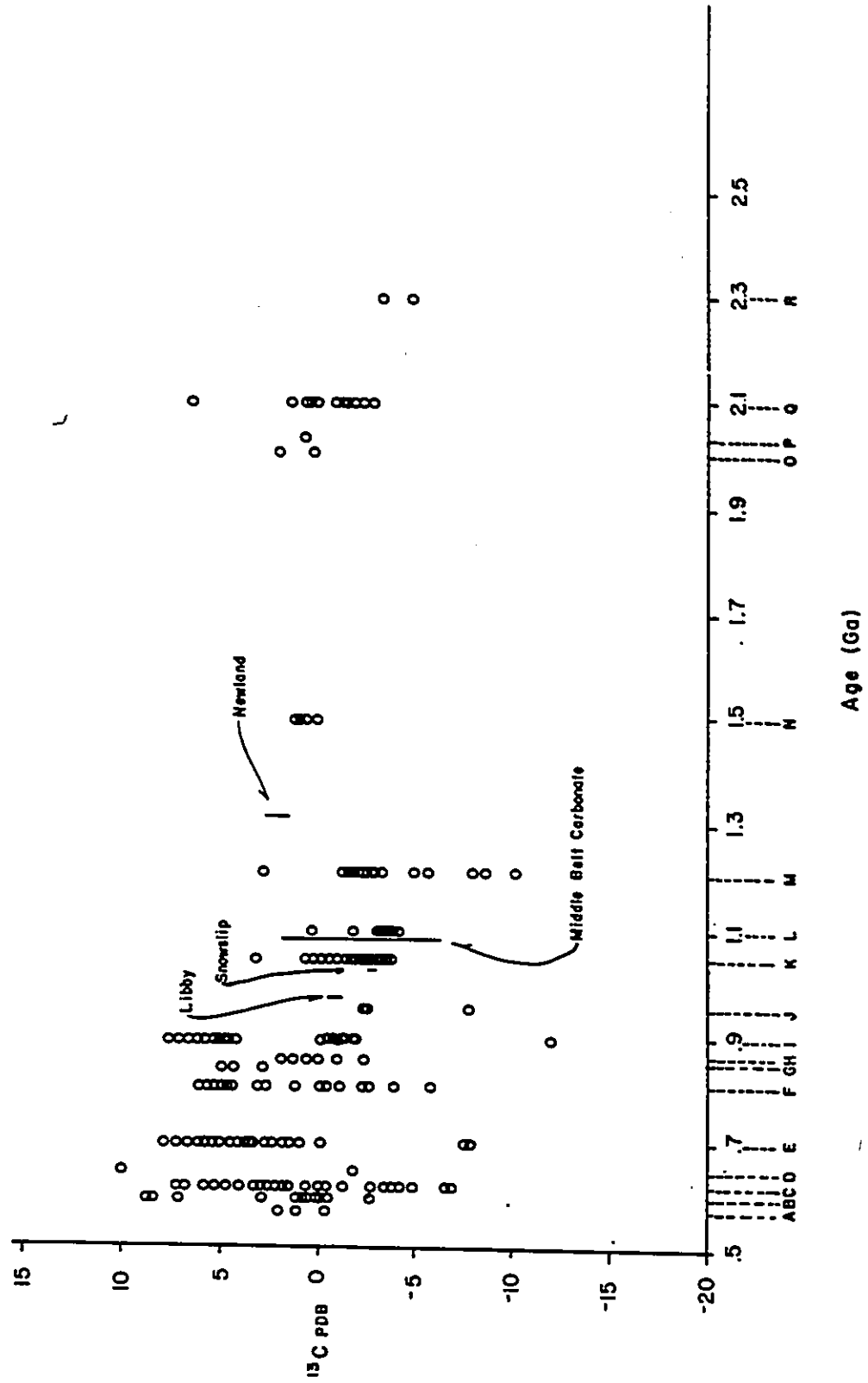
Newland
Snowslip
Libby
Middle Belt Carbonate
15
10
5
0
-5
-10
-15
-20
^{13}C PDB
.5
.7
.9
1.1
1.3
1.5
1.7
1.9
2.1
2.3
2.5
Age (Ga)
A B C D E F G H I J K L M N O P Q R

Figure 6-9
$\delta^{13}C$ distribution in Proterozoic dolomites as summarized from data listed in Appendices C and E. The ranges of values for Belt dolostones from this thesis are indicated as bars.
A-India: Krol-Tal succession;
B-S. Africa: Cango and Malmesbury Fms.;
C-Greenland; Nordauslandet; Spitsbergen succession;
D-Namibia: Damara System;
E-Greenland; Nordauslandet; Spitsbergen succession;
Australia: Adelaide Geosyncline, Brighton Lmst.; Amadeus Basin, Pertataka Fm.;
F-Australia: Amadeus Basin, Bitter Springs Fm.; Greenland; Nordauslandet; Spitsbergen Fm.;
G-India: Belha Series, Bhatapara Do.; Mauritania: Taoudenni Syncline;
H-Greenland; Nordauslandet succession;
I-Zambian Cu-belt: Katanga System;
J-U.S.: Noonday Do.;
K-U.S.: Belt, Mt.Shields, Australia: Bangemall Group;
L-India: Badami Group;
M-Canada: Oakway Fm.;
N-U.S.: Belt Ravalli Group (from literature); Beck Spring Dolomite;
O-India: Cuddapah System; Canada: Sibley Fm.;
P-India: Kaladgi Group;
Q-Australia: Bungle Bungle Do., McArthur Group;
R-Australia: Earaheedy Group;
S-Canada: Coronation Geosyncline;
T-Fennoscandia Shield: Karelian/Svecofennian Fms.;
U-Canada: Maintounuk Group;
V-Australia: Hammersley Basin, Mt.Bruce Supergroup, S-Africa: Transvaal Supergroup;
W-Canadian Shield: Epworth Group;
X-Zimbabwe: Lomagundi Group;
Y-Australia: Hammersley Group.

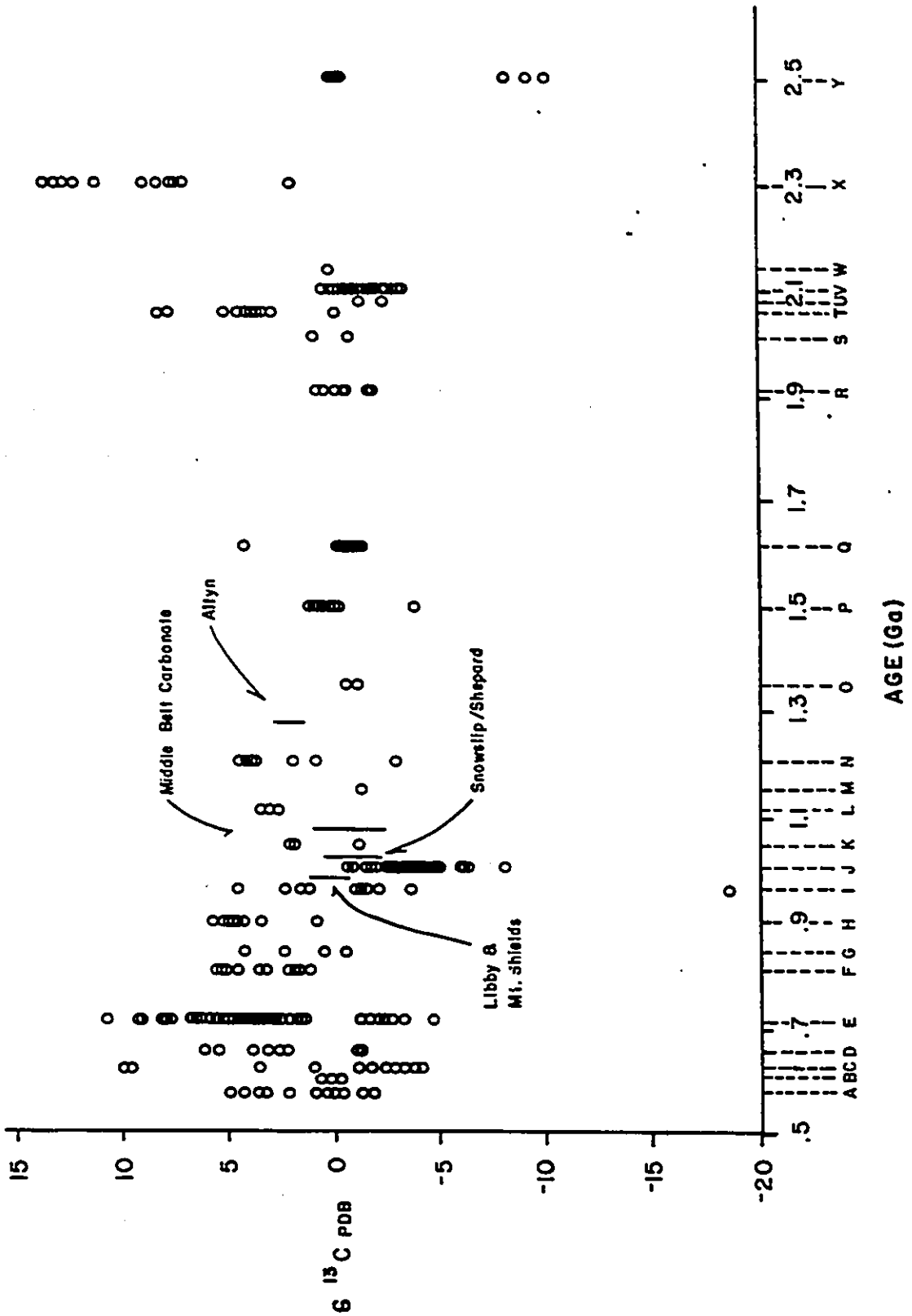
Middle Belt Carbonate
Allyn
Snowslip/Shepard
Libby &
Mt. shields
δ 13C PDB
15
10
5
0
-5
-10
-15
-20
AGE (Ga)
.5
.7
.9
1.1
1.3
1.5
1.7
1.9
2.1
2.3
2.5
A B C D E
F G H I J K L M N
O P Q
R
S T U V W
X
Y

values reported for rocks of comparable age (Figures 6-8, 6-9), and similar to modern values. No secular variations of $\delta^{13}C$ are immediately obvious in this compilation, but with increased sample density ^{13}C variations noted for Phanerozoic rocks (Veizer et al., 1980; Garrels and Lerman, 1981; Schidlowski et al., 1983; Veizer, 1985) may be extended into the Proterozoic. If the Belt basin were completely intracratonic, the carbonates might be expected to be either enriched (cf. Proterozoic Lomagundi carbonates, Schidlowski et al., 1975; U. Carboniferous to U. Permian Sverdrup basin, Beauchamp et al., 1987) or depleted in ^{13}C (Clayton and Degens, 1959).

The maximal $\delta^{18}O$ calcite values, as reported in literature and this thesis, are used to estimate the $\delta^{18}O$ of Proterozoic seawater as summarized in Figure 6-10. Lower $\delta^{18}O$ values may have resulted from diagenetic interaction with meteoric waters and/or from exchange reactions at higher temperatures (Chapter 3) and are not therefore considered in this discussion. This, at the moment, is the best approximation of the primary isotopic composition for calcites, because the diagenetic rank of sections other than the Belt has not been reported in the literature. Dolomites, because of the uncertainty in the fractionation factor at low temperatures and because of their diagenetic origin, are not a suitable indicator of marine $\delta^{18}O$. This criterion effectively eliminates several sequences, such

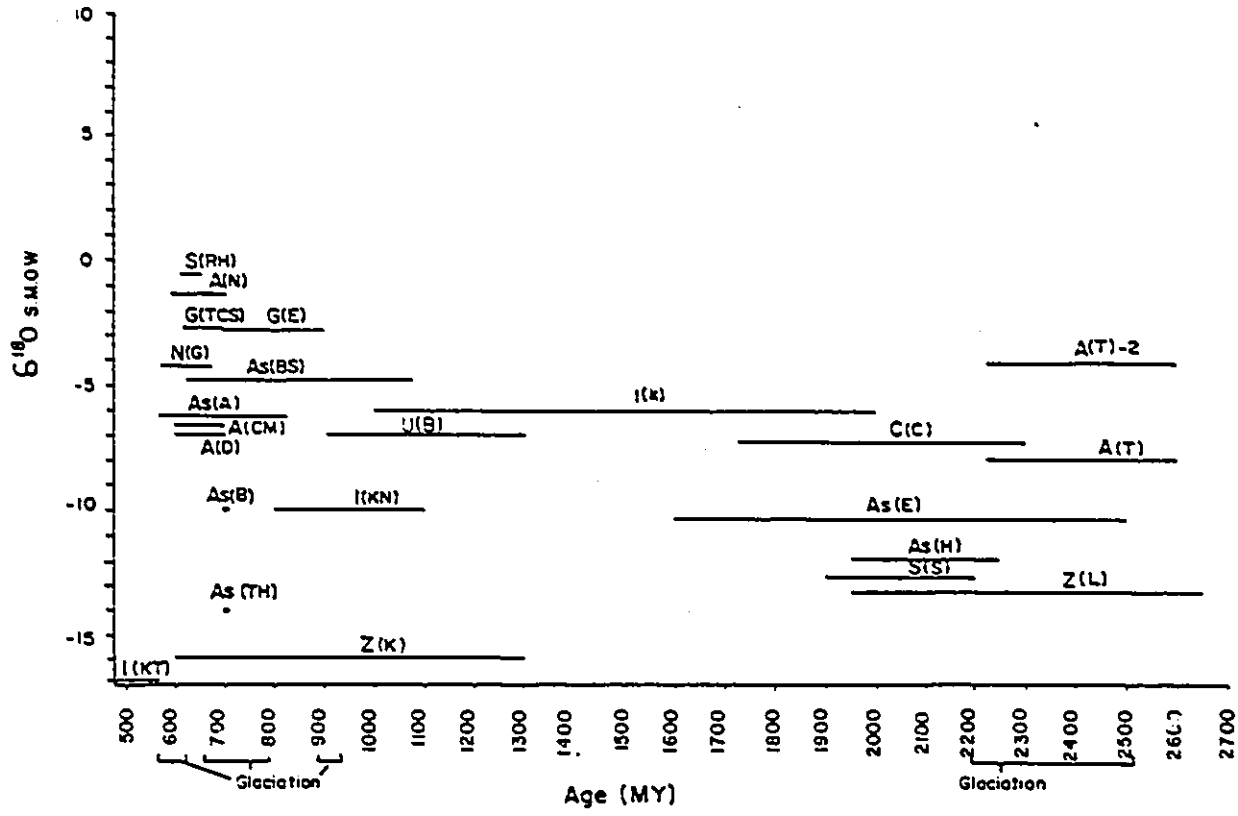

Figure 6-10
$\delta^{18}O$ of 'seawater' based on maximum $\delta^{18}O$ values of Proterozoic limestones (Appendix E). Bars indicate time limits for each sequence as reported in the literature. Those sequences for which only a single date was reported are plotted as points. A - Africa (T) Transvaal Supergroup, (Schidlowski et al., 1983), (T)-2 Transvaal Supergroup, (Schidlowski et al., 1975), (D) Damara System, (CM) Congo and Malmesbury Fms., (N) Nama System: AS-Australia (A) Adelaide Geosyncline, (BS) Bitter Springs Fm., (H) Hammersley Basin, (E) Earaheedy Group, (B) Balcanoona Fm., (TH) Tapley Hill Fm.: C - Canada (C) Coronation Geosyncline: G - Greenland (E) Eleonore Bay Fm., (TCS) Tillite, Canyon, Spiral Creek Fms.: I - India (k) Kaladgi Group, (KN) Kurnool system: N - Nordaustandet (G) Gotia Fm.: Z- Zimbabwe (L) Lomagundi Group: S - Spitsbergen (RH) Rysso and Hunnberg Fms.: S - Scandinavian Shield (S) Svecofennian and Karelian Fms.: U - U.S.A. (B) Belt Supergroup: Z - Zambia (K) Katanga System (Cu-Belt). Glacial ranges summarized from Windley (1977).

as the McArthur Group and the Beck Spring and Noonday Dolomites. The best estimate for $\delta^{18}O$ of Belt seawater, assuming a depositional temperature of 20 °C, is -7 $^{0}/_{00}$ SMOW (Figure 4-22). This value is intermediate between estimates based on the heaviest values from the Zambian copper belt (-15.87 $^{0}/_{00}$), the Indian Kurnool system (-10 $^{0}/_{00}$) and Kaladgi Group (-6.1 $^{0}/_{00}$), and the Australian Bitter Springs Fm. (-4.94 $^{0}/_{00}$: Figure 6-10; Appendix E) and argues against isolation of the Belt sea from the world ocean.

The $\delta^{18}O$ of Archean calcites (and possibly sea water) was supposedly 7 $^{0}/_{00}$ lighter than that of their Cenozoic counterparts (Veizer, 1983c, 1989a,b). If so, the oxygen isotopic composition of seawater at the beginning of the Proterozoic seems to have been similar to the Archean (-5 to -12 $^{0}/_{00}$; Figure 6-10) and increased in the late Proterozoic towards the modern value of 0 $^{0}/_{00}$. In the Phanerozoic, second order variations in $\delta^{18}O$ of 4 $^{0}/_{00}$, and $\delta^{13}C$ of 3 $^{0}/_{00}$, are superimposed on these overall secular trends (Veizer et al., 1986), but such variations are not resolvable in the Proterozoic. The chemistry of the Archean ocean was strongly influenced by mantle flux via cycling of ocean water through oceanic basalt (Veizer, 1983c) and the weathering of relatively abundant young volcanic material on the continents and the sea floor. As discussed earlier, low temperature weathering of silicates is a sink for ^{18}O whereas high

temperature basalt/sea water interaction contributes ^{18}O to seawater. The magnitude of these fluxes is not well known (cf. discussion in Veizer et al., 1986) and silicate weathering may or may not effectively buffer the $^{18}O/^{16}O$ ratio of the oceans through time (Muehlenbachs and Clayton, 1971, 1972; Walker and Lohman, 1989). Analysis of fluid inclusions in Phanerozoic rocks suggests that $\delta^{18}O$ of seawater may have been unchanged since at least the Silurian (Knauth and Beeunas, 1986). Although this finding casts some doubt on the existence of second order fluctuations in the Phanerozoic $\delta^{18}O$ record, it may have little effect on the argument that a fundamental shift in oceanic $\delta^{18}O$ occurred between the Archean and the Phanerozoic.

The best ^{13}C and ^{18}O values of Belt carbonates fall well within limits of coeval sequences (Figures 6-6, 6-7, 6-8, 6-9) and are thus perhaps indicative of the world ocean.

Conclusions

Carbonates of the Belt Supergroup have a geochemical signature expected from theoretical redistribution of trace elements and isotopes during diagenetic-epigenetic alteration. Each formation in the Belt Supergroup has achieved its own diagenetic rank. Progressive post-depositional alteration is recorded by decreasing Sr, increasing Mn, ^{13}C and ^{18}O depletions, and corresponding textural variations. Variations in the degree of diagenesis of particular formations are overprinted by a regional temperature trend shown by a westward depletion in ^{18}O and ^{13}C of limestones. Because of this regional overprint, the 'degree of alteration' for particular formations increases from the oldest Newland to the youngest Libby Formations. The $\delta^{13}C$ may reflect a secular component of about 2 $^{0}/_{00}$ within the Belt depositional interval, but overall the observed $\delta^{13}C$ of $\pm$ 1 $^{0}/_{00}$ are comparable to that of the Phanerozoic carbonates. Relatively high Sr concentrations in the Newland and possibly Libby Formations indicate that these limestones may have had an aragonitic precursor. For the Middle Belt Carbonates, the low Sr contents at comparable Mn concentrations indicate an original high-Mg calcite mineralogy. $^{87}Sr/^{86}Sr$ ratios of Belt carbonates are best preserved in limestones of the Newland Formation (.70484) and in dolostones and become more radiogenic as post-depositional alteration, indexed by

decreasing elemental Sr, ^{13}C and ^{18}O, increased.

Carbon, oxygen and strontium isotope values of the least altered limestones in the Belt Supergroup are similar to those in contemporaneous units worldwide and suggest a connection of the Belt basin with the world ocean. If compared to modern oceans, the Proterozoic ones may have been depleted up to 7 $^{0}/_{00}$ in ^{18}O.

^{34}S values of sulfates and sulfides in the basin and small $\Delta\ ^{34}S$ for sulfate-sulfide pairs, hints that the Belt basin had: 1) a limited supply of sulfate, 2) limited activity of sulfate reducing bacteria, or 3) the sulfides were formed from ^{34}S enriched diagenetic fluids. The absence of Raleigh fractionation trends for either the $\delta^{34}S$ or the $\delta^{13}C$ data militates against either periodic or total restriction of the basin.

The bulk of dolostones in the Belt basin (Spokane/Greyson, Newland, Empire, Snowslip, Middle Belt Carbonate and Shepard Formations) are dominantly of the 'early' micritic type, characterized by good textural preservation. They may have been generated in an evaporitic environment. The observed paucity of widespread evaporites may be a consequence of periodic salinity variations, resulting in dissolution of salts during 'wet' intervals. In contrast, the Altyn and Mt. Shields Formations contain dolostones with pervasive and destructive styles of dolomitization and such

dolostones have formed from ^{18}O depleted waters or at higher temperatures.

References Cited

Adams, J.E. and Rhodes, M., 1960, Dolomitization by seepage refluxing, Amer. Assoc. Petrol. Geol. Bull. v.44, p.1912-1920

Aharon, P., Schidlowski, M., and Singh, I.B., 1987, Chronostratigraphic markers in the end-Precambrian carbon isotope record of the Lesser Himalaya, Nature, v.327, No. 6124, p.699-702

Al-Aasm, I.S., and Veizer, J., 1982, Chemical stabilization of low-Mg calcite: an example of Brachiopoda, Journ. Sed. Pet., v.52, p.1101-1109

Al-Aasm, I.S., and Veizer, J., 1986, Diagenetic stabilization of aragonite and low-Mg calcite, I., Trace elements in rudists: Journ. Sed. Pet., v.56, p.138-152.

Albarede, F., Michard, A., Minster, J.F. and Michard, G., 1981, $^{87}Sr/^{86}Sr$ ratios in hydrothermal waters and deposits from the East Pacific Rise at 21^{0} N, Earth and Planet. Sci. Letters, v.55, p.229-236

Allan, J.R., and Matthews, R.K., 1982, Isotope signatures associated with early meteoric diagenesis, Sedimentology, v.29, p.797-817

Alleman, D.G., 1983, Stratigraphy and sedimentation of the Precambrian Revett Formation, northwest Montana and northern Idaho, M.S. Thesis, Univ. of Montana, Missoula, 103p.

Anderson, T.F. and Arthur, M.A., 1983, Stable isotopes of oxygen and carbon and their application to sedimentologic and paleoenvironmental problems, S.E.P.M. Short Course No. 10, Stable isotopes in sedimentary geology, p.1-1 - 1-151

Andrews, J.E., Hamilton, P.J., and Fallick, A.E., 1987, The geochemistry of early diagenetic dolostones from a low-salinity Jurassic lagoon, Journ. Geol. Soc. London, v.144, p.687-698

Armin, R.A. and Mayer, L., 1983, Subsidence analysis of the Coordilleran miogeocline: implications for timing of Late Proterozoic rifting and amount of extension, Geology, v.11, p.702-705

Badiozamini, K., 1973, The Dorag dolomitization model-application to the Middle Ordovician of Wisconsin, Journ. Sed. Pet., v.43, p.965-984

Baertschi, P., 1957, Messung und Deutung relativer Haufigkeitsvariotionen von ^{18}O und ^{13}C in karbonatgesteinen und mineralien, Schweiz. Mineral. Petrog. Mitt., v.37, p.73-152 in Veizer, J., Fritz, P. and Jones, B., Geochemistry of Brachiopods: oxygen and carbon isotopic records of Paleozoic oceans, Geochem. Cosmochim. Acta, v.50, p.1679-1696

Baker, P.A. and Burns, S.J., 1985, Occurrence and formation of dolomite in organic-rich continental margin sediments, Amer. Ass. Petrol. Geol. Bull. v.69, p.1917-1930

Baker, P.A., Gieskes, J.M., and Elderfield, H., 1982, Diagenesis of carbonates in deep-sea sediments-evidence from Sr/Ca ratios and interstitial dissolved Sr^{+2} data, Journal of Sed. Pet., v.52, no.1, p.71-82

Baker, P.A. and Kastner, M., 1981, Constraints on the formation of sedimentary dolomite, Science, v.213, p.214-216

Bathurst, R.G.C., 1975, Carbonate sediments and their diagenesis, Elsevier, N.Y. 658p

Bathurst, R.G.C., 1986, Carbonate diagenesis and reservoir development: conservation, destruction and creating of pores, Colorado School of Mines Quarterly, v.81, p.1-24

Bausch, W. and Hoefs, J., 1972, Die isotopen zusammensetzung von dolomiten und kalken aus dem suddeutschen Malm, Contrib. Mineral. Petrol., v.37, p121, from Hoefs, J., 1980, Stable isotope geochemistry, 2nd edition, Springer-Verlag, Berlin, 208p

Beauchamp, B., Oldershaw, A.E., and Krouse, H.R., 1987, Upper Carboniferous to Upper Permian ^{13}C enriched primary carbonates in the Sverdrup Basin, Canadian Arctic: comparissons to coeval western N. American Ocean Margins, Chem. Geol., v.65, p.391-413

Bell, K., and Blenkinsop, J., 1984, Multiple collection in solid-source mass spectrometry, Geoscience Canada, v.10, p.210-212

Bloomfield, S.L., 1983, The Proterozoic Greyson-Spokand transition sequence: a stratigraphic and gravity study, west-central Montana, unpubl. M.S. thesis, Univ. of Montana, 93p.

Bogdanov, Y.V. and Golubchina, M.N., 1971, Sulphide sulphur isotope compositions as an important criterion of the genesis of stratigied copper deposits, Soc. Mining Geol. Japan, Spec. Issue 3, p.304-306

Bond, G.C. and Kominz, M.A., 1984, Construction of tectonic subsidence curves for the early Paleozoic miogeocline, southern Canadian Rocky Mountains: Implications for subsidence mechanisms, age of breakup and crustal thinning, Geol. Soc. Amer. Bull., v.95, p.155-173

Both, R.A. and Smith, J.W., 1975, A sulfur isotope study of base metal mineralization in the Willyama complex, western New South Wales, Australia, Econ. Geol., v.70, p.308-318

Bowden, T.D., 1977, Depositional processes and environments within the Revett Formation, Precambrian Belt Supergroup, northwestern Montana and northern Idaho: M.S. thesis, Univ. of Calif., Riverside, 161p.

Bowers, T.S. and Taylor, H.P.Jr., 1985, An integrated chemical and stable - isotope model of the origin of midocean ridge hydrothermal hot spring systems, Journ. Geophys. Res., 90B, 12583-12606

Boyle, E.A., 1981, Cadmium, zinc, copper and barium in foraminifera tests, Earth. Planet. Sci. Lett., v.53, p.11-35

Brand, U., 1989, Aragonite-calcite transformation based on Pennsylvanian molluscs, Geol. Soc. Amer. Bull., v.101, p.377-390

Brand, U. and Morrison, J.O., 1987, Paleoscene #6. Biogeochemistry of Fossil Marine Invertebrates, Geoscience Canada v.14, #2, p.85-107

Brand, U. and Veizer, J., 1980, Chemical diagenesis of a multicomponent carbonate system - 1: trace elements, Journ. Sed. Pet., v.50, p11219-1236

Brand, U. and Veizer, J., 1981, Chemical diagenesis of a multicomponent system - 2: stable isotopes, Journ. Sed. Pet., v.51, p.987-998

Brass, G.W., 1975, The effect of weathering on the distribution of strontium isotopes in weathering profiles, Geochim. Cosmochim. Acta, v.39, p.1647-1653

Brass, G.W., 1976, The variation of the marine $^{87}Sr/^{86}Sr$ ratio during Phanerozoic time: interpretation using a flux model, Geochim. Cosmochim. Acta, v.40, p.721-730

Broecker, W.S., 1963, Radioisotopes and large-scale oceanic mixing in Hill, M.N., ed., The Sea, v.2, Wiley-Interscience: N.Y., p.108-188

Broecker, W.S., 1982, Ocean chemistry during glacial time, Geochim. Cosmochim. Acta, v.46, p.1689-1705

Buddington, A.G., Jensen, M.L. and Mauger, R.L., 1969, Sulfur isotopes and origin of northwest Adirondack sulfide deposits, Geol. Soc. Am. Mem. 115, p.423-451

Burke, W.H., Denison, R.E., Hetherington, E.A., Koepnick, R.B., Nelson, N.F., and Otto, J.B., 1982, Variation of seawater $^{87}Sr/^{86}Sr$ throughout Phanerozoic time, Geology v.10, p.516-519

Burnie, S.W., Schwarcz, H.P. and Crocket, J.H., 1972, A sulfur isotopic study of the White Pine mine, Michigan, Econ. Geol., v.67, p.895-914

Burwash, R.A., 1984, pers. comm. cited in Harrison, J.E., 1984b, Session on geochronology and geophysics (summary): Abstracts with Summaries, Belt Symposium II, Montana Bur. Mines and Geol. Spec. Publ. 90, p.98-100.

Busenberg, E. and Plummer, L.N., 1985, Kinetic and thermodynamic factors controlling the distribution of SO_4^{-2} and Na^+ in calcites and selected aragonites, Geochim. Cosmochim. Acta, v.49, p.713-725

Cameron, E.M., 1982a, Genesis of Proterozoic iron-formation: Sulphur isotope evidence, Geochim. Cosmochim. Acta, v.47, p.1069-1074

Cameron, E.M., 1982b, Sulphate and sulphate reduction in early Precambrian oceans, Nature, v.296, p.145-148

Cameron, E.M., 1983, Evidence from early Proterozoic anhydrite for sulphur isotopic partitioning in Precambrian oceans, Nature, v.304, p.54-56

Cameron, E.M. and Garrels, R.M., 1980, Geochemical composition of some Precambrian shales from the Canadian shield, Chem. Geol., v.28, p.181-197

Cameron, E.M., and Hattori, K., 1987, Archean sulphur cycle: evidence from sulphate minerals and isotopically fractionated sulphides in Superior Province, Canada: Isotope Geoscience, v.65, p.341-358

Campbell, F.A., Ethier, V.G., Krouse, H.R., and Both, R.A., 1978, Isotopic composition of sulfur in the Sullivan Orebody British Columbia, Econ. Geol., v.73, p.246-268

Carballo, J.D. and Land, L.S., 1984, Holocene dolomitization of Sugarloaf sediments by active tidal pumping, Sugarloaf Key, Florida, Amer. Ass. Petrol. Geol. Bull., v.68, p.459

Carr, G.R. and Smith, J.W., 1977, A comparative isotopic study of the Lady Loretta zinc-lead-silver deposit, Mineral. Deposita, v.12, p.105-110

Chambers, L.A., Trudinger, P.A., Smith, J.W. and Burns, M.S., 1975, Fractionation of sulfur isotopes by continuous cultures of Desulfovibrio desulfuricans, Can. Journ. Microbiol., v.21, p.1602-1607

Chase, C.G. and Perry, E.C., 1972, The oceans: growth and oxygen isotope evolution, Science, v.177, p.992-994

Chevillon, C.V., 1977, Tectonically induced Proterozoic soft sediment deformation at the Atlas property, Coeur d'Alene mining district, Idaho, Geol. Soc. Amer. Abstr. w/Prog., Rocky Mtn. Section Mtng., Missoula, Montana

Choquette, P.W. and Steinen, R.P., 1980, Mississippian non-supratidal dolomite, Ste. Genevive limestone, Illinois Basin, evidence for mixed-water dolomitization, Soc. of Econ. Paleont. Mineral. Special Publ. 28, p163-196

Chukrov, F.V., 1971, Isotopic compositions of sulfur and genesis of copper ores of Dzhezkazgan and Udokan, Internat. Geol. Review, 13, p.1429-1434

Cisne, J.L., 1985, Depth-dependent sedimentation and the flexural edge effect in epeiric seas: measuring water depth relative to the lithosphere's flexural wavelength, Journal of Geology, v.93, no.5, p.567-576

Claypool,, G.E., Holser, W.T., Kaplan, I.R., Sakai, H. and Zak, I., 1980, The age curves of sulfur and oxygen isotopes in marine sulfate and their mutual interpretation, Chem. Geol., v.28, p.199-259

Clayton, R.M. and Degens, E.T., 1959, Use of C isotope analyses for differentiating fresh-water and marine sediments, Amer. Ass. Petrol. Geol. Bull., v.43, p.890-897

Clayton, R.N., Jones, B.F. and Berner, R.A., 1968, Isotope studies of dolomite formation under sedimentary conditions, Geochim. Cosmochim. Acta, v.32, p.415-432

Collerson, K.D., Ullman, W.J. and Torgersen, T., 1988, Ground waters with unradiogenic $^{87}Sr/^{86}Sr$ in the Great Artesian Basin, Australia, Geology, v.16, no.1, p.1-96

Connor, J.J., Reynolds, M.W. and Whipple, J.W., 1984, Stratigraphy of the Ravalli Group, Belt basin, Montana and Idaho: Abstracts with Summaries, Belt Symposium II, Montana Bur. Mines and Geol. Spec. Publ. 90, p.13-15.

Craig, H. and Lupton, J.E., 1981, Helium-3 and mantle volatiles in the ocean and the oceanic crusts, in C. Emiliani ed., The Sea, vo. 7, Wiley, New York, p.391-428

Cressman, E.R., 1982, Generalized Stratigraphic section of the Prichard Formation, basal Belt Supergroup, Proterozoic Y near Plains, Montana: U.S. Geol. Survey Open File Report 82-495, 1p.

Cressman, E.R., 1984a, Paleogeography and paleotectonic setting of the Prichard Formation - a preliminary interpretation: Abstracts with Summaries, Belt Symposium II, Montana Bur. Mines and Geol. Spec. Publ. 90, p.8-9.

Cressman, E.R., 1984b, Summary of session on lower Belt and Ravalli group stratigraphy: Abstracts with Summaries, Belt Symposium II, Montana Bur. Mines and Geol. Spec. Publ. 90, p.19-22.

Dasch, E.J., 1969, Strontium isotopes in weathering profiles, deep-sea sediments and sedimentary rocks, Geochim. Cosmochim. Acta, v.33, p.1521-1552

Davies, G.R., 1977, Former magnesian calcite and aragonite submarine cements in upper Paleozoic reefs of the Canadian Arctic: A summary, Geology, v.5, p.11-15

Davis, J.A., Fuller, C.C. and Cook, A.D., 1987, A model for trace metal sorption processes at the calcite surface: adsorption of Cd^{+2} and subsequent solid solution formation, Geochim. Cosmochim. Acta, v.51, p.1477-1490

Degens, E.T. and Epstein, S., 1962, Relationship between $^{18}O/^{16}O$ ratios in coexisting carbonates, cherts and diatomites, Amer. Ass. Petrol. Geol. Bull., v.46, p.534-542

Degens, E.T., and Epstein, S., 1964, Oxygen and carbon isotope ratios in coexisting calcites and dolomites from recent and ancient sediments, Geochm. Cosmochm. Acta, v.28, p.23-44

Deines, P., 1980, The carbon isotopic composition of diamonds: Relationship to diamond shape, color, occurrence and vapor composition, Geochim. Cosmochim. Acta, v.46, p.943-961

Demaiffe, D. and Fieremans, 1981, Strontium isotopic geochemistry of the Mbuji Mayi and Kundelungu kimberlites, Zaire, central Africa, Chem. Geol., v.31, p.311-324

DePaolo, D.J., 1987, Correlating rocks with strontium isotopes, Geotimes, December, 1987, p.16-18

Deuser, W.G. and Degens, E.T., 1967, Carbon isotope fractionation CO_2(gas)-CO_2(aq.)-HCO_3^-(aq.), Nature, v.215, p.1033

Donnelly, T.H. and Ferguson, J., 1980, A stable isotope study of three deposits in the Alligator Rivers uranium field in J. Ferguson and A.B. Goleby (eds.) Uranium in the Pine Creek Geosyncline, Int. Atom. Energy Authority, Viewwn Proc. Ser., p.387-406

Dontsova., E. I., 1970, Oxygen isotope exchange in rock forming processes, Geochem. Int., v.7, p.624-636

Dontsova, E.I., Migdisov, A.A. and Ronov, A.B., 1972, On the causes of variation of oxygen isotopic composition in the carbonate strata of the sedimentary column, Geochem. Int., v.9, p.885-891

Drever, J.I., 1982, The geochemistry of natural waters, Prentice-Hall, Englewood Cliffs, N.J., 388p.

Dunham, R.J., 1962, Classification of carbonate rocks according to depositional texture, in W.E. Ham (ed.) Depositional Environments in Carbonate Rocks, Am. Ass. Petrol. Geol., Tulsa, Ok., pp.108-121

Eby, D.E., 1977, Sedimentation and early diagenesis within eastern portions of the 'Middle Belt Carbonate Interval' (Helena Formation), Belt Supergroup (Precambrian Y), western Montana: PhD. thesis, State University of New York at Stony Brook, Stony Brook, New York, 712 p.

Eckelman, W.R., Broecker, W.S., Whitlock, D.W., and Allsup, J.R., 1962, Implications of carbon isotopic composition of total organic carbon of some recent sediments and ancient oils, Bull. Amer. Ass. Petrol. Geol., v.46., p.699-704

Eichmann, R. and Schidlowski, M., 1975, Isotopic Fractionation between coexisting organic carbon-carbonate pairs in Precambrian sediments, Geochm. Cosmochm. Acta., v.39, p.585-595

Eisbacker, G.H., 1981, Sedimentary tectonics and glacial record in the Windermere Supergroup, Mackenzie Mtns., N.W. Canada, Canad. Geol. Surv. Paper 80-27, 40p

Elderfield, H. and Gieskes, J.M., 1982, Sr isotopes in interstitial waters of marine sediments from deep sea drilling project cores, Nature, v.300, p.493-497

Elston, D.P., 1984, Magnetostratigraphy of the Belt Supergroup - A symposium: Abstracts with Summaries, Belt Symposium II, Montana Bur. Mines and Geol. Spec. Publ. 90, p.88-90.

Emrich, K., Enhalt, D.H., and Vogel, J.C., 1970, Carbon isotope fractionation during the precipitation of calcium carbonate, Earth Planet Sci. Lett, v.8, p.363-371

Eslinger, E.V., and Savin, S.M., 1973, Oxygen isotope geothermometry of burial metamorphic rocks of the Precambrian Belt Supergroup, Glacier National Park, Montana: Geol. Soc. Amer. Bull., v.84, p.2549-2560.

Farley, K.J., Dzombak, D.A. and Morel, F.M.M., 1985, A surface precipitation model for the sorption of cations on metal oxides, Journ. Colloid Interface Sci., v.106, p.226-242

Faure, G., 1977, Principles of Isotope Geology, John Wiley, New York, 464p.

Faure, G., 1986, Principles of Isotope Geology, 2nd edition, John Wiley and sons, New York, 589p

Fenton, C.L. and Fenton, M.A., 1937, Belt Series of the north, stratigraphy, sedimentation, paleontology, Geol. Soc. Amer. Bull., v.84, p.1114-1120

Fermor, P.R. and Price, R.A., 1984, Stratigraphy of the lower part of the Belt-Purcell Supergroup (middle Proterozoic) in the Lewis Thrust Sheet of southern Alberta and British Columbia: Montana Geol. Soc. 1984 Field Conf. N.W. Montana

Finch, J.C. and Baldwin, D.O., 1984, Stratigraphy of the Prichard Formation, Belt Supergroup, Abstracts with Summaries, Belt Symposium II proceedings, Montana Bureau Mines and Geol. Spec. Publ. 90, p.5-8.

Fisher, R. and Stueber, A.M., 1976, Strontium isotopes in selected streams within the Susquehanna River basin, Water Resources Res., v.12, p.1061-1068

Folk, R.L., 1962, Spectral subdivision of limestone types, in W.E. Ham (ed.), Classification of Carbonate Rocks, Am.Ass. Petrol. Geol., Tulsa, Ok., pp.62-84

Folk, R.L., and Land, L.S., 1975, Mg/Ca ratio and salinity, two controls over crystallization of dolomite, Amer. Ass. Petrol. Geol. Bull., v.59, p.60-68

Folk, R.L. and Pittman, J.S., 1971, Length-slow chalcedony: a new testament for vanished evaporites, Jour. of Sed. Pet., v.41, p.1045-1058.

Frakes, L.A., 1979, Climates throughout geologic time, Amsterdam, Elsevier, 310p

Freidrichsen, H., 1984, Oxygen and hydrogen isotope studies in glauconites, Terra Cognita, v.4, p.218

Frey, M., 1969, Beitr. Geol. Karte Schweiz Neue Folge 137 from Winkler, H.G.F., Petrogenesis of metamorphic rocks 4th edition, Springer-Verlag, N.Y., 334p.

Fritz, P., 1971, Geochemical characteristics of dolomites and the ^{18}O content of middle Devonian oceans, Earth Planet Sci. Lett., v.11, p1277-282

Fritz, P. and Katz, A., 1972, The sodium distribution of dolomite crystals, Chem. Geol., v.72, p.170-194

Fritz, P. and Smith, D.C.W., 1970, The isotopic composition of secondary dolomites, Geochim. Cosmochim. Acta, v.34, p.1161-1173

Frost, C.D. and Winston, D., 1987, Nd isotope systematics of coarse- and fine-grained sediments: examples from the middle Proterozoic Belt-Purcell Supergroup, Journ. of Geology, v.95, p. 309-327

Gabrielse, H., 1972, Younger Precambrian of the Canadian Cordillera: Amer. Jounr. of Sci., v.272, p.421-536

Gabrielse, H. and Reesor, J.E., 1964, Geochronology of plutonic rocks in two areas of the Canadian Cordillera: in Geochronology Can. Roy. Soc. Can. Special Pub. No. 8, p.96-129.

Garrels, R.M., and Lerman, A., 1981, Phanerozoic cycles of sedimentary carbon and sulfur, Proc. Nat. Acad. Sci., U.S.A., v.78, p.72-78

Garrels, R.M. and Mackenzie, F.T., 1971,Evolution of sedimentary rocks, W.W. Norton and Co., N.Y., 397p

Garrels, R.M. and Perry, E.A., 1974, Cycling of carbon, sulfur and oxygen through geologic time in Goldberg, E.D. (ed.), The sea, Wiley-Interscience, New York, p.303-336

Gearing, J.N., Gearing, P.J., Rudnick, D.T., Requejo, A.G. and Hutchins, M.J., 1984, Isotopic variability of organic carbon in phytoplankton-based temperate estuary, Geochim. Cosmochim. Acta, v.48, p.1089-1098

Gieskes, J.M. and Lawrence, J.M., 1981, Alteration of volcanic matter in deep sea sediments: evidence from the chemical composition of interstitial waters from deep sea driling cores, Geochim. Cosmochim. Acta, v.45, p.1687-1703

Godlewski, D.W., 1977, The origin of the middle Wallace breccias (abs.) Geol. Soc. of Amer. Abstr. w/Prog., v.9, no.61, p.727

Godlewski, D.W. and Zieg, G.A., 1984, Stratigraphy and depositional setting of the Precambrian Newland Limestone, Abstracts and Summaries, Belt Symposium II, Montant Bur. of Mines and Geol. Spec. Publ. 90, p.2-4

Goldberg, E.D., 1963, The oceans as a chemical system, in The sea, Hill, M.N. (ed.), Wiley-Interscience, p.3-25

Goldstein, S.J. and Jacobsen, S.B., 1987, The Nd and Sr isotopic systematics of river-water dissolved material: implications for the sources of Nd and Sr in seawater, Chem. Geol., Isotope Geoscience Sect., v.66, p.245-272

Goldstein, S.J. and Jacobsen, S.B., 1988, Nd and Sr isotopic systematics of river water suspended material: implications for crustal evolution, Earth Planet. Sci. Lett., v.87, p.249-265

Goodfellow, W.D. and Jonasson, I.R., 1984, Ocean stagnation and ventilation defined by $\delta^{34}S$ secular trends in pyrite and barite, Selwyn Basin, Yukon, Geology, v.12, p.543-586

Goodwin, A.M., Monster, J. and Thode, H.G., 1976, Carbon and sulfur isotope abundances in Archean iron formations and early Precambrian life, Econ. Geol., v.71, p.870-891

Gordon, L., Salutsky, M.L., and Willard, H.H., 1959, Precipitation from homogenous solution, John Wiley and sons, N.Y. from Veizer, J., 1983a, Chemical diagenesis of carbonates: theory and application of trace element technique, S.E.P.M. Short Course no. 10, Stable isotopes in sedimentary geology, p.3-1 - 3-100

Graf, D.L., 1960, Minor element distribution in Geochemistry of carbonate sediments and carbonate sedimentary rocks, Illinois State Geol. Surv. Circular 301

Graham, D.W., Bender, M.L., Williams, D.F. and Keighwin, L.D., 1981, Strontium and calcium ratio in Cenozoic planktonic foraminifera, Geochim. Cosmochim. Acta, v.46, p.1281-1292

Gregory, R.T. and Taylor, H.P., 1981, An oxygen isotope profile in a section of Cretaceous ocean crust, Samoil ophiolite, Oman: evidence for ^{18}O buffering of the oceans by deep (>5km) seawater hydrothermal circulation at mid ocean ridges, Journ. Geophys. Res., v.86, p.2737-2755

Grotzinger, J.P., 1981, The stratigraphy and sedimentation of the Wallace Formation, northwest Montana and northern Idaho, M.S. thesis, Univ. of Montana, Missoula, 153p.

Grotzinger, J.P., 1986, Shallowing-upward cycles of the Wallace Formation, Belt Supergroup, northwestern Montana and northern Idaho: in Belt Supergroup, a guide to Proterozoic rocks of western Montana and adjacent areas, Sheila Roberts, ed., Mont. Bur. Mines and Geol. Spec. Publ. 94, p.143-161.

Hall, F.B. II, 1968, Bedrock geology, north half of Missoula 30' quadrangle, Montana, unpubl. PhD. dissertation, Univ. of Montana, Missoula

Hall, S.M., 1984, Metallogenesis and stable isotope systematics of stratabound lead/silver deposits in the Precambrian Noonday Dolomite, Death Valley, Ca., unpubl. M.S. thesis, Univ. of Calif., Davis, 133p.

Hambrey, M.J. and Harland, W.B., 1985, The late Proterozoic glacial era, Paleogeog. Paleoclim. Paleoecol., v.51, p.255-272

Hamilton, J.M., Delaney, G.D., Hauser, R.L., and Ransom, P.W., 1983, Geology of the Sullivan deposit, Kimberly, B.C., Canada, in Sediment-hosted stratiform lead-zinc deposits, D.F. Sangster (ed.), Mining Assn. Canada short course notes, p.31-83

Hanshaw, B.B., Back, W., and Deike, R.G., 1971, A geochemical hypothesis for dolomitization by ground water, Econ. Geol., v.66, p.719-724

Harrison, J.E., 1972, Precambrian Belt Basin of the northwestern United States, it's geometry, sedimentation and copper occurrences, Geol. Soc. Amer. Bull., v. 83, no.5, p.1215-1240.

Harrison, J.E., 1984, Stratigraphy and lithocorrelation of the Wallace Formations: Abstracts with summaries, Belt Symposium II, Montana Bur. Mines and Geol. Spec. Publ. 90, p.24-26.

Harrison, J.E. and Grimes, D.J., 1970, Mineralogy and geochemistry of some Belt rocks, U.S. Geol. Surv. Bull., 1312-O, 49 p.

Harrison, J.E., and Jobin, D.A., 1963, Geology of the Clark Form quadrangle, Idaho-Montana: U.S.Geol. Survey Bull., 1141-K, p. KI-K39

Harrison, J.E., Griggs, A.B. and Wells, J.D., 1974, Tectonic features of the Belt basin and their influence on post-Belt structures: U.S. Geol. Surv. Prof. Paper 866, 15p.

Harrison, J.E., Kleinkopf, M.D. and Wells, J.D., 1980, Phanerozoic thrusting in Proterozoic Belt rocks, northwestern United States: Geology, v. 8, p.407-411.

Hattori, K., Krouse, H.R. and Campbell, F.A., 1983, The start of sulfur oxidation in continental environments: about 2.2 x 10^9 years ago, Science, v.221, p.549-551

Helgeson, H.C., Delany, J.M., Nesbitt, H.W. and Bird, D.K., 1978, Summary and critique of the thermodynamic properties of rock-forming minerals, Amer. Journ. Sci., v.278-A, 229p

Hemzacek, J.M., Larue, D.K., Montgomery, C.A. and Perry, E.C., 1984, The ^{34}S age curve of the Precambrian: clues from replaced evaporites, unpublished manuscript, Northern Illinois University, 14p. in Ueda, A., Cameron, E.M. and Krouse, H.R., in press, ^{34}S-enriched sulphate in the Belcher Group, N.W.T., Canada: evidence for dissimilatory sulphate reduction in the early Proterozoic ocean

Hietanen, A., 1963, Metamorphism of the Belt Series in the Elk River-Clarkia area, Idaho, U.S.G.S. Prof. Paper 344-C, 49p.

Hobbs, W.S. (ed.), 1984, Preface to Belt symposium II, 1984, Abstracts and summaries, Montana Bureau of Mines and Geology Special Publ. 90, p.v,vi

Hobbs, S.W., Griggs, A.B., Wallace, R.E. and Campbell, A.B., 1965, Geology of the Coeur d'Alene district, Shoshone County, Idaho, U.S. Geol. Sur. Prof. Paper 478, 139p.

Hoefs, J., 1980, Stable Isotope Geocheimstry, 2nd edition, Springer-Verlag, Berlin, 208p.

Hoefs, J. and Frey, M., 1976, Isotopic composition of carbonaceous matter in a metamorphic profile from the Swiss Alps, Geochm. Cosmochm. Acta, v.40, p.945-951

Hoffman, A.W. and Hart, S.R., 1978, An assessment of local and regional isotopic equilibrium in the mantle, Earth Planet. Sci. Lett., v.38, p.95-116

Holland, H.D., 1978, The chemistry of the atmosphere and oceans, Wiley, N.Y., 351p

Holland, H.D., 1984, The chemical evolution of the atmosphere and oceans, Princeton series in geochemistry, Princeton Univ. Press, N.J., 582p.

Holser, W.T., 1977, Catastrophic chemical events in the history of the ocean, Nature, v.267, p.403-408

Holser, W.T., 1984, Gradual and abrupt shifts in ocean chemistry during Phanerozoic time, in Patterns of Chamge in Earth Evolution, H.D. Holland and A.J. Trendal, eds., Berlin, Springer, p.123-143

Holser, W.T. and Kaplan, I.R., 1966, Isotope geochemistry of sedimentary sulfates, Chem. Geol., v.1, p.93-135

Horodyski, R.J., 1983, Sedimentary geology and stromatolites of the middle Proterozoic Belt Supergroup, Glacier National Park, Montana: Precambrian Res., v.20, p.391-425.

Hoy, T., 1982, The Purcell Supergroup in southeastern British Columbia: sedimentation, tectonics and stratiform lead-zinc deposits in Hutchinson, R.W., Spence, C.D. and Franklin, J.M., eds., Precambrian sulphide deposits, H.S. Robinson memorial volume, Geol. Ass. Canada Special Paper 25, p.127-147

Hoy, T., 1984, The Purcell Supergroup near the Rocky Mountain Trench southeastern British Columbia, in Hobbs, W.S. (ed.) Belt Symposium II, 1984, Abstracts and summaries, Montana Bureau of Mines and Geology, Special Publ. 90, p.36-38

Hrebar, S.V., 1971, Stratigraphy and depositional environment of the St. Regis Formation of the Ravalli Group (Precambrian Belt Megagroup) northwestern Montana and Idaho: PhD. dissertation, Univ. of Cincinnati, 188p. (abs.), Dissertation Abstracts International, v.32, no.6, p.3438b-3439b.

Hudson, J.D., 1977, Stable isotopes and limestone lithification, J.Geol. Soc. London, v.133, p.637-660

Hunt, G.H., 1964, Chemical correlation of the Purcell igneous rocks, Bull. Can. Petrol. Geol., v.12, spec. issue guidebook, p.544-555

Illich, H.A. and Winston, D., 1968, Belt-Middle Cambrian gradational boundary, western Montana (abstr.), Geol. Soc. Amer. Special Paper 101, p.101

Illing, G.U., Wells, A.J. and Taylor, C.M., 1965, Penecontemporary dolomite in the Persian Gulf in Pray, A.C. and Murray, R.C., eds., Dolomitization and Limestone Diagenesis, Soc. Econ.Paleontol. Mineral. Special Publ. No.13, p.89-111

Ishikawa, M. and Ichikuni, M., 1984, Uptake of sodium and potassium by calcite, Chem. Geol., v.42, p.137-147

James, N.P. and Choquette, P.W., 1984, Diagenesis 9. limestones - the meteoric environment, Geoscience Canada, v.11, #4, p.161-193.

Jenkins, W.J., Edmond, J.M. and Corliss, J.B., 1978, Excess ^{3}He and ^{4}He in Galapagos submarine hydrothermal waters, Nature, v.272, p.156-158

Kaplan, I.R., and Rittenberg, S.C., 1964, Microbiological fractionation of sulfur isotopes, Journ. Gen. Microbiol., v.34, p.195-212

Keith, M.L. and Weber, J.N., 1964, Carbon and oxygen isotopic composition of selected limestones and fossils, Geochim. Cosmochim. Acta, v.28, p.1787-1816

Keppens, E. and O'Neil, J.R., 1985, Isotope geochemistry of glauconitic sediments: II- Stable isotopes, in Isotopes in the Sedimentary Cycle, Abstracts, Obernai, France from Veizer, J., Fritz, P. and Jones, B., 1986, Geochemistry of brachiopods: oxygen and carbon isotopic records of Paleozoic oceans, Geochim. Cosmochim. Acta, v.50, p.1679-1696

Kiba, T., Takagi, T., Yoshimura, Y. and Kishi, I., 1955, Tin (II)-strong phosphoric acid. A new reagent for the determination of sulphate by reduction to hydrogen sulphide, Bull. Chem. Soc. Japan, v.28, p.641-644

Kidder, D.L., 1985, Stratigraphy and depositional environments of the Libby Formation, Preterozoic Belt Supergroup, N.W. Montana, Geol. Soc. Amer. Abstr. w/prog., Cordilleran section mtng. Boise, Id.

Kidder, D.L., and Hall, S.M., in prep., Petrology and trace element geochemistry of mixed aragonite and calcite ooids of the Libby Formation, Belt Supergroup, Montana

King, R. H., 1947, Sedimentation in Permian Castile Sea, Am. Ass. Petrol. Geol. Bull., v.31,p.470-477

Kinsman, D.J.J., 1969, Interpretation of Sr^{+2} concentrations in carbonate minerals and rocks, J. Sed. Petrol., v.39, p.486-508.

Kleinkopf, M.D. and Reynolds, M.W., 1982, Tectonic framework of western Montana interpreted from regional magnetic-anomaly data (abs.), Geol. Soc. Amer. Abstr. w/Prog., Rocky Mtn. Section, v.14, no.6, p317

Knauth, L.P. and Beeunas, M.A., 1986, Isotope geochemistry of fluid inclusions in Permian halite with implications for the isotopic history of ocean water and the origin of saline formation waters, Geochim. Cosmochim. Acta, v.50, p.419-433

Knauth, L.P. and Epstein, S., 1976, Hydrogen and oxygen isotope ratios in nodular and bedded cherts, Geochim. Cosmochim. Acta, v.40, p.1095-1108

Knauth, L.P. and Lowe, D.R., 1978, Oxygen isotope geochemistry of cherts from the Onverwacht Group (3.4 billion years), Transvaal, S. Africa, with implications for secular variations in the isotopic composition of cherts, Earth Planet. Sci. Lett., v.41, p.209-222

Knoll, A. H., Hayes, J.M., Kaufman, A.J., Swett, K. and Lambert, I.B., 1986, Secular variation in carbon isotope ratios from the upper Proterozoic succession of Svalbard and East Greenland, Nature, v.321, p.832-838

Kolodny, Y. and Epstein, S., 1976, Stable isotope geochemistry of deep sea cherts, Geochim. Cosmochim. Acta, v.40, p.1195-1209

Kroopnick, P., 1980, The distribution of ^{13}C in the Atlantic Ocean, Earth Planet Sci. Letters, v.49, p.469-484

Kubler, B. 1967, Bull. Centre Recherches PAU-SNPAI: 259-278 in. Winkler, H.G.F., Petrogenesis of metamorphic rocks, 4th edition, Springer-Verlag, N.Y., 334p.

Lambert, I.B., Donnelly, T.H., Dunlop, J.S.R. and Groves, D.I., 1978, Stable isotope compositions of early Archean sulphate deposits of probable evaporitic and volcanogenic origin, Nature, v.276, p.808-811

Lambert, I.B., Donnelly, T.H., Etminan, H., and Rowlands, N.J., 1984, Genesis of Late Proterozoic copper mineralization, Copper Claim, South Australia, Econ. Geol., v.79, p.461-475

Lambert, I.B., Walter, M.R., Wenlong, Z., Songnian, L., and Guogan, M., 1987, Paleoenvironment and carbon isotope stratigraphy of Upper Proterozoic carbonates of the Yangtze Platform, Nature, v.325, No.7000, p.140-142

Land, L.S., 1980, The isotopic and trace element geochemistry of dolomite: the state of the are, Soc. of Econ. Paleont. Mineral. Spec. Publ. 28, p.87-110

Land, L.S., 1986, Environments of limestone and dolomite diagenesis: some geochemical considerations, in Carbonate depositional environments, modern and ancient, Part 5: diagenesis 1, Colorado School of Mines Quarterly, v.81, No.4, p.26-41

Land, L.S. and Hoops, G.K., 1973, Sodium in carbonate sediments and rocks: a possible index to the salinity of diagenetic solutions, Journ. Sed. Pet., v.43, p.614-617

Lang, H.M., 1983, Relative timing of thrusting and metamorphism in Belt series rocks north of the Idaho batholith (abs.): Geol. Soc. Amer. Abstr. w/prog., v.15, p.437

Lang, H.M. and Rice, J.M., 1981, Low-variance mineral paragenesis in metapelites of the Snow Peak area, northern Idaho (abs.): Geol. Soc. Amer. Abst. w/prog., v.13, p.494

Lange, I.M., Moore, J.N. and Krouse, H.R., 1987, Diagenesis and copper mineralization in carbonates inn the Spokane Formation, Belt Supergroup, at Wolf Creek, Montana, Econ. Geol. v.82, p.1334-1347

Lawrence, J.R. and Gieskes, J.M., 1981, Constraints on water transport and alteration in the oceanic crust from the isotopic composition of pore water, J. Geophys. Res., v.86, p.7924-7934

Leech, G.B., 1962, Metamorphism and granitic intrusions of Precambrian age in southeastern British Columbia: Can. Geol. Surv. Paper 62-13, 8p.

Lippman, F., 1973, Sedimentary Carbonate Minerals, Springer, Berlin, 228p

Lohman, K.C., 1983, Unravelling the diagenetic history of carbonate reservoirs: integration of petrographic and geochemical techniques in A.A.P.G. Short course notes, Dallas mtng.

Lohman, K.C. and Walker, J.C.G., 1989, The delta-18 record of Phanerozoic abiotic marine cements, Geophys. Res. Lett., v.16, p.319-322

Longinelli, A. and Nuti, S., 1968, Oxygen isotope composition of phosphorites from marine formations, Earth Planet. Sci. Lett., v.5, p.13-16

Lorens, R.B., 1981, Sr, Cd, Mn and Co distribution coefficients in calcite as a function of calcite precipitation rate, Geochim. Cosmochm. Acta, V.45, p.553-561.

Lucchitta, I. and Hendricks, J.D., 1983, Characteristics, depositional environment and tectonic interpretations of the Proterozoic Cardenas lavas, eastern Grand Canyon, Arizona, Geology, v.11, p.177-181

Luz, B., Kolodny, Y. and Kovach, J., 1984, Oxygen isotope variations in phosphate of biogenic apatites, III, Conodonts, Earth Planet. Sci. Lett, v.69, p.255-262

Machel, H.G. and Mountjoy, E.W., 1986, Chemistry and environments of dolomitization - a reappraisal, Earth-Science Reviews, v.23, p.175-222

Magaritz, M., Holser, W.T., and Kirschvink, L., 1986, Carbon-isotope events across the Precambrian/Cambrian boundary on the Siberian Platform, Nature, v.320, No.6059, p.258-259

Magaritz, M. and Taylor, H.P., Jr., 1976, Oxygen, hydrogen and carbon isotope studies of the Franciscan formation, Coast Ranges, California, Geochim. Cosmochim. Acta, v.40, p.215-235

Makela, M., 1974, A study of sulfur isotopes in the Outokumpu ore deposit, Finland, Geol. Surv. Finland Bull., v.267, p.1-45

Malvia, R.G. and Siever, R., 1988, Diagenetic replacement controlled by force of crystallization, Geology, v.6, p.685-691

Manghnani, M.H., Schlanger, S.O. and Milholland, P.E., 1980, Elastic properties related to depth of burial, strontium content and age, and diagenetic stage in pelagic carbonate sediments, in Bottom-interacting ocean acoustics, W.A. Kupferman and B.F. Jensen eds., New York, Plenum Press, p. 41-51

Matthews, A. and Katz, A., 1977, Oxygen isotope fractionation during the dolomitization of calcium carbonate, Geochm. Ccsmochm. Acta, v.27, p1209-1264

Mauk, J.L., 1983, Stratigraphy and sedimentation of the Proterozoic Burke and Revett Formations, Belt Supergroup, Flathead Reservation, western Montana (abs.): Geol. Soc. Amer. Abstr. w/prog., v.15, no.5, p.424.

Maxwell, D.T. and Hower, J., 1967, High grade diagenesis and low-grade metamorphism of illite in the Precambrian Belt series: American Mineral., v.52, p.843-857.

McBride, M.B., 1979, Chemisorption and precipitation of Mn^{+2} at $CaCO_3$ surfaces, Soil Sci. Soc. Amer. Journ., v.43, p.693-698

McIntire, W.L., 1963, Trace element partition coefficients - a review of theory and application to geology, Geochm. Cosmochm. Acta, v.27, p.1209-1264.

McKirdy, D.M. and Powell, T.G., 1974, Metamorphic alteration of carbon isotopic composition in ancient sedimentary organic matter: new evidence from Australia and South Africa, Geology, v.2, p.591-595

McMannis, W.J., 1963, LaHood Formation - a coarse facies of the Belt Series in southwestern Montana: Geol. Soc. Amer. Bull. v.74, p.407-436.

McMechan, M.E., 1981, The middle Proterozoic Purcell Supergroup in the southwest Purcell mountains, British Columbia , and the initiation of the Cordilleran miogeocline, southern Canada and adjacent United States: Bull. Can. Soc. Petrol. Geol., v.29, p.583-621.

McRae, S.G., 1972, 'Glauconite': Earth Sci. Rev., 8, p.397-440

Michard, G., Michard, A., Albarede, F., Minster, J.R. and Charlou, J.L., 1984, Chemistry of solutions from 13°N East Pacific Rise hydrothermal site, Earth Planet. Sci. Lett., v.67, p.297-307

Miller, F.K. and Clark, L.D., 1975, Geology of the Chewelah-Loon Lake area, Stevens and Spokane Counties, Washington, U.S. Geol. Surv. Prof. Paper 806, 74p.

Monson, K.D. and Hayes, J.M., 1982, Carbon isotopic fractionation in the biosynthesis of bacterial fatty acids, Ozonolysis of unsaturated fatty acids as a means of determining the intramolecular distribution of carbon isotopes, Geochim. Cosmochim. Acta, v.34, p.525-527

Monster, J., Appel, P.W.U., Thode, H.G., Schidlowski, M., Carmichael, C.M. and Bridgewater, D., 1979, Sulfur isotope studies in early Archaean sediments from Isua, W. Greenland: implications for the antiquity of bacterial sulfate reduction, Geochim. Cosmochim. Acta, v.43, p.405-413

Morrow, D.W., 1982, Diagenesis I. Dolomite - part I: The chemistry of dolomitization and dolomite precipitation, Geoscience Canada, v.9, p.5-13

Morton, J.L. and Sleep, N.H., 1985, A mid-ocean ridge thermal model: constraints on the volume of axian hydrothermal heat flux, Journ. Geophys. Res., 90B, 11345-11353

Mucci, A. and Morse, J.W., 1983, The incorporation of Mg^{+2} and Sr^{+2} into calcite over-growths; influences of growth rate and solution composition, Geochim. Cosmochim. Acta, v.47, p.217-233

Mucci, A., Morse, J.W. and Kaminski, M.S., 1985, Auger spectroscopy analysis of magnesian calcite overgrowths precipitated from seawater and solutions of similar composition, Am. Journ. Sci., v.285, p.289-305

Mudge, M.R., 1970, Origin of the disturbed belt in northwestern Montana, Geol. Soc. Amer. Bull., v.81, p.377-392.

Muehlenbachs, K. and Clayton, R.N., 1971, Oxygen isotope ratios of submarine diorites and their constituent minerals, Can. Journ. Earth Sci., v.8, p.1591-1595

Muehlenbachs, K. and Clayton, R.N., 1972, Oxygen isotope geochemistry of submarine greenstones, Can. Journ. Earth Sci., v.9, p.471-478

Muir, M., Lock, D., and von der Borch, C., 1980, The Coorong model for penecontemporaneous dolomite formation in the Middle Proterozoic McArthur Group, Northern Territory, Australia, Soc. Econ. Paleon. Mineral. Special Publ. 28, Concepts and Models of Dolomitization, p.51-68

Mullins, H.T., Wist, S.W., Gardulski, A.F., Hinchey, E.J., Masters, P.M. and Siegel, D.I., 1986, Shallow subsurface diagenesis of Pleistocene periplatform ooze, northern Bahamas, Sedimentology, v.32, p.473-494

Myers, W.B., 1952, Geology and mineral deposits of the northwest quarter Willis quadrangle and adjacent Browns Lake area, Beaverhead County, Mt., U.S. Geol. Surv. Trace Elements Inv. Rept. 259, 46p.

Nelson, W.H., 1963, Geology of the Duck Creek Pass quadrangle, Montana: U.S. Geol. Sur. Bull. 1121J, 56p.

Nelson, W.H. and Dobell, J.P., 1961, Geology of the Bonner quadrangle, Montana, U.S. Geol. Surv. Bull., 111-F, p.189-235

Nielsen, H., 1965, Schwefelisotope in marinen Kreislauf und das $\delta^{34}S$ des fruheren Meere, Geol. Rdsch, v.55, p.160-172 from Mackenzie, F.T. and Pigott, J.D., 1981, Tectonic controls of Phanerozoic sedimentary rock cycling, Journ. Geol. Soc. London, v.138, p.183-196

Northrop, D.A. and Clayton, R.N., 1966, Oxygen isotope fractionations in systems containing dolomite, Journ. Geol., v.74, p.174-196

Norwick, S., 1977, Precambrian amphibolite facies metamorphism in the Belt rocks of northern Idaho (abs.): Geol. Soc. Amer. Abstr.w/prog. v. 9, p.753.

O'Connor, M.P., 1967, Stratigraphy and petrology across the Precambrian Piegan Group-Missoula Group boundary, southern Mission and Swan ranges, Montana, Unpubl. PhD. Thesis, 269p.

O'Connor, M.P., 1972, Classification and environmental interpretation of the cryptalgal organosedimentary 'molar tooth' structure from the Late Precambrian Belt-Purcell Supergroup: Journ. Geol., v.80, p.592-610.

O'Neil, J.R., Clayton, R.N. and Mayeda, T.K., 1969, Oxygen isotope fractionation in divalent metal carbonates, Journ. Chem. Physics, v.51, p.5547-5548

O'Neil, J.R. and Ghent, E.D., 1975, Stable isotope study of coexisting metamorphic minerals from the Esplanade Range, British Columbia, Geol. Sco. Amer. Bull., v.86, p.1708-1712

Obradovich, J.D. and Peterman, Z.E., 1968, Geochronology of the Belt Supergroup, Montana: Can. Journ. Earth Sci., v.5, p.737-747.

Obradovich, J.E., Zartman, R.E. and Peterman, Z.E., 1984, Update of the Geochronology of the Belt Supergroup: Abstracts with programs, Belt Symposium II, Montana Bur. Mines and Geol., Spec. Publ. 90, p.82-84.

Ohde, S., and Yasuski, K., 1984, Coprecipitation of strontium with marine Ca-Mg carbonates, Geochem. Journ., v.18, p.143-146

Ohmoto, H. and Felder, R.P., 1987, Bacterial activity in the warmer sulphate-bearing, Archean oceans, Nature, v.328, p.244-246

Park, R. and Epstein, S., 1960, Carbon isotope fractionation during photosynthesis, Geochim. Cosmochim. Acta, v.21, p.110-126

Patterson, R.J., 1972, Hydrology and carbonate diagenesis of a coastal sabkha in the Persian Gulf, Unpubl. PhD thesis, Princeton Univ., N.J., 498p. from Machel, H.G. and Mountjoy, E.W., 1986, Chemistry and environments of dolomitization - a reappraisal, Earth-Science Reviews, v.23, p.175-222

Perry, E.C., 1967, The oxygen isotope chemistry of ancient cherts, Earth Planet. Sci. Letters, v.3, p.62-66

Perry, E.C. and Tan, F.C., 1972, Significance of oxygen and carbon isotope variations in early Precambrian cherts and carbonate rocks of southern Africa, Bull. Geol. Soc. Amer., v.83, p.647-664

Perry, E.C., Ahmad, S.N. and Swulius, T.M., 1978, The oxygen isotope composition of 3800 m.y. old metamorphosed chert from Isukasia west Greenland, Journ. Geol., v.86, p.223-239

Perry, E.C., Monster, J. and Reiner, T., 1971, Sulfur isotopes in the Swaziland system barites and the evolution of the Earth's atmosphere, Science, v.171, no.3975, p.1015-1016

Peterman, Z.E., Hedge, C.E., and Tourtelot, H.A., 1970, Isotopic composition of strontium in sea water throughout Phanerozoic time, Geochim. Cosmochim. Acta, v.34, p.105-120

Piepgras, D.J., and Wasserburg, G.J., 1985, Strontium and neodymium isotopes in hot springs on the East Pacific Rise and Guaymas Basin, Earth Planet. Sci. Lett., v.72, p.341-356

Piper, J.D.A., 1982, The Precambrian paleomagnetic record: the case for the Proterozoic supercontinent, Earth Planet. Sci. Letters, v.59, p.61-89

Popp, B.N., Podosek, F.A., Brannon, J.C., Anderson, T.F. and Pier, J., 1986, $^{87}Sr/^{86}Sr$ ratio in Permo-Carboniferous sea water from the analyses of well preserved brachiopod shells, Geochim. Cosmochim. Acta, v.50, p.1321-1328

Price, R.A., 1964, The Precambrian Purcell System in the Rocky Mountains of southern Alberta and British Columbia: Bull. Can. Petrol. Geol., v. 12, special issue, Guidebook, August 1964, p.399-426.

Qin Zhengyong, Yang Xiuen and Jiang Mingmei, 1985, Chemostratigraphic correlation of the middle and upper Preterozoic between the Yanshan and Shennongjia Basins, Precambrian Res., v.29, p.77-91

Randazzo, A.G. and Cook, D.J., 1987, Characterization of dolomitic rocks from the coastal mixing zone of the Floridan aquifer, Florida, U.S.A., Sedimentary Geol., v.54, p.169-192

Reeder, R.J. and Sheppard, C.E., 1984, Variation of lattice parameters in some sedimentary dolomites, Amer. Mineral., v.69, p.520-527

Renard, M., 1986, Pelagic carbonate chemostratigraphy (Sr, Mg, ^{18}O, ^{13}C), Marine Micropaleo., v.10, p.117-164

Reynolds, M.W., 1977, Character and significance of deformation at the east end of the Lewis and Clark line, Montana (abs.), Geol. Soc. Amer. Abs. w/Prog., v.9, p.758

Reynolds, M.W. and Kleinkopf, M.D., 1977, The Lewis and Clark line, Montana-Idaho; a major intraplate tectonic boundary (abs.): Geol. Soc. Amer. Abstr. w/Prog., v.9, p.1140-1141.

Reynolds, M.W. and Lindsey, D.A., 1979, Eastern extent of the Proterozoic Y Belt Basin, Montana: U.S. Geol. Surv. Prof. Paper 1150, p.68.

Rice, H.M.A., 1941, Nelson map area, east half, British Columbia, Geol. Surv. Canada Mem. 228, 86p

Rickard, D.T., Zweifel, H., and Donnelly, T.H., 1979, Sulphur isotope systematics in the Asen pyrite-barite deposits, Skellefte District, Sweden, Econ. Geol., v.74, p.1060-1068

Ross, C.P., Andrews, D.A. and Witkind, I.J., 1955, Geologic map of Montana, 1:500,000, U.S. Geol. Survey geologic map series

Rye, D.M. and Rye, R.O., 1974, Homestake gold mine, South Dakota: Stable isotope studies, Econ. Geol., v.69, p.293-317

Rye, R.O., Whelan, J.F., Harrison, J.E., and Hayes, T.S., 1984, The origin of copper-silver mineralization in the Ravalli Group as indicated by preliminary stable isotope studies, Belt Symposium II, Abstract and Summaries, Montana Bur. Mines and Geol. Spec. Publ. 90, S.W. Hobbs ed., p.104-107

Sackett, W.M. and Thompson, R.R., 1963, Isotopic organic carbon composition of recent continental derived clastic sediments of eastern gulf coast, Gulf of Mexico, Bull. Amer. Ass. Perol. Geol., v.47, p.525-531

Saller, A.H., 1984, Petrologic and geochemical constraints on the origin of subsurface dolomite, Enewatak Atoll: an example of dolomitization by normal seawater, Geology, v.12, p.217-220

Sathyanarayan, S., Arneth, J.D. and Schidlowski, M., 1987, Stable isotope geochemistry of sedimentary carbonates from the Proterozoic Kaladgi, Badami and Bhima Groups, Karnataka, India, Precambrian Res., v.37, p.147-156

Schieber, J., 1985, The relationship between basin evolution and genesis of stratiform sulfide horizons in mid-Proterozoic sediments of central Montana (Belt Supergroup), PhD. thesis, Univ. of Oregon, 811p.

Schieber, J., 1986, Stratigraphic control of rare-earth pattern types in mid-Proterozoic sediments of the Belt Supergroup, Montana, U.S.A., implications for basin analysis, Chem. Geol., v.54, p.135-148

Schidlowski, M., Eichman, R. and Junge, C.E., 1975, Precambrian sedimentary carbonates: carbon and oxygen isotope geochemistry and implications for the terrestrial oxygen budget, Precambrian Res., v.2, p.1-69

Schidlowski, M., Hayes, J.M., and Kaplan, I.R., 1983, Isotopic inferences of ancient biochemistries: carbon, sulfur, hydrogen and nitrogen, in Schopf, J.W., ed., Earth's earliest biosphere, its origin and evolution, Princeton Univ. Press, N.J., p.149-186

Schultz, D.J., and Calder, J.A., 1976, Organic carbon $^{13}C/^{12}C$ variations in estuarine sediments, Geochim. Cocmochim. Acta, v.40, p.381-386

Sears, J.W., and Price, R.A., 1978, The Siberian connection - a case for Precambrian separation of the North American and Siberian Craton, Geology, V.6, no.5, p.267-270

Shackleton, N.J., and Kennett, J.P., 1975a, Paleotemperature history of the Cenozoic and the initiation of Antarctic glaciation: oxygen and carbon isotope analyses in DSDP sites 277, 279 and 281, in Kennett, J.P., Houtz, R.E., et al. (eds.), Initial reports of the Deep Sea Drilling Project, v.29, U.S. Govt. Printing Office, p.743-755

Shegelski, R.J., 1982, Depositional environment of the Gunflint Formation, Ontario, Canada, I.G.C.P. Joint Mtng. 157 & 160, Mexico City, Abstract Volume

Shemesh, A., Kolodny, Y., and Lux, B., 1983, Oxygen isotope variations in phosphate of biogenic apatites, II. Phosphorite rocks, Earth Planet. Sci. Lett., v.64, p.405-416

Sheppard, S.M.F., 1981, Stable isotope geochemistry of fluids, in Chemistry and Geochemistry of Solutions at High Temperature and Pressure, D.T. Rickard and F.E. Wickmann, eds., Physics and Chemistry of the Earth, v13-14, p419-445

Sheppard, S.M.F., 1986 Characterization and isotopic variations in natural waters in Reviews in Mineralogy v.16, Stable Isotopes in High Temperature Geological Processes, J.W. Valley, H.P.Taylor and J.R. O'Neil eds., Mineralogical Society of America, Washington D.C., p.165-184

Sheppard, S.M.F., and Schwarcz, H.P., 1970, Fractionation of carbon and oxygen isotopes and magnesium between coexisting metamorphic calcite and dolomite, Contrib. Mineral. Petrol., v.26, p.161-198

Shieh, Y.H., and Taylor, H.P., 1969, Oxygen and carbon isotope studies of contact metamorphism of carbonate rocks, J.Petrol., v.10, p.307-331

Singh, U., 1987, Ooids and cements from the late Precambrian of the Flinders Ranges, South Australia, Journ. Sed. Pet., v.57, no.1, p.117-127

Smith, B.N. and Epstein, S., 1971, Two categories of $^{13}C/^{12}C$ ratios for higher plants, Plant Physiol., v.47, p.380-384

Smith, J.W., Burnes, M.S. and Croxford, N.J.W., 1978, Stable isotope studies of the origins of mineralisation at Mt.Isa, Mineral. Deposita, v.13, p.369-381

Smith, J.W. and Croxford, N.J.W., 1975, An isotopic investigation of the environment of deposition of the McArthur mineralization, Mineral. Deposita, v.10, p.269-276

S.P.S.S.x., 1986, Statistical package for the social sciences, version x, user's guide, 2nd edition, SPSSx Inc., 444 N. Michigan Ave, Chicago Ill, 988p.

Stewart, J.H., 1972, Initial deposits in the Cordilleran Geosyncline: evidence of a Late Precambrian (< 850 m.y.) continental separation, Geol. Soc. Amer. Bull., v.83, p.1345-1360

Stewart, J.H., 1976, Late Precambrian evolution of North America: plate tectonic immplications, Geology, v.4, p.11-15

Taylor, H.P., 1974, The application of oxygen and hydrogen isotope studies to problems of hydrothermal alterations and ore deposition, Econ. Geol., v.69, p.843-883

Taylor, S.R., and McLennan, S.M., 1985, The continental crust: its composition and evolution, Blackwell Scientific, 312p.

Thode, H.G., Dunford, H.B. and Shima, M., 1962, Sulfur isotope abundances in rocks of the Sudbury district and their geological significance, Econ. Geol., v.57, p.565-578

Thode, H.G. and Monster, J., 1965, Sulfur isotope geochemistry of petroleum, evaporites and ancient seas, Amer. Assn. Petrol. Mem. 4, p.367-377

Trendall, A.F., 1979, A revision of the Mt. Bruce Supergroup, Geol. Surv. W. Aust. Ann. Rep-t., 1978: 63-71

Tucker, M.E., 1982, Precambrian dolomites: Petrographic and isotopic evidence that they differ from Phanerozoic dolomites, Geology, v.10, p.7-12

Ueda, A., Cameron, E.M. and Krouse, H.R., in press, ^{34}S-enriched sulphate in the Belcher Group, N.W.T., Canada: evidence for dissimilatory sulphate reduction in the early Proterozoic ocean

Ueda, A., Campbell, F.A., Krouse, H.R., and Spencer, R.J., 1987, $^{34}S/^{32}S$ variations in trace sulphide and sulphate in carbonate rocks of a Devonian reef, Alberta, Canada, and the Precambrian Siyeh Formation, Montant, U.S.A., Chem. Geol., v.65, p.383-390

Vahrenkamp, V.C., Swart, P.K., Ruiz, J., 1988, Contstraints and interpretation of $^{87}Sr/^{86}Sr$ ratios in dolomites, in special section on the isotopic history of sea water, Geophysical Research Letters, v.15(4), p.385-388

Veizer, J., 1983a, Chemical diagenesis of carbonates: theory and application of trace element technique, S.E.P.M. Short Course no. 10, Stable Isotopes in Sedimentary Geology, p.3-1 - 3-100

Veizer, J., 1983b, Trace elements and isotopes in sedimentary carbonates, Reviews in Mineralogy, v.II, Carbonates, mineralogy and chemistry, Mineral. Soc. Amer., Bookcrafters, Michigan, p.265-394

Veizer, J., 1983c, Geologic evolution of the Archean-early Proterozoic earth, in Schopf, J.W., ed., Earth's earliest biosphere, Princeton University Press, Princeton N.J., p.240-259

Veizer, J., 1985, Carbonates and ancient oceans: isotopic and chemical record on time scales of 10^7-10^9 years, in The carbon cycle and atmorpheric CO_2: Natural variations Archean to present, Geophysical Monograph 32, Amer. Geophys. Union, p.595-601

Veizer, J. and Compston, W., 1974, $^{87}Sr/^{86}Sr$ composition of seawater during the Phanerozoic, Geochim. Cosmochim. Acta, v.38, p.1461-1484

Veizer, J. and Compston, W., 1976, $^{87}Sr/^{86}Sr$ in Precambrian carbonates as an index of crustal evolution, Geochim. Cosmochim. Acta, v.40, p.905-915

Veizer, J. and Demovic, R., 1974, Strontium as a tool in facies analysis, Journ. Sed. Pet., v.44, p.93-115

Veizer, J. and Hoefs, J., 1976, The nature of $^{18}O/^{16}O$ and $^{13}C/^{12}C$ secular trends in sedimentary carbonate rocks, Geochm. Cosmochim. Acta, v.40, p.1387-1395

Veizer, J., Compston, W., Clauer, N, and Schidlowski, M., 1983, $^{87}Sr/^{86}Sr$ in late Proterozoic carbonates: evidence for a 'mantle' event at 900 Ma. ago, Geochim. Cosmochim. Acta, v.47, p.295-302

Veizer, J. Compston, W., Hoefs, J. and Nielsen, H., 1982, Mantle buffering of the early oceans, Naturwissenschaften 69, p.173-180

Veizer, J., Fritz, P., and Jones, B., 1986, Geochemistry of brachiopods: oxygen and carbon isotopic records of Paleozoic oceans, Geochim. Cosmochim. Acta, v.50, p.1679-1696

Veizer, J., Hoefs, J., Lowe, D.R., and Thurston, P.C.; 1989b, Geochemistry of Precambrian carbonates: II. Archean greenstone belts and Archean sea water, Geochm. Cosmochim. Acta, v.53, no.4, p.859-871

Veizer, J., Hoefs, J., Ridler, R.H., Jensen, L.S. and Lowe, D.R., 1989a, Geochemistry of Precambrian carbonates: I. Archean hydrothermal systems, Geochm. Cosmochim. Acta, v.53, no. 4, p.845-858

Veizer, J., Holser, W.T., and Wilgus, C.K., 1980, Correlation of $^{13}C/^{12}C$ and $^{34}S/^{32}S$ secular variations, Geochim. Cosmochim. Acta, v.44, p.579-587

Veizer, J., Lemieux, J., Jones, B., Gibling, M.R. and Savelle, J., 1978, Paleosalinity and dolomitization of a lower Paleozoic carbonate sequence, Somerset and Prince of Wales Islands, Arctic Canada, Can. Journ. Earth Sci., v.15, p.1448-1461

Visser, J.N.J., 1971, The deposition of the Griquatown glacial member in the Transvaal Supergroup, Geol. Soc. S. Africa Trans., v.74, p.187-199

Vogel, J.C., Grootes, P.M. and Mook, W.G., 1970, Isotopic fractionation between gaseous and dissolved carbon dioxide, Z.Phys, v.230, p.225-238, from Faure, G., 1986, Principles of Isotope Geology, John Wiley and sons, New York, 589p

Wadleigh, M.A., 1982, Marine geochemical cycle of strontium, MSc. thesis, Univ. of Ottawa, 187p

Wadleigh, M. A., Veizer, J., Brooks, C., 1985, Strontium and its isotopes in Canadian rivers: fluxes and global implications, Geochim. Cosmochim. Acta, v.49, p. 1727-1736

Walcott, C.D., 1899, Precambrian fossiliferous formations: Geol. Soc. Amer. Bull., v.10, p.199-244

Walcott, C.D., 1914, Pre-Cambrian Algonkian algal flora, in Cambrian geology and paleontology III, Smithsonian Misc. Coll., v.64, no.2, p.77-156

Walker, J.C.G. and Lohman, K.C., 1989, Why the ozygen isotope composition of sea water changes with time, Geophys. Res. Lett., v.16, p.323-326

Wallace, C.A., Harrison, J.E., Klepper, M.R. and Wells, J.D., 1976, Carbonate sedimentary breccias in the Wallace Formation (Belt Supergroup), Idaho and Montana, and their paleogeographic significance (abs.): Geol. Soc. Amer. Abstr. w/Prog., v.8, p.1159

Wallace, C.A., Harrison, J.E., Ruppel, E.T., Schmidt, R.G. and Whipple, J.W., 1984, A summary of the stratigraphy of the Missoula Group: Abstracts with summaries, Belt Symposium II, Montana Bur. of Mines and Geol. Spec. Publ. 90, p.27-29

Wallace, R.E. and Hosterman, J.W., 1956, Reconnaissance geology of western Mineral County, Montana, U.S. Geol. Surv. Bull. 1027-M, p.572-612

Wardlaw, N., Oldershaw, A., and Stout, M., 1978, Transformation of aragonite to calcite in a marine gasteropod, Can. Journ. Earth Sci., v.15, p.1861-1866

Weber, J.N., 1965, Evolution of the ocean and the origin of fine-grained dolomites, Nature, v.207, p.930-933

Webster, T.A., 1981, Faulting and slumping during deposition of the Precambrian Prichard Formation, near Quinns, Montana: a model for sulfide deposition: M.S. Thesis, Univ. of Montana, 71p

Wells, J.D., 1972, Pers. comm. to Harrisson, J.E., 1972: in Precambrian Belt Basin of the northwestern United States: it's geometry, sedimentation, and copper occurrences: Geol. Soc. Amer. Bull., v.83, no.5, p.1215-1240

Welte, D.H., Kalkreuth, W., and Hoefs, J., 1975, Age-trend in carbon isotopic composition in Paleozoic sediments, Naturwissenschaften, v.62, p.482-483

Wendt, I., 1968, Fractionation of carbon isotopes and its temperature dependence in the system CO_2 gas-CO_2 in solution and HCO_3^- - CO_2 in solution, Earth Planet. Sci. Letters, v.4, p.64-68

Weyl, P.K., 1960, Porosity through dolomitization: conservation mass requirements, Journ. Sed. Pet., v.30, p.85-90

Whelan, J.F., Rye, R.O. and DeLorraine, W., 1984, The Balmat-Edwards zinc-lead deposits - synsedimentary ore from Mississippi Valley-type fluids, Econ. Geol., v.79, p.239-265

Whelan, T.W., Sackett, W.M. and Benedict, C.R., 1973, Enzymatic fractionation of carbon isotopes by phosphoenophryvate carboxylase from C_4 plants, Plant Physiol., v.51, p.1051-1054

White, A.F., 1977, Sodium and potassium coprecipitation in aragonite, Geochim. Cosmochim. Acta, v.41, p.613-625

White, B., 1977, Stratigraphy of the Altyn Formation, lower Belt Supergroup, Glacier National Park, Montana (abs.): Geol. Soc. Amer. Abstr. w/Prog. v.9, no.6, p.772-773

White, B.G. and Winston, D., 1982, The Revett St.Regis 'transition zone' near the Bunker Hill Mine, Coeur D'Alene District, Idaho, Idaho Bureau of Mines and Geol. Bull. 24

Windley, B.F., 1977, The evolving continents, John Wiley and Sons, New York, 385p

Winston, D., 1973, The Bonner Formation as a late Precambrian pediplain: Northwest Geology, v.2, p.53-58

Winston, D., 1981, Late Precambrian block faulting in the Belt basin and it's effect on the Laramide, Int. Geol. Cong. Abstr., v.2, no.26, p.624

Winston, D., 1982, The effect of Precambrian Belt basin blocks on Cretaceous to Eocene compression and middle to late Cenozoic extension, Montana and Idaho, Geol. Soc. Amer. Abstr. w/Prog., Rocky Mtn. Sect. Mtng., Bozeman, Mt.

Winston, D., 1983, Middle Proterozoic Belt basin syndepositional faults and their influence on Phanerozoic thrusting and extension (abs.) A.A.P.G. Rocky Mountain Section mtng., A.A.P.G. Bull. 67(8), p.1361

Winston, D., 1986, Tectonics and sedimentation of the middle Proterozoic Belt basin, and their influence on Cretaceous compression and Cenozoic extension in western Montana and northern Idaho: Amer. Assoc. Petrol. Geol. for inclusion in Peterson, J.A., (ed.) Paleotectonics and sedimentation in the Rocky Mountain Region, United States, Amer. Assoc. Petrol. Geol. Memoir 41, p.87-118

Winston, D., Woods, M., Byer, G.B. 1984, The case for an intracratonic Belt-Purcell Basin; tectonic, stratigraphic and stable isotopic considerations: Montana Geol. Soc. 1984 Field Conf., N.W. Montana, p.103-120

Young, G.M., 1973, Tillites and aluminous quartzites as possible time markers for middle Precambrian (Aphebian) rocks of North America, in Huronian stratigraphy and sedimentation, G.M. Young ed., Geol. Assn. Can. Spec. Pap. 12: p.97-127

Zartman, R.E., Peterman, Z.E., Obradovich, J.D., Gallego, M.D. and Bishop, D.T., 1982, Age of the Cressport C sill near Eastport, Idaho: Soc. of Econ. Geol. Coeur d'Alene Field Conf., R.R.Rein and G.A.Williams (eds.): Idaho Bur. of Mines and Geol. Bull. 24, p.61-69

Zieg, G.A., 1981, Stratigraphy, sedimentology and diagenesis of the Precambrian upper Newland Limestone, central Montana: M.S. thesis, Univ. of Montana, 182p

Appendix A

Sample Locations and Descriptions

Samples of the Belt Supergroup were collected mostly from measured sections throughout Montana and Idaho. Their locations and sources are described below. The samples collected throughout measured sections are plotted directly on these sections (Figures A-1 through A-9). The exception is the location 6 (Holland Lake) taken from O'Connor (1967) for which a stratigraphic section was not available. No section was measured by this author. Some samples were collected on a reconnaissance scale (the 7/28 and 7/29 series, DF-1 to 3, RR-1 & 2, PH-1 to 3, Af/Al-1 to 3) and only their locations are listed. Following the descriptions of sample locations are the field characteristics of the samples.

The numbers of the following sample locations correspond to those plotted on Figure 2-1.

1 - CF - Clark Fork, Idaho, U.S. Geol. Survey 1:250,000 Western U.S. series V502 Map, Sandpoint Idaho, T28N R2E sections not projected, between Hope and Clark Fork, Idaho from a roadcut on Rte. 10., Location from Grotzinger (1981).

2 - DF,RR - Delye Fork and Ruen Road - geologic map of Clark Fork Quadrangle, Idaho-Montana (Harrison and Jobin, 1963; Plate 1). RR - T55N R2E NE/4 Section 27, DF - T54N R2E SE/4

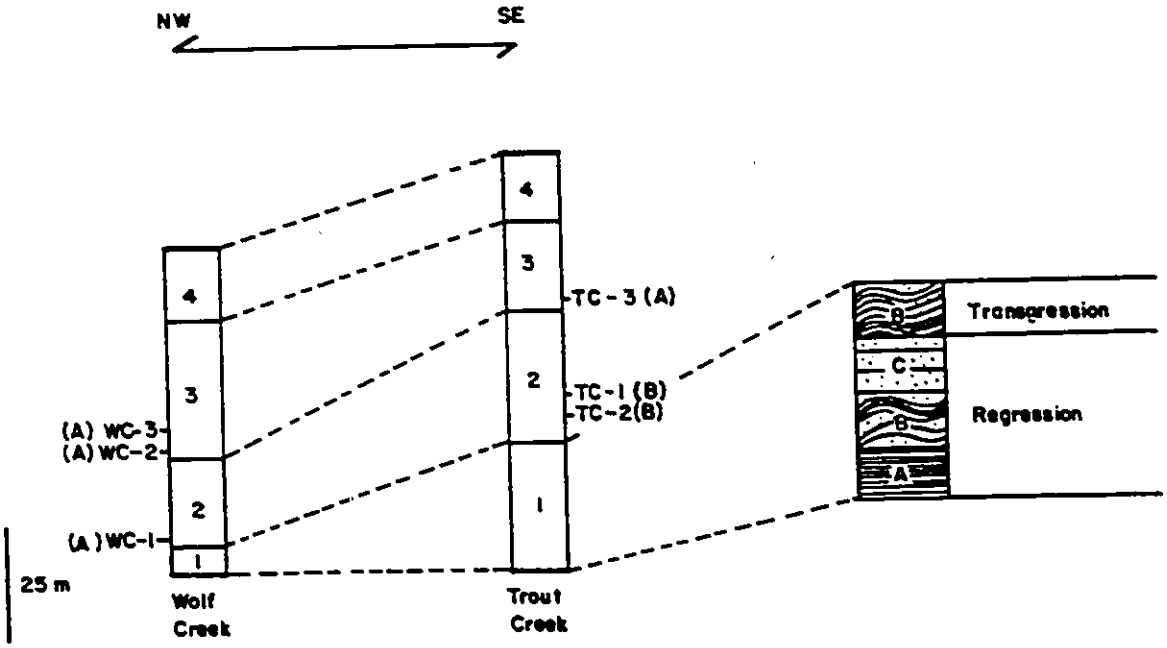

Figure A-1
Spokane/Greyson sample locations TC-1 to 3 and WC-1 to 3. Cycles 1 to 4 are regressive/transgressive cycles composed of sediment types A, microlaminated silt, clay and carbonate with molar tooth structures representing a sub-tidal deposit, B, wavy couplets of fine sand, silt and mud deposited in an intertidal zone and C, horizontally laminated coarse-sand and wavy couplets of fine sand, silt and mud deposited in an intertidal zone. The letter (in parentheses next to the sample number) represents the sediment type from which the sample was collected. Diagram modified from Bloomfield (1983).

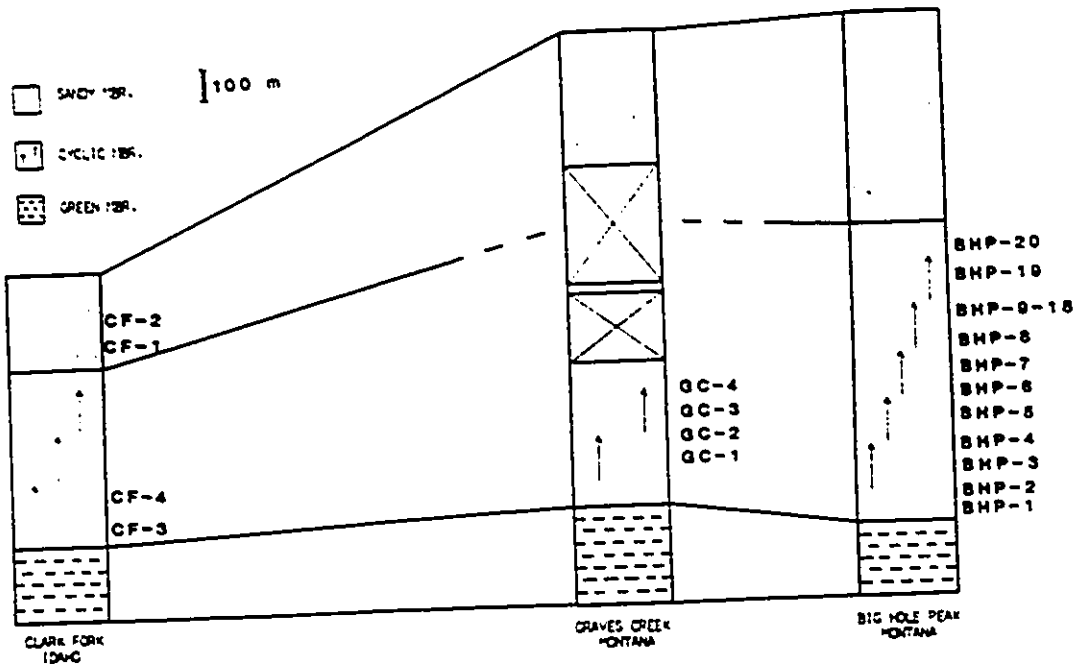

Figure A-2
Samples collected from sections of the Wallace Formation measured and correlated by Grotzinger (1981). The sections are Clark Fork (CF), Graves Creek (GC) and Big Hole Peak (BHP). BHP-9 to 18 were collected from one locality and are more thoroughly described in the following figure.

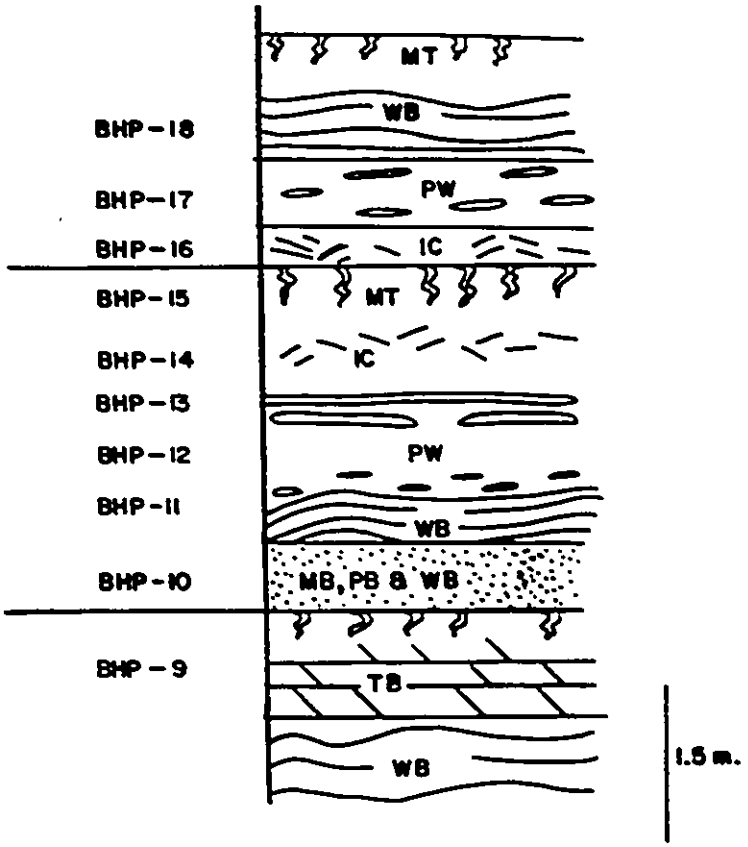

Figure A-3
Samples collected in depositional cycles of the Big Hole Peak section of the Wallace Fm. (see Figure 2-8 for idealized Wallace Fm. cycle). BHP-9 was collected from carbonate at the top of a cycle, BHP-10 to BHP-15 and BHP-16 to BHP-18 were collected upward through two sedimentary cycles. WB - wavy bedding, MB - medium bedding, PB - parallel bedding, PW -pods of brown carbonate weathering in dominantly grey weathering carbonate, IC - intraclast conglomerate, MT - molar tooth carbonate.

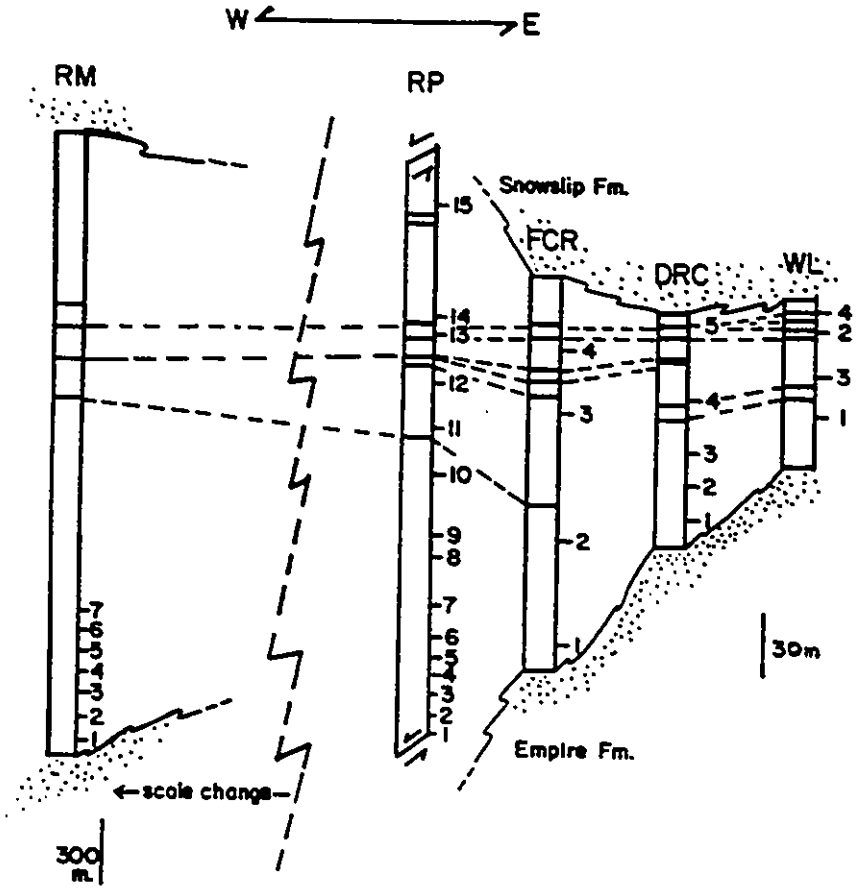

Figure A-4
Sample location from sections of the Helena Fm. measured and correlated by Eby (1977). The sections are Red Mountain (RM), Rogers Pass (RP), Falls Creek Ridge (FCR), Dearborn River Canyon (DRC) and Wood Lake (WL). This cross section shows major correlative units between the sections. For a more complete description see Eby (1977).

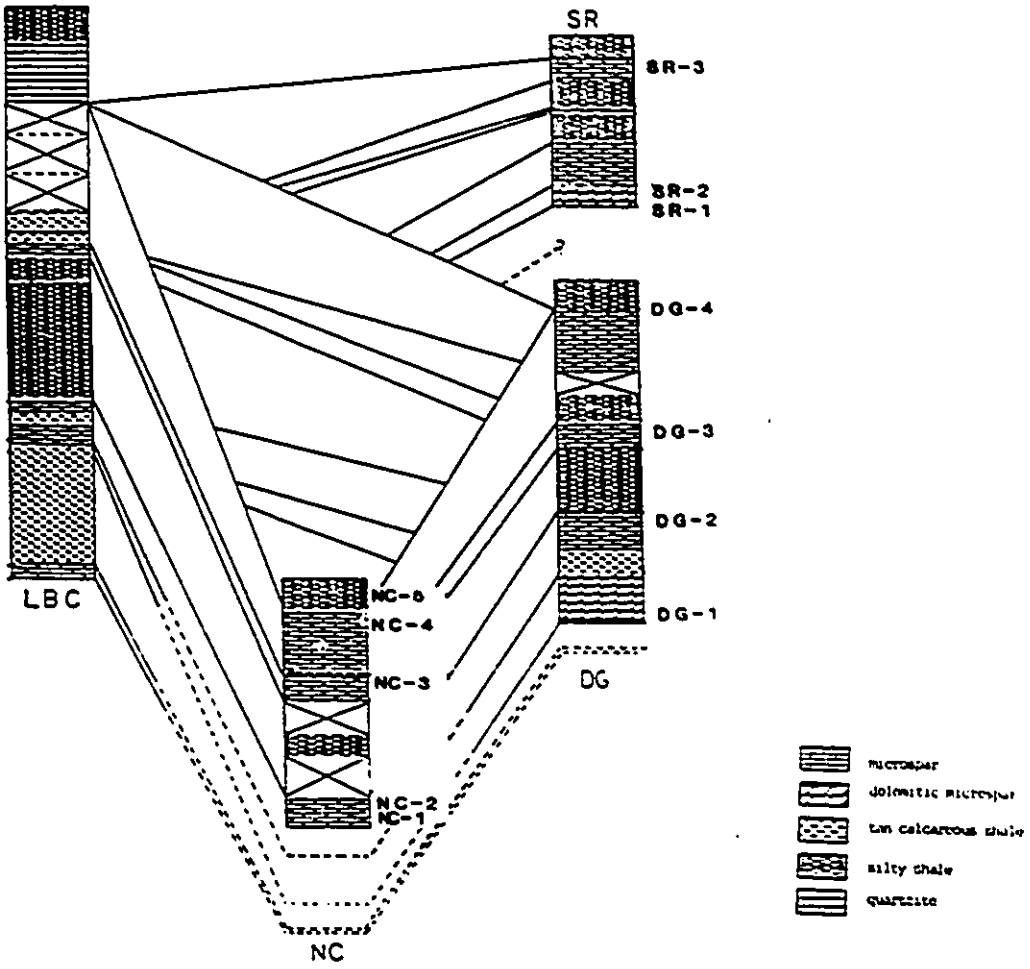

Figure A-5
Location of samples collected from stratigraphic sections of the Newland Formation measured by Zieg (1981). The sections are Newlan Creek (NC), Smith River (SR) and Deckers Gulch (DG). The Little Birch Creek (LBC) section was not sampled and is shown here for correlative purposes only.

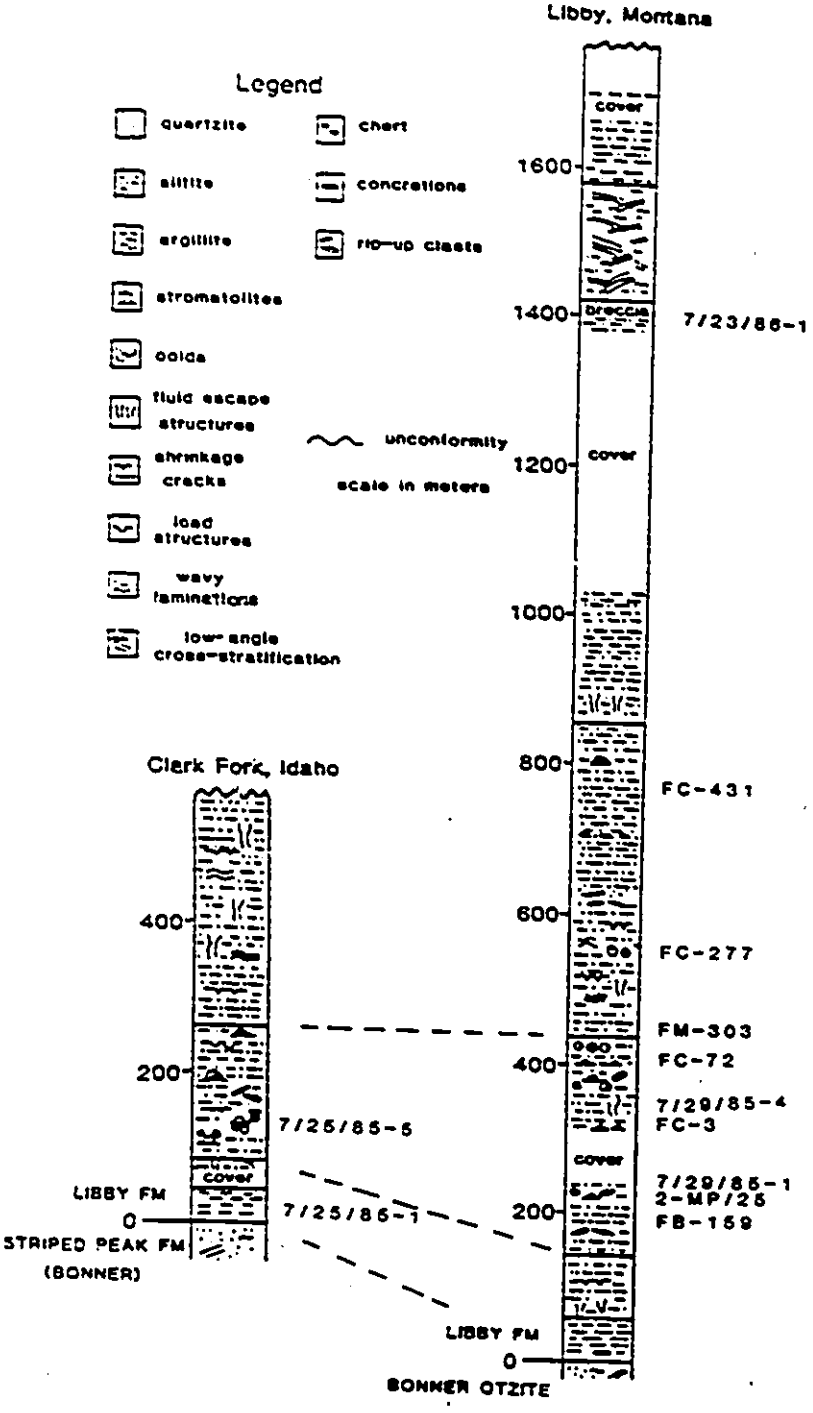

Figure A-6
Location of samples collected from stratigraphic sections of the Libby Formation which were measured and provided to me by D. Kidder (pers. comm., 1986).

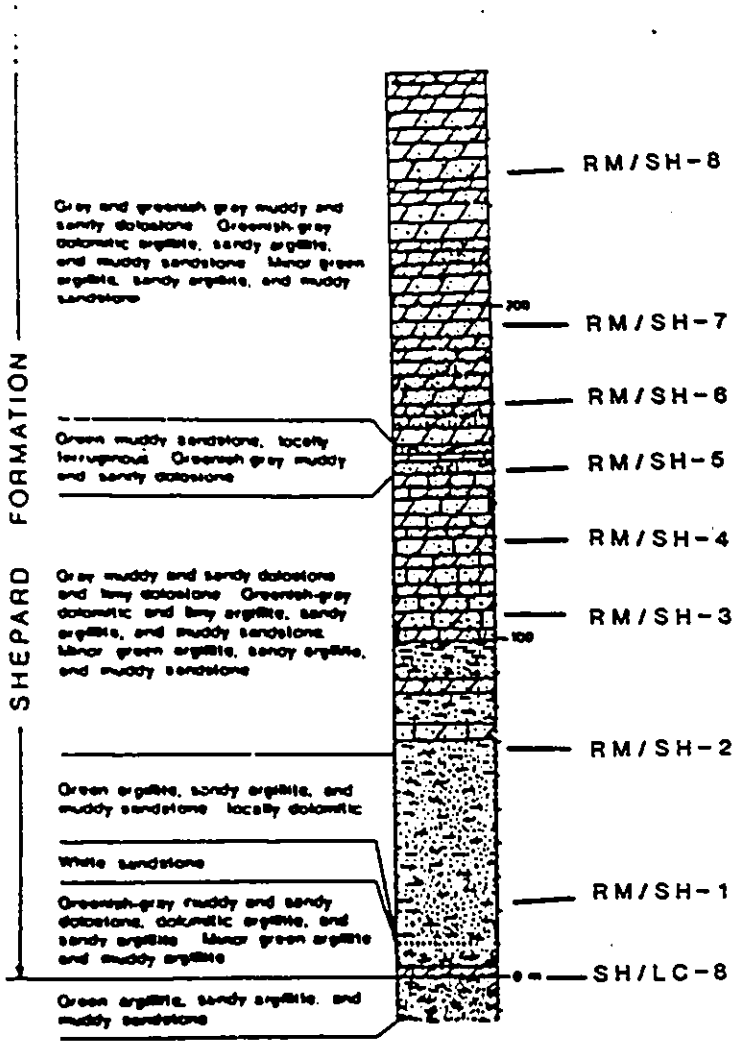

Figure A-7
Sample locations from the Reynolds Mountain stratigraphic section of the Shepard formation as described by Horodyski (1983). SH/LC-8 was collected at the Lunch Creek locality, and the remainder from Reynolds Mountain (See previous sample location descriptions).

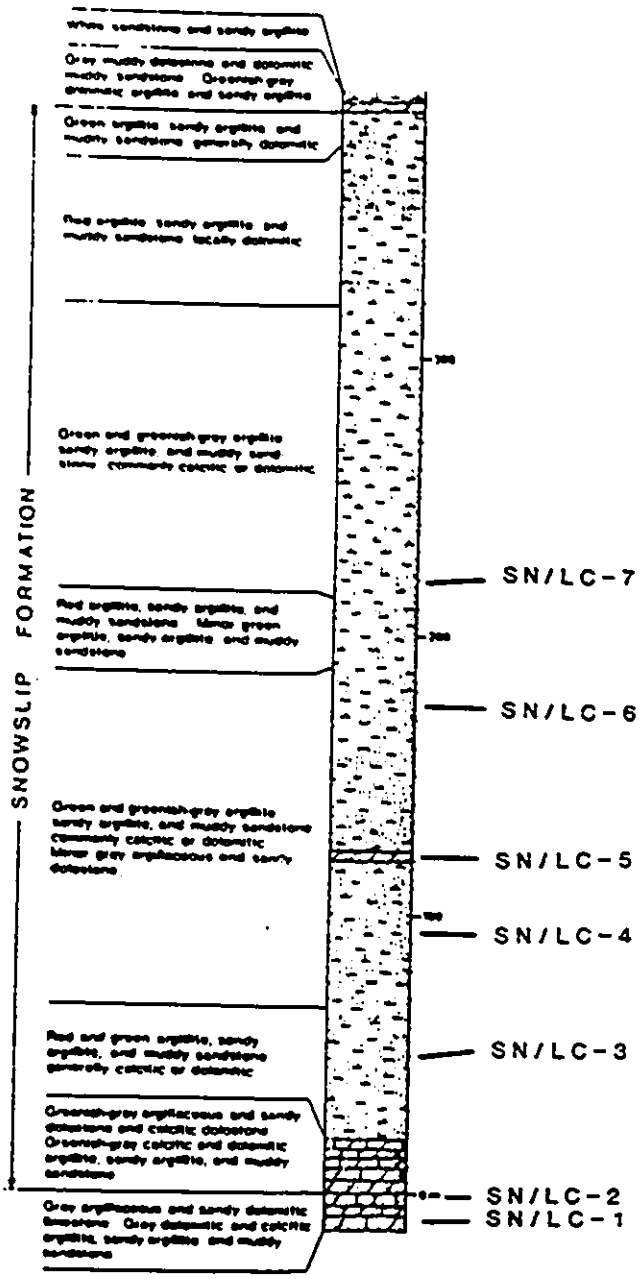

Figure A-8
Stratigraphic location of samples collected from the Snowslip Formation as described by Horodyski (1983). Samples were collected in the Lunch Creek (LC) locale.

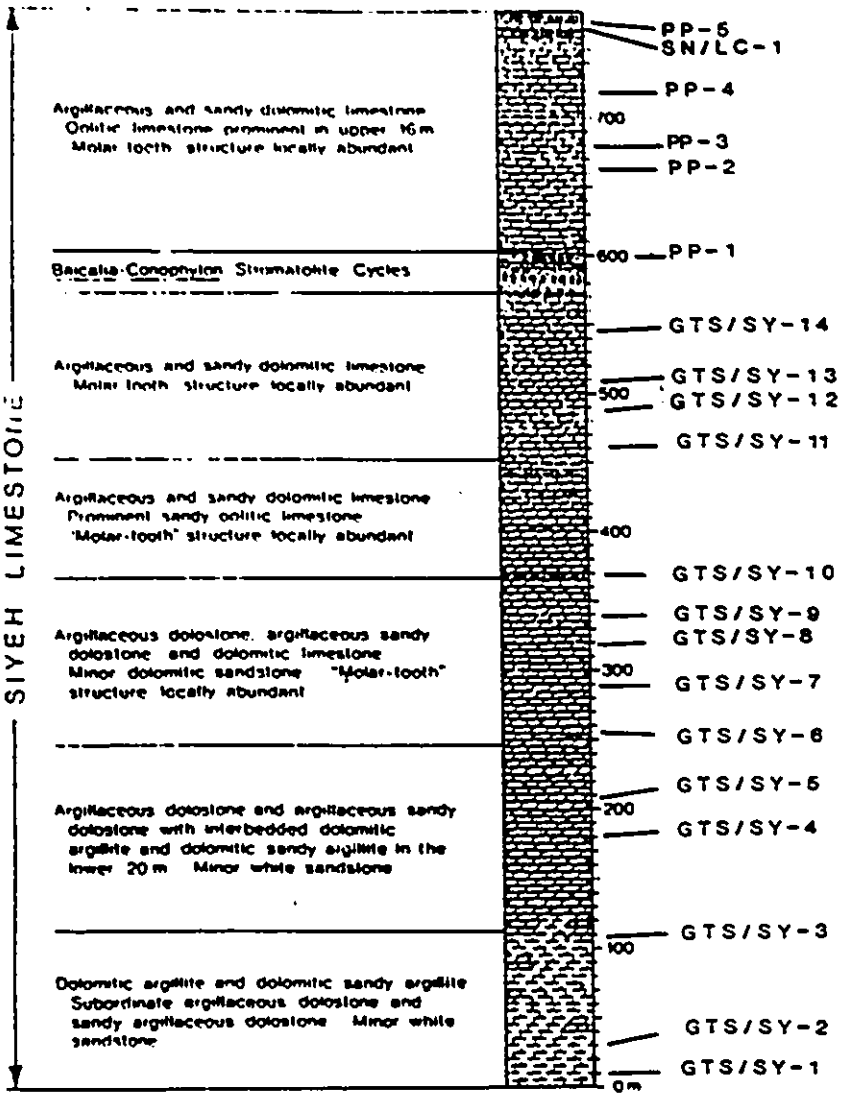

Figure A-9
Stratigraphic location of samples collected from the Siyeh Formation as described by Horodyski (1983). Samples were collected in the Piegan Pass (PP) and Going to the Sun Mountain (GTS) locales.

Section 11.

3 - 7/28/85-1 to 3 Tony Peak 7.5 minute quadrangle: T30N R29W N. centre section 28; top of Shepard Fm. on W. side of road.

7/28/85-4 to 6 Alexander Mountain 7.5 minute quadrangle: T31N R29W W. centre 1/2 section 32; lower 1/4 to 1/3 of Helena Fm. which is 2400 feet here in the basin.

7/28/85-7 Alexander Mountain 7.5 minute quadrangle: T31N R29W NW/4 section 33; lower 1/3 of the Helena Fm. which is 950 feet thick here in the basin.

7/28/85-8 Alexander Mountain 7.5 minute quadrangle: T31N R29W middle of section 33, east side of river next to dam; Empire Fm.

7/28/85-9 Volcour 7.5 minute quadrangle: T32N R28W Top 1/2 of section 8, east side of Hwy. 37; upper Prichard Fm.

7/28/85-10 Volcour 7.5 minute quadrangle: T32N R28W SW/2 of section 34, east side of Hwy. 37; Prichard Fm.

7/28/85-11 Inch Mountain 7.5 minute quadrangle: T33N T28W S/2 section 23; upper Prichard Fm. transition

7/28/85-12 Inch Mountain 7.5 minute quadrangle: T34N T29W NE/4 section 23, near McGuire Creek; upper Prichard Fm. transition

7/28/85-13 Alexander Mountain 7.5 minute quadrangle: T31N R29W section 33; Helena Fm. / Empire Fm. contact

7/29/85-1 Scenery Mountain 7.5 minute quadrangle: T31N R32W SW/4 section 15, at Kootenai River milepost 25; Libby Fm.

7/29/85-2 Kootenai Falls 7.5 minute quadrangle: T31N R33W S/2 of NE/4 section 14, near footbridge over Kootenai River; Mt. Shields 3

7/29/85-3 Kootenai Falls 7.5 minute quadrangle: T31N R33W SE/4 section 15, south of Rte. 2, Libby Fm.

7/29/85-4 Kootenai Forest Service map; T58N R32W W/2 section 7; near the quarry, Libby Fm.

7/29/85-5 Kootenai Falls Quadrangle map; T31N R33W E/2 middle of section 2, .1 mile SE of Kootenai Cr.

7/29/85-6 Rt.2 SE of Libby near Schreiber Creek, Mt.Shields 3

Fc, Fb, Fm, and Mp were supplied to me by Dave Kidder and are plotted on the following stratigrpahic section. No exact sample locations were provided, but the samples were collected from measured sections in the Libby area.

4 - GC - Graves Creek - Lolo National Forest Service Map and Thompson Falls Montana 15' quadrangle, T.23N R29W Sections 19, 20 and 30, location from Grotzinger (1981).

5 - BHP - Big Hole Peak - Big Hole Peak Montana 7.5' quadrangle, T.21N R27W Sections 22, 23, 24 and 26, location from Grotzinger (1981).

6 - HL - Holland Lake - Holland Lake Montana 7.5' quadrangle, T20N R16W NE/4 Section 36, location from O'Connor (1967).

7 - PH - Phillipsburg - Deerlodge National Forest Service Map, Montana, T8N R14W Sections 13, 15 and 23, location from Ross et al., 1955.

8 - NC - Newlan Creek - Lewis and Clark Forest Service Map (Jefferson Division), T11N R7E Section 29, west of Highway 89, location from Zieg, 1981

9 - DG - Decker Gulch, Whitetail Reservoir, Montana 7.5' quadrangle, DG-1 to DG-3; T11N R6E Section 7, DG-4; T11N, R5E, Section 12, location from Zieg (1981).

10 - SR - Smith River, Fort Logan, Montana 7.5' quadrangle, T11N, R4E, W/2 Section 1, location from Zieg (1981).

11 - TC/WC - Trout Creek, Canyon Ferry quadrangle, T11N, R1W, W/2 Section 9, location from Bloomfield (1983). Wolf Creek, Sheep Creek, Montana 7.5' quadrangle, T14N R4W SE/4 Section 15

12 - DRC - Dearborn River Canyon - Steamboat Mountain, Montana 7.5' quadrangle, T18N R7W section 32, locations from Eby (1977) and Marvin Woods (Pers. Comm., 1985; DRC-SI-345).

13 - FCR - Falls Creek Ridge - Blowout Mountain, Montana 7.5' quadrangle, T17N R6W section 19, Location from Eby (1977).

14 - RP - Rogers Pass - Rogers Pass Montana 7.5' quadrangle, T16N R6W W/2 section 34, E/2 section 33, location from Eby (1977).

15 - RM - Red Mountain - Stonewall Mountain Montana 7.5' quadrangle T15N R8W section 33 (projected), location from Eby (1977).

16 - WL - Wood Lake - Wood Lake Montana 7.5' quadrangle (unsurveyed), projections from Lewis and Clark National Forest Service map (Rocky Mountain Division) T19N R9W S/2 section 6,

location from Eby (1977).

17 - Glacier National Park, Glacier National Park 1:100,000 map - SN/LC - Lunch Creek, SW slope of Piegan Mountain, Lunch Creek Drainage, E. of Logan Pass Visitor Centre, north of Going to the Sun Highway; GTS/SY - S slope of Going to the Sun Mountain north of Going to the Sun Highway, E. of Logan Pass Visitor Centre; RM/SH - SE slope of Reynolds Mountain, S of Logan Pass Visitor Centre, PP/SY - NE slope of Piegan Mountain, S of Piegan Pass above Siyeh Bend in Going to the Sun Highway, E. of Logan Pass Visitor Centre, AF/AL - Apikuni Falls, Above Apikuni Flat next to Apikuni Falls, near Swiftcurrent Gauging station, north of road to Many Glacier Lodge, locations from Horodyski (pers. comm. 1985).

Sample Descriptions

Mineralogy of the samples described in the Table A-1 is based on Ca and Mg concentrations, do = dolomite; cc = calcite, docc = dolomitized calcite. Those samples with no designated composition had an insoluble residue content greater than 25 % and have been excluded from further consideration. All other descriptions were gathered in the field with some classifications based on thin-section work. Classification is based on both Folk's (1962) and Dunham's (1962) systems. Sample descriptions use the following abbreviations:

Table A-1: Description of Belt Supergroup Carbonate Samples

Sample #	Composition	Depositional Environment	Classification	Description
Libby:				
7/25/85-1	DO	IT	oosparite/wackestone	OO,IC
7/25/85-5a	DOCC	IT	micrite/mudstone	PLL
7/25/85-5b	DOCC	IT	oomicrite/packstone	OO
7/29/85-1	DOCC	APZ	biolithite/boundstone	MB,STR
7/29/85-4	DOCC	IT	oosparite/grainstone	MB,OO
FM-303	DOCC	ST	micrite/mudstone	
FC-72	N.A.	ST	oomicrite/wackestone	OO,O
FC-3	N.A.	APZ	biolithite/boundstone	OO,STR
FB-159	DOCC	IT	biolithite/boundstone	OO,STR
FC-431	CC	APZ	biolithite/boundstone	STR
FC-277	N.A.	ST	micrite/mudstone	CB
2-MP-25-1	CC	APZ	biolithite/boundstone	STR
7/23/86-1	N.A.	IT	biolithite/boundstone	STR,TLL
Mt.Shields:				
DF-1	DO	SWB	sparite/mudstone	THB,TKL,PLL,IC
DF-2	DO	SWB	initrasparite/wackestone	THB,TKL,PLL
DF-3	DO	SWB	micrite/mudstone	THB,TKL,PLL
DF-4	DO	SWB	micrite/mudstone	THB,TKL,PLL
RR-1	DO	SWB	micrite/mudstone	THB,PB
RR-2	DO	SWB	sparite/mudstone	THB,PB
7/29/85-2	DOCC	APZ	biolithite/boundstone	MB,STR
7/29/85-5	DO	ST	micrite/mudstone	MB,RXB
7/29/85-6	DO	SWB	biolithite/boundstone	STR
Shepard:				
DRC-SI-345	DOCC	APZ	biolithite/boundstone	STR
SH/LC-8-5	DOCC	SWB	initramicrite/wackestone	THB
RM/SH-1	DOCC	ST	micrite/mudstone	MB,PLL,PB
RM/SH-2	DOCC	ST	sparite/mudstone	THB,RXB
RM/SH-3	DOCC	SWB	micrite/mudstone	THB,TKL,PLL,PB
RM/SH-4	N.A.	SWB	micrite/mudstone	THB,TKL,PLL,PB

RM/SH-5	DOCC	ST	micrite/mudstone	
RM/SH-6	DOCC	ST	micrite/mudstone	THB
RM/SH-8	DO	ST	intramicrite/packstone	
7/28/85-1	DOCC	SWB	micrite/mudstone	MB
7/28/85-2	DOCC	SWB	micrite/mudstone	THB,TKL,couplets
7/28/85-3	DOCC	SWB	micrite/mudstone	MB
7/29/85-3	DOCC	SWB	micrite/mudstone	THB,PLL
Snowslip:				
SN/LC-2-0	DO	ST	intramicrite/wackestone	THB,WB,IC
SN/LC-3-50	DOCC	IT	oomicrite/wackestone	MB,OO,MC
SN/LC-4-95	DOCC	APZ	biolithite/boundstone	THL,STR
SN/LC-5-125	DOCC	SWB	micrite/mudstone	THB,THL
SN/LC-6-175	DOCC	SWB	sparite/mudstone	THB
SN/LC-7-228	CC	APZ	biolithite/boundstone	THL,STR
Middle Belt Carbonate:				
Helena:				
RP-1-121	DO	SPT	micrite/mudstone	TB,ECC
RP-2-156	DO	SWB	micrite/mudstone	TB
RP-3-196	DO	SWB	micrite/mudstone	TB,CF
RP-4-212	DO	SWB	micrite/mudstone	TB
RP-5-242	DO	SWB	micrite/mudstone	TB
RP-6-264	DO	SWB	micrite/mudstone	THB
RP-7-329	DOCC	SWB	micrite/mudstone	MB,WB,PB,CF
RP-8-407	DOCC	IT	micrite/mudstone	TKL,PB,AR
RP-9-446	DOCC	SWB	micrite/mudstone	THB,MT,WB,PB
RP-10-560	DOCC	SWB	micrite/mudstone	THB,PB
RP-11-673	DOCC	SWB	micrite/mudstone	THB
RP-12-730	DOCC	SWB	micrite/mudstone	THB,WB,MT
RP-13-865	DOCC	ST	micrite/mudstone	THB,WB
RP-14-887	N.A.	SWB	micrite/mudstone	THB,WB,PB
RP-15-1091	CC	SWB	micrite/mudstone	TNL,TKL,WB,PB
WL-1-50	DOCC	SPT	intramicrite/wackestone	THL,THB,PB,WB,ECC,DS
WL-2-209	DOCC	SWB	oomicrite/packstone	THL,PB

WL-3-120	DOCC	SWB	mudstone/micrite	THL,PB,IC
WL-4-236	DOCC	IT	oomicrite/mudstone	TB,OO
DRC-1-25	DO	IT	intramicrite/mudstone	THL,MB,WB,OO,IC
DRC-2-64	DO	SWB	micrite/mudstone	MB
DRC-3-141	DO	SWB	micrite/mudstone	THB
DRC-4-275	DO	SWB	micrite/mudstone	MB
DRC-5-385	DOCC	SWB	oomicrite/packstone	THL,THB,PLL,OO
RH-1	DOCC	SWB	micrite/mudstone	THB,PLL,WB
RH-2	DOCC	SWB	micrite/mudstone	THB,WB,PLL
RH-3	DOCC	SWB	micrite/mudstone	THB,WB,PLL
RH-4	DOCC	ST	micrite/mudstone	THB,WB,RXB,CR,IR
RH-5	DOCC	SWB	micrite/mudstone	THL,THB,WB,PLL
RH-6			gabbro sill	
RH-7	CC	ST	micrite/mudstone	THB,CR,WB
FCR-1-5	DO	ST	micrite/mudstone	THL,THB
FCR-2-113	DOCC	SWB	micrite/mudstone	THL,THB
FCR-3-345	DO	ST	micrite/mudstone	THB
FCR-4-443	DOCC	APZ	biolithite/boundstone	THB,STR
HL-1	N.A.	SWB	micrite/mudstone	THB,THL,WL,PLL
HL-2	DOCC	SWB	micrite/mudstone	THB,THL,WL,PLL
HL-3	N.A.	SWB	micrite/mudstone	THB,PLL
HL-4	N.A.	SWB	micrite/mudstone	THB,PLL
HL-5	N.A.	SWB	micrite/mudstone	MB,THL,PLL
HL-6	N.A.	SWB	micrite/mudstone	TB,THL,PLL couplets
PH-1	CC	SWB	micrite/mudstone	deformed
PH-2	N.A.	SWB	micrite/mudstone	THB,PB,MC
PH-3	DOCC	SPT	micrite/mudstone	THB,PB,MC
7/28/85-4	DOCC	IT	micrite/mudstone	
7/28/85-5	DOCC	SWB	micrite/mudstone	MT
7/28/85-6	DOCC	SWB	micrite/mudstone	
7/28/85-7	DOCC	SWB	micrite/mudstone	TKL,PLL
Wallace:				
BHP-1-320	N.A.	SWB	micrite/mudstone	TB
BHP-2-640	N.A.	SWB	micrite/mudstone	THB
BHP-3-840	N.A.	SWB	micrite/mudstone	THB
BHP-4-1120	CC	IT	micrite/mudstone	MB,MT

BHP-5-1400	CC	SWB	micrite/mudstone	THB,WB,couplets
BHP-6-1580	N.A.	SWB	intramicrite/packstone	THB,TKL,WB,PLL
BHP-7-1800	CC	ST	micrite/mudstone	TB,WB,PB
BHP-8-1940	CC	SWB	micrite/mudstone	MB,WB,PB
BHP-9	CC	SWB	micrite/mudstone	TB,MT
BHP-10	DOCC	ST	micrite/mudstone	MB,PB,WB
BHP-11	N.A.	SWB	micrite/mudstone	WB
BHP-12	N.A.	SWB	micrite/mudstone	pods of carbonate
BHP-13	N.A.	SWB	micrite/mudstone	carbonate couplets
BHP-14	CC	IT	intramicrite/packstone	IC
BHP-15	DOCC	IT	micrite/mudstone	MT
BHP-16	CC	IT	intramicrite/mudstone	IC
BHP-17	DOCC	SWB	intramicrite/mudstone	
BHP-18	N.A.	SWB	micrite/mudstone	WB
BHP-19	CC	IT	micrite/mudstone	MB,MT
BHP-20	DOCC		micrite/mudstone	
GC-1	DOCC	ST	biolithite/boundstone	TB,TNL,PLL,WB,STR,O
GC-2	DOCC	IT	micrite/mudstone	THB,THL,PLL,WB,STR
GC-3	DOCC	SWB	intramicrite/mudstone	THB,PB
GC-4	DOCC	IT	intramicrite/wackestone	MB,MT
CF-1-2910	N.A.	SWB	micrite/mudstone	TB,PLL
CF-2-3000	N.A.	SWB	intramicrite/grainstone	MB,PB
CF-3-400	N.A.	SWB	micrite/mudstone	THB,PB
CF-4-500	DOCC	SWB	intramicrite/grainstone	MB,PB
Siyeh:				
GTS/SY-1-10	DO	ST	micrite/mudstone	MB,AR
GTS/SY-2-30	DO	ST	micrite/mudstone	MB,AR
GTS/SY-3-100	DO	SWB	micrite/mudstone	MB,WB
GTS/SY-4-170	DOCC	APZ	micrite/mudstone	THB
GTS/SY-5-210	DO	APZ	micrite/mudstone	THB
GTS/SY-6-254	DOCC	APZ	micrite/mudstone	THB
GTS/SY-7-295	DOCC	SWB	micrite/mudstone	MB
GTS/SY-8-320	DOCC	ST	intramicrite/packstone	THB,IC
GTS/SY-9-345	DOCC	SWB	micrite/mudstone	TKL,MB
GTS/SY-10-373	DOCC	IT	micrite/mudstone	THB
GTS/SY-11-455	N.A.	SWB	micrite/mudstone	THB
GTS/SY-12-490	DOCC	SWB	micrite/mudstone	THB

GTS/SY-13-510	DOCC	SWB	micrite/mudstone	THB
GTS/SY-14-545	DOCC	SWB	micrite/mudstone	THB,MT
PP/SY-1-605	DOCC	IT	micrite/mudstone	THB,RXB,CR,PLL,WL
PP/SY-2-660	CC	ST	micrite/mudstone	THB,PLL,WL
PP/SY-3-686	CC	IT	micrite/mudstone	TNL,TK1,PLL,MT
PP/SY-4-725	DOCC	ST	micrite/mudstone	TKL
PP/SY-5-775	DOCC	IT	micrite/mudstone	CB
SN/LC-1- -10	CC	ST	micrite/mudstone	PLL/WL,MC,RXB,STR,MT
Empire:				
7/28/85-8	DOCC	SWB	micrite/mudstone	TKL,MB
7/28/85-13	DOCC	SWB	micrite/mudstone	MB
Spokane/ Greyson:				
TC-1	DOCC	IT	intramicrite/wackestone	TNL
TC-2	DOCC	IT	micrite/mudstone	THB,MT,WB
TC-3	DOCC	IT	micrite/mudstone	THB,MT
WC-1	DOCC	IT	micrite/mudstone	TNL
WC-2	DOCC	IT	micrite/mudstone	TN1,WL,RC
WC-3	N.A.	IT	intramicrite/wackestone	WL,SSD/RXB
ALtyn:				
AF/AL-1- -150	DO	IT	biolithite/boundstone	TH1,RXB,STR
AF/AL-2- -30	DO	IT	sparite/mudstone	THB,RXB
AF/AL-3- -80	DO	IT	oosparite/grainstone	THL,RXB
Newland:				
NC-1-10	CC	SWB	micrite/mudstone	TNL,THB,PB,CF
NC-2-100	CC	SWB	intrasparite/wackestone	TNL,THB,PB
NC-3-400	CC	ST	micrite/mudstone	THL,THB,PB,CR,IR
NC-4-440	CC	SWB	micrite/mudstone	THL,THB,PB
NC-5-440	N.A.	SWB	shale	PB
SR-1-520	DOCC	SWB	micrite/mudstone	THL,MB,PB
SR-2-596	DOCC	SWB	micrite/mudstone	THL,PB
SR-3-1260	DOCC	SWB	micrite/mudstone	THL,THB,PB
DG-1-20	DOCC	SWB	micrite/mudstone	THL,THB,PB
DG-2-140	CC	SWB	micrite/mudstone	THL,THB,PB
DG-3-540	CC	SWB	intramicrite/wackestone	THL,THB,PB
DG-4-1000	CC	SWB	micrite/mudstone	THL,PB,LC

Prichard:				
7/28/85-9			amphibol.-grade cc vein	
7/28/85-10			amphibol.-grade cc vein	
7/28/85-11	N.A.	SWB	micrite/mudstone	THL,PLL
7/28/85-12	N.A.	ST	micrite/mudstone	THL,RXB

N.A. indicates insufficient soluble fraction to determine composition

AR - asymmetrical ripples
CB - cross-bedding
CF - channel fill
CR - climbing ripples
DS - domal stromatolites
ECC - evaporite crystal casts
GB - graded bedding
IC - intraclasts
IR - isolated ripples
LC - load casts
MB- medium bedded (10-30 cm)
MC - mudcracks
MT - molar tooth structures
O - organic-rich
OO - oolites
PB - planar bedding
PLL - parallel laminations
RC - rip-up clasts
RXB - ripple cross-beds
SR - symmetrical ripples
SSD -soft sediment deformation
STR - stromatolites
TB -thickly bedded (30-100cm)
THB - thinly bedded (1-10cm)
TKL-thickly laminated(.3-1cm)
TNL -thinly laminated (<.3 cm)
WB - wavy bedding
WL - wavy laminations

The determination of depositional environments within Belt limestones which, except for stromatolites, are devoid of diagnostic fossils is very generalized. Supratidal (SPT) facies have emergent features such as mudcracks and evaporites (although the latter are not accepted as independently diagnostic of a supratidal facies). Intertidal (IT) facies show strong current indicators such as cross-beds and oolites. The use of the term intertidal is not meant to imply the presence of any true tidal indicators such as herringbone cross-stratification. The designation of an intertidal facies indicates close proximity to the paleoshoreline where more wave and current ripples would have been preserved. Subtidal (ST) carbonates have some current indicators, wavy bedding or channels, but the degree of rippling is subordinate to that found in intertidal deposits. Those carbonates that are stromatolitic are classified as having been formed in the photic zone (APZ) which implies proximity to the paleo-shoreline or at least proximity to light and may fall within any of the above four environmental groupings.

Appendix B

Petrography of Selected Belt Samples

Selected samples of Belt carbonate sediments were examined petrographically. These petrographic analyses are summarized below in ascending stratigraphic order. The following format was followed in the description of the rocks:

Sample Number Rock Classification

Composition

Primary Depositional Textures:

Post Depositional Textures:

The sample number is the same as that used throughout the text. The rock is classified using the Folk (1962) and Dunham (1962) classification systems, separated by a slash. The composition of the rock is that determined petrographically, not geochemically; percentages and grain sizes are approximate. Grain sizes listed are average diameters of the grains or crystals. Quartz and feldspar clasts are considered intraclasts. All thin sections were stained with Alizarin Red S to distinguish between calcite and dolomite and with Potassium Ferricynide to distinguish iron rich and iron poor carbonate phases. Most carbonate phases are iron poor, but deviations are noted in the thin section descriptions. The thin sections were not stained to distinguish quartz from

feldspar. Because the size of these siliciclastic grains was often very small, quartz is often difficult to distinguish from untwinned feldspar. The percentages of quartz and feldspar are therefore often approximate. Post depositional textures are arranged in a diagenetic sequence. The determination of whether the carbonate in the rocks is a primary cement or diagenetic in origin is made following Bathurst's (1975) criteria.

Libby:

7/29/85-4
Oosparite/Grainstone
60 % calcite .005 to .25 mm.
30 % quartz including chert
10 % dolomite
Primary Depositional Textures:
Intraclasts dominantly of ooids with chert and monocrystalline quartz clasts cemented by sparry calcite. Some calcite ooids have retained their primary radial and tangential textures throughout diagenesis.
Post-Depositional Textures:
Ooids are rimmed with isopachous calcite spar and silicified in some areas. Sparry calcite cements these silicified ooids, but the calcite looks secondary with no size gradations away from the substrate (ooids): this calcite also cross-cuts the ooids, indicating it formed after silicification and at the expense of the silica in the replaced ooids. Sparry calcite grew at the expense of some of these previously silicified ooids. Sparry iron-rich dolomite occurs in certain layers and along the rims of some calcitic ooids. Most ooids are still calcite and have been recrystallized. Stylolites cross-cut the rock.

Mt. Shields:

DF-1
Sparite to Intrasparite/Mudstone
96 % Dolomite .025 to .05 mm.
3 % Quartz and chert fragments .05 mm.
1 % Muscovite .025 mm.
Primary Depositional Textures:
Laminations are defined by concentrations of organic material,

gradations of dolomitic crystals and concentrations of chert and quartz fragments.
Post-Depositional Textures:
The contacts between laminations are now crenulated organic layers created by compaction of the rock and wrapping of the organic laminations around dolomite crystals and silica fragments. The dolomite in this sample has begun to undergo aggrading neomorphism to sparite. This neomorphic sparite is patchy and ubiquitous throughout the rock. Organic coatings are seen on some of the larger grains of sparite as if the organics had been excluded from the dolomite during recrystallization. Dolomite crystals have both straight and wavy contacts, showing characteristics of both neomorphic and primary carbonate cement. Larger grained, texturally late, dolomite is more iron rich along crystal cleavages. Muscovite cross cuts rock fabrics.

DF-2
Intrasparite/Wackestone
95 % Dolomite .005 to .05 mm.
5 % Monocrystalline and polycrystalline quartz, .05 to .25 mm.
tr. muscovite
tr. opaques
Primary Depositional Textures:
The rock is composed of about 50 % micritic dolomite intraclasts with 5 % quartz intraclasts in a micritic dolomite matrix. Chert and some rock fragments were coated with micrite before deposition. Rock fragments are metamorphic as evidenced by abundant stressed quartz (with undulose extinction) and crenulated contacts. Some dolomite intraclasts are rounded and resemble ooids, their origin is hard to pinpoint as their original shapes have been obscured by recrystallization. Some intraclasts appear to have been algae that was coated with micrite and rounded before deposition. Some intraclasts are composed of composite grains and other intraclasts which were cemented together with micrite before being redeposited in this rock. Intraclasts are oriented with their longest axis lying parallel to bedding. Bedding in this sample is further defined by concentrations of organics separating the beds.
Post-Depositional Textures:
Micritic dolomite is being neomorphosed to sparry dolomite. Compaction has wrapped organic laminations around clasts. Fractures transect the sample are filled with chert, as are some vugs in the rock. Small dolomite crystals have wavy crystal contacts. Larger dolomite crystals are found in patches and have straight crystal contacts and many enfacial junctions which are characteristic of primary carbonate cements. These larger dolomite crystals are iron rich and some form at the expense of quartz clasts.

RR-2
Sparite/Mudstone
95 % Dolomite .0025 to .025 mm.
5 % Quartz and Feldspar Intraclasts .05 mm.
tr. muscovite
tr. opaques
Primary Depositional Textures:
Alternating coarse- and fine-grained dolomite crystals define laminations in the rock. Intraclasts are concentrated in layers and are dominantly sub-angular quartz grains with occasional polycrystalline quartz grains. Opaque minerals are concentrated along bedding and as stringers (which may be disrupted laminations).
Post-Depositional Textures:
50 % of the dolomite (that with smaller grain sizes) has textures that would indicate that it is secondary (wavy crystal boundaries, a low number of enfacial junctions, patchy recrystallization to sparite). Diagenetic dolomite rhombs are growing in the coarser grained sections of the rock. Trace muscovite is disseminated throughout the rock.

7/29/85-2
Biolithite/Boundstone
97 % Dolomite < .0025 to .025 mm.
3 % Chert .005 mm.
Primary Depositional Textures:
1.5 mm. thick laminations are arranged in larger cycles .9 mm. thick.
Post-Depositional Textures:
The laminations in this rock are often bounded by chert and coarser grained dolomite which are growing outward from micritic dolomite in an apparent open space filling structure.

Shepard:
DRC-SI-345
Intrasparite/Packstone
76 % Calcite .005 mm
20 % Quartz and Feldspar .5 mm
3 % Glauconite .5 mm
1 % opaques (lath and equant shaped) .025 mm
tr Dolomite less than .005 mm
Primary Depositional Textures:
This intraclast conglomerate is grain supported, the grains dominantly angular 1-5 mm sized stromatolitic intraclasts. Well-rounded quartz, feldspar and glauconite clasts are also found in this sample surrounded by a micritic matrix. The calcite in this sample is 60 % stromatolitic intraclasts in 40 % calcite cement. Some geopetal textures are present; siliciclastic intraclasts show normal graded bedding. Intraclasts of stromatolitic calcite are randomly

oriented and concentrated in layers. These intraclasts contain sulfides which have weathered into iron oxide haloes.
Post-Depositional Textures:
Some calcite and trace amounts of dolomite is embaying quartz and feldspar grains in the coarser grained sections of the rock.

RM/SH-3-105
Micrite/Mudstone
79 % Dolomite .012 mm.
20 % Quartz .007 to .01 mm.
1 % Calcite .005 mm.
tr. Muscovite
tr. Opaques
Primary Depositional Textures:
.1 mm intraclasts of chert, calcite and monocrystalline quartz are well rounded and all coated with opaque minerals which are also disseminated throughout the intraclast. The intraclasts compose less than 10 % of the rock and are aligned along laminations. Micritic dolomite surrounds these intraclasts and makes up the bulk of the sample.
Post-Depositional Textures:
Trace muscovite cross-cuts intraclasts and dolomitic matrix. The dolomite in this rock has wavy indistinct crystal boundaries, no enfacial junctions and is uniform in grain size implicating a diagenetic origin. Some larger grained dolomite is iron rich, but the bulk of the dolomite is iron poor to iron free.

RM/SH-6-170
Micrite/Mudstone
95 % Dolomite .0025 mm.
4 % Quartz and Feldspar .005 mm.
1 % Opaques .003 mm.
Primary Depositional Textures:
Laminations are defined by concentrations of quartz and feldspar intraclasts and gradations in their size in layers in this rock.
Post-Depositional Textures:
Streaks of opaques, some with iron oxide haloes and disseminated opaque minerals are found throughout the sample.

RM/SH-8-270
Intramicrite/Packstone
50 % Dolomite .005 mm.
45 % Quartz .01 mm.
5 % Orthoclase and Plagioclase .01 mm.
tr. Muscovite
tr. Opaques up to .01 mm.

Primary Depositional Textures:
Intraclasts of dominantly quartz with some feldspar are sub-angular to sub-rounded, evenly distributed and grain supported within a micritic dolomite matrix.
Post-Depositional Textures:
Micritic dolomite has some straight and some wavy crystal boundaries, a uniform grain size and has characteristics of neomorphic cement. The dolomite is growing at the expense of silica and feldspar grains and is iron rich. Muscovite cross cuts all previous textures.

SH/LC-8-5
Intramicrite/Wackestone
50 % Dolomite .01 to .05 mm.
20 % Quartz .025 to .05 mm.
30 % Orthoclase .025 to .05 mm.
tr. Muscovite .05 mm to .1 mm
tr. Opaques (sulfides?)
Primary Depositional Textures:
Dolomite and silicate grains are equally mixed. Most of the quartz clasts are monocrystalline and strained.
Post-Depositional Textures:
Iron rich dolomite rhombs cross-cut the silicates. The crystals in this sample are somewhat aligned. probably caused by compaction. Muscovite cuts all other textures.

7/28/85-1
Intramicrite and Micrite/Packstone and Mudstone by layers
70 % Dolomite .005 mm.
15 % Quartz (both mono- and polycrystalline) .15 mm.
15 % Feldspar .15 mm.
tr. Muscovite .5 mm.
tr. Calcite
Primary Depositional Textures:
No laminations are present in the micritic portions of this rock, but laminations are defined by angular quartz clasts in higher energy intramicrite layers. Cross laminations are common.
Post-Depositional Textures:
Micritic dolomite has indistinct and wavy crystal boundaries. Few enfacial junctions are seen in this dolomite. The micritic dolomite is recrystallizing to sparite in patches, undergoing aggrading neomorphism. Adjacent to some clasts dolomite spar sized as opposed to the predominant micrite matrix. Fractures in the rock have been filled with calcite spar. The calcite in these fractures accounts for less that .5 % of the total rock volume. Dolomite spar is growing at the expense of quartz clasts in siliciclastic rich areas of the rock. Some dolomite rhombs are forming in the intramicrite areas of the rock.

7/29/85-3
Micrite/Mudstone
85 % Dolomite <.0025 mm. to .0025 mm.
10 % Quartz and Feldspar .015 mm.
5 % Calcite .010 mm.
tr. Muscovite .02 mm.
Primary Depositional Textures:
Micritic dolomite is interlaminated with coarser grained quartz clasts.
Post-Depositional Textures:
Dolomite crystals are so small that a determination of the origin of the dolomite is impossible. Fluidization, molar tooth, structures disrupt the primary laminations. Calcite spar cements the siliciclastic minerals found in the molar tooth structures and is also preferentially formed in areas of siliciclastic concentration. Muscovite is formed in quartz rich layers and cross-cuts all previous textures.

Snowslip:

SN/LC-1- -10
Micrite/Mudstone
60 % Calcite .01 to .025 mm.
40 % Dolomite .01 to .025 mm.
tr. opaques .03 mm.
Primary Depositional Textures:
Equidimensional, uniformly sized calcite and dolomite crystals make up this rock.
Post Depositional Textures:
Patches of microcrystalline dolomite are surrounded by more coarsely crystalline dolomite and calcite implicating that the finer grained carbonate could have been an earlier cement with the more coarsely crystalline a recrystallization product of this earlier cement. Some dolomite rhombs are seen in the rock, and some of these rhombs are being replaced by calcite (dedolomitization).

SN/LC-2-0
Intramicrite/Wackestone
60 % Dolomite .005 to .05 mm.
20 % Quartz .025 mm to .1 mm
20 % Feldspar (Plagioclase and Orthoclase)
tr. Muscovite max. length 1mm.
tr. opaques
Primary Depositional Textures:
.5 mm thick laminations of alternating clastic and carbonate-rich layers and faint cross-laminations are visible in this sample. Most of the primary textures of the rock have been obscured by dolomitization, but faint microcrystalline dolomitic intraclasts remain.

Post-Depositional Textures:
Small iron rich dolomite rhombs dominate the texture of this rock, obscuring primary depositional textures.

SN/LC-4-95
Intrasparite/Boundstone
60 % Calcite .005 to .01 mm.
15 % Quartz
15 % Feldspar (Plagioclase and Orthoclase)
10 % Dolomite .01 to .05 mm. rhombs
Primary Depositional Textures:
Stromatolitic laminations in this rock are seen in thin section to consist of alternating pure calcite and mixed calcite/siliciclastic layers and changing grain sizes of the siliciclastic fraction of the rock.
Post-Depositional Textures:
Dolomite rhombs cross-cut both the calcite and siliciclastic fraction of the rock. Large crystals (.4 mm.) of calcite are forming in the more siliciclastic rich sections of the rock; replacing quartz and feldspar as it grows. This diagenetic calcite cement makes up about 3 % of the volume of this rock.

SN/LC-7-228
Intramicrite/Boundstone
80 % Calcite 90% less than .005 mm.; 10 % 5 mm.
10 % Feldspar (Orthoclase and Plagioclase) .005 to .05 mm.
4 % Chlorite less than .005 mm. needles
5 % Quartz .005 to .05 mm.
1 % Opaques
tr. Organics
Primary Depositional Textures:
Most of the calcite in this rock is very fine grained with indistinguishable crystal boundaries. 1 mm. thick stromatolitic laminations consist of siliciclastic rich layers alternating with fine-grained calcite layers which are rich in organics. These laminae are arranged in 10 mm. thick units which are defined, and separated, by concentrations of organics. The quartz in this rock is both monocrystalline, polycrystalline and chert with some of the monocrystalline grains showing overgrowths.
Post-Depositional Textures:
Coarser grained (5 mm.) calcite is growing in (and replacing) the more siliciclastic rich layers of the rock. Chlorite is growing in the siliciclastic rich layers of the rock as well. Muscovite is metamorphic and cuts all previous grains.

Middle Belt Carbonate:

RP-1-121
Micrite/Mudstone
60 % Dolomite less than .005 up to .01 mm.
40 % Calcite less than .005 mm.
trace opaques (pyrite?)
Primary Depositional Textures:
Laminations are faintly visible and defined by calcite rich and poor layers. Calcite and Dolomite are mixed as interlocking crystals.
Post Depositional Textures:
Diagenetic dolomite rhombs cross-cut calcite composing 5 % of the rock volume. The bulk of the dolomite in this rock is much finer grained and not obviously diagenetic in origin. Two sets of veinlets cross-cut the rock, one set parallel to laminations one set perpendicular to laminations. The veins perpendicular to bedding are larger than those parallel to bedding and are filled with two stages of cement; the first stage is isopachous calcite and the second stage is blocky dolomite which fills the centre of the veinlets. In the smaller veins which parallel bedding only blocky calcite cement is found.

RP-5-242
Micrite/Mudstone
85 % Dolomite: 90% less than .005 to .01 mm: 10% .1 mm.
15 % Quartz and Orthoclase Feldspar .03 to .05 mm.
tr opaques
Primary Depositional Textures:
Silicates are scattered throughout the crystalline dolomite. Micritic dolomite with occasional spar-sized crystals compose most of the rock. Crystal boundaries are indistinct.
Post-Depositional Textures:
Dolomite is recrystallizing to coarser grained microspar in a patchy fashion. Veinlets and vugs are filled with silica (chert and grains of quartz) then cross cut by iron rich dolomite crystals. These veinlets are offset along stylolites along which iron oxides and sparite are concentrated. This sparite is less than 3% of the volume of the rock.

RP-8-407
Micrite/Mudstone
100% Dolomite .0025 mm.
tr. silica grains .05 mm.
tr. opaques .0025 mm.
Primary Depositional Textures:
.005 mm thick laminations are faintly visible and are grouped into larger (1 cm.) thick beds. Dolomite is uniformly sized with indistinct crystal boundaries.

Post-Depositional Textures:
.005 mm. sized dolomite crystals, which are slightly larger than the majority of the dolomite in this rock, fills conduits created by fluidization of the carbonates, (molar tooth structures). Compaction of the rock is mirrored in the crenulation of lamination boundaries.

RF-12-730
Micrite/Mudstone
99 % Dolomite less than .0025 to .007 mm.
1 % Quartz and Feldspar clasts .025 mm.
tr opaques
Primary Depositional Textures:
.1 mm. thick laminations of micritic dolomite with indistinct crystal boundaries and disseminated angular quartz and feldspar clasts dominate this rock.
Post-Depositional Textures:
Micritic dolomite is undergoing aggrading neomorphism to microspar. Quartz grains are wrapped by laminations of opaques indicating compaction.

RF-15-1091
Micrite/Mudstone
99 % Calcite .01 mm.
1 % Quartz (and feldspar?) .01 mm.
Primary Depositional Textures:
Uniformly sized micritic calcite crystals were uniformly sized with interlocking crystals with silicates disseminated throughout this micrite. The grain size of the silicates was so small it was impossible to accurately determine their composition petrographically but those few grains that were large enough to determine were quartz.
Post-Depositional Textures:
Veinlets composing about 1% of the total rock volume running parallel to each other transect the rock and are filled with slightly larger calcite crystals.

WL-1-50
Intramicrite/Wackestone
70 % Calcite .05 mm.
27 % Quartz and/or Feldspar(to small to distinguish).005 to .05mm 3 % Opaques
tr. Chlorite
Primary Depositional Textures:
.5 mm. laminations are separated by concentrations of opaque minerals. Interlocking calcite crystals are distributed throughout the rock in a mottled manner with very fine grained quartz and feldspar.

Post-Depositional Textures:
The silicate minerals in this rock are now altering to chlorite, and in some places are completely replaced. In some places the silicates are unaltered chemically, but are highly fractured, which makes them very difficult to identify. The calcite in this rock may be secondary: the crystal size is fairly large and the crystal boundaries are sharp.

WL-2-209
Oomicrite/Packstone
60 % Dolomite: 40 % Ooids 1 mm in diameter
20 % Intraclasts 2 to 5 mm. long
40 % mixed calcite and dolomite matrix .05 mm.
tr. quartz clasts .05 to .4 mm.
Primary Depositional Textures:
Ooids, intraclasts and occasional quartz clasts are intermixed in this grain supported rock. The matrix of the rock is about 40 % calcite and 6 % dolomite.
Post-Depositional Textures:
The intraclasts and ooids have been recrystallized, some layers preferentially replaced by dolomite rhombs, some layers are calcitic. The ooids have lost any original radial textures and many have no concentric textures either, distinguishable only by their round outline. The dolomite in the matrix of the rock has well shaped rhombs and is replacing calcite cement.

DRC-1-25
Intramicrite/Mudstone
100 % Dolomite .005 to .01 mm
tr. sulfides .01 mm
Primary Depositional Textures:
The rock is crystalline dolomite with some faint rhombic crystal shapes, but dominantly indistinct crystal boundaries. Faint laminations are visible. Some micritic dolomite intraclasts are present. These intraclasts are 2.5mm by .5mm with 2 to 3 % sulfides in them.
Post-Depositional Textures:
The crystal shapes in this rock are not distinct enough to determine their origin and no remnants of a possible protolith are visible in this sample.

DRC-2-64
Micrite/Mudstone
98 % Dolomite .0025 to .025 mm
1 % Quartz .025 mm
1 % Feldspar (Orthoclase) .025 mm
tr. opaques
Primary Depositional Textures:
Faint laminations are seen in this crystalline micritic dolomitic sample, quartz and feldspar fragments are very small and scattered uniformly throughout the rock.

Post-Depositional Textures:
Molar tooth structures are filled with dolomite of the same grain size as the bulk of the rock. Stylolites have developed in the rocks and are defined by iron-oxide concentrations. Two sets of fractures have developed in this sample, the first set is filled with carbonate, the second has a silica filling.

RM-4
Micrite/Mudstone
40 % Calcite .005 mm
20 % Dolomite .0025 mm
20 % quartz .01 mm
20 % feldspar (some plagioclase) .01 mm
1 % opaques .025 mm
tr. muscovite .01 mm
Primary Depositional Textures:
4 mm thick laminations, cross-beds and climbing ripples are visible in this thin section. These features are created by alternating silicate rich and silicate poor layers. Calcite and dolomite are concentrated in alternating layers. Well rounded dolomite intraclasts are occasionally seen.
Post-Depositional Textures:
Trace (less than 1%) dolomite rhombs have formed in this rock.

FCR-1-5
Micrite/Mudstone
100 % Dolomite; 90% .01 mm, 10% .05 mm
tr. calcite .05 mm
tr. opaques .0025 mm
Primary Depositional Textures:
Laminations are visible in otherwise featureless interlocking dolomite crystals.
Post-Depositional Textures:
Veinlets cross-cut this mudstone and are filled with two cement phases, .05 mm dolomite then .05 mm blocky calcite crystals.

BHP-4-443
Micrite/Mudstone (Intramicrite in molar tooth fill)
90 % Calcite .007 mm.
9 % Quartz/Feldspar .05 mm.
1 % Muscovite
Primary Depositional Textures:
This rock consists of interlocking grains of micritic calcite, which show faint laminations.
Post-Depositional Textures:
Two stages of fluidization, resulting in the formation of molar tooth structures, have affected this rock. The first stage of molar tooth is filled with intraclasts of quartz, muscovite and very severely altered plagioclase. The second episode of molar tooth is filled with dolospar with isolated

and fairly well preserved plagioclase grains. The calcite in the molar tooth is iron rich calcite. The total volume of this sample that is molar tooth fill is 30 %: dolomicrite makes up the remaining 70 % of the rock. The molar tooth structures are cut by iron poor dolomite veins.

BHP-6-1580
Intramicrite/Packstone
composition changes dramatically in pods:

50 % Feldspar .025 mm.	to	60 % Calcite .05 mm.
30 % Muscovite .025 mm.		20 % Quartz .025 mm.
20 % Quartz .025 mm.		10 % Feldspar .025 mm.
		10 % Muscovite .025 mm.

Primary Depositional Textures:
Laminations are defined by large, strained quartz and feldspar clasts. Where calcite occurs it is a cement in the siliciclastic matrix.
Post-Depositional Changes:
This rock is undergoing low-grade metamorphism. Two generations of muscovite are seen in this rock, the 1st generation in parallel to bedding, the second generation is perpendicular to bedding. The calcite in this sample is a cement in the dominantly siliciclastic rock and forms a pod-shape in this thin section resembling a concretion.

BHP-9
Micrite to Intramicrite/Mudstone
78 % Dolomite .012 mm.
20 % Calcite .012 mm.
2 % Allochems (quartz, muscovite, feldspars) .012 - .05 mm.
tr. opaques .025 mm.
Primary Depositional Textures:
Interlocking crystals of micritic dolomite make up the bulk of this sample. Laminations are defined in this rock by alternating concentrations of quartz, muscovite and feldspar in layers.
Post-Depositional Textures:
Molar tooth (fluidization) textures cross-cut the dolomitic micrite. These molar tooth structures are filled with .01 to .05 mm clasts of feldspar and quartz in a micritic calcite matrix. Calcite grades outward from molar tooth structures into pure dolomitic micrite implicating that the calcite may have formed by outward percolation of fluids from the molar tooth structures. Dolomite rhombs are dominantly iron poor, but the latest in the diagenetic sequence are iron rich. Calcite veinlets cross-cut molar tooth structures, these veinlets are in turn cut by haematite (perhaps formed by weathering of diagenetic pyrite?). Surrounding this haematite are quartz halos.

BHP-10
Micrite to Intramicrite (in patches)/Mudstone
90 % Dolomite .005 to .012 mm.
10 % allochems quartz .05 mm
muscovite .1mm
tr. opaques
Primary Depositional Textures:
Faint laminations are visible in this sample, intraclasts of detrital quartz and muscovite are concentrated along these laminations.
Post-Depositional Textures:
Diagenetic opaque minerals are concentrated in patches in the dolomite matrix. Quartz haloes are found around some of these opaques, some opaques contain calcite indicating that the opaque might be a rock fragment. Late stage 'beefcake'-type calcite veins have developed perpendicular to bedding.

BHP-15
Micrite/Mudstone
64 % Dolomite < .0025 mm.
30 % Calcite .005 mm.
5 % Muscovite
1% Quartz clasts
Primary Depositional Textures:
Faint laminations of quartz and feldspar grains.
Post-Depositional Textures:
Calcite is concentrated in pods in this sample, these concentrations grading outward into the dolomitic mudstone which dominates the rock. The calcite pods often have calcite spar veins at their centers which may have acted as an initial site of nucleation for the diagenetic calcite cement. The iron content of the pod increases outward along with the dolomite content. Muscovite is metamorphic, cross-cutting underlying minerals and faintly aligned.

BHP-17
Intramicrite/Mudstone
40 % Dolomite .005 mm.
20 % Feldspar (orthoclase and plagioclase) .005 to .025 mm.
20 % Quartz .005 to .025 mm.
10 % Calcite .005 mm.
10 % Muscovite .1 mm.
Primary Depositional Textures:
Laminations are well developed with normally graded bedding and sharp lower contacts defining the laminations. Calcite is concentrated in layers, but grades outward into siltstone from these layers implicating the possibility of a diagenetic, permeability controlled, origin for the calcite.
Post-Depositional Textures:
Iron rich dolomite rhombs cross-cut siliciclastic clasts in the coarser grained sections of the rock. This same

relationship may be ubiquitous throughout the rock, but the grain size is too small to be sure of this relationship. Calcite veinlets cross-cut the rock, making up about 3 % of the rock volume. Muscovite is metamorphic in origin and is concentrated along faint foliations in the rock.

GC-3
Intramicrite/Mudstone
30 % Calcite .013 mm.
30 % Dolomite < .0025 mm.
20 % Quartz .01 to .2 mm.
10 % Orthoclase .2 mm.
10 % Plagioclase .01 to .2 mm.
Primary Depositional Textures:
Laminations are the only primary depositional textures remaining in this rock.
Post-Depositional Textures:
Minerals are oriented by pressure, stylolites cut primary fabrics, fluidization breccia (molar tooth) has moved up through and disrupted primary laminated layers. The fluidization breccia is a fine grained breccia with a calcite matrix and silicate breccia clasts. Some of the larger clasts are micritic calcite.

GC-4
Intramicrite/Wackestone
60 % Calcite .01mm.
30 % Dolomite < .0025 mm.
10 % Quartz .01 to .07 mm.
Primary Depositional Features:
Microlaminations of fine-grained calcite and quartz clasts.
Post-Depositional Features:
Molar-tooth features cut across the rock and are filled with higher concentrations of calcite, less quartz, and more brecciated and larger silica clasts.

HL-3
Micrite/Mudstone
50 % quartz and feldspar .025 mm.
40 % dolomite .02 mm.
10 % calcite .013 mm.
tr. opaques, some pyrite .5 mm. cubes and .025 mm. amorphous opaques
tr. muscovite .05 mm.
Primary Depositional Textures:
This rock is a featureless mosaic of very fine grained quartz, calcite and dolomite.
Post-Depositional Textures:
Quartz shows some sutured grain boundaries. Large diagenetic pyrite crystals cross-cut the micrite matrix. Fine grained metamorphic muscovite cross-cuts the fine grained silica and

carbonate matrix.

HL-4
Micrite/Mudstone
Quartz .025 mm.
Plagioclase .025 mm.
Calcite .025 mm.
Dolomite .025 mm rhombs. .005 mm. crystal.
Muscovite .05 mm.
Primary Depositional Textures:
Laminations, graded laminations and cross-beds are seen in this sample. The cross-beds are defined by coarser grained sediments. Calcite is found in these coarser grained sections of the rock.
Post-Depositional Textures:
Some dolomite rhombs are found in this sample, but are much less volumetrically important than the finer grained dolomite. Calcite appears to be diagenetic in origin, found in the coarser grained sections of the rock it seems to be a permeability controlled cement. Muscovite is metamorphic in origin and is growing oriented parallel to bedding.

CF-2-380
Intramicrite/Grainstone
50 % Feldspar, Orthoclase and Plagioclase .01 to .07 mm.
40 % Quartz .01 to .07 mm.
8 % Dolomite .005 to .025 mm.
2 % Muscovite .07 mm.
Primary Depositional Textures:
This is a clast supported conglomerate, the average clast size is about .05 mm.; the clasts are angular, and are oriented parallel to bedding.
Post-Depositional Textures:
Dolomite rhombs and muscovite are found randomly cross-cutting quartz and feldspar clasts. The dolomite rhombs are composites of iron-rich and iron-poor dolomite intergrown in a rhombic shape. I found it impossible to determine the order of these iron-rich and iron-poor dolomites.

CF-4-500
Intramicrite/Grainstone
50 % Feldspar .1 mm.
37 % Quartz .1 mm.
10 % Dolomite .2 mm.
2 % Chert .05 mm.
1 % Muscovite .15 mm. in longest direction
Primary Depositional Textures:
Laminations are created by alignment of mineral grains.

Post-Depositional Textures:
Silica grains are sutured, metamorphic muscovite cross-cuts siliciclastic grains. Dolomite rhombs have grown in this rock but have little of their rhomb shapes left; they have been etched and dissolved, but not replaced by another mineral. As in CF-2, iron-rich and iron-poor dolomites have intergrown in a rhombic shape.

PH-1
Micrite/Mudstone
98 % Calcite .012 mm.
2 % quartz .025 mm.
tr iron oxides
Primary Depositional Textures:
Laminations are present in this rock, but are highly deformed by soft sediment deformation processes. Quartz intraclasts are scattered throughout the carbonate.
Post-Depositional Textures:
The calcite in this rock has indistinct crystal boundaries, patches of neomorphic spar is found amid micrite and microspar which has indistinguishable crystal boundaries. Stylolites are common and have concentrations of iron oxide and quartz clasts along them.

PH-2
Micrite/Mudstone; Intramicrite/Grainstone layers
64 % Quartz and Feldspar (hard to distinguish) .1 mm.
30 % Dolomite <.0025 mm.
5 % Calcite <.0025 mm.
1 % Muscovite .15 mm.
Primary Depositional Textures:
Faintly graded laminations alternate between intramicrite, micrite and mudstone. Calcite is evenly disseminated throughout the dominantly dolomitic laminae.
Post-Depositional Textures:
Fluidization features (Molar Tooth) are filled with blocky calcite and quartz clasts. Muscovite has formed paralleling bedding planes.

GTS/SY-3-100
Micrite/Mudstone
100 % Dolomite .005 mm.
tr. Quartz and Feldspar .025 mm.
tr. Opaques .025 mm.
Primary Depositional Textures:
Faint Laminations are visible with quartz and feldspar clasts scattered evenly throughout the sample.
Post Depositional Textures:
Crystal boundaries of dolomite are unclear, but look wavy where visible. There are no enfacial junctions and occasional partial rhombs of dolomite are seen.

GTS/SY-4-170
Micrite/Mudstone
100 % Dolomite <.0025 mm.
tr. quartz/feldspar clasts <.0025 mm.
tr. opaques <.0025 mm.
tr. organics
Primary Depositional Textures:
Laminations are visible with some layers consisting of up to 50 % clastics. This rock is very dark coloured, caused by wisps of organics that are found intergranularly throughout this sample.
Post-Depositional Textures:
Organic laminations show compaction of the rock by being crenulated and wrapped around quartz and feldspar clasts.

GTS/SY-10-373
Micrite/Mudstone
100 % Dolomite .005 to .01 mm.
tr. Quartz and Feldspar .01 mm.
tr. Opaques .0025 mm.
tr. Muscovite .05 mm.
Primary Depositional Textures:
1 mm. to 1 cm. thick bedding is visible in this sample.
Post-Depositional Textures:
Soft sediment deformation has disrupted the bedding in this rock. Dolomite has wavy crystal boundaries, uniform grain size and no enfacial junctions, implying a diagenetic origin.

GTS/SY-11-455
Micrite to Sparite (by layers)/Mudstone
78 % Dolomite .01 mm.
20 % Calcite .01 mm.
2 % Quartz/Feldspar intraclasts .01 to .05 mm.
tr. Muscovite
tr. Opaques .01 mm.
Primary Depositional Textures:
2 mm. to 2 cm. thick laminations are visible in this sample. Calcite is concentrated in layers in the rock. Dolomite and silicates are distributed uniformly throughout the rock.
Post-Depositional Textures:
Compaction has produced aligned mineral grains. Some dolomite rhombs are visible in coarser grained sections of the rock. Dolomite and calcite both have wavy crystal boundaries, no enfacial junctions, and grain size gradation typical of a diagenetic origin. Muscovite cuts all other grains in the rock.

GTS/SY-14-545
Micrite to Sparite by layers/ Mudstone
50 % Dolomite <.0025 to .025 mm.
30 % Calcite <.0025 to .025 mm.
20 % Quartz and Feldspar .025 mm.
tr. Muscovite .15 mm.
tr. Opaques
Primary Depositional Textures:
1 mm. to 1 cm. thick laminated siliciclastic graded beds cemented by calcite compose this sample.
Post-Depositional Textures:
Stylolites, diagenetic pyrite crystals and calcite veinlets are noted. Crenulated opaque layers (carbon concentrations?) are found in some beds. Dolomite rhombs are growing in this rock at the expense of silicate clasts, although the bulk of the dolomite is so fine grained that the crystal texture is unclear. Calcite has wavy crystal boundaries and no enfacial junctions.

PP/SY-2-660
Micrite/Mudstone
73 % Calcite .01 to .02 mm.
10 % Quartz .01 to .025 mm.
10 % Feldspar (Plagioclase and Orthoclase) .01 to .025 mm.
5 % Dolomite .01 to .025 mm.
2 % Muscovite .01 mm.
tr. Opaques
Primary Depositional Textures:
Calcite has straight and wavy crystal boundaries, and grades into silicate rich layers of rock. Opaques are deposited in discontinuous bands and disseminated throughout the calcite. Silicate rich and poor layers alternate forming .5 to 1 cm. thick laminations. Quartz and feldspar clasts form sharp boundaries at the bottom of the beds they are found in and grade upward into more calcite rich layers.
Post-Depositional Textures:
Opaque bands in the calcite wrap around the calcite crystals indicating compaction or displacement of the opaques by calcite crystal growth. Rhombs of dolomite cross-cut calcite, muscovite cross-cuts silicate minerals. Calcite crystals are forming at the expense of silica and feldspar rich grains.

PP/SY-4-725
Micrite/Mudstone
60 % Calcite .01 to .025 mm
39 % Dolomite .002 mm with occasional .04 mm. crystals
1 % Quartz .015 mm.
tr. pyrite .005 mm.
tr. haematite

Primary Depositional Textures:
Interlocking anhedral dolomite and calcite have wavy crystal boundaries. Dolomite is concentrated in layers and grades into more calcite-rich layers where they become equally mixed in a mottled fashion.
Post-Depositional Textures:
Stylolites, defined by concentrations of opaque minerals transect this sample. Trace amounts of sulfides and haematite are scattered throughout the rock. Trace amounts of .01 mm. dolomite rhombs are found occasionally in this rock and are being patchily replaced by calcite.

PP/SY-5-775
Micrite/Mudstone
78 % Calcite .005 to .025 mm
20 % Dolomite .005 to .025
2 % Quartz .02 mm.
tr. pyrite .0005 mm.
tr. muscovite max. length .05 mm.
Primary Depositional Textures:
Uniformly sized dolomite and calcite crystals are equally intermixed.
Post-Depositional Textures:
Carbonate crystal boundaries are wavy, there are few enfacial junctions, and crystal sizes are uniform. .025 mm. wide veinlets are filled with .01 mm to .05 mm calcite crystals. These veinlets show two generations of formation, two sets occur perpendicular to each other. Stylolites with opaque organic concentrations concentrated along them cross-cut the rock. Dolomite is also found concentrated along the stylolites.

7/28/85-4
Intramicrite to Micrite/ Wackestone or Grainstone and Mudstone by layers
90 % Dolomite .01 mm.
5 % Quartz .02 mm.
5 % Feldspar .02 mm.
tr. Muscovite .05 mm.
tr. Pyrite .005 mm.
tr. Organics
Primary Depositional Textures:
Alternating light and dark colored laminae are 1mm. to 1cm. thick; the dark colored laminae are created by interstitial organic carbon concentrations.
Post-Depositional Textures:
Laminations are disrupted by fluidization (molar tooth) which is filled with coarser grained calcite and quartz clasts. The dolomite is being recrystallized to spar in patches as aggrading neomorphism affects the rock. Muscovite and diagenetic pyrite both cross-cut the carbonate and quartz

clasts. Dolomite, with wavy indistinct crystal boundaries, is forming at the expense of quartz and feldspar clasts in this rock.

Empire:

7/28/85-13
Micrite/Mudstone
99 % Dolomite .005 mm.
1 % Quartz/Feldspar grains .005 mm.
tr. muscovite .01 mm.
tr. opaques .01 mm.
Primary Depositional Textures:
This rock is a faintly laminated crystalline dolomite.
Post-Depositional Textures:
Dolomite crystal boundaries are indistinct, but where visible are wavy, have a uniform grain size, have no entacial junctions and are interpreted to be diagenetic. Muscovite cross-cuts all other rock textures.

7/28/85-8
Micrite/Mudstone
99 % Dolomite < .0025 mm.
1 % Calcite .01 mm.
tr. iron oxides
Primary Depositional Textures:
Dolomite is dominantly of a uniform grain size with wispy, wavy carbon-rich layers interstitial to the carbonate grains.
Post-Depositional Textures:
Patches of dolomitic spar are scattered throughout the micritic matrix. These patches of spar are a result of aggrading porphyrid neomorphism of the dolomite and compose about 3% of the total rock volume. One pod of haematite is surrounded by sparry calcite. The dolomite in this sample shows abundant diagenetic textures; wavy crystal boundaries, uniform grain size and random grain orientation etc.

Spokane/Greyson Transition

TC-1-285
Intramicrite/Wackestone or Mudstone
50 % Calcite .02 to .05 mm
10 % Dolomite .02 mm
30 % Quartz .05 mm
10 % Orthoclase Feldspar .05 mm
trace opaques (pyrite?) .01 to .05 mm
trace muscovite .07 mm average length
Primary Depositional Textures:
Dolomite and calcite crystals are interlocking and equally distributed with silicates.

Post Depositional Textures:
Stylolites, with concentrations of opaques along them, are offset by .1 mm veinlets of .05 mm calcite. The grains and crystals show some preferred orientation. There is some dedolomitization (calcite replacement) of dolomite crystals.

TC-2-185
Micrite/Mudstone
90 % Calcite .01 to .05 mm
6 % Quartz .025 to .05 mm
2 % Orthoclase .025 to .05 mm
2 % Plagioclase .025 to .05 mm
tr. Muscovite .1 mm avg. length
Primary Depositional Textures:
Interlocking calcite crystals are distributed with silicates. Primary laminations are about 5 mm. thick; fine grained calcite alternates with coarser grained calcite intermixed with feldspar and quartz.
Post Depositional Textures:
Stylolites, defined by concentrations of iron-oxides, larger calcite crystals and silicate minerals have developed along many primary lamination boundaries.

WC-3-120
Intramicrite/Wackestone
50 % Quartz grains and vein fill: 90% less than .005 mm., 10% .03 mm.
30 % Chlorite less than .005 mm.
10 % Plagioclase vein fill .07 mm.
10 % Calcite less than .005 mm.
tr opaques
Primary Depositional Textures:
Primary laminations are visible in hand sample but not in thin section. Calcite and silica is evenly intermixed, but crystal boundaries are indistinct and therefore their relationship is hard to interpret.
Post Depositional Textures:
Molar tooth structures (fluidization textures) are still visible although this is a low-grade metamorphic rock. 2 phases of cement; gypsum and halite are replaced by albite and silica. Chlorite is growing in this rock at the expense of both siliciclastics and carbonates.

Altyn:

AF/AL-1- -150
Intrasparite/Boundstone
99 % Dolomite .012 to .05 mm.
.5 % Quartz (chert and monocrystalline quartz) .005 to .1 mm.
.5 % Feldspar .005 to .015 mm.
tr. Opaques .01 mm.
tr. Muscovite
Primary Depositional Textures:
Stromatolitic laminae are defined by alternating sparite and micrite sized dolomite crystals with siliclastic intraclasts concentrated along some layers. There is an area of intermound infill, intraclasts of quartz, feldspar and chert in a micrite matrix filling in between algal mats.
Post-Depositional Textures:
Some patches of larger dolomitic spar are found in the intramicritic portions of the rock. This dolomite is growing at the expense of silica clasts. Muscovite in trace amounts cross-cuts all previous textures.

AF/AL-3- -80
Oosparite/Grainstone
99 % Dolomite: 74 % Ooids .25 to .5 mm.
20 % Sparite .05 mm.
5 % Intraclasts .5 mm.
1 % Rock Fragments .1 mm.
Primary Depositional Textures:
Radial and concentric ooids and intraclasts are surrounded by a sparry dolomitic matrix. Chloritized igneous rock fragments are scattered throughout this carbonate conglomerate.
Post-Depositional Textures:
Many of the ooids have been diagenetically altered so much that they are merely ghosts of their former selves. Some ooids have been silicified (are now chert) and some are recrystallized dolomite. This process of recrystallization has destroyed primary textures and left only concentrically banded ooids. Two stages of cement can be seen in vugs in this rock, first an isopachous dolomite cement followed by a chert cement. Recrystallization of the carbonate in this rock (or the process of dolomitization) has obliterated many of the original textures. Dolomite rhombs are growing at the expense of silicified ooids.

Newland:

NC-1-10
Micrite/Mudstone
89 % Calcite .0025 mm
10 % Dolomite .0025 mm
1 % Opaques .0025 mm
tr. Organics
Primary Depositional Textures:
Dolomite and calcite crystals are interlocking and evenly distributed throughout the rock. Faint 1 mm. thick laminations are defined by concentrations of organics.
Post-Depositional Textures:
Diagenetic opaque minerals are scattered throughout the rock.

NC-2-100
Intrasparite and Sparite (by layers)/Wackestone
80 % Calcite .025 mm
2 % Rock Fragments .25 mm
8 % Quartz .2 mm
8 % Feldspar .2 mm
2 % Chlorite less than .0025 mm
Primary Depositional Textures:
1 cm. thick laminations are defined by alternating grain sizes of carbonate and silicates. Rock fragments are angular to subangular and are dominantly chloritized metamorphic fragments and chert. Ooids are found in some silicate layers. The matrix is composed of spar-sized calcite crystals.
Post-Depositional Textures:
Many of the ooids have been extensively recrystallized most are almost unrecognizable with only faint outlines of the original shapes remaining. Stylolites have developed perpendicular to bedding. The rock is fractured after stylolite formation, also perpendicular to laminations these fractures are filled with coarser grained calcite.

DG-3-540
Micrite to Intramicrite/Wackestone
60 % Calcite .025 mm
28 % Chlorite (?) less than .0025 mm
10 % Quartz/Feldspar .025 mm
2 % Muscovite max length .05 mm
tr. organics
Primary Depositional Textures:
Laminations are defined by alternating layers of quartz-rich and calcite rich layers. Some laminations have concentrations of organics along them. Quartz clasts are very angular with their long axes parallel to bedding and are concentrated in layers.

Post-Depositional Textures:
Compaction has caused the chlorite and organic rich layers to wrap around the quartz and feldspar grains. Fractures developed perpendicular to bedding and are filled with calcite. Muscovite cross-cuts the other carbonate and silicate minerals. Chlorite is growing at the expense of silicates in this rock.

Appendix C

Analytical Techniques and Chemical Composition of Belt Carbonates

The techniques for determination of trace element and isotopic ratios are summarized below. Following this discussion, the results of trace element and carbon and oxygen isotope analyses are reported.

Sample Preparation

All samples were soaked in 5% HCl for at least 5 hours to remove weathered rinds and thus avoid any possible contamination from surficial weathering. The average Belt carbonate sample lost 10 weight percent after 100 minutes exposure to HCl, with dissolution rate exponentially decreasing thereafter. Thus 5 hours was more than sufficient to pre-treat these carbonates. In order to further reduce the possibility of contamination, weathered rinds were cut off from rock samples after soaking in HCl and before crushing. The samples were crushed in an iron Chipmunk jaw crusher and then ground in a tungsten carbide shatterbox for 2 minutes. The resulting powder was less than 250 phi as determined by sieving of selected samples. The jaw crusher was cleaned with acetone and a large bottle brush between samples. The

shatterbox was cleaned first by grinding pure quartz sand for 2 minutes then with acetone.

Trace Element Analytical Procedures

The optimal digestion time for Belt carbonates was determined by trial digestions. Several samples were digested for .5, 1, 2, 4, 6 and 24 hours in 8% (v/v) HCl. After 3 hours, most of the carbonate in the sample has been dissolved. Between 3 and 4 hours significant aluminum began to be leached from the aluminosilicate phases. As a result, the Belt samples have been digested for 3 to 4 hours in 8% HCl.

The powdered rock samples were oven dried for one hour at 100 degrees C, then transferred to a desiccator to cool to room temperature. Between 1 and 1.5 grams (to .0003 grams accuracy) was weighed and placed in a 100 mL beaker. All glass and plastic ware was cleaned with aqua regia, rinsed in deionized water and dried. After addition of 25mL8% HCl, the samples were covered with watch glasses, swirled and then placed on a Jr. Orbit shaker plate. The samples were occasionally swirled manually to keep the particulate matter in suspension. The digested samples were filtered through ashless filter paper which took an average of 3 hours. To determine if the carbonate fraction of the sample was completely reacted, 8% HCl was sprayed on the particulate matter in the filters. Those samples which showed any reaction

with the HCl were re-digested using a smaller initial sample size. The filtered liquid was diluted in 50 mL volumetric flasks by addition of 5 mL of 20,000 ppm KCl and deionized water. The final solutions, utilized for Atomic Absorption measurements, were dissolved in 3% HCl and were stored in polyethelyne bottles. The undigested portions of the samples were combusted with the filter paper at 400° C for 2 hours in ceramic crucibles. For each sample, the weight of this insoluble residue was subtracted from the total sample weight. Consequently all trace element concentrations are reported for the insoluble residue free, or total carbonate, portion of the rock.

For each 15 samples digested, 2 samples were duplicated for an estimate of analytical precision and one blank was analyzed for evaluation of laboratory contamination. An internal laboratory standard (LMS-1) was run with each set of 15 samples to determine the accuracy of the techniques. This accuracy is summarized in Table C-1. The high Ca determination likely represents systematic error by previous analysts. With the exception of Ca of the LMS-1 standard, all analytical data are within acceptable limits of precision and accuracy with the exception of sodium. Sodium contamination was noted in several blanks. Analyses in the same sample set were corrected for this contamination by subtraction of a mean sodium value in the contaminated blanks. LMS-1 standards were overcorrected

Table C-1

LMS-1 Trace Element Accuracy

Univ. of Ottawa 'Accepted' Values for the LMS-1 Standard

Sample #[1]	Fe(ppm)	Mn(ppm)	Mg(%)	Ca(%)	Na(ppm)	Sr(ppm)
JL X	490	232	0.169	41.62	156	440
JL X	510	248	0.169	42.58	141	443
JL X	430	232	0.169	41.90	148	440
JL X	380	256	0.169	41.70	148	445
JL X	400	240	0.169	42.46	148	439
JL X	420	240	0.169	42.22	148	439
JL X	400	217	0.169	41.65	141	425
JL X	420	240	0.163	42.50	156	444
JL X	380	225	0.175	41.70	156	420
JL X	490	240	0.169	42.20	148	425
DG S	215	279	0.169	47.75		427
DG Tr	466	52	0.174	43.68		411
JL S		262	0.199	45.59		503
JL S	284	254	0.179	45.10	100	498
JL S	301	259	0.198	49.26	126	
JL S	310	262	0.185	48.21	110	
JL S	272	264	0.193		107	490
JL S	445	262	0.214	49.78	110	
JL S	338					498
H McGill	398	280			95	495
H McGill	411	276			99	499
H McGill	407	281			101	494
H McGill	446				121	
Average	392	243	0.178	44.11	129	457
St.Dev.	75	46	0.014	2.82	22	32
% St.Dev.	19.2	19.1	7.7	6.4	17.0	7.0
LMS-1 standards run for this thesis:						
LMS-1	343	295	0.170	42.01	93	439
LMS-1		254	0.168	40.05	101	263
LMS-1	353	294	0.167	41.90	90	419
LMS-1	349	289	0.170		80	430
LMS-1	336	286	0.161	41.58	85	421
LMS-1	345	289	0.169	42.46	93	419
LMS-1		264	0.152	36.27	78	345
LMS-1	338	277	0.168	42.43	79	437
Average	343	283	0.166	40.94	87	398
St.Dev.	6	14	0.006	1.92	8	55
LMS-1 Percent Accuracy:						
	-12.5	16.5	-6.7	-7.2	-32.6	-12.9

[1] Analyses performed by other analysts at the Univ. of Ottawa

and are consistently depleted in sodium. KH standards show depletion in sodium, the reason for which is not immediately obvious (Table C-2). To determine the accuracy of spectroscopic (AA) determinations, 0.5 grams of the international limestone standard (KH of Zentrales Geologisches Institut, ZGI, Berlin) was dissolved in 4ml of perchloric acid and 10 mL of HF. The sample was digested overnight and diluted to 25 mL with 3% HCl. The accuracy for the KH standard is summarized in Table C-2. This accuracy is substantially better than that of the LMS-1 internal standard, probably due to the limited number of determinations for the latter. The precision has been ascertained from duplicate analyses of 34 samples and is summarized in Table C-3.

Trace element analyses were performed on a Varian AA-175 series atomic adsorption spectrophotometer. Standard element concentrations were prepared with Fisher Scientific Company stock standards. They were within acceptable sensitivity for AA analyses, as determined by restricting the standard solutions to a slope = 1 in the graphs of absorbance vs. concentration for each element (see the Varian Tecktron manual of analytical methods for flame spectroscopy). The results of these analyses are reported in Table C-4. Despite my best efforts, some Ca and Mg values are 1-2% too high, an error that does not, however, affect the general diagenetic trends determined for these samples.

Table C-2

Accuracy as determined for KH Standards

Recommended Values for KH Standards:

Laboratory	Fe(ppm)	Mn(ppm)	Na(ppm)	Sr(ppm)	Al(ppm)	Mg(ppm)
ZGI	6435	682		545	12649	0.446
AGI KH-2	6015	650	816	537	12437	0.404
KH ZGI	6435	682		545	12649	0.446
KH GSN	6505	674	801		12755	0.436
Mean	6348	672	809	542	12622	0.433
St.Dev.	194	13	8	4	116	0.017

Present Measurements:

KH	5842	662	685	559	12781	0.406
KH	6153	663	513	511	12381	0.393
Mean	5998	662	599	535	12581	0.400

Accuracy in, Relative Percent, for KH Standard:

-5.5	-1.5	-25.9	-1.3	-0.3	-7.6

Standard values ZGI, AGI KH-2 and KH ZGI are from the Zentrales Geologisches Institut, Berlin and were supplied with the standard. The KH GSN value is from Geostandards Newsletter v.Viii, July, 1984.

Table C-3

Precision of Trace Elements

Sample #	Ca	Mg	Mn	Sr	Al	Na	Fe	%Sol.
RP-5	0.1	0.1	0.0	0.0	0.0	0.0	0.0	0.0
RP-7	1.3	10.4	0.7	0.0	1.7	1.1	0.0	0.0
RM-1	0.0	0.0	0.0	0.0	0.0	0.1	0.0	0.0
DRC-SI	5.3	1.3	NA	1.0	1.0	2.6	33.4	1.0
FCR-4	0.6	1.2	3.2	7.4	11.8	2.1	6.0	1.4
BHP-5	NA	2.1	4.9	1.4	2.8	9.8	3.6	0.0
BHP-11	5.1	10.7	3.2	15.3	8.5	2.4	13.5	5.3
BHP-12	3.1	9.0	1.1	0.0	15.3	14.6	6.8	5.3
BHP-14	6.9	7.3	6.1	0.6	8.7	9.2	7.3	0.0
BHP-17	4.8	4.4	5.8	4.8	0.8	3.5	1.5	2.4
BHP-20	0.0	0.0	0.0	0.0	0.1	0.0	0.0	0.0
GC-3	3.5	1.9	12.7	0.8	0.6	0.3	6.3	0.0
GC-4	0.0	0.0	0.0	0.2	0.0	0.1	0.0	0.0
HL-1	0.6	9.0	4.9	0.9	2.0	2.6	2.5	0.0
RR-1	1.5	0.2	0.8	0.9	14.9	0.3	NA	0.6
GTS-13	0.0	4.1	0.7	18.0	4.2	0.8	6.5	0.9
PP/SY-3	1.2	NA	1.5	1.0	1.4	5.7	1.9	1.2
RM/SH-3	3.8	2.3	0.5	6.0	0.8	7.8	4.8	0.0
RM/SH-6	1.2	1.6	1.6	0.0	2.4	4.6	9.7	2.4
RM/SH-8	3.3	2.5	3.2	12.9	0.0	28.7	17.0	3.0
SN/LC-6	0.0	0.0	0.0	0.0	0.1	0.0	0.0	0.0
AF/AL-3	0.0	0.0	0.0	0.0	0.0	0.1	0.0	0.0
7/25/855b	0.0	0.1	0.0	0.0	0.0	0.1	0.0	0.0
7/28/85-1	7.5	6.3	2.3	0.0	2.0	13.4	NA	1.2
7/28/85-3	2.3	5.6	3.1	0.0	4.2	29.7	NA	0.0
7/28/85-4	2.0	1.6	0.6	3.4	2.4	30.9	20.7	2.0
7/28/85-5	4.5	2.4	2.1	9.1	4.8	9.1	17.3	0.0
7/28/85-8	3.6	2.4	1.3	0.4	5.7	18.5	NA	2.5
7/29/85-4	2.8	3.5	3.2	7.7	4.7	0.6	NA	0.0
FM-303	0.0	0.0	0.0	0.0	0.0	0.0	0.0	0.0
FC-3	0.0	0.0	0.0	0.0	0.0	0.1	0.0	0.0
FB-159	0.0	0.0	0.0	0.0	0.0	0.0	0.0	0.0
FC-431	0.0	0.0	0.0	0.0	0.0	0.1	0.0	0.1
2-MP-25-1	0.1	0.1	0.0	5.0	5.0	0.1	0.0	0.0
Average Percent Precision	1.9	2.7	1.9	2.8	3.0	5.7	5.3	1.0

NA - No repeat analysis available.
All above samples were run twice

Table C-4: Trace and Major Element Analyses of Belt Carbonates

Sample Number	% soluble	Ca %	Mg %	Mn ppm	Sr ppm	Al ppm	Na ppm	Fe ppm
Libby:								
7/25/85-1	72.00	22.77	11.59	2268	90	419	172	16149
7/25/85-5a	48.00	39.03	3.25	4487	155	1249	63	4049
7/25/85-5b	51.00	37.29	3.21	4650	147	460	52	6010
7/29/85-1	57.00	40.88	2.05	7693	309	607	72	6333
7/29/85-4	65.00	37.68	1.94	4712	188	233	82	3381
FH-303	70.00	37.48	5.09	11359	253	1478	70	25499
FB-159	54.00	21.30	10.27	5535	101	1482	112	33921
FC-431	44.00	34.77	0.15	6543	338	829	150	2926
2-MP-25-1	40.00	35.26	0.33	5795	322	2291	159	7834
Mt.Shields:								
DF-1	83.00	21.46	12.67	541	32	281	160	8640
DF-2	70.00	19.10	11.82	739	44	264	11	5671
DF-3	70.00	21.34	12.96	1021	36	1075	146	7325
DF-4	74.00	21.16	12.96	1002	57	923	207	6903
RR-1	80.00	21.40	12.70	809	55	252	169	202
RR-2	73.00	21.79	12.19	675	53	171	192	4841
7/29/85-2	64.00	16.58	10.47	818	49	57	55	4947
7/29/85-5	63.00	22.99	11.79	1244	42	1082	133	20640
7/29/85-6	73.00	22.08	13.34	2704	60	278	75	8065
Shepard:								
DRC-SI-345	50.00	34.44	3.44	3227	104	1233	129	1094
SH/LC-8-5	38.00	20.86	9.78	8610	186	5469	311	46123
RM/SH-1	31.00	18.51	8.45	7644	154	13056	360	53905
RM/SH-2	33.00	20.30	9.74	3583	168	7009	353	37826
RM/SH-3	43.00	21.30	9.17	3496	181	6027	248	40098
RM/SH-5	45.00	21.97	10.64	2541	166	7239	246	36646
RM/SH-6	43.00	22.60	10.83	2619	117	3423	269	19110
RM/SH-8	51.00	22.46	11.23	1971	81	2383	149	29015
7/28/85-1	42.00	19.80	9.28	2017	164	2880	199	3713

Sample Number	% soluble	Ca %	Mg %	Mn ppm	Sr ppm	Al ppm	Na ppm	Fe ppm
7/28/85-2	33.00	32.43	3.58	2198	140	3584	172	10578
7/28/85-3	50.00	26.33	11.30	2201	241	1908	137	4254
Snowslip:								
SN/LC-2-0	44.00	23.84	11.82	1375	41	2760	191	11394
SN/LC-3-50	80.00	37.15	3.31	1785	136	113	64	1860
SN/LC-6-175	33.00	22.75	7.54	5885	172	5989	402	30700
SN/LC-7-228	57.00	35.62	0.51	5367	283	2144	89	6245
Middle Belt Carbonate:								
RP-1-121	59.00	20.78	11.87	688	73	2115	175	9515
RP-2-156	65.00	23.84	12.85	751	52	1391	139	8988
RP-3-196	61.00	22.16	12.68	716	46	1663	130	9172
RP-4-212	60.00	22.23	12.74	627	53	1132	111	8892
RP-5-242	60.00	22.84	12.03	672	74	1481	97	10310
RP-6-264	63.00	24.56	12.23	741	75	2984	170	9571
RP-7-329	49.20	20.75	9.94	665	78	2385	182	8925
RP-8-407	88.00	28.02	8.13	441	187	217	84	5340
RP-9-446	50.00	21.96	11.33	686	100	3979	180	17692
RP-10-560	70.00	33.94	2.81	356	130	1783	139	3347
RP-11-673	59.00	22.27	5.49	636	126	3133	160	8521
RP-12-730	49.00	22.83	10.67	868	56	4464	207	12736
RP-13-865	59.00	27.10	7.93	875	89	2787	137	12213
RP-15-1091	68.00	37.43	1.07	461	105	1681	140	5408
WL-1-50	62.00	32.03	4.99	3489	90	5746	123	10393
WL-2-209	68.00	17.40	10.20	572	18	1725	80	5747
WL-3-120	55.00	27.67	6.97	1958	86	1892	178	3602
WL-4-236	83.00	30.16	9.97	2007	67	345	32	5399
DRC-1-25	74.00	21.79	12.90	2355	21	1048	88	6864

Sample Number	% soluble	Ca %	Mg %	Mn ppm	Sr ppm	Al ppm	Na ppm	Fe ppm
DRC-2-64	75.00	22.03	13.08	1219	24	705	74	6143
DRC-3-141	74.00	32.57	12.87	888	32	979	73	6355
DRC-4-275	65.00	22.57	12.59	676	33	1249	88	6805
DRC-5-385	36.00	23.30	9.67	1904	53	5396	377	13195
RM-1	33.00	35.56	1.88	868	234	3852	216	5958
RM-2	32.00	34.16	1.34	1551	169	5366	192	8462
RM-3	36.00	31.36	1.97	659	163	2882	215	5318
RM-4	55.00	36.24	2.65	837	201	2057	107	5695
RM-5	31.00	36.20	1.57	889	200	5264	299	6882
RM-7	46.00	35.73	0.93	1103	182	3281	163	5661
FCR-1-5	78.00	23.44	12.57	4896	22	450	116	8848
FCR-2-113	65.00	24.96	9.83	693	56	1420	161	8745
FCR-3-345	77.00	22.71	12.21	907	35	714	148	8821
FCR-4-443	72.00	26.86	8.64	2935	51	630	98	19943
BHP-4-1120	44.00	38.68	1.06	955	81	4140	101	7604
BHP-5-1400	40.00	35.29	0.71	890	144	4943	55	6342
BHP-7-1800	33.00	36.09	0.84	1452	10	5010	33	4856
BHP-8-1940	38.00	34.93	0.61	806	230	5040	164	7333
BHP-9	29.00	29.35	0.53	922	163	3764	158	16197
BHP-10	47.00	21.70	11.25	1323	110	2783	74	3374
BHP-14	64.00	28.28	0.90	655	242	931	79	5523
BHP-15	43.00	26.95	6.32	888	153	2645	58	2195
BHP-16	70.00	38.19	0.48	496	239	73	7	96
BHP-17	43.00	29.28	4.35	815	167	2642	56	14113
BHP-19	41.00	41.40	0.51	954	208	2888	42	4654
BHP-20	35.00	35.93	2.32	1146	254	4800	158	12240
GC-1	33.00	34.21	2.32	1258	329	5015	265	16889
GC-2	41.00	32.60	1.98	1152	301	3063	158	18569
GC-3	51.00	34.12	1.79	895	253	2510	168	9011
GC-4	70.00	35.81	2.69	713	306	1368	44	10990

Sample Number	% soluble	Ca %	Mg %	Mn ppm	Sr ppm	Al ppm	Na ppm	Fe ppm
HL-2	30.00	30.78	2.55	946	157	5113	201	7340
PH-1	89.00	39.01	0.51	466	462	421	20	3066
PH-3	31.00	38.09	1.47	1552	94	3739	169	6136
GTS/SY-1-10	71.00	22.09	12.49	2072	53	982	125	12158
GTS/SY-2-30	54.00	22.28	11.70	1962	58	2305	116	17374
GTS/SY-3-100	51.00	22.58	11.91	2169	55	1888	121	13110
GTS/SY-4-170	50.00	19.35	10.13	1379	31	2150	110	10632
GTS/SY-5-210	57.00	22.54	12.05	731	31	1455	123	9203
GTS/SY-6-254	54.00	22.14	11.30	870	103	2961	81	18327
GTS/SY-7-295	59.00	22.50	11.41	785	104	1424	65	15492
GTS/SY-8-320	63.00	20.15	11.36	737	121	2094	58	26881
GTS/SY-9-345	56.00	21.38	10.56	895	115	2428	69	18758
GTS/SY-10-373	46.00	28.13	4.34	599	118	2260	96	8333
GTS/SY-12-490	53.00	22.91	11.14	1522	57	1926	115	31844
GTS/SY-13-510	57.00	27.21	6.06	946	177	1501	66	18569
GTS/SY-14-545	54.00	30.44	3.71	548	156	1439	67	8670
PP/SY-1-605	32.00	29.11	5.04	777	116	3270	170	15956
PP/SY-2-660	62.00	39.10	0.66	562	101	1373	67	4666
PP/SY-3-686	41.00	34.13	0.74	790	104	2480	124	10995
PP/SY-4-725	56.00	28.03	7.00	1093	112	1524	102	14124
PP/SY-5-775	63.00	32.39	3.02	854	116	1709	81	8035
SN/LC-1- -10	74.00	40.16	1.23	752	126	922	84	3388
7/28/85-4	50.00	22.69	11.56	1233	130	1697	148	3317
7/28/85-5	37.00	25.13	5.31	813	126	2964	145	9560
7/28/85-6	46.00	20.40	11.29	1280	127	1879	86	2592
7/28/85-7	34.00	24.76	9.78	1998	172	2510	157	31315
Empire:								
7/28/85-8	41.00	25.63	7.13	2614	264	2632	186	20069
7/28/85-13	38.00	22.76	10.04	2107	205	2766	133	32384

Sample Number	% soluble	Ca %	Mg %	Mn ppm	Sr ppm	Al ppm	Na ppm	Fe ppm
Spokane/ Greyson:								
TC-1	34.00	34.08	5.49	3410	742	3724	398	6781
TC-2	72.00	39.94	3.30	1617	484	773	120	7290
TC-3	64.00	38.77	2.97	2473	321	1705	98	7553
WC-1	27.00	32.77	6.90	5592	374	171	563	4411
WC-2	61.00	38.62	4.04	2638	401	3724	169	2535
ALtyn:								
AF/AL-1- -150	89.00	22.53	13.49	179	25	175	147	3311
AF/AL-2- -30	86.00	22.40	12.99	457	53	390	197	7718
AF/AL-3- -80	86.00	22.55	12.86	211	44	< 20	53	2034
Newland:								
NC-1-10	69.00	38.80	0.83	375	1271	1028	83	8378
NC-2-100	78.00	36.89	0.68	707	1786	840	82	5914
NC-3-400	68.00	35.78	1.25	465	1468	1428	97	7920
NC-4-440	70.00	38.28	0.73	466	1699	1295	92	7525
SR-1-520	43.00	17.17	9.94	2591	162	4666	153	8925
SR-2-596	27.00	12.05	6.86	3485	89	9585	252	39389
SR-3-1260	77.00	24.10	9.27	1103	428	186	68	9688
DG-1-20	45.00	35.13	1.59	666	5521	2761	130	9367
DG-2-140	43.00	35.21	0.87	327	2876	3041	240	6801
DG-3-540	51.00	35.43	1.33	644	3914	1997	76	8187
DG-4-1000	56.00	34.37	1.27	390	1950	2673	114	7382

Geochemistry of carbonates containing > 75% insoluble residue are not reported here.
Duplicate analyses of selected samples are not reported here.

Carbon and Oxygen Isotopic Analyses

Powdered carbonate samples were weighed to the nearest hundredth of a gram and loaded into glass reaction vessels. Between 10 and 150 mg of sample were used, depending on the carbonate content of the sample. 3 mL of dehydrated phosphoric acid was added to the reaction vessels, which were immediately capped, sealed and evacuated on a vacuum line for one hour. The acid was heated immediately after the samples were placed on the line to drive off any water. The sealed vessels were then placed in a 25 degree circulating water bath overnight. They were then tipped to allow the acid to react with the powdered carbonate for 4 to 5 hours at 25 ° C. The evolved CO_2, dominantly from calcite, was collected after extraction of water and non-condensible gasses by liquid nitrogen and a slush of CO_2-acetone. This CO_2 was sealed in glass tubes. The vessels containing the residual solid samples were immediately resealed and placed in a 50° C circulating antifreeze bath overnight. The CO_2 evolved from the samples after 18-26 hours was mostly from dolomite. Carbon and oxygen isotopic compositions from these two mineral phases were often similar (Table C-5) which indicates dolomite might have begun to dissolve during the 'calcite' extraction step.

The $\delta^{13}C$ and $\delta^{18}O$ were measured on a V.G. Isogas SIRA 12 triple collecting mass spectrometer and are reported in the standard delta notation in Table C-5. For carbon the standard

Table C-5: Carbon and Oxygen Isotope Geochemistry of Belt Carbonates

Sample Number	$^{18}O_{cc}$	$^{13}C_{cc}$	$^{18}O_{do}$	$^{13}C_{do}$
Libby:				
7/25/85-1	20.1	-0.5	19.6	-0.4
7/25/85-5a	13.6	-1.7		
7/25/85-5b	not analyzed			
7/29/85-1	13.4	-1.6		
7/29/85-4	13.6	-0.9		
FM-303	13.7	-1.4	16.8	-1.0
FC-72	low yield			
FC-3	12.9	-2.9		
FB-159	15.4	-1.5	14.9	-1.8
FC-431	13.4	-1.0		
FC-277	12.4	-12.4		
2-MP-25-1	13.6	-0.6		
7/23/86-1	14.5	-0.2		
Mt. Shields:				
DF-1	22.5	0.0	23.5	0.6
DF-2	22.3	0.3	23.1	0.9
DF-3	21.9	0.8	21.7	1.1
DF-4	22.0	1.0	22.5	1.3
RR-1	22.5	0.4	22.8	0.7
RR-2	22.6	0.8	23.3	1.2
7/29/85-2	18.7	-1.0	19.4	-0.9
7/29/85-5	17.0	-0.9	18.1	-0.8
7/29/85-6	20.7	-1.3	21.6	-0.9
Shepard:				
DRC-SI-345	21.1	-3.5		
SH/LC-8-5			19.9	-2.9
RM/SH-1	20.7	-4.0	21.4	-3.8
RM/SH-2	21.6	-3.1	22.6	-2.9
RM/SH-3	20.8	-2.9	21.1	-2.9
RM/SH-4	not analyzed			
RM/SH-5	21.4	-2.0	21.9	-1.9
RM/SH-6	21.7	-1.8	22.5	-8.1
RM/SH-8	23.5	-2.3	23.5	-2.2
7/28/85-1	17.7	-2.1		
7/28/85-2	15.2	-5.3	20.1	-1.5
7/28/85-3	17.2	-2.0	17.1	-1.7
7/29/85-3	16.2	-4.0	16.7	-3.5
Snowslip:				
SN/LC-2-0	24.8	0.3	25.3	0.4
SN/LC-3-50	18.0	-2.2	26.0	0.4
SN/LC-4-95			16.4	-2.1

Sample Number	$^{18}O_{cc}$	$^{13}C_{cc}$	$^{18}O_{do}$	$^{13}C_{do}$
SN/LC-5-125	19.2	-2.1	22.3	-1.2
SN/LC-6-175	19.3	-2.6	21.9	-1.6
SN/LC-7-228	15.7	-3.2		
Middle Belt Carbonate:				
Helena:				
RP-1-121	25.3	0.2	25.7	0.3
RP-2-156	25.3	0.3	25.6	0.4
RP-3-196	25.4	0.1	25.8	0.1
RP-4-212	25.4	0.0		
RP-5-242	24.4	-0.3	24.8	-0.2
RP-6-264	25.2	-0.4	25.4	-0.3
RP-7-329	24.8	-0.2	25.5	-0.1
RP-8-407	23.3	-0.7	25.4	0.4
RP-9-446	23.7	0.6	24.0	0.9
RP-10-560	20.3	0.3	24.7	0.8
RP-11-673	22.5	0.3	25.4	0.9
RP-12-730	25.5	1.7	25.9	1.8
RP-13-865	23.1	1.7	25.5	2.2
RP-14-887	21.8	1.9	24.7	2.6
RP-15-1091	20.8	1.3		
WL-1-50	21.3	-2.0	21.7	-2.2
WL-2-209	21.2	-1.5		
WL-3-120	23.0	-1.1	25.3	-0.3
WL-4-236	23.2	-0.2	24.3	0.4
DRC-1-25	26.0	-1.4	26.4	-1.1
DRC-2-64	25.6	0.1	26.2	0.4
DRC-3-141	26.2	0.2	26.2	0.3
DRC-4-275	26.5	0.8	27.0	0.9
DRC-5-385	25.2	-1.0	27.4	-0.1
RM-1	16.7	-2.2	19.9	-1.1
RM-2	17.7	-2.5		
RM-3	18.1	-1.0	19.4	-0.9
RM-4	22.2	-0.5		
RM-5	18.3	-1.1	20.1	-0.6
RM-6	not analyzed			
RM-7	16.5	-2.5		
FCR-1-5	26.0	-1.5	26.4	-1.4
FCR-2-113	22.2	0.9	25.3	1.2
FCR-3-345	25.2	1.4	25.6	1.7
FCR-4-443	22.5	-0.2	26.2	0.8
HL-1	17.8	-1.9		
HL-2	17.1	-1.9	17.7	-2.1

Sample Number	$^{18}O_{cc}$	$^{13}C_{cc}$	$^{18}O_{do}$	$^{13}C_{do}$
HL-3			16.8	-2.6
HL-4	18.1	-2.2	20.7	-1.6
HL-5	18.0	-3.3		
HL-6	17.7	-12.8		
PH-1	15.0	-1.8		
PH-2	15.7	-3.9		
PH-3	17.0	-1.0		
7/28/85-4	18.0	-2.4		
7/28/85-5	18.1	-0.3	19.0	-0.2
7/28/85-6	13.2	-0.8	18.9	-0.2
7/28/85-7	18.6	-1.3	18.1	-1.3
Wallace:				
BHP-1-320	14.6	1.3		
BHP-2-640	low yield			
BHP-3-840	not analyzed			
BHP-4-1120	16.0	-2.2		
BHP-5-1400	16.8	-2.7		
BHP-6-1580	17.2	-1.1		
BHP-7-1800	15.3	-5.6		
BHP-8-1940	17.2	0.1		
BHP-9	17.2	-0.8	17.8	-0.4
BHP-10	19.0	-0.4	18.4	-0.3
BHP-11	17.4	-0.8	18.5	-0.3
BHP-12	low yield			
BHP-13	16.7	-2.1		
BHP-14	17.4	-0.8	18.5	-0.3
BHP-15	17.7	-0.6	18.4	-0.2
BHP-16	17.2	-0.6	19.1	-0.6
BHP-17	17.5	-0.7	18.2	-0.7
BHP-18	19.1	-0.3	18.4	-0.2
BHP-19	16.4	-1.7		
BHP-20	16.4	-2.0	18.2	-0.7
GC-1	16.2	-1.1	17.1	-0.7
GC-2	16.7	1.3	17.2	1.6
GC-3	16.2	-0.6	17.7	-0.1
GC-4	16.6	-0.4	17.6	-0.2
CF-1-2910	dirty gas			
CF-2-3000	14.4	-2.6	16.0	-3.4
CF-3-400	14.4	-4.4	14.7	-3.7
CF-4-500	15.9	-4.1	15.6	-4.1
Siyeh:				
GTS/SY-1-10	22.7	-1.3	23.0	-1.2
GTS/SY-2-30	22.3	-1.9	23.1	-1.6

Sample Number	$^{18}O_{cc}$	$^{13}C_{cc}$	$^{18}O_{do}$	$^{13}C_{do}$
GTS/SY-3-100	21.9	-1.3	22.3	-1.1
GTS/SY-4-170	23.0	-0.6	23.6	-0.1
GTS/SY-5-210	23.6	0.0	23.9	0.2
GTS/SY-6-254	21.3	0.1	20.8	0.2
GTS/SY-7-295	21.0	-0.1	21.8	0.0
GTS/SY-8-320	21.7	0.1	21.4	0.3
GTS/SY-9-345	22.1	0.3	22.0	0.4
GTS/SY-10-373	19.8	0.4	23.0	-0.7
GTS/SY-11-455	low yield			
GTS/SY-12-49C	24.3	1.6	24.2	1.5
GTS/SY-13-510	20.0	1.5	22.2	2.1
GTS/SY-14-545	20.8	1.9	22.7	2.1
PP/SY-1-605	20.0	0.6	21.3	0.8
PP/SY-2-660	19.5	-0.8		
PP/SY-3-686	19.5	-0.6	22.6	0.2
PP/SY-4-725	20.6	-0.3	23.9	0.1
PP/SY-5-775	19.6	-0.3	23.9	0.5
SN/LC-1- -10	19.1	0.3	23.3	0.6
Empire:				
7/28/85-8	15.5	-3.5		
7/28/85-13	17.9	-1.6	17.2	-1.6
Spokane/ Greyson:				
TC-1	16.3	1.5		
TC-2	17.0	2.8		
TC-3	16.2	1.7		
WC-1	16.4	0.4		
WC-2	16.6	1.9		
WC-3	16.3	1.0		
Altyn:				
AF/AL-1- -150	27.4	1.4	27.9	1.6
AF/AL-2- -30	26.5	1.3	27.4	1.5
AF/AL-3- -80	24.2	1.7	24.5	1.9
Newland:				
NC-1-10	18.2	2.1	19.5	0.8
NC-2-100	18.3	1.9		
NC-3-400	19.5	2.4	21.5	2.4
NC-4-440	18.9	2.4	20.6	1.8
NC-5-440	18.3	0.2	23.3	0.9
SR-1-520	25.0	0.1	24.8	-0.3
SR-2-596	23.5	-1.6	25.4	-1.8

Sample Number	$^{18}O_{cc}$	$^{13}C_{cc}$	$^{18}O_{do}$	$^{13}C_{do}$
SR-3-1260	22.3	0.4		
DG-1-20	20.7	1.7		
DG-2-140	20.7	2.4		
DG-3-540	22.9	1.5	16.7	-4.5
DG-4-1000	20.6	2.4		
Prichard:				
7/28/85-9	low yield			
7/28/85-10	low yield			
7/28/85-11	low yield			
7/28/85-12	low yield			

is the Pee Dee Belemnite (PDB) and for oxygen isotopic analyses it is Standard Mean Ocean Water (SMOW). The accuracy of the determinations is better than .025 $^{o}/_{oo}$ and the precision, including extraction of gas, is .1 $^{o}/_{oo}$ for both $\delta^{13}C$ and $\delta^{18}O$. All elemental and isotope work has been performed at the University of Ottawa Derry Laboratory.

Strontium Isotopic Analyses

Strontium was concentrated by the column ion-exchange technique. Glass columns were loaded with a slurry of 200-400 mesh Biorad Laboratories hydrogen form cation exchange resin in 2.5 N ultrapure HCl. The purified HCl has been prepared and titrated at the Carleton University dust-free clean laboratory. Glass wool was placed on the top of the resin columns to prevent its disruption during addition of the fluid. The height of the 4 columns thus prepared was 18, 18.5, 19 and 17.5 cms, and their diameter was 1 cm. Carbonates were dissolved in 8% ultrapure HCl and filtered as described in the section on trace element extraction. Depending on the Sr concentration of the solution, 1-4 mL was dropped directly on the resin column. This was followed by three 1mLadditions of 2.5N HCl, each allowed to sink into the resin. A final 2 mL portion of 2.5 N HCl was added and allowed to sink into the resin. For calibration of the columns, 150mLof 2.5N HCl was then added to the columns. The columns were calibrated for Sr

and Ca throughout by collection of the effluent in 5 mL increments and analyzed for these cations by atomic adsorption mass spectrometry. After calibration, when the Sr peak was determined, the initial 5 mls of 2.5 N HCl was added in 1mLincrements as described above. Then between 90 and 100 mls of 2.5 N HCl were added to the columns, the amount of HCl increasing with the height of the column. This elutant was allowed to pass through the columns uncollected. 20 mLs of 2.5 N HCl was then added to the column and this portion was collected as it contained concentrated Sr^{+2}. This 20mLof effluent was heated to about 100°C in teflon watch glasses until the liquid was evaporated to such a degree that it could be placed in cone-shaped teflon containers and evaporated to powder which collected at the tip of the cone. The solid Sr was covered with parafilm and placed in a desiccator prior to mass spectrometric analysis.

The mass spectrometric analysis was carried out at Carleton University on a Finnigan-MAT 261 multi-collector mass spectrometer (Bell and Blenkinsop, 1984). Sr was run as the phosphate using a single tantalum filament. Masses 85 through 88 were measured simultaneously. Reproducibility of the $^{87}Sr/^{86}Sr$ ratios is considered to be 0.004% of the quoted value at the 2 sigma level. The NBS 987 standard gives a $^{87}Sr/^{86}Sr$ ratio of 0.71023 ± 0.00003 and the E. and A. standard had a value of 0.70802 ± 0.00003.

Unfortunately, 12 samples were stored for 1 year at Carleton University in polyethelyne bottles prior to evaporation. Of this group, one contained a white precipitate and was not run, one failed to produce a strong enough beam, and two ran poorly on the mass spectrometer resulting in sub-standard precision (samples 7/28/85-5 and 7/28/85-8). The remaining samples (GC-1, DRC-4, DRC-5, 7/28/85-4, 7/28/85-6, DF-4, TC-1, FM-303) produced credible results and are listed here. The results of $^{87}Sr/^{86}Sr$ analyses are listed in Table 5-1.

Sulfur Isotope Analyses

25 carbonate samples were selected for sulfur isotope analysis based on the possibility that these samples contained sufficient sulfur. Some samples has visible trace (< 1%) sulfides, dominantly pyrite and subordinate pyrrhotite. Others were chosen for their low solubility which increases the chance for the presence of a sulfides. Samples were pretreated by dissolution in 6% (v/v) HCl for 3 to 4 hours to remove excess carbonate. This pretreatment should have effectively removed sulfates and some sulfide species, leaving pyrite and pyrrhotite intact. 5 to 12 grams of powdered carbonate was reacted with Kiba agent (dehydrated phosphoric acid containing stannous ions; Kiba et al., 1955) under vacuum for a minimum of 30 minutes at >300^{0}C to extract H_2S from sulfide and any SO_2 from sulfate remaining in the sample. Those samples with

significant carbonate were allowed to react slowly (with no heat) with the Kiba agent until this carbonate was consumed, usually within 45 minutes. SO_2 evolved by this reaction, after passing through a distilled water trap to remove unwanted chemical species, was oxidized to cadmium sulfate by reaction with cadmium acetate in two liquid traps. 13 samples contained insufficient sulfur, even after multiple reactions, to produce measurable sulfur yields. The cadmium sulfate was then reduced to silver sulfide through addition to silver nitrate. The silver sulfide was filtered, washed with distilled water, then dried at least 1 hour prior to weighing. Between 9 and 52 mg of silver sulfide was mixed with copper oxide with a ratio of AgS/CuO of 0.6 and placed in a quartz sample boat, capped with glass wool. The sample was then burned at 1050^{0}C for 15 minutes in a closed sample tube which was stoppered with copper filings, and for an additional 15 minutes open to a liquid nitrogen trap. Any CO_2 or H_2O evolved during sample burning was separated by alternating baths of ethanol + liquid nitrogen and CO_2 (dry ice) and liquid nitrogen. The SO_2 sample evolved was sealed in a glass tube then analyzed on a V.G. Micromas 602E double collector mass spectrometer with a resulting accuracy, including KIBA extraction, of 2.5 $^0/_{00}$. The error on these types of analyses is high because of the significant percentage of carbonate. Determinations of $\delta^{34}S$ from mixtures of carbonate and sulfide of known composition, using the above

described KIBA extractions in the stable isotope laboratory at the University of Ottawa, have been shown to reproduce $\delta^{34}S$ with an accuracy of only 2.5 $^{o}/_{oo}$.

Percent sulfur was determined by ion liquid chromatography. The sample was weighed and intimately mixed with 0.6 g of vanadium pentoxide. The mix was placed in a nickel 'boat', and the boat inserted into a muffle furnace at 1030 °C under a stream of heated, water saturated oxygen. Oxygen was bubbled into 50 mL of 'pure water' containing 25 µl of hydrogen peroxide. The liquid sample was then separated using a DIONEX HPLC, the anions are determined after separation and compared to standard solutions. The detection limit is 50 µg/ml. These analyses were performed at the Geological Survey of Canada. Percent accuracy is .008. Sulfur concentrations and $\delta^{34}S$ for those Belt carbonates that produced measurable yield are listed below:

Sample #	% Sulfur	$\delta^{34}S$
BHP-11	0.006	
7/29/85-2	<0.005	
7/28/85-11	<0.005	
BHP-10	<0.005	
Sn/Lc-3	0.062	
RR-1	0.007	
WC-3	0.290	8.78/9.58
Gts/Sy-11	0.054	7.75
FC-72	0.010	2.70
7/25/85-5	0.334	0.18
7/29/85-5		7.91
7/29/85-3		5.65
Rm/Sh-1		6.61
Hl-6		2.82
Nc-5		7.26

Appendix D

SPSSx Program for Factor Analysis

The SPSSx program (SPSSx, 1986) for factor analysis was applied to the geochemical and compositional determinations as listed in Tables C-4 and C-5 and entered in the input data file SBELT. Pairwise deletion on input data was utilized. In order to circumvent possible problems with negative values, $\delta^{13}C$ was reported as a positive value in SBELT by adding 10 to all original values. The factor analyses were performed at The Colorado College, Colorado Springs, Colorado and at the University of Ottawa. The data in SBELT was the geochemical data collected for Belt carbonates as reported in this thesis. The following sample program performed factor analysis on dolostones of the Altyn Formation.

```
FILE HANDLE SBELT/NAME ="BELT SYSDATA A1"
GET FILE = SBELT/
 KEEP=SOL. COMP FM. CA MG MN SR AL NA FE O18CC C13CC O18DO
O13DO  SRISO/MAP
VARIABLE LABLES
 SOL. 'PERCENT SOLUBLE'
 COMP 'CARBONATE COMPOSITION'
 FM. 'FORMATION'
 CA 'PERCENT CA'
```

```
 MG 'PERCENT MG'
 MN 'MN (PPM)'
 SR 'SR (PPM)'
 AL 'AL (PPM)'
 NA 'NA (PPM)'
 FE 'FE (PPM)'
 O18CC 'DELTA O18CC'
 C13CC 'DELTA C13CC'
 O18DO 'DELTA O18DO'
 C13DO 'DELTA C13DO'
 SRISO 'STRONTIUM ISOTOPES'
SELECT IF (COMP EQ 'DO    ')
SELECT IF (FM. EQ 'AL     ')
COMPUTE LOS = LG10(SOL.)
COMPUTE AC = LG10(CA)
COMPUTE GM = LG10(MG)
COMPUTE NM = LG10(MN)
COMPUTE RS = LG10(SR)
COMPUTE LA = LG10(AL)
COMPUTE AN = LG10(NA)
COMPUTE EF = LG10(FE)
FACTOR VARIABLES=LOS AC GM NM RS LA AN EF O18DO TO SRISO
/MISSING=PAIRWISE
/PRINT=ALL
```

Appendix E

Summary of Isotope Data for Proterozoic Carbonates

The following tables (E-1 and E-2) summarize oxygen, carbon and strontium isotope data from literature. The carbon and oxygen isotope composition of rocks from the Siberian Platform (Magaritz et al., 1986) and the Yangtze Platform (Lambert et al., 1987) were read from graphs. As a result, oxygen and carbon isotopes of these sequences are not listed here. The geochemistry of Belt Supergroup data is not included in this compilation as it is listed in Table C-5.

Table E-1

Strontium Isotope Data From Proterozoic Carbonate Sequences

Locality	Composition	Age(Ma)	$^{87}Sr/^{86}Sr$
Cango and	cc	600	0.70789
Malmesbury Formations	cc	600	0.70808
	do	600	0.70811
	cc	600	0.70806
	cc	600	0.70836
	cc	600	0.70763
	cc	600	0.70755
	cc	600	0.70883
	cc	600	0.70871
Nama System	cc	620	0.70951
	do	620	0.70854
	cc	620	0.70840
	cc	620	0.70851
	cc	620	0.70837
	cc	620	0.70846
	cc	620	0.70842
Adelaide Geosyncline:			
Wonoka Fm.	cc	645	0.70915
Nuccaleena Fm.	do	645	0.70944
Willochra Fm.	do	645	0.71285
	do	645	0.70973
Trezona Fm.	cc	645	0.70735
	cc	645	0.70730
	cc	645	0.70823
Etina Fm.	cc	645	0.70761
	cc	645	0.70750
Brighton Limestone	do	725	0.70739
	cc	725	0.70734
	cc	725	0.70734
	cc	725	0.70911
	cc	725	0.70833
	cc	725	0.70833
	cc	725	0.70857
Tapley Hill Fm.	cc	725	0.71447
	cc	725	0.71236
	cc	725	0.71236
Tindelpina Shale Mbr.	do	725	0.71037
Apilla Tillite	do	725	0.71937
	do	725	0.71711

Locality	Composition	Age(Ma)	$^{87}Sr/^{86}Sr$
Adelaide Geosyncline cont.:			
Skillogalee Dolomite	do	785	0.70893
	do	785	0.70903
	do	785	0.71323
	do	785	0.71156
	do	785	0.71108
River Wakefield Grp.	do	860	0.71051
	do	860	0.71048
	do	860	0.71062
	do	860	0.71972
Amadeus Basin:			
Pertatataka Fm.	do	645	0.71264
	do	645	0.70995
Bitter Springs Fm.	do	1000	0.70860
	cc	1000	0.71149
	do	1000	0.71058
	cc	1000	0.70739
	cc	1000	0.70732
	do	1000	0.70730
	do	1000	0.70755
	cc	1000	0.70739
	cc	1000	0.70837
	cc	1000	0.70998
	do	1000	0.70877
	do	1000	0.70876
	do	1000	0.70796
	cc	1000	0.70848
	cc	1000	0.70665
Adrar Fm., Mauritania	cc	900	0.71352
	cc	900	0.71843
	cc	900	0.71655
	cc	900	0.71330
	do	900	0.71015
	cc	900	0.71456
	cc	900	0.71032
	cc	900	0.71763
	do	900	0.70841
	cc	900	0.72127
	cc	900	0.70555
	cc	900	0.70707
	do	900	0.70873
	do	900	0.71220
	do	900	0.71475
	do	900	0.71636
	cc	900	0.70731
	do	900	0.71446
	do	900	0.70742

Locality	Composition	Age(Ma)	$^{87}Sr/^{86}Sr$
Hammersely Basin:			
Bangemal Group	do	1050	0.70831
	do	1050	0.70861
	do	1050	0.70851
	do	1050	0.70496
	do	1050	0.70824
	do	1050	0.72025
	do	1050	0.71428
McArthur Basin:			
Reward Do.	do	1550	0.70694
	do	1550	0.70611
Cooley Mbr.	do	1550	0.70696
Mitchell Yard Mbr.	do	1550	0.70604
Mara Do.	do	1550	0.70667
Leila Sst.	do	1550	0.71306
Wollogonang Fm.	cc	1800	0.71390
	do	1800	0.73460
Hammersley Basin:			
Mt. Bruce Supergroup:			
Duck Creek Do.	cc	2095	0.70496
	do	2095	0.70930
Wittenoom Do.	do	2095	0.74331
	do	2095	0.75035
	do	2095	0.72847
	do	2095	0.70711
	do	2095	0.72110
Pillingani Tuff	?	2095	0.74086
Yangtzee Gorges:			
Dengying Fm.	do	700	0.70890
Doushantou Fm.	cc	700	0.71290

All strontium isotope ratios are from Veizer and Compston (1976). Exceptions are the Yangtzee Gorges and the Wollogonang Fm. of the McArthur Basin (Lambert et al., 1984), the Cango and Malmesbury Formations, the Nama system, and the Adrar Fm. (Veizer et al., 1983). The strontium ratios are normalized to E. and A. standard 0.70802 or NBS-987 0.71023 except those from the Yangtzee Gorges and Wollogonang Fm. for which no standards were reported. The normalized strontium isotope ratios can be compared directly to strontium isotopes listed in Appendix C and in Table 5-1.

Table E-2: Oxygen and Carbon Isotope Data from Proterozoic Carbonate Sequences

Location	Age/Comp	^{18}O	^{13}C	Source
Zimbabwe, Lomagundi Group	2300 do	23.7	12.5	Schidlowski
1950-2650 Ma	2300 do	24.6	12.9	et al., 1975
" "	2300 do	24.3	11.4	" "
" "	2300 do	24.0	13.4	" "
" "	2300 do	22.3	8.1	" "
" "	2300 do	21.9	7.3	" "
" "	2300 do	21.1	8.0	" "
" "	2300 do	22.0	7.8	" "
" "	2300 do	18.5	8.6	" "
" "	2300 do	17.9	8.0	" "
" "	2300 do	22.5	9.2	" "
" "	2300 do	22.1	2.2	" "
" "	2300 cc	15.6	-4.9	" "
" "	2300 cc	15.6	-4.9	" "
Zimbabwe, Umkondo Group	300 do	26.9	14.0	" "
S. Africa, Transvaal	100 cc	16.1	1.5	" "
" "	2100 do	23.2	0.4	" "
" "	2100 do	20.9	-0.9	" "
" "	2100 do	23.1	-0.9	" "
" "	2100 do	22.7	-1.0	" "
" "	2100 do	22.8	-0.5	" "
" "	2100 do	22.4	-0.9	" "
" "	2100 do	23.2	-0.8	" "
" "	2100 do	24.2	-0.2	" "
" "	2100 do	23.4	-1.2	" "
" "	2100 do	23.2	-1.1	" "
" "	2100 do	24.5	-0.7	" "
" "	2100 do	23.4	-1.1	" "
" "	2100 do	23.4	-0.3	" "
" "	2100 do	23.5	-0.3	" "
" "	2100 do	23.5	-0.7	" "
" "	2100 do	23.0	-0.9	" "
" "	2100 do	23.1	0.3	" "
" "	2100 do	15.6	-0.8	" "
" "	2100 do	21.2	0.2	" "
" "	2100 docc	18.9	0.0	" "
" "	2100 cc	19.2	-1.1	" "
" "	2100 cc	18.9	-0.7	" "
" "	2100 cc	19.3	-1.3	" "
" "	2100 cc	19.2	-0.8	" "
" "	2100 do	20.1	0.2	" "
" "	2100 do	22.2	0.0	" "
" "	2100 do	16.0	-0.7	" "

Location	Age/Comp	^{18}O	^{13}C	Source
S.Africa, Transvaal	2100 cc	19.3	0.3	Schidlowski
" "	2100 cc	20.2	-0.7	et al., 1975
" "	2100 cc	20.9	0.5	" "
" "	2100 cc	28.7	6.6	" "
" "	2100 do	17.2	0.7	" "
" "	2100 do	22.2	0.2	" "
" "	2100 do	25.4	-0.2	" "
" "	2100 do	22.2	-0.6	" "
" "	2100 do	23.0	-1.0	" "
" "	2100 do	21.4	-0.5	" "
" "	2100 do	25.8	-0.8	" "
" "	2100 do	22.6	-1.3	" "
" "	2100 do	21.9	-0.9	" "
" "	2100 do	22.5	-1.2	" "
" "	2100 do	21.5	-1.0	" "
" "	2100 do	22.6	-0.8	" "
" "	2100 do	21.8	-0.5	" "
" "	2100 cc	16.1	-2.3	" "
" "	2100 do	18.8	-2.1	" "
" "	2100 cc	17.3	-2.8	" "
" "	2100 do	22.9	-0.6	" "
" "	2100 do	22.2	-0.0	" "
" "	2100 do	21.5	-1.9	" "
" "	2100 do	22.5	-1.0	" "
" "	2100 do	21.9	0.3	" "
" "	2100 do	22.3	-0.3	" "
" "	2100 do	21.1	-0.8	" "
" "	2100 do	23.5	-0.6	" "
" "	2100 do	22.3	-0.9	" "
" "	2100 do	22.3	-1.3	" "
" "	2100 do	21.5	-1.0	" "
" "	2100 do	19.6	-1.3	" "
" "	2100 do	24.9	-0.5	" "
" "	2100 do	21.7	-0.3	" "
" "	2100 do	22.2	-1.3	" "
" "	2100 do	15.5	-3.0	" "
" "	2100 do	15.3	-2.9	" "
" "	2100 do	15.1	-3.0	" "
" "	2100 cc	19.5	-2.3	" "
" "	2100 do	21.5	-2.7	" "
" "	2100 do	22.4	-0.5	" "
" "	2100 do	19.6	-0.8	" "
" "	2100 do	22.4	-0.6	" "
" "	2100 do	22.1	-0.8	" "
S. Africa, Cango and	600 cc	15.6	-0.9	" "
Malmesbury Formations	600 cc	20.9	7.0	" "

Location	Age/Comp	^{18}O	^{13}C	Source
S.Africa, Cangc and	600 cc	22.2	2.6	Schidlowski
Malmesbury Formations	600 cc	19.6	-3.0	et al., 1975
" "	600 cc	22.4	-0.4	" "
" "	600 cc	22.1	-0.9	" "
" "	600 do	18.5	-0.1	" "
" "	600 do	14.5	0.0	" "
" "	600 cc	18.2	8.5	" "
" "	600 cc	19.3	8.3	" "
" "	600 cc	18.6	0.8	" "
" "	600 cc	17.3	0.1	" "
" "	600 cc	19.1	0.0	" "
" "	600 cc	18.7	0.3	" "
S-S.W. Africa, Nama System	620 cc	21.8	-1.4	" "
" "	620 do	20.5	-3.8	" "
" "	620 cc	20.1	-2.9	" "
" "	620 do	23.0	-3.1	" "
" "	620 cc	26.6	-4.0	" "
" "	620 docc	24.4	-2.8	" "
" "	620 do	24.2	-3.7	" "
" "	620 cc	20.1	-6.7	" "
" "	620 do	24.9	1.0	" "
" "	620 docc	20.2	-0.6	" "
" "	620 cc	24.4	-0.6	" "
" "	620 cc	23.2	-0.2	" "
" "	620 cc	23.9	4.8	" "
" "	620 cc	23.5	3.1	" "
" "	620 cc	26.3	1.5	" "
" "	620 cc	26.8	1.4	" "
" "	620 cc	27.1	1.8	" "
" "	620 cc	26.6	2.0	" "
" "	620 cc	27.6	1.7	" "
" "	620 do	24.0	-1.9	" "
" "	620 do	22.7	-2.6	" "
S.W. Africa, Damara System	650 do	27.3	2.3	" "
600-700 Ma.	650 do	24.5	2.8	" "
" "	650 cc	22.1	9.9	" "
" "	650 do	24.0	6.2	" "
" "	650 do	26.5	5.5	" "
" "	650 do	26.5	3.9	" "
" "	650 do	24.1	-1.1	" "
" "	650 do	23.5	-1.0	" "
" "	650 docc	24.4	-0.8	" "
" "	650 do	23.8	2.5	" "
" "	650 cc	21.0	-2.1	" "

Location	Age/Comp	^{18}O	^{13}C	Source
Zambian Cu-belt,	950 do	26.2	1.3	Schidlowski
Katanga System	950 do	26.4	-3.5	et al., 1975
600-1300 Ma.	950 docc	20.8	6.8	" "
" "	950 do	17.5	-1.9	" "
" "	950 cc	10.8	-2.4	" "
" "	950 do	21.9	4.6	" "
" "	950 do	19.0	-1.5	" "
" "	950 cc	18.3	-1.0	" "
" "	950 cc	4.3	-2.3	" "
" "	950 do	19.2	1.3	" "
" "	950 cc	18.5	1.6	" "
" "	950 do	18.7	2.4	" "
" "	950 docc	21.2	0.7	" "
" "	950 do	13.5	-18.5	" "
" "	950 cc	13.2	-7.6	" "
Mauritania, Taoudenni	870 do	22.9	0.7	" "
Syncline	870 do	23.5	-0.4	" "
< 870 Ma.	870 cc	18.6	1.8	" "
" "	870 cc	15.4	0.1	" "
" "	870 cc	20.1	-0.9	" "
" "	870 cc	17.2	-2.2	" "
" "	870 cc	18.4	0.7	" "
" "	870 cc	21.7	1.3	" "
Finland/Sweden-	2050 do	17.8	8.1	" "
Fennoscandian Shield	2050 do	23.6	3.1	" "
Karelian/Svecofennian Fms.	2050 do	21.2	4.1	" "
1900-2200 Ma.	2050 do	22.5	4.5	" "
" "	2050 do	22.9	4.1	" "
" "	2050 do	17.7	8.6	" "
" "	2050 do	21.5	3.5	" "
" "	2050 do	20.9	5.2	" "
" "	2050 cc	16.3	0.9	" "
" "	2050 do	17.9	0.1	" "
Greenland, Eleonore-Bay Fm.	900 do	16.4	5.2	" "
<1000 Ma.	900 do	20.4	5.6	" "
" "	900 cc	20.9	7.2	" "
" "	900 do	16.7	4.9	" "
" "	900 cc	17.6	5.2	" "
" "	900 do	21.7	5.1	" "
" "	900 do	26.1	3.7	" "
" "	900 do	22.6	4.6	" "
" "	900 cc	15.1	5.4	" "
" "	900 cc	19.3	5.1	" "

Location	Age/Comp	^{18}O	^{13}C	Source
Canadian Shield: Oakway Fm.	1150 do	18.6	-1.1	Schidlowski
Sibley Fm.	1350 do	24.1	-0.3	et al., 1975
Maintounuk Group	2075 do	23.6	-2.2	" "
" "	2075 do	22.9	-1.1	" "
Epworth Group	2130 do	21.2	0.2	" "
Espanola Limestone	2325 cc	9.2	-3.4	" "
India: Belha Series	850 do	25.7	2.5	" "
India: Nadini Series	850 cc	21.2	4.4	" "
" "	850 cc	19.8	5.0	" "
Bhatapara Dolomite	850 do	25.4	4.4	" "
Chhattisgarh System	850 cc	23.2	3.0	" "
Kurnool System	900 cc	18.7	-0.6	" "
Lower Kurnool System	1050 cc	19.0	3.4	" "
Cuddapah System	1350 do	21.9	-0.9	" "
Australia: Brighton Lmst.	700 docc	18.7	2.1	" "
Balcanoona Fm.	700 cc	17.2	6.1	" "
Brighton Lmst.	700 do	24.3	1.6	" "
Tapley Hill Fm.	700 cc	14.7	-0.2	" "
Skillogalee Dolomite	1000 docc	22.2	-2.0	" "
India, Krol-Tal Succession	570 do	19.6	0.9	Aharon et al.
" "	570 do	28.0	0.5	1987
" "	570 do	29.3	4.4	" "
" "	570 do	26.1	4.9	" "
" "	570 do	29.4	3.6	" "
" "	570 do	29.0	-1.3	" "
" "	570 do	21.0	2.1	" "
" "	570 do	29.2	3.6	" "
" "	570 do	22.4	1.0	" "
" "	570 do	20.7	0.9	" "
" "	570 do	26.4	3.4	" "
" "	570 cc	18.4	1.9	" "
Adelaide Geosyncline	710 cc	18.4	-7.2	Veizer and
570-850 Ma.	710 do	22.3	-2.0	Hoefs, 1976
" "	710 docc	22.5	3.3	" "
" "	710 cc	19.7	-7.4	" "
" "	710 cc	20.0	-7.5	" "
" "	710 cc	18.7	-7.7	" "
" "	710 do	22.6	9.5	" "
" "	710 do	22.1	9.4	" "
" "	710 cc	22.3	3.8	" "
" "	710 cc	21.1	2.7	" "
" "	710 cc	18.7	2.2	" "
" "	710 cc	19.2	2.1	" "
" "	710 cc	18.7	1.8	" "
" "	710 do	25.1	1.8	" "

Location	Age/Comp	^{18}O	^{13}C	Source
Adelaide Geosyncline	710 do	28.0	4.4	Veizer and
" "	710 do	27.6	3.3	Hoefs, 1976
" "	710 do	23.0	5.0	" "
" "	710 do	27.9	-4.5	" "
" "	710 do	22.4	4.1	" "
" "	710 do	22.3	4.1	" "
" "	710 cc	21.4	3.7	" "
" "	710 cc	22.8	6.1	" "
" "	730 do	23.7	4.8	" "
Amadeus Basin: Pertataka Fm	730 do	24.8	5.5	" "
A. Basin: Bitter Springs Fm	800 do	25.2	2.2	" "
" "	800 cc	16.2	-2.1	" "
" "	800 cc	24.0	-3.8	" "
" "	800 cc	21.7	-2.6	" "
" "	800 cc	23.0	5.3	" "
" "	800 do	25.9	2.2	" "
" "	800 do	26.0	1.4	" "
" "	800 cc	17.6	-0.9	" "
" "	800 cc	16.9	0.0	" "
" "	800 cc	19.8	3.1	" "
" "	800 cc	23.7	0.1	" "
Australia: Hammersley Basin	2095 cc	16.7	0.6	" "
Mt. Bruce Supergroup	2095 do	20.9	0.4	" "
1950-2240 Ma.	2095 do	20.5	0.0	" "
" "	2095 do	20.6	0.0	" "
" "	2095 do	21.3	-0.1	" "
" "	2095 do	18.0	0.1	" "
" "	2095 do	19.6	-0.2	" "
" "	2095 cc	11.6	-1.6	" "
Bangemall Group	1050 do	24.7	2.3	" "
1000-1100 Ma.	1050 do	23.8	2.2	" "
" "	1050 do	22.7	-1.0	" "
Canada: Coronation Geosyncl.	2012 cc	14.0	0.4	" "
1725-2300 Ma.	2012 cc	21.5	2.1	" "
" "	2012 do	21.1	1.2	" "
" "	2012 do	21.9	-0.6	" "
India: Badami Group	1100 do	20.6	3.2	Sathyanarayn
" "	1100 docc	21.2	3.9	et al., 1987
" "	1100 do	20.0	2.8	" "
" "	1100 do	22.8	3.8	" "
India: Kaladgi Group	1500 do	24.4	0.6	" "
" "	1500 do	19.6	0.0	" "
" "	1500 do	21.8	1.2	" "
" "	1500 cc	22.8	1.1	" "

Location	Age/Comp	^{18}O	^{13}C	Source
India: Kaladgi Group	1500 cc	19.5	0.3	Sathyanarayan
" "	1500 cc	22.9	1.5	et al.,1987
" "	1500 cc	21.4	1.0	" "
" "	1500 do	21.4	1.3	" "
" "	1500 do	21.9	0.0	" "
" "	1500 do	21.0	0.6	" "
" "	1500 do	21.5	0.0	" "
" "	1500 do	22.3	0.2	" "
" "	1500 do	23.2	0.5	" "
" "	1500 do	22.0	-3.6	" "
" "	1500 do	21.0	0.2	" "
" "	1500 do	20.0	0.2	" "
East Greenland	620 do	26.0	-4.0	Knoll et al.,
570-900 Ma.	620 do	21.6	-1.1	1986
" "	620 do	25.6	-2.4	" "
" "	620 do	22.7	-3.0	" "
" "	620 cc	24.4	0.5	" "
" "	620 cc	19.3	2.8	" "
" "	620 cc	22.8	-4.2	" "
" "	620 cc	19.7	-6.7	" "
" "	620 cc	26.2	-5.0	" "
" "	620 cc	21.3	3.2	" "
" "	620 cc	23.9	2.9	" "
" "	620 cc	22.8	3.0	" "
" "	620 cc	22.9	6.6	" "
" "	620 cc	30.7	5.5	" "
" "	620 cc	22.9	7.2	" "
" "	700 do	18.9	4.8	" "
" "	700 do	21.2	-3.1	" "
" "	700 cc	23.6	7.2	" "
" "	700 cc	22.8	7.2	" "
" "	700 do	30.4	11.0	" "
" "	700 cc	16.2	7.3	" "
" "	800 do	21.8	5.6	" "
" "	800 cc	12.5	4.4	" "
" "	800 do	26.5	4.7	" "
" "	800 do	13.7	1.7	" "
" "	800 cc	15.4	1.4	" "
" "	800 cc	26.1	5.6	" "
" "	800 cc	23.0	6.0	" "
" "	800 cc	20.2	4.8	" "
" "	800 do	21.8	4.8	" "
" "	800 docc	21.7	-1.4	" "
" "	900 cc	20.5	4.6	" "

Location	Age/Comp	^{18}O	^{13}C	Source
East Greenland	900 cc	13.8	5.9	Knoll et al.,
" "	900 cc	17.5	5.7	1987
" "	900 cc	22.6	5.8	" "
" "	900 cc	26.2	7.7	" "
" "	900 cc	18.8	7.7	" "
" "	900 cc	21.6	4.3	" "
" "	900 cc	15.4	6.6	" "
Northwest Spitsbergen	570 cc	18.2	-0.4	" "
" "	570 cc	20.9	-0.4	" "
" "	570 do	19.3	-0.2	" "
" "	570 do	17.5	-1.8	" "
" "	570 do	22.9	0.4	" "
" "	570 cc	24.6	1.1	" "
" "	620 do	23.3	10.0	" "
" "	620 cc	22.6	-3.9	" "
" "	620 cc	23.8	4.0	" "
" "	620 do	28.7	3.7	" "
" "	620 cc	24.8	2.7	" "
" "	620 cc	28.2	2.1	" "
" "	620 cc	26.7	4.7	" "
" "	700 cc	24.0	3.9	" "
" "	700 cc	24.4	5.7	" "
" "	700 do	26.5	5.0	" "
" "	700 cc	23.9	6.6	" "
" "	700 do	27.9	7.8	" "
" "	700 do	28.3	3.4	" "
" "	700 do	25.1	5.5	" "
" "	700 do	25.5	5.3	" "
" "	700 do	25.8	5.2	" "
" "	700 do	26.1	6.8	" "
" "	700 cc	24.1	2.9	" "
" "	700 cc	27.0	4.5	" "
" "	700 do	29.0	5.2	" "
" "	700 do	28.0	6.6	" "
" "	700 do	26.7	7.8	" "
" "	700 cc	28.4	6.6	" "
" "	700 cc	30.4	5.4	" "
" "	700 cc	24.5	4.8	" "
" "	700 cc	24.3	4.6	" "
" "	700 do	22.6	2.4	" "
" "	700 do	23.3	-2.5	" "
" "	700 cc	20.3	0.9	" "
" "	700 cc	20.6	7.0	" "
" "	700 cc	23.0	6.6	" "

Location	Age/Comp	$^{18}\delta$	^{13}C	Source
Northwest Spitsbergen	700 cc	22.4	5.1	Knoll et al.,
" "	700 cc	24.0	3.1	1986
" "	700 cc	20.2	4.4	" "
" "	800 cc	23.2	3.3	" "
" "	800 cc	14.4	4.4	" "
" "	800 cc	25.0	-5.8	" "
" "	900 cc	17.5	4.5	" "
" "	900 cc	17.2	5.0	" "
" "	900 cc	20.5	5.5	" "
" "	900 cc	13.9	0.1	" "
Nordauslandet	620 do	21.4	9.8	" "
" "	620 cc	22.5	-4.3	" "
" "	620 cc	20.2	-7.0	" "
" "	620 cc	20.9	3.6	" "
" "	620 cc	23.7	5.3	" "
" "	620 cc	23.1	5.5	" "
" "	620 cc	24.7	2.7	" "
" "	700 do	22.7	4.4	" "
" "	700 cc	21.9	6.1	" "
" "	700 do	23.2	5.2	" "
" "	700 cc	24.6	7.7	" "
" "	700 do	24.5	8.0	" "
" "	700 do	23.1	8.2	" "
" "	700 cc	17.3	5.1	" "
" "	700 do	26.1	4.6	" "
" "	700 do	25.4	3.0	" "
" "	700 do	28.8	4.3	" "
" "	700 do	21.3	5.8	" "
" "	700 do	25.2	-1.9	" "
" "	700 d0	22.9	3.2	" "
" "	700 do	25.9	-2.1	" "
" "	700 do	24.5	-1.1	" "
" "	700 cc	19.2	3.7	" "
" "	700 do	22.4	2.6	" "
" "	800 do	23.4	3.6	" "
" "	800 do	22.7	3.4	" "
" "	900 cc	18.3	5.1	" "
" "	900 cc	17.1	5.1	" "
" "	900 cc	17.9	4.7	" "
" "	900 cc	17.7	5.3	" "
" "	900 do	12.5	1.1	" "
" "	900 do	12.5	1.1	" "

Location	Age/Comp	^{18}O	^{13}C	Source
Australia: Burra Group	800	21.6	4.6	Schidlowski,
Australia: Bungle Bungle Do.	1600	24.7	-0.8	et al. 1983
" "	1600	22.7	-0.9	" "
" "	1600	23.3	-0.7	" "
" "	1600	19.8	-0.5	" "
" "	1600	21.5	-0.3	" "
" "	1600	22.4	-0.2	" "
" "	1600	20.8	-1.0	" "
Australia: Bitter Springs	900	22.5	3.3	" "
Australia: McArthur Group	1600	20.5	0.0	" "
" "	1600	23.0	0.1	" "
" "	1600	17.7	-2.4	" "
" "	1600	20.7	-1.5	" "
" "	1600	19.4	-1.2	" "
" "	1600	19.2	-1.1	" "
Australia: Earaheedy Group	1800	18.1	-0.8	" "
" "	1800	19.2	-1.7	" "
" "	1800	21.3	-1.1	" "
" "	1800	23.3	1.0	" "
" "	1800	17.9	0.5	" "
" "	1800	13.8	-1.1	" "
" "	1800	18.5	0.0	" "
Canada: Kahochella Group	2000	16.5	-0.1	" "
" "	2000	17.0	-0.7	" "
Canada: Pethei Group	2000	18.3	1.6	" "
" "	2000	15.7	1.2	" "
Australia: Wyloo Group	2000	16.5	0.9	" "
" "	2000	15.9	0.6	" "
" "	2000	15.3	0.5	" "
" "	2000	15.1	0.3	" "
" "	2000	18.3	0.7	" "
Canada: Albanel Fm.	2100	23.7	0.9	" "
" "	2100	21.8	6.3	" "
S. Africa: Transvaal	2200	21.6	-1.4	" "
" "	2200	21.6	-1.3	" "
" "	2200	22.4	-0.5	" "
" "	2200	21.3	-0.5	" "
" "	2200	21.9	-0.7	" "
" "	2200	22.5	-0.8	" "
" "	2200	21.9	-0.9	" "
" "	2200	23.4	-0.1	" "
" "	2200	21.4	-0.9	" "
" "	2200	21.5	-0.9	" "
" "	2200	21.6	-0.8	" "

	Location	Age/Comp	^{18}O	^{13}C	Source
S. Africa:	Transvaal	2200	24.8	-0.7	Schidlowski,
"	"	2200	19.9	-0.8	et al. 1983
Australia:	Hammersley Group	2500	20.9	-12.0	" "
"	"	2500	22.2	0.5	" "
"	"	2500	19.6	0.0	" "
"	"	2500	20.5	0.3	" "
"	"	2500	16.9	0.0	" "
"	"	2500	16.9	0.0	" "
"	"	2500	20.4	-9.3	" "
"	"	2500	20.1	-8.5	" "
California:	Noonday Dolomite	1000 do	21.0	-2.8	Hall, 1984
"	"	1000 do	25.4	-1.1	" "
"	"	1000 do	25.2	-2.1	" "
"	"	1000 do	24.5	-1.9	" "
"	"	1000 do	23.2	-2.8	" "
"	"	1000 do	22.6	-2.4	" "
"	"	1000 do	20.6	-3.9	" "
"	"	1000 do	22.5	-3.4	" "
"	"	1000 do	24.5	-2.6	" "
"	"	1000 do	18.8	-6.2	" "
"	"	1000 do	17.1	-2.2	" "
"	"	1000 do	17.8	-3.3	" "
"	"	1000 do	16.8	-4.0	" "
"	"	1000 do	22.8	-3.2	" "
"	"	1000 do	21.9	-2.6	" "
"	"	1000 do	21.9	-2.7	" "
"	"	1000 do	22.0	-3.0	" "
"	"	1000 do	21.9	-3.2	" "
"	"	1000 do	18.3	-4.8	" "
"	"	1000 do	22.7	-2.8	" "
"	"	1000 do	20.4	-3.6	" "
"	"	1000 do	18.3	-4.6	" "
"	"	1000 do	16.7	-5.9	" "
"	"	1000 do	20.0	-3.1	" "
"	"	1000 do	16.6	-4.5	" "
"	"	1000 do	20.2	-3.3	" "
"	"	1000 do	20.4	-3.4	" "
"	"	1000 do	22.3	-3.7	" "
"	"	1000 do	19.5	-3.1	" "
"	"	1000 do	21.2	-3.1	" "
"	"	1000 do	22.4	-2.6	" "
"	"	1000 do	23.2	-2.9	" "
"	"	1000 do	21.8	-3.1	" "
"	"	1000 do	20.9	-3.5	" "

Location	Age/Comp	^{18}O	^{13}C	Source
Belt Supergroup: Helena	1050 cc	19.5	-1.6	Winston et al.
" "	1050 cc	19.2	-2.2	1984
Mt. Shields	1080 do	23.8	0.8	" "
" "	1080 do	23.0	0.5	" "
Spokane	1080 cc	18.2	-3.0	" "
" "	1080 cc	17.2	-3.3	" "
" "	1080 cc	17.5	-3.6	" "
" "	1080 cc	17.5	-3.7	" "
" "	1080 cc	16.9	-3.8	Lange et al.
" "	1080 cc	16.9	-3.2	1987
" "	1080 cc	17.2	-3.8	" "
" "	1080 cc	17.1	-3.7	" "
" "	1080 cc	14.0	-3.2	" "
" "	1080 cc	16.7	-3.6	" "
" "	1080 cc	16.5	-4.0	" "
" "	1080 cc	16.6	-1.4	" "
" "	1080 cc	15.6	-1.4	" "
" "	1080 cc	17.1	-3.7	" "
Ravalli Group	1180 cc	15.2	-10.5	Rye et al.
" "	1180 cc	9.8	-5.8	1984
" "	1180 cc	14.7	-5.7	" "
" "	1180 cc	13.8	-5.0	" "
" "	1180 cc	14.6	-3.2	" "
" "	1180 cc	15.5	-2.8	" "
" "	1180 cc	17.8	-3.1	" "
" "	1180 cc	16.2	-2.3	" "
" "	1180 cc	14.3	-2.1	" "
" "	1180 cc	17.0	-1.8	" "
" "	1180 cc	17.0	-1.5	" "
" "	1180 cc	17.3	-2.0	" "
" "	1180 cc	18.8	-2.2	" "
" "	1180 cc	18.3	-2.4	" "
" "	1180 cc	16.1	-1.3	" "
" "	1180 cc	18.2	3.2	" "
" "	1180 do	25.5	2.4	" "
" "	1180 do	21.7	1.3	" "
" "	1180 cc	10.8	-8.8	" "
" "	1180 cc	12.1	-8.3	" "
Missoula Group	1025 cc	12.2	-5.7	" "
" "	1025 cc	14.3	-2.8	" "
" "	1025 cc	14.0	0.5	" "
" "	1025 cc	17.9	-0.8	" "
" "	1025 cc	18.4	-1.3	" "
" "	1025 cc	19.5	-2.4	" "

Location	Age/Comp	^{18} 0	^{13} C	Source
Missoula Group	1025 do	24.2	-2.5	Rye et al.
Middle Belt Carbonate	1050 cc	12.4	-2.5	1984
" "	1050 cc	15.0	-3.5	" "
" "	1050 cc	16.3	-3.6	" "
" "	1050 cc	16.3	-2.8	" "
" "	1050 cc	20.2	-1.0	" "
" "	1050 cc	21.2	-0.8	" "
" "	1050 cc	15.3	-0.6	" "
" "	1050 cc	17.2	0.9	" "

Oxygen isotopes are reported as SMOW,
Carbon isotopes are reported as PDB,
Age is in Ma.
do = dolostone
cc = limestone
docc = dolomitic limestone
composition was determined from descriptions of samples in literature